

The Early Detection of Apple Scab
Using Multispectral Imagery
Under Natural Illumination Conditions

Alexander Bleasdale

Lancaster Environment Centre

This thesis is submitted for the degree of Doctor of Philosophy

Lancaster
University



June 2024

“An Apple a Day Keeps the Doctor Away”

Abstract

Apples are a nutritious, globally significant crop, yet their production has a substantial environmental impact due to the reliance on heavy pesticide use within disease management strategies. Apple scab, caused by the fungus *Venturia inaequalis*, is the primary cause of yield losses among all the pathogens that affect apples globally, leading to the highest protection costs and volumes of fungicides used for control. Conventional disease management strategies rely on uniform spraying of protective fungicides, repeated frequently throughout the growing season. This expensive, chemical-intensive approach contributes to widespread environmental contamination in many apple-growing regions worldwide. The early detection of apple scab infections offers a promising alternative for disease control by enabling targeted fungicide spraying, thereby improving the effectiveness of control measures and reducing chemical usage. Remote sensing systems are powerful tools for the early detection of plant pathogens; however, practical solutions for apple scab monitoring in commercial orchards are limited. The challenges of early detection in orchards arise from diverse symptom variations, variable illumination conditions, tree physiologies, and influences from other stress factors. Demonstrating the feasibility of early apple scab detection by remote sensing systems in uncontrolled conditions represents a significant step towards applying such systems in commercial orchards.

This thesis aims to develop a remote sensing strategy for the early detection of apple scab infections under natural illumination conditions. The research rationale will first be introduced, followed by a review of the requirements for early disease detection in orchards and the current strategies and technologies available, including imaging sensors, classification methods and acquisition platforms. The capabilities of several low-cost sensing systems (multispectral, thermal, and 3D cameras) for detecting early apple scab infections under natural illumination are then assessed. Results indicate that apple scab symptoms could be manually identified several days earlier from high-resolution near-infrared (NIR) imagery than equivalent RGB imagery due to major differences in NIR radiation absorption potential between healthy and infected tissue. RGB and NIR time series datasets comprising 150 individual plants were then acquired and used to train convolutional neural networks (CNNs) to enable rapid, automated classification of apple scab symptoms. These CNNs consistently classified apple scab infections earlier and more accurately from NIR imagery than RGB imagery. This research shows that NIR imagery is effective for early apple scab detection under natural illumination conditions, and automated identification of the disease can be achieved accurately and rapidly with CNN classification models. This represents a significant advancement towards applying remote sensing systems for disease monitoring in apple orchards.

Declaration

The following thesis is the result of my original work and has not been submitted to qualify for another academic degree at any other institution. All published sections of the thesis have been identified. Many of the ideas contained within this work were the product of discussions with my supervisors: Professor James Duncan Whyatt, Professor George Alan Blackburn, and Professor Elizabete Carmo-Silva at Lancaster University.

Alexander Bleasdale

June 2024

Statement of Authorship

The work presented in this thesis is organised into chapters, each reflecting a key objective achieved during this project towards the research aim. Much of this research is intended for publication in peer-reviewed journals. Chapter 3 is adapted from a manuscript published in a peer-reviewed journal. Chapter 4 is adapted from a manuscript currently under review, and Chapter 5 has been prepared for submission. All chapters include contributions from multiple authors within my supervisory team.

Chapter 3 is an adapted version of a manuscript published as:

Bleasdale, A. J., Blackburn, G. A., & Whyatt, J. D. (2022). Feasibility of detecting apple scab infections using low-cost sensors and interpreting radiation interactions with scab lesions. *International Journal of Remote Sensing*, 43(13), 4984–5005. <https://doi.org/10.1080/01431161.2022.2122895>

Chapter 4 is adapted from a manuscript in review at *Artificial Intelligence in Agriculture* as:

Bleasdale, A. J., Whyatt, J. D. (2024). Classifying early apple scab infections in multispectral imagery using convolutional neural networks

Chapter 5 is adapted from a manuscript prepared for submission to *Computers and Electronics in Agriculture* as:

Bleasdale, A. J., Whyatt, J. D. (2024). Monitoring Apple Scab Progression from Visible and Near-Infrared Time Series Imagery using Convolutional Neural Networks

Acknowledgements

Completing this PhD has been a long and arduous journey that would not have been possible without the support and encouragement of those around me. I would like to take this opportunity to express my sincere gratitude to everyone who helped me along the way.

To begin with, I want to acknowledge both of my academic supervisors. First, I am deeply grateful to the late Professor Alan Blackburn, who inspired the initial project. Your knowledge and precious time were invaluable to me; this project could never have happened without you. I must also express my profound thanks to Professor Duncan Whyatt for the support, freedom, and trust you gave me that allowed me to thrive. Your kind words and critical feedback have helped me develop as a scientist, and your little red pen has made this a thesis I can be proud of.

Next, I would like to thank everyone who has contributed to this project. I am thankful to everyone in the Waitrose Collaborative Training Partnership for keeping this project organised. I must also acknowledge the Biotechnology and Biological Sciences Research Council for funding this project. To those at Worldwide Fruit, the apple growers, and agronomists I have met during my research whose time, knowledge, and passion have been instrumental in helping me understand the reality of the apple industry. I also wish to express my appreciation to Professor Elizabete Carmo-Silva for her advice and expertise as well as the administrative, technical, and academic staff at Lancaster University for always being able to help whenever possible.

Thank you to my friends and family for always asking me how the apples are doing. Thank you to my Nana and Grandad for all the bananas, biscuits, cans of Coke, and cash you slipped me through the years. Thank you to Buddy, Minnie, Pearl, and Hugo for all being such good cats. I also thank all my surviving apple trees as well as those who were sacrificed in the name of science.

To my mum, Michaela, your love and support throughout the years and your assistance during the final stages of writing have been invaluable. I never could have made it to this stage of my life without you. Finally, thank you to Eva Bukina for her patience and kindness during this PhD, for all the laughter, food and experiences we share, and for inspiring me to be the best version of myself.

Table of Contents

- Abstract.....3
- Declaration.....4
- Statement of Authorship4
- Acknowledgements.....5
- Table of Contents.....6
- List of Figures 10
- List of Tables 15
- 1 Introduction..... 17
 - 1.1 Smart Farming and the Sustainable Intensification of Agriculture..... 17
 - 1.2 Precision Agriculture Strategies for Crop Disease Management..... 18
 - 1.3 The Impact of Apple Scab 20
 - 1.4 Thesis Overview 24
 - 1.4.1 Thesis Aims and Objectives 24
 - 1.4.2 Thesis Structure 25
- 2 Remote Sensing Strategies for Disease Monitoring in Apple Orchards 27
 - 2.1 Introduction 27
 - 2.2 Disease Monitoring in Apple Orchards 30
 - 2.2.1 Taxonomy of Apple Diseases..... 30
 - 2.2.2 Conventional Methods of Disease Monitoring..... 34
 - 2.3 Remote Sensors for Disease Detection..... 35
 - 2.3.1 Leaf Optical Properties 35
 - 2.3.2 Colour Cameras (RGB Imaging) 37
 - 2.3.3 Hyperspectral Sensing..... 40
 - 2.3.4 Multispectral Cameras..... 43
 - 2.3.5 Chlorophyll Fluorescence Imaging 46
 - 2.3.6 Thermography 47
 - 2.3.7 3D Imaging Systems..... 49
 - 2.3.8 Sensor Selection 51
 - 2.4 Classification Techniques for Disease Identification..... 52
 - 2.4.1 Traditional Machine Learning Classification..... 52
 - 2.4.2 Deep Learning Convolutional Neural Network Models 54
 - 2.4.3 Classification Model Selection 57
 - 2.5 Acquisition Platforms for Orchard Monitoring..... 58
 - 2.5.1 Requirements for Acquisition Platforms in Orchards 58

2.5.2	Ground-based Sensing Platforms.....	59
2.5.3	Aerial Sensing Platforms.....	62
2.5.4	Platform Selection	62
2.6	Potentiality and Practicalities of Remote Sensing for Disease Monitoring.....	63
2.6.1	Recommendations for Remote Sensing System Technologies and Opportunities for Further Research	63
2.6.2	Practical Considerations for Orchard Use.....	65
2.6.3	Prospective Applications of Disease Monitoring Systems	66
2.7	Conclusion.....	68
3	Feasibility of Detecting Apple Scab Infections using Low-Cost Sensors and Interpreting Radiation Interactions with Scab Lesions.....	70
	Abstract.....	70
3.1	Introduction	71
3.2	Methodology	75
3.2.1	Plant Material and Inoculation.....	75
3.2.2	Low-Cost Sensing Setup.....	76
3.2.3	Disease Assessment.....	79
3.3	Results	80
3.3.1	Multispectral Imagery.....	80
3.3.2	Thermal Imagery	84
3.3.3	3D Imagery	86
3.4	Discussion	87
3.4.1	Radiation Interaction with Scab Lesions.....	87
3.4.2	Apple Foliar Sensing Requirements.....	88
3.4.3	Directions for Future Research	89
3.5	Conclusion.....	90
4	Classifying Early Apple Scab Infections in Multispectral Imagery using Convolutional Neural Networks	91
	Abstract.....	91
4.1	Introduction	92
4.2	Methodology	95
4.2.1	Apple Disease Identification Dataset.....	95
4.2.2	Fine-Tuning Convolutional Neural Networks.....	99
4.2.3	Performance Assessment	101
4.3	Results and Discussion	102
4.3.1	Model Training and Convergence	102
4.3.2	Classification Performance on the ADID Dataset	103

4.3.3	Apple Scab Classification from the Multispectral Time Series.....	105
4.3.4	Comparing Classification Performance on RGB and NIR Imagery	107
4.3.5	Experimental Limitations and Recommendations for Further Research.....	109
4.4	Conclusion.....	111
5	Monitoring Apple Scab Progression from Visible and Near-Infrared Time Series Imagery with Convolutional Neural Networks	112
	Abstract.....	112
5.1	Introduction	113
5.2	Materials and Methods	116
5.2.1	Apple Plant Material.....	116
5.2.2	Multispectral (VIS-NIR) Time Series Imagery	118
5.2.3	Apple Disease Dataset.....	119
5.2.4	Convolutional Neural Networks	124
5.2.5	CNN Classification Performance Evaluation.....	127
5.3	Results	128
5.3.1	CNN Model Training Convergence.....	128
5.3.2	CNN Classification Performance.....	129
5.3.3	Enhancing Classification Performance Through Localisation.....	133
5.3.4	Time Series Assessment.....	136
5.4	Discussion	140
5.4.1	CNN Classifiers for Apple Scab Monitoring.....	140
5.4.2	Multispectral Imagery for the Early Detection of Apple Scab	141
5.4.3	Experimental Challenges and Limitations.....	144
5.4.4	Recommendations for Future Research	147
5.5	Conclusions.....	149
6	General Discussion.....	151
6.1	Introduction	151
6.2	Apple Plant Samples	152
6.3	High-Resolution Multispectral Sensing.....	156
6.4	Multispectral Apple Disease Dataset	160
6.5	Automated Classification of Apple Scab	166
6.6	Early Detection of Apple Scab	170
6.7	Recommendations for Further Work.....	172
6.7.1	Designing a Practical High-resolution Multispectral Imaging System.....	172
6.7.2	Collecting and Annotating a Large Multispectral Apple Disease Dataset.....	173
6.7.3	Enhancing Apple Scab Classification Methods	173
6.7.4	Performing Controlled Early Detection of Apple Scab Assessments	174

7	Conclusions and Future Research.....	175
7.1	General Conclusion.....	175
7.2	Future Research for Disease Monitoring in Orchards.....	177
7.2.1	Assessment of Acquisition and Classification in High-Density Orchards.....	178
7.2.2	Informing Integrated Pest and Disease Management Strategies	178
7.2.3	Understanding the Impact on Sustainable Intensification of Apple Production	179
8	References	180
9	Appendices.....	209
9.1	Appendix A – Experimental Weather Conditions	209
9.2	Appendix B – Convolutional Neural Network Model Code Structure.....	214
9.2.1	Chapter 4 Model Code.....	214
9.2.2	Chapter 5 Model Code.....	218
9.2.3	Pre-Trained CNN Classifier.....	222
9.3	Appendix C – Convolutional Neural Network Classification Results	224
9.3.1	Model Training Metrics	224
9.3.2	Classification Results.....	227
9.4	Appendix D - Multispectral Time Series Imagery	230

List of Figures

Figure 2.1 Changes in fungicide usage within the UK from 2012 – 2022 (adapted from Garthwaite et al., 2013; Garthwaite et al., 2015; Garthwaite et al., 2017; Mace et al., 2019; Ridley et al., 2022; Ridley et al., 2024). 28

Figure 2.2 Common biotic and abiotic stresses monitored in apple orchards 31

Figure 2.3 Severe foliar and fruit symptoms of apple scab, powdery mildew and fireblight (adapted from Ayer et al., 2020; Strickland et al., 2020; Wallis et al., 2020)..... 34

Figure 2.4 The electromagnetic spectrum (excluding Gamma Rays) 36

Figure 2.5 RGB imagery displaying the symptom variance of late-stage apple diseases (adapted from Thapa et al., 2020) 39

Figure 2.6 Simplified diagram of a hyperspectral imaging hypercube and vegetation reflectance spectrum..... 40

Figure 2.7 Hyperspectral imaging principal component analysis scores for healthy and apple scab- infected (adapted from Nouri et al., 2018) 42

Figure 2.8 Multispectral imaging (component bands and false colour composite) of apple trees in an orchard (adapted from Jarolmasjed et al., 2018)..... 44

Figure 2.9 Thermal assessment of apple scab progression where white circles denote initial symptom development (adapted from Oerke et al., 2011)..... 48

Figure 2.10 The basic structure of a CNN for apple disease classification (adapted from Liu & Wang, 2021) 55

Figure 2.11 Example imagery of apple foliar diseases from public datasets. PV – PlantVillage (Hughes & Salathe, 2015); PP - PlantPathology2020 (Thapa et al., 2020) 57

Figure 2.12 Remote sensing platforms for agricultural applications (adapted from Shakoor et al., 2017)..... 59

Figure 2.13 Apple scab symptom variation with stage and severity (adapted from Thapa et al., 2021)..... 64

Figure 2.14 Extrinsic factors influencing accurate disease classification. Column A) Presence of strong shadows. Column B) Strong illumination and specular lighting. Column C) Occlusion of leaves by overlaying foliage. (Adapted from Thapa et al., 2021)..... 65

Figure 2.15 Intrinsic factors influencing accurate disease classification. Column D) Differing symptom presence from the same pathogen. Column E) Similar symptom presence from differing pathogens. Column F) Multiple pathogens present on individual leaves (adapted from Thapa et al., 2021) 66

Figure 3.1 The lifecycle of the hemibiotrophic fungus *V. inaequalis* on apple trees..... 72

Figure 3.2 Low-cost, high-resolution stereoscopic multispectral camera..... 77

Figure 3.3 Low-cost image acquisition setup consisting of a multispectral camera, thermal camera, and 3D imager on a variable friction arm	78
Figure 3.4 Ordinal scale of categorical apple scab infection severities and example RGB imagery.	80
Figure 3.5 The progression of apple scab from low to severe infection in RGB, NIR and red-edge imagery over the experiment with imagery acquired at 9 (low severity), 17 (moderate severity), and 35 (high severity) days past inoculation (d.p.i.)	81
Figure 3.6 The progression of apple scab symptoms on a single leaf from initial symptoms at 12 d.p.i. to moderate severity at 22 d.p.i. Arrows indicate initial infection locations identified through retrospective analysis.	82
Figure 3.7 A single apple leaf with moderate-severity infection in A) RGB and B) NIR imagery at 18 days post inoculation. Features labelled include: 1) mature coalesced lesions, 2) large circular lesions growing along venules, 3) small lesions with individual points of infection on main veins 4) asymptomatic leaf tissue	83
Figure 3.8 Influence of ambient light environment on the perception of scab. Irradiance was measured at 13 d.p.i. as 0.048 kW/m ² , at 22 d.p.i. as 0.353 kW/m ² , and at 23 d.p.i. as 0.149 kW/m ² . Observe the influence of shadow on infected leaf 1, and specular light on infected leaves 2 and 3. Bright spots in NIR imagery at 13 d.p.i. are an artefact from the NIR structured light from the 3D camera.....	84
Figure 3.9 Progression of apple scab infection in Thermal, RGB and NIR imagery over a 28-day period from 7 d.p.i. to 35 d.p.i.. Length of leaf in pixels from base to tip of a 50 mm leaf, and diameter of a 4 mm scab lesion included to highlight difference in image resolution between thermal and multispectral systems.	85
Figure 3.10 Temperature variation across different features of a A) thermogram and corresponding B) RGB.....	85
Figure 3.11 3D models of young apple plants with an A) RGB texture overlay and B) NIR texture overlay observed from 1) isometric viewpoints, 2) side viewpoints 3) top-down viewpoints. Artefacts labelled include *overlay stretching between different depths, ** flattening of plant height, *** incorrect background depth between leaves, **** gaps in models due to shadowing from leaves.....	86
Figure 3.12 Interaction of NIR light with infected and asymptomatic leaf cross-sections	88
Figure 4.1 Manual classification results of the RGB and NIR time series datasets. Each cell represents a single image.	96
Figure 4.2 Example images of the variation of symptoms in the early and late stages of apple scab infection. *PlantVillage contains only well-established symptoms of scab, although this still includes variations in the stage and severity of lesions.....	97
Figure 4.3 Example images of characteristic symptoms of each of the six classes from the PlantPathology2021 dataset	98
Figure 4.4 Flow diagram of the ADID Dataset multi-class classification process.....	100
Figure 4.5 Graphs displaying the convergence speed for training accuracy (left) and loss (right) for both MobileNetV2 and EfficientNetV2L models	103

Figure 4.6 Confusion matrices of CNN predictions for each of the six classes in the ADID dataset for the MobileNetV2 and EfficientNetV2L models.....	104
Figure 4.7 Confusion matrices of the scab category in the multispectral dataset for the MobileNetV2 and EfficientNetV2L models. 0 indicates negative labels (healthy) and 1 positive labels (scab)	106
Figure 4.8 Heatmap of the scab prediction confidence in the multispectral time series classification for the MobileNetV2 (left) and EfficientNetV2L (right) models. Each cell represents the confidence score output for an individual image.....	107
Figure 4.9 Above) Heatmap of the scab prediction confidence in the RGB (left) and NIR (right) time series imagery for the MobileNetV2 model. Below) Heatmap of the scab prediction confidence in the RGB (left) and NIR (right) time series imagery for the EfficientNetV2L model. Each cell represents the confidence score output for an individual image.....	108
Figure 5.1 RGB and NIR time series imagery displaying examples of control (C16) and experimental (E08) samples at an early and late stage of the experiment.....	119
Figure 5.2 Example imagery for each disease class from the secondary validation (public - PlantPathology2021) data. The three lower images display examples of multiple diseases occurring within a single leaf.....	121
Figure 5.3 Example images within the training set from primary and secondary sources demonstrating the variance within the 'HEALTHY' and 'SCAB' classes in RGB and NIR imagery	123
Figure 5.4 The class label distribution across the training and testing sets of the apple disease dataset	124
Figure 5.5 Flow diagram of the apple disease dataset multi-label classification process	125
Figure 5.6 Process of fine-tuning the final fully-connected layer of the pre-trained MobileNetV2, InceptionResNetV2, and EfficientNetV2L models.....	126
Figure 5.7 Convergence in training accuracy (left) and training loss (right) for MobileNetV2, InceptionNetV2 and EfficientNetV2L models	128
Figure 5.8 Example of whole-plant and localised images of experimental samples E01 and E13 in RGB and NIR imagery	134
Figure 5.9 Time series of manually classified data (Yellow - Healthy; Aqua/Blue - Scab) for control (C01-C20) and experimental (E01-E20) samples	137
Figure 5.10 Time series heatmap of 'SCAB' confidence scores for RGB imagery. (Yellow - Healthy; Aqua/Blue - Scab) for control (C01-C20) and experimental (E01-E20) samples	138
Figure 5.11 Time series heatmap of 'SCAB' confidence scores for NIR imagery. (Yellow - Healthy; Aqua/Blue - Scab) for control (C01-C20) and experimental (E01-E20) samples	138
Figure 5.12 Smoothed 3-day moving mean time series of the sum of manual classification scores (green) and confidence scores of all 40 experimental and control samples in RGB (light blue) and NIR (dark blue) imagery from 1 to 56 days post-inoculation.....	139

Figure 5.13 The influence of strong sunlight on apple scab prominence in sample E09. Lesions on leaves marked 1 and 2 become visible at 49 d.p.i. compared to the previous day.....	142
Figure 5.14 Example of abiotic (heat) stress on control sample C04 in RGB and NIR imagery. Characteristic symptoms of damaged leaf tissue are present on leaves marked 1, 2 and 3	143
Figure 5.15 Example of powdery mildew (white fungal mycelium on leaf surface) and scab on experimental sample E09. While characteristic scab lesions are clearly visible in the NIR imagery, powdery mildew cannot be detected.....	144
Figure 5.16 Occlusion of scab lesions on Sample E13 in both the RGB and NIR time series. Scab lesions on leaf 1 at 52 d.p.i. are masked by the overlaying leaf 2 at 53 d.p.i., presenting no scab symptoms in the whole-plant imagery.....	146
Figure 6.1 Control and Experimental SolarDome Glasshouses.....	152
Figure 6.2 Comparison of sizes of Raspberry Pi (Sensor 1) and Canon (Sensor 2) systems. A) Size of stereoscopic sensing system. B) CMOS sensor size	158
Figure 6.3 Exposure Triangle	159
Figure 6.4 Above) Example of healthy image (Sample C07 at 47 d.p.i.). Below) Example of Scab imagery (Sample E13	161
Figure 6.5 Above) Examples of brown necrotic tissue damage due to heat stress in the imagery, which are identifiable on leaves labelled 1, 2, and 3 (Sample C03 at 14 d.p.i.). Below) Examples of white fungal mycelium of powdery mildew in imagery (Sample T69 at 45 d.p.i.).	162
Figure 6.6 Above) Combination of apple scab and powdery mildew in imagery (Sample E08 at 45 d.p.i.). Below) Example of Apple Scab, powdery mildew, and heat stress (Sample T75 at 56 d.p.i.)	163
Figure 6.7 Label distribution in the Final Apple Disease Dataset generated over Experiment 1 and Experiment 2.....	164
Figure 6.8 Apple scab symptoms on leaves and fruits in multispectral imagery acquired by handheld means from orchards around Lancaster, UK.....	165
Figure 6.9 Heatmap of confidence prediction of combined multispectral (RGB+NIR) imagery. 169	
Figure 6.10 Smoothed 3-day moving mean time series of the sum of manual classification scores (green) and confidence scores of all experimental and control samples in combined multispectral (RGB+NIR) imagery.....	169
Figure 6.11 Early detection of scab time series from RGB and NIR imagery in Experiment 1 and Experiment 2	171
Figure 9.1 Temperature within the Experimental Dome (Feb 2021- Jan 2022) captured by TinyTag Data Logger (Gemini Data Loggers, Chichester, UK)	210
Figure 9.2 Humidity within the Experimental Dome (Feb 2021- Jan 2022) captured by TinyTag Data Logger (Gemini Data Loggers, Chichester, UK)	210
Figure 9.3 Experiment 1 ‘Sample (S)’ time series 7-21 d.p.i. (Sample S17).....	231

Figure 9.4 Experiment 1 'Sample (S)' time series 22-35 d.p.i. (Sample S17)	232
Figure 9.5 Experiment 2 'Control (C) - large' time series 1-14 d.p.i. (Sample C07).....	233
Figure 9.6 Experiment 2 'Control (C) - large' time series 15-28 d.p.i. (Sample C07).....	234
Figure 9.7 Experiment 2 'Control (C) - large' time series 29-42 d.p.i. (Sample C07).....	235
Figure 9.8 Experiment 2 'Control (C) - large' time series 43-56 d.p.i. (Sample C07).....	236
Figure 9.9 Experiment 2 'Training (T) - large' time series 01-14 d.p.i. (Sample T23).....	237
Figure 9.10 Experiment 2 'Training (T) - large' time series 15-28 d.p.i. (Sample T23).....	238
Figure 9.11 Experiment 2 'Training (T) - large' time series 29-42 d.p.i. (Sample T23).....	239
Figure 9.12 Experiment 2 'Training (T) - large' time series 43-56 d.p.i. (Sample T23).....	240
Figure 9.13 Experiment 2 'Experimental (E) – medium' time series 01-14 d.p.i. (Sample E06)	241
Figure 9.14 Experiment 2 'Experimental (E) – medium' time series 15-28 d.p.i. (Sample E06)	242
Figure 9.15 Experiment 2 'Experimental (E) – medium' time series 29-42 d.p.i. (Sample E06)	243
Figure 9.16 Experiment 2 'Experimental (E) – medium' time series 43-56 d.p.i. (Sample E06)	244
Figure 9.17 Experiment 2 'Experimental (E) - small' time series 01-14 d.p.i. (Sample E09).....	245
Figure 9.18 Experiment 2 'Experimental (E) - small' time series 15-28 d.p.i. (Sample E09).....	246
Figure 9.19 Experiment 2 'Experimental (E) - small' time series 29-42 d.p.i. (Sample E09).....	247
Figure 9.20 Experiment 2 'Experimental (E) - small' time series 43-56 d.p.i. (Sample E09).....	248

List of Tables

Table 2.1 Remote sensors utilised in literature for the detection of apple diseases	52
Table 2.2 Key image analysis phases and techniques used in plant disease detection studies	53
Table 2.3 Previous studies utilising CNN models for apple disease classification (ALS – Alternaria Leaf Spot; AMV – Apple Mosaic Virus; AS – Apple Scab; BS -Brown Spot; CAR – Cedar-Apple Rust; FLS – Frogeye Leaf Spot; GS – Grey Spot; H – Healthy; MB – Marssonina Blotch; PM – Powdery Mildew)	56
Table 3.1 Low-cost camera specifications.....	78
Table 4.1 Composition of classes from the public and primary datasets of the 29,000 images used in the final ADID dataset	98
Table 4.2 The distribution of class labels for the training and testing datasets.....	99
Table 4.3 The hardware and software environment of the experiment.....	100
Table 4.4 CNN model training and testing metrics for the MobileNetV2 and EfficientNetV2L models. Training and testing accuracy and training loss were recorded after Epoch 20.....	103
Table 4.5 Performance metric scores for each of the six classes for the MobileNetV2 and EfficientNetV2L models.....	104
Table 4.6 Performance scores for the scab classifications in the multispectral imagery by the MobileNetV2 and EfficientNetV2L models.....	106
Table 4.7 Performance scores for the scab classifications in the RGB and NIR imagery by the MobileNetV2 and EfficientNetV2L models.....	108
Table 5.1 Quantity of each plant size across control and experimental samples	117
Table 5.2 Quantity of ‘HEALTHY’, ‘MILDEW’ and ‘SCAB’ label classes in the RGB and NIR imagery in the primary dataset.....	120
Table 5.3 Hardware configuration parameters.....	127
Table 5.4 Training and testing runtimes for MobileNetV2, InceptionNetV2 and EfficientNetV2Lmodels.....	128
Table 5.5 CNN prediction accuracies for each class in the test set from secondary (public) data sources.....	130
Table 5.6 Model prediction accuracy and recall for the ‘SCAB’ class for RGB and NIR imagery and the total count of ‘SCAB’ predictions (True Positives (TP) and False Negatives (FN))	132
Table 5.7 EfficientNetV2L prediction accuracy and recall for the ‘SCAB’ class for RGB and NIR imagery for each plant samples and the total count of ‘SCAB’ predictions (True Negative (TN), False Positives (FP), True Positives (TP) and False Negatives (FN))	133

Table 5.8 Cumulative EfficientNetV2L prediction accuracies and sensitivities for the 'SCAB' class for RGB and NIR imagery and the total count 'SCAB' predictions (True Positives (TP) and False Negatives (FN))	135
Table 5.9 Model prediction accuracies and recall scores for the 'SCAB' class for cropped RGB and NIR imagery. The total count of 'SCAB' labels True Positives (TP) and False Negatives (FN) are also displayed.	136
Table 6.1 Average monthly temperatures over 2021 recorded at Hazelrigg Field Station (Outdoor) and SolarDome (Indoor)	153
Table 6.2 Mills' infection period table showing temperature and hours of leaf wetness required for scab germination. (Adapted from Stensvand et al., 1997)	155
Table 6.3 Impact of threshold value on classification performance of Chapter 5 dataset	168
Table 6.4 The earliest detection dates of each positively tested plant sample in Experiment 1 and Experiment 2. The overall earliest date of detection is highlighted in yellow	171
Table 9.1 Weather conditions regarded at 10AM from Hazelrigg Field Station (UK Meteorological Office - Climatological Station Number 7236) during Experiment 1 – Round 1.....	211
Table 9.2 Weather conditions regarded at 10AM from Hazelrigg Field Station (UK Meteorological Office - Climatological Station Number 7236) during Experiment 1 – Round 2.....	212
Table 9.3 Weather conditions regarded at 10AM from Hazelrigg Field Station (UK Meteorological Office - Climatological Station Number 7236) during Experiment 2	213
Table 9.4 MobileNetV2 training metrics (Chapter 4)	224
Table 9.5 EfficientNetV2L training metrics (Chapter 4)	225
Table 9.6 MobileNetV2 training metrics (Chapter 5)	225
Table 9.7 InceptionResNetV2 training metrics (Chapter 5)	226
Table 9.8 EfficientNetV2 training metrics (Chapter 5)	226
Table 9.9 Classification results for the full ADID Dataset	227
Table 9.10 Classification results for the multispectral ADID subset.....	227
Table 9.11 Classification results for the validation data	227
Table 9.12 Classification results of fine-tuned CNN for multispectral imagery (whole-plant)....	227
Table 9.13 Classification results for multispectral imagery (localised)	228
Table 9.14 EfficientNetV2L classification results for Control samples	228
Table 9.15 EfficientNetV2L classification results for Experimental samples (whole-plant)	229
Table 9.16 EfficientNetV2L classification results for Experimental samples (localised).....	229

Introduction

1.1 Smart Farming and the Sustainable Intensification of Agriculture

Global food security is essential for an equitable society, although achieving this is a significant challenge amidst population growth and environmental decline. Conventional agricultural policies and practices have promoted cropland expansion, intensive irrigation and reliance on external inputs (chemical pesticides, inorganic fertilisers, and heavy machinery) as the primary means to increase yields (Pretty, 1995). These high-input, resource-intensive strategies are major sources of pollution and greenhouse gas emissions and lead causes of water scarcity, soil depletion, and biodiversity loss, which pose serious threats to agricultural yields (Gomiero, 2016; Lanz et al., 2018; Anderson et al., 2020; Rosa et al., 2020). The world must move towards a sustainable method of increasing agricultural production to ensure global food security without causing further environmental and ecological damage. Sustainable intensification is a system that increases crop yields without cultivating additional land or causing adverse environmental impacts (Pretty & Bharucha, 2014). The concept emphasises the efficient utilisation of resources to manage soils and nutrition, irrigation, and pest and disease management while reducing reliance on cropland expansion and chemical inputs (Pretty, 1997). Sustainable intensification offers an alternate approach to agriculture that can concurrently tackle crop production-based food security issues and environmental degradation.

Large-scale sustainable intensification methodologies rely upon the appropriate implementation of smart agricultural technologies. (Dicks et al., 2019). Smart farming, also known as Agriculture 4.0 or “the fourth agricultural revolution”, utilises modern innovations and developments in information and communication technologies to increase efficiencies in crop production and provide environmental and social benefits to growing regions (Rose & Chilvers, 2018). The increasing accessibility of emerging technologies, including robotics, the Internet of Things (IoT), Unmanned Aerial Vehicles (UAVs), cloud computing, wireless sensor networks, and Artificial Intelligence (AI), allows for decision-making and management tasks to be informed by real-time data (Wolfert et al., 2014; Javaid et al., 2022). Practical solutions have been utilised in agricultural operations to estimate evapotranspiration, soil moisture, and crop phenotyping, enabling automated irrigation and precise application of fertilisers and pesticides (Sishodia et al., 2020). As the global population increases, agricultural yields must also increase in order to maintain the availability of nutritious food. Smart farming is increasingly important in providing

solutions for sustaining productivity and adapting to environmental decline and climate change. Precision agriculture, the most prominent methodology used within smart farming, aims to improve production efficiency by applying information and technology to understand the spatiotemporal variability of agricultural production to inform targeted, site-specific crop management (Stafford, 2000; Auernhammer, 2001; Pierce & Nowak, 1999). Precision agriculture came to prominence at the turn of the millennium with the widespread introduction of Geographic Information Systems (GIS), Global Positioning Systems (GPS), remote sensing and other data generators into agricultural operations (Karunathilake et al., 2023). These technologies enable management strategies to consider variability in geography, soil properties, crop physiology, historical yield distributions, and the influence of external biotic and abiotic stresses (Zhang et al., 2002). Monitoring crop health and yield variability can inform decision-making to improve resource input efficiency and maximise yields, providing widespread economic and environmental benefits. Appropriate integration of Smart farming technologies and precision agriculture strategies into current agricultural practices can provide an essential route to the sustainable intensification of agriculture.

1.2 Precision Agriculture Strategies for Crop Disease Management

Plant pathogens pose a major threat to global food security. Crop diseases, borne of fungal, bacterial, and viral pathogens, reduce the quality and quantity of agricultural yields, exacerbating food supply deficits and threatening the financial viability of crop production (Strange & Scott, 2005; Ristaino et al., 2021). Intensive farming practices with high-density monocultures increase the risk of substantial losses caused by pathogens (Newton et al., 2009). Intensive protection measures are implemented to minimise crop losses by spraying high doses of pesticides (fungicides, bactericides, and insecticides) to prevent and control pests and diseases proliferating within the field and during storage (Oerke, 2006). With their abundant pesticide use, specifically fungicides, these disease management routines incur some of the highest economic costs and environmental impacts within agricultural production. The excessive use of these inputs has led to them contaminating the natural environment, destroying beneficial ecosystems, and leading to pests developing resistance to specific modes of action (Aktar et al., 2009; Sharma et al., 2019; Tudi et al., 2021). Furthermore, routine fungicide spray techniques are expensive, and significant disease-related crop losses still occur (Popp et al., 2013). Current crop protection strategies based on homogenous fungicide spraying are unsustainable. Alternative methods that reduce overall fungicide use while also minimising crop losses due to disease are essential to improve the environmental impacts associated with agriculture.

Precision agriculture strategies for crop disease management have the potential to improve sustainability within agricultural production and increase marketable yields (Mahlein et al., 2012; Balasundram et al., 2020). Precision crop protection can reduce the reliance on treating crops homogeneously and instead tackle plant pathogens through rapid, site-specific targeted treatment (Roberts et al., 2021). GIS has long been used to map the spatial heterogeneity of disease epidemics over their regions (Nelson et al., 1999) and provide an accessible platform for monitoring and forecasting crop disease with visual assessments and spatial analysis (Dong et al., 2019; Dong et al., 2020). Novel IoT-based monitoring systems and wireless technologies enable real-time monitoring and analysis of environmental and crop information, feeding into dynamic forecasting models or decision-making to determine infection risk more accurately and rapidly (Khattab et al., 2019). Precision pesticide applications through Variable-Rate Spray (VRS) systems are increasingly utilised in commercial growing environments. VRS technologies adjust agrochemical applications in real time depending on location, inoculum levels and canopy densities to address the specific needs of the area, improve spray deposition and minimise pesticide waste while maintaining high efficacy in control (Zhang et al., 2018; Manandhar et al., 2020).

Essential to all these precision technologies is detailed information on the temporal and spatial variability of crop health parameters within fields collected from remote sensors (Mulla et al., 2013). Remote sensing is a non-contact method of obtaining information by measuring electromagnetic energy reflected or radiated by a surface, which can then be analysed to determine information on crop health (Martinelli et al., 2015). Optical sensors are powerful tools that allow for rapid, automated, non-destructive measurements that can be used to diagnose disease in plants in real time under field conditions (Sankaran et al., 2010). Various remote sensing options exist for plant disease detection, including spectral, thermal and fluorescence imaging systems, each with unique benefits and limitations for different diseases and field conditions (Mahlein, 2012; Kuska et al., 2018). To be effective, remote disease detection systems need to be able to i) detect symptoms of the disease early, ii) identify the causal pathogen and differentiate it from other stress sources, and iii) quantify the severity of infection (Mahlein, 2016; Ray et al., 2017).

Optical sensors are sensitive to biological changes but do not measure plant parameters directly, so advanced data analysis methods rapidly interpret information for decision-making (Behmann et al., 2015). Supervised and unsupervised machine learning techniques have been utilised to enable the early detection and diagnosis of plant diseases without labour-intensive manual techniques. Deep learning techniques, notably Convolutional Neural Networks (CNNs), have

quickly become the most common method for plant disease diagnosis (Saleem et al., 2019; Hasan et al., 2020; Li et al., 2021). These CNN models can accurately and rapidly identify many diseases despite considerable symptom variance. Importantly, CNNs perform well on images captured in laboratory conditions as well as in natural, real-world settings, where weather, illumination and background conditions vary. Utilising deep learning classification models to diagnose diseases accurately and rapidly from images acquired by remote sensors means that new approaches to crop management are feasible at scale.

The adoption of precision technologies for crop disease detection and management has been slow. The high cost and uncertainty of using novel methods, along with the high risk and extreme consequences if they fail, can cause apprehension in adopting technologies. It is essential that these technologies are thoroughly researched and utilised correctly to maximise their potential. Precision crop protection, enabled by accurate, early detection and identification from remote sensors and machine learning algorithms, can inform targeted fungicide use. Judicious fungicide use can remove the need for unnecessary homogenous spraying, improving the efficiency and efficacy of crop disease treatment. Improving crop disease management efficiency can improve the sustainability of agricultural production while also increasing the quantity of agricultural yields.

1.3 The Impact of Apple Scab

Apples are among the most important horticultural crops due to their high economic and nutritional value. They are also one of the most produced fruits worldwide, with 95.84 million tonnes grown over an area of 4.86 million hectares (Food and Agriculture Organization of the United Nations, 2024). Apple orchards are subject to some of the most chemically intensive disease management regimes in agriculture (Simon et al., 2011). Commercial apple production involves typically high-density monoculture rows that maximise the productivity and profitability of orchards (Reig et al., 2019). The conditions created by these high-density orchards of susceptible cultivars are conducive to pest and disease epidemics, putting them at high risk of major crop losses (Peil et al., 2009; Lindell et al., 2023). These may occur from direct losses from fruit infection, which can cause lesions or rots in apples preharvest within orchards and postharvest in cold storage, or through indirect losses through reduced productivity of trees. Severe infections from foliar pathogens, such as powdery mildew, can stunt trees and produce lower-quality fruit (Holb, 2013). Extreme examples of destructive diseases, including European canker (Weber, 2014) and Fireblight (Khan et al., 2012), can even lead to the death of entire plants. Due to the numerous threats to their orchards, growers rely heavily on inorganic

pesticides to maintain their yields despite the economic and environmental impact of the chemicals. This chemical-intensive management is characteristic of apple orchards in all growing regions worldwide. The scale of apple production and the intensity of disease control applied across all growing regions has significant potential for sustainable intensification.

Apple scab is the most important disease facing global apple production because of the high susceptibility of most commercial varieties, its widespread presence, and the economic cost of required management techniques (MacHardy et al., 2001). Apple scab is caused by the ascomycete fungus *V. inaequalis*, which occurs in all commercial growing regions but has the most severe effects in countries with cool, moist springs and high summer rainfall (MacHardy, 1996; Bowen et al., 2011). Epidemics of apple scab rapidly spread throughout orchards, and poor disease management can result in the loss of an entire orchard. The major economic costs of the disease come from direct losses due to fruit infection developing within orchards and storage. Apple scab causes symptomatic olive-brown lesions to develop on the fruit; these lesions grow, darken, and coalesce, eventually developing a corky texture as the pathogen and apple flesh become necrotic (Belete & Boyraz, 2017). Apple fruits that display any symptom of apple scab are lost as they do not meet the market requirement for a high-quality, blemish-free product (Berrie & Xu, 2003). The primary infection cycle of *V. inaequalis* begins as the fungus overwinters as pseudothecia in leaf litter on the orchard floor. In spring, rainfall and sunlight promote the release of ascospores, which are wind-dispersed long distances throughout the orchard and germinate on young leaf tissue. Infected leaves develop characteristic lesions comprised of a dense layer of fungal conidia. As the infection matures, these conidia penetrate through the leaf cuticle and are splash-dispersed over short distances to infect surrounding plant tissue and fruits. (Oerke & Steiner, 2024). This secondary infection cycle repeats throughout the growing season, increasing the severity of orchard epidemics.

Due to the polycyclic nature of the pathogen, the repeated and intensive application of fungicides remains the primary method of controlling scab (Koller et al., 2005; Chatzidimopoulos et al., 2020). Orchards in the UK receive an average of 13 fungicidal sprays for apple scab control per growing season at 7–14-day intervals (Berrie & Xu, 2003; Mace et al., 2019; Ridley et al., 2024). The abundant use of fungicides significantly increases production costs, and concerns over the impact on human health and the agroecosystem mean alternate methods to optimise fungicide use are being sought. Improving the fungicide-use efficiency of apple scab management could reduce the environmental impact of disease control and the losses of this major horticultural crop.

Integrated Pest and Disease Management (IPM) is considered the best practice for controlling *V. inaequalis* and other pathogens and pests in orchards. IPM is a practical and environmentally sensitive approach that relies on a combination of sanitation and treatment through cultural and biological controls, supported by tactical chemical use, to manage pests and diseases in orchards. Comprehensive knowledge of the pathogens and their interactions with host plants is the basis of IPM strategies. Treatment decisions are made to prevent diseases from exceeding an economic damage threshold using the most economical and environmentally friendly means. (MacHardy, 2000; Beckerman et al., 2013).

Numerous non-chemical IPM options are available for treating apple scab. Orchard sanitation measures can include pruning trees to improve air circulation or by removing overwintering inoculum on the orchard floor. Sanitation provides an alternative solution to fungicide use but is laborious and may often result in higher scab incidence and lower yields if used in place of chemical treatment (Antal et al., 2023). Scab-resistant apple varieties are another option for managing apple scab using fewer fungicides, with several cultivars containing specific scab-resistant genes currently grown in commercial orchards (Belfante et al., 2004; Papp et al., 2016; Patocchi et al., 2020). Consumer and company preferences regarding taste, aesthetics, and shelf life drive commercial apple production; breeding resistant varieties is an extremely long and arduous process to identify which plants carry these valuable traits (Petkovsek et al., 2007; Papp et al., 2020). Developing resistant crops only offers a partial solution to intensive fungicide use in the long term.

Efficient fungicide application is currently the best defence against apple scab. Orchards that received no fungicide applications had higher scab severities and lower fruit quality than both conventional management and IPM with tactical fungicide use (Holb et al., 2017). Disease forecasting is another key method used in IPM strategies to optimise fungicide use based on weather-related risks and historical and current inoculum levels. ADEM (Apple Disease East Malling) and RIMpro are computer programs that provide warnings on a range of diseases, including apple scab, powdery mildew, European canker, and fireblight infection. These programs use information on weather variables: rainfall, surface wetness duration, ambient temperature, and ambient relative humidity to generate warnings. Scab forecasting models have been successfully deployed to inform reductions in fungicide applications, but there is evidence to suggest that this approach has led to increased incidences of scab infection in orchards (Berrie & Xu, 2003; Garofalo et al., 2018).

All IPM strategies rely on accurate information on disease incidence, location, severity, and phenological stages to inform cultural control or fungicide use (Whalon & Croft, 1984; MacDonald & Glynn, 1994; Cirjak et al., 2022). Visual assessments made through crop scouting are the most common techniques of orchard health monitoring (Ray et al., 2017). Crop scouting is performed primarily by agronomists, crop consultants, and other field specialists (Thapa et al., 2020). Scouts must have extensive knowledge and training before becoming effective at orchard disease diagnostics. As a result, only a limited number of experienced scouts are available, and so most are required to cover many orchards in a region within a narrow time-frame. Scouts establish a random sampling system throughout an orchard to avoid assessing every tree, which can inadvertently lead to missed disease symptoms. Scouts evaluate risk and scout based on specific susceptible cultivars, specific regions of orchards, or known presence of the disease in the region or previous seasons. These scouts also provide growers and clients with further treatment recommendations (spray schedule, pesticide use, and cultural control). Crop scouting is an essential resource for growers. However, it is time-consuming, expensive, and prone to errors from sampling biases and missing latent infections (Bock et al., 2010). While crop scouting provides growers with vital information on orchard health and treatment recommendations, these are often ancillary to the homogenous, repeated protective spraying of trees over the growing season.

The lower input costs associated with reduced fungicide applications are often offset by the high cost of consultants, scouting, weather-monitoring equipment, sanitation equipment, hardware, and software programs that are required for IPM. Furthermore, there is concern that current IPM strategies have contributed to increased resistance due to the dependency on broad-spectrum fungicides. Inappropriate reduction in fungicide spraying has led to increasing incidence within orchards. Higher levels of overwintering inoculum can drive the selection and the evolution of fungicide resistance through simple stochastic processes (Beckermann, 2013). IPM implementation may suffer due to a lack of well-qualified IPM experts, and it is too difficult compared to conventional management (Parsa et al., 2014).

The labour-intensive demands of disease monitoring limit the practical use of the method without the use of state-of-the-art monitoring and information systems to aid decision-making (Barzman et al., 2015). Although our in-depth understanding of the epidemiology of apple scab has reduced fungicide usage, scab control in most apple-growing regions still depends on the significant input of agrochemicals. This will likely continue until effective and durable scab resistance is incorporated into new apple cultivars. (Bowen et al., 2011). Many growers operate a zero-tolerance for scab due to the risk to their harvests. As IPM strategies can increase infections

in commercial orchards, heavy fungicide use is still the most common control method worldwide (Damos et al., 2015). Apple scab management will rely on fungicide application in the future, and so tactical spraying, based on disease risk and presence is the most feasible way of improving the sustainability of disease control.

Precision agriculture technologies offer the potential to improve orchard health monitoring by acquiring objective information from imagery, acquired over wider areas, more regularly than crop scouts. Despite this, the successful deployment of remote sensing systems for disease detection in orchards has been limited. This can be attributed to previous research focusing on successful imaging in controlled laboratory conditions. Sensors must demonstrate their ability to detect apple scab early in the complex environments of orchards, where illumination and plant stress conditions are uncontrollable. Applying deep learning CNN models to this data can provide rapid, precise, and objective classifications of disease presence even under these heterogeneous conditions. The capabilities of both technologies must be demonstrated by reliably providing the rapid and accurate identification of apple scab at different phenological stages, under a range of illumination conditions, on complex apple plants. Early detection of apple scab can inform intelligent decision-making within orchards for effective cultural control measures and improving fungicide-use efficiency. Applying precision agricultural methodologies to improve apple scab management could reduce yield losses due to the disease while also reducing the environmental impact of control, making sustainable intensification of apple production feasible.

1.4 Thesis Overview

1.4.1 Thesis Aims and Objectives

The aim of this thesis is to develop an effective remote-sensing strategy for the early detection of apple scab. The intention is to provide an alternate solution to manual disease monitoring in apple orchards to enhance the decision-making process. Producing a feasible method is paramount, with the accurate detection of apple scab infections under real-world conditions being the major focus.

The thesis addresses this aim with the following objectives:

- 1) Identify potential precision agriculture technology strategies (sensors, models, and platforms) for the detection and diagnosis of apple disease (Chapter 2).
- 2) Perform a feasibility study of several low-cost sensors and their capabilities of detecting apple scab in real-world conditions (Chapter 3).
- 3) Examine the viability of deep learning CNNs for classifying early apple scab from a novel multispectral imagery time series (Chapter 4).
- 4) Provide a robust assessment of the performance of CNNs in classifying apple scab at progressing severities under natural illumination conditions from near-infrared and visible-band (Chapter 5).
- 5) Reflect on the experimental design and the use of high-resolution multispectral imagery for apple disease detection (Chapter 6).

1.4.2 Thesis Structure

The thesis is composed of seven chapters, some of which have been published, submitted, or intended to be submitted to peer-reviewed journals. The full list of references is provided at the end of the thesis. Supplementary material is provided in the appendices at the end of the thesis.

Chapter 2 – Remote Sensing Strategies for Disease Monitoring in Apple Orchards

This chapter reviews the use of current and prospective precision agriculture technologies to detect apple diseases. Examples of remote sensors, data analytics, and acquisition platforms are obtained from the literature and discussed. A critical evaluation of the advantages and disadvantages of the numerous potential solutions and provides recommendations for future research. Through the literature review, it was found that apple scab would provide the greatest potential for developing the technology, and that successful early detection had only been demonstrated in controlled laboratories, rather than uncontrolled orchard conditions

Chapter 3 – Feasibility of Detecting Apple Scab Infections using Low-Cost Sensors and Interpreting Radiation Interactions with Scab Lesions

This chapter investigates the use of three low-cost sensors for the early detection of apple scab. Multispectral, thermal, and 3D imaging sensors were used to acquire daily information on apple scab development on seedlings. The novel use of high-resolution multispectral imagery showed considerable potential. The interactions between near-infrared radiation and apple scab lesions were discussed for the first time.

Chapter 4 – Classifying Early Apple Scab Infections in Multispectral Imagery using Convolutional Neural Networks

This chapter utilises CNN models to provide automated classifications of scab infections from multispectral imagery. Multispectral imagery and publicly available data of 6 apple disease classes were used to train CNN models. The trained CNN models were then used to classify apple scab infection from the multispectral time series to determine if automated classification of early apple scab was feasible from multispectral imagery. This would demonstrate if there was an improvement in early detection compared to RGB imagery alone.

Chapter 5 – Monitoring Apple Scab Progression from Visible and Near-Infrared Time Series Imagery using Convolutional Neural Networks

This chapter further examines the performance of CNNs to classify apple scab on a larger variety of more complex plants. By utilising a larger sample selection, including a control set, more robust training can be performed and reliable assessments of model performance. This chapter explores methods of improving model performance and demonstrates the differences in classification capabilities under different illumination conditions, plant health and structure conditions and disease severity and phenological stages.

Chapter 6 – General Discussion

This chapter discusses the novel contributions made by this thesis, including the experimental design, technology development, multispectral imagery, and assessment measures. The strengths and weaknesses of each methodological stage are explored and used to offer suggestions for improving techniques. These are summarised to provide recommendations for further work to improve apple scab detection. Opportunities for future research and how these technologies may be implemented for the sustainable intensification of apple production are given.

Chapter 7 – Conclusions and Future Research

This chapter provides a summary of the findings from the research, discusses the use of high-resolution multispectral imaging, and combines with CNNs to detect diseases in orchards. This chapter concludes with suggestions for further research that can provide a route to practical use.

2 Remote Sensing Strategies for Disease Monitoring in Apple Orchards

2.1 Introduction

Apples (*Malus x domestica*) are among the most widely cultivated and valuable fruit crops in the world. The threat of plant pathogens and resulting disease epidemics significantly impacts the economic and environmental sustainability of apple production. Crop diseases lower fruit quality, reduce tree productivity and render yields unmarketable. Commercial, high-density orchards are particularly vulnerable to rapid-onset disease epidemics (Peil et al., 2009), which can lead to major economic losses both in the field (MacHardy, 1996) and postharvest (Ivić et al., 2013). Consequently, apple orchards receive some of the highest volumes of pesticides applied in agricultural production (Simon et al., 2011; Penvern et al., 2012; Mouron et al., 2012). A significant proportion of orchard production costs are devoted to pest and disease management (Taylor & Granatstein, 2013). Moreover, the intensive application of pesticides negatively impacts the orchard environment and ecosystem. Reducing pesticide use while minimising losses through informed, targeted control can improve farm economics by increasing yields and lowering input costs while simultaneously reducing the environmental impacts of global apple production. Enhancing disease management within orchards can thus facilitate the sustainable intensification of apple production.

Conventional disease control methods within orchards are intensive, involving repeated applications of large volumes of pesticides, primarily fungicides, for disease protection (MacHardy, 2000; Alaphilippe et al., 2013). The abundant usage of fungicides is inefficient and expensive. There are concerns over the contamination effects of these fungicides on terrestrial (Martínez-Toledo et al., 1998; Kumari et al., 2020) and aquatic environments (Mohr et al., 2023), as well as their impact on beneficial pollinators (Piechowicz et al., 2021) and human health for both farmers (Hines et al., 2008) and consumers (Lozowicka et al., 2016). Furthermore, the non-targeted application of fungicides in apple orchards has led to pathogens developing resistance to certain chemicals, further increasing the challenges of managing apple diseases (Beckerman et al., 2013; Cox, 2015; Heaven et al., 2023). Despite intensive spray regimes, growers still experience major crop losses due to disease each year, and large volumes of fungicides continue to be applied to commercial orchards each season (Figure 2.1)

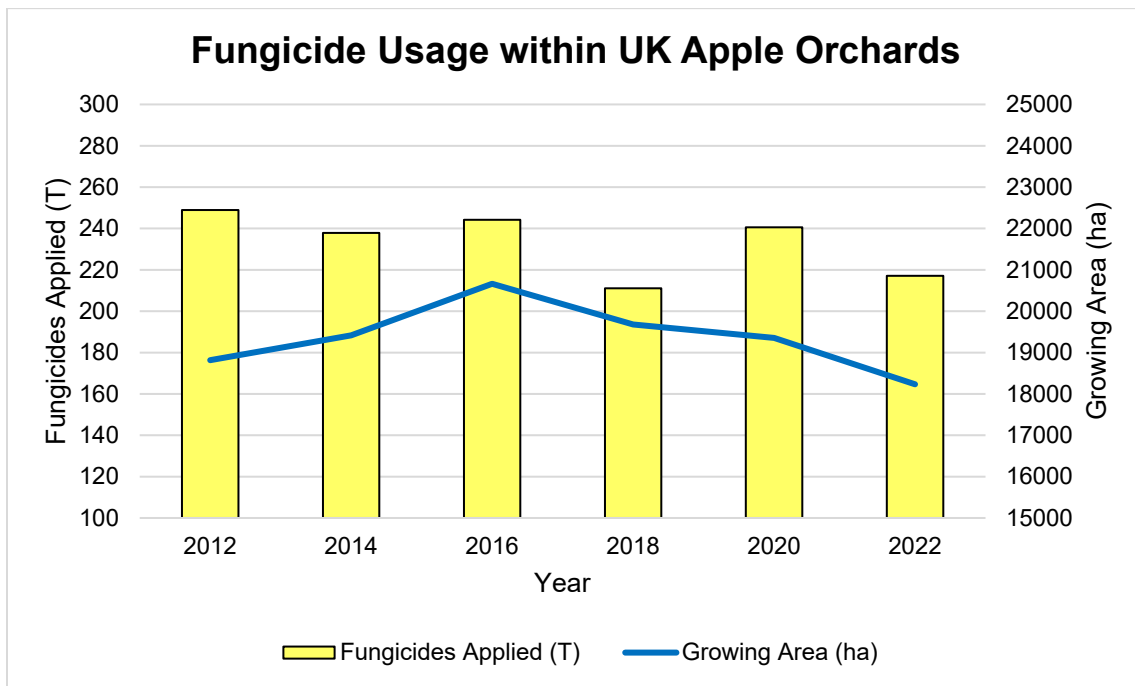


Figure 2.1 Changes in fungicide usage within the UK from 2012 – 2022 (adapted from Garthwaite et al., 2013; Garthwaite et al., 2015; Garthwaite et al., 2017; Mace et al., 2019; Ridley et al., 2022; Ridley et al., 2024).

Precision agriculture offers a potential solution for improving disease management routines within orchards. Precision methodologies aim to enhance agricultural production efficiency by collecting data on the spatial and temporal variability of crop factors, which can then inform targeted, site-specific crop management (Stafford, 2000; Auernhammer, 2001). Targeted pesticide applications help reduce the volume of chemicals used by minimising drift and applying pesticides only when necessary, maintaining adequate disease protection while achieving significant economic savings in management costs (Berk et al., 2020; Sedlar et al., 2013). Site-specific disease management based on disease incidence can provide more effective control than homogeneous spraying, reducing the volume of pesticides applied (Behmann et al., 2015; Mahlein et al., 2018; Chawade et al., 2019).

Remote sensors are essential to precision agriculture. They are powerful tools with the potential for objective, non-invasive disease detection and diagnosis through real-time measurements of plant parameters (Mulla, 2013). Remote sensors detect variability in the reflectance and emissivity of plants, which can be used to evaluate anatomical, physiological, and biochemical properties and identify stress caused by pests and diseases (Prabhakar et al., 2012). Remote sensing technologies can detect diseases early and map sites of infection, informing efficient and effective crop spraying, therefore reducing pesticide volume and disease control costs (Zanin et al., 2022). Despite the successful use of remote sensors for disease detection in arable crops, limited progress has been made in applying these technologies to disease detection in orchards (Jarolmasjed et al., 2019). Although developing a system to diagnose disease in orchards poses

significant challenges, there is substantial potential for improving pesticide efficiency in many orchards worldwide. This improvement would create widespread global economic and environmental benefits, as well as higher production yields (Delalieux et al., 2007).

An effective orchard disease monitoring system should be capable of performing three specific tasks: (i) Early Detection, (ii) Classification, and (iii) Quantification (Mahlein, 2016; Ray et al., 2017). Early detection has no clear definition but has been used synonymously with presymptomatic detection of latent infection (Bock et al., 2020). For precision agriculture purposes, early detection typically refers to identifying diseases in the initial stages of symptom development when severity is low (Chawade et al., 2019; Pallotino et al., 2019; Oerke, 2020). Early detection is critical for targeted pesticide application, as once symptoms develop, they can reduce plant productivity, damage fruits, and increase the risk of secondary infections (Chaerle & Van Der Straeten, 2000; Barbedo, 2019a). Classification, also referred to as identification, involves diagnosing diseases by separating biotic stress from abiotic causes and differentiating the causative pathogen from other potential sources of stress (Mahlein, 2016). Inaccurate disease assessments and false diagnoses can lead to incorrect management decisions, resulting in greater host plant damage and increased risk of disease spread (Thapa et al., 2020). Quantification of infection measures disease severity, indicating the extent of infection symptoms displayed on the measured plant area (Bock et al., 2010). Severity estimates are often provided on an ordinal scale, typically based on a percentage, although qualitative descriptions of symptom development may also be used (Chiang & Bock, 2022). Severity estimates are fundamental for establishing disease management thresholds, determining crop losses, evaluating treatment efficacy, and forecasting disease epidemics (Pethybridge & Nelson, 2015; Bock et al., 2020).

A remote sensing strategy that detects stress early, accurately identifies the causative pathogen and estimates severity can provide an invaluable asset for growers in making informed decisions on disease management (Delalieux et al., 2007). Early disease detection can further improve the efficiency of disease control by facilitating site-specific management strategies through targeted fungicide application or sanitation techniques to reduce disease spread and severity (Sankaran et al., 2010; Ray et al., 2017; Khaled et al., 2018). However, incorrect or delayed diagnosis can result in improper treatment, allowing diseases to proliferate. As many fungal pathogens produce similar symptoms, it is crucial to distinguish between different species through an appropriate disease detection process. Sensing systems for precision agricultural operations consist of three key components: remote sensors, classification methods, and acquisition platforms (Olsen & Anderson, 2021). Selecting the appropriate technology for each component is

essential for the early detection of diseases in apple plants. Furthermore, these systems must be capable of operating effectively under the complex conditions experienced within commercial orchards.

A wealth of high-impact literature provides comprehensive reviews of utilising precision agriculture technologies for plant disease monitoring (Li et al., 2014; Mahlein, 2016; Chawade et al., 2019; Zhang et al., 2019; Pallotino et al., 2019; Oerke et al., 2020; Buja et al., 2021). Despite the prevalence of early detection and classification studies for apple diseases, there has yet to be a thorough review of these technologies within the context of orchard operations. Therefore, this is the first review to focus on each of the three components of a remote sensing strategy exclusively for apple disease monitoring. The aim of this work is to identify optimal technologies that could be applied for orchard monitoring and opportunities for further research and future implementation. First, the report will discuss the numerous diseases that affect apple production and current practices for monitoring these diseases. Second, it will review the potential of remote sensors to detect early stages of apple diseases, specifically RGB, multispectral, hyperspectral, thermal, fluorescence, and 3D imaging sensors. Third, methods of classifying images will be reviewed to facilitate rapid and accurate identification of plant pathogens. Fourth, acquisition platforms that provide the spatial coverage necessary for orchard monitoring will be assessed. Fifth and final, all the information will be synthesised to discuss the potential and practicalities of a remote sensing system for disease detection within apple orchards and to provide recommendations for further research.

2.2 Disease Monitoring in Apple Orchards

2.2.1 Taxonomy of Apple Diseases

Apple orchards are host to over 70 different infectious diseases that can impact yields through rots, decays, blights, lesions, and cankers (Belete & Boyraz, 2017). High-density orchards provide a hospitable environment for pathogens to overwinter and spread rapidly under ideal conditions. Crop pruning and thinning techniques offer many potential sites for infection (Simon et al., 2011). Additionally, high-density orchards of susceptible monocultures create a conducive environment for pathogen proliferation (Peil et al., 2009; Lindell et al., 2023). Climate change can further exacerbate disease risk by introducing favourable conditions earlier in the season, increasing the number of infection periods, especially in temperate regions (Gautam et al., 2013; Garrett et al., 2021). Fungi are by far the most common and diverse group of pathogens affecting

agricultural production, with their spores spreading easily throughout the growing environment, causing crop losses and reducing plant productivity (Fisher et al., 2012). However, many other sources of stress are present within apple orchards (Figure 2.2).

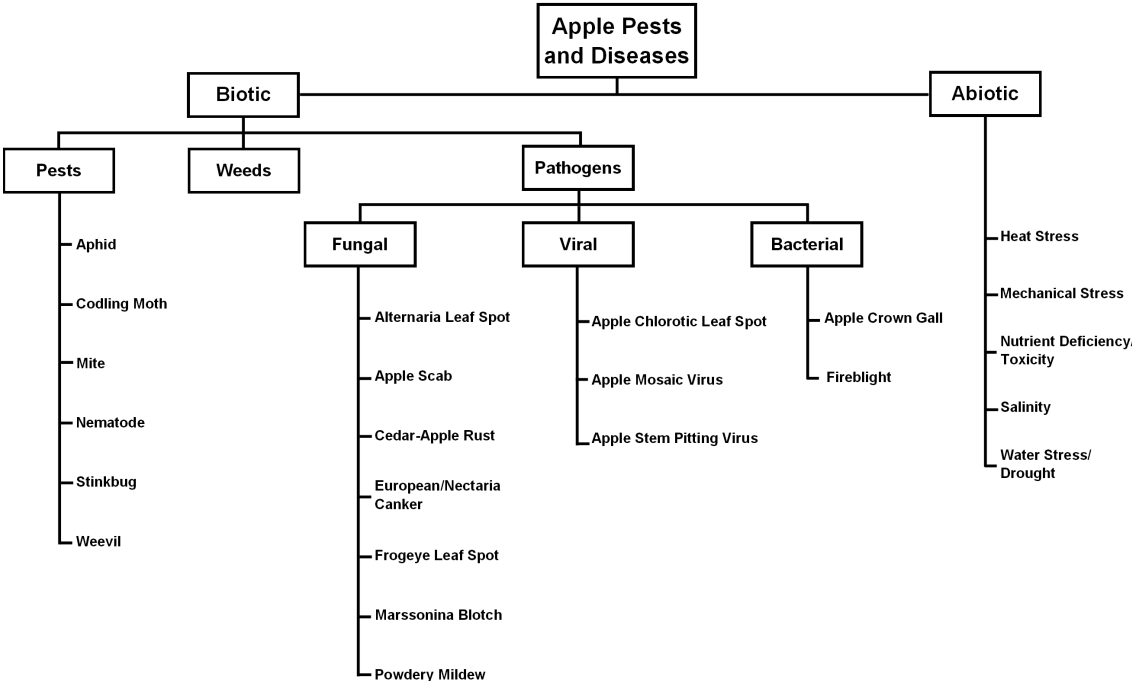


Figure 2.2 Common biotic and abiotic stresses monitored in apple orchards

Plants under stress develop symptoms on their organs that can reduce tree productivity, render fruit unmarketable, and act as sources for secondary infections. There are generally four types of visible disease symptoms used to detect and diagnose diseases: (i) reduction in biomass, (ii) change in pigment concentrations, (iii) presence of pathogens (such as pustules, lesions, mycelium, and ooze), and (iv) wilts (Zhang et al., 2019). The appearance, incidence, and severity of disease symptoms are influenced by climatic conditions, the quantity of inoculum present in the environment, susceptibility, host vigour and physiological development stage, and the presence of multiple stress factors. Moreover, several stresses can result in similar symptoms, further increasing the complexity of quick and accurate diagnosis (Barbedo et al., 2016). While plant diseases can manifest in fruits, shoots, blossoms, and other plant regions, foliage is the most common organ of interest. The leaves of stressed plants undergo non-visible physiological changes, affecting their photosynthetic capabilities, internal chemical and structural composition, as well as leaf water content and transpiration rates (Berger et al., 2007). These changes are often the first indicators of plant disease and can be treated before infections become severely destructive to yields.

According to MacHardy (2000), three major diseases threaten apple production: apple scab, powdery mildew, and fireblight (Figure 2.3). However, many other apple diseases also significantly impact orchards across the world. The following sections provide a brief description of key apple diseases that have received considerable research attention for disease detection and management.

2.2.1.1 *Apple Scab (Venturia inaequalis)*

Apple scab is widely considered the most economically impactful disease affecting apples worldwide (MacHardy, 1996), with most commercial cultivars being susceptible (Holb, 2007). Apple scab, caused by the hemibiotrophic fungus *Venturia inaequalis*, significantly impacts apple production yields through infectious lesions that develop on fruit in orchards and storage, rendering them unmarketable (Bowen et al., 2011). Infections can be easily identified on leaves, shoots, blossoms, pedicels, petioles, and fruits. Heavy scab infection can debilitate trees through defoliation, reduced formation of leaf buds and fruits, and increased susceptibility to injury (Belete & Boyraz, 2017). Apple scab is characterised by distinctive olive-brown lesions with a velvety texture developing on the leaves and fruits. Severe infection of leaves results in dwarfing, necrotic tissues, and senescence, whereas severe fruit infections cause deformations, cork-textured lesions, and early drops (Crassweller et al., 2020). The symptoms of apple scab are highly variable due to the ontogenic resistance of certain genotypes or phenological stages (Gessler et al., 2006).

2.2.1.2 *Powdery Mildew (Podosphaera leucotricha)*

Powdery mildew, caused by the obligate biotrophic fungus *Podosphaera leucotricha*, is endemic to all apple production regions worldwide (Strickland et al., 2021). Infected plants experience reduced photosynthesis and transpiration, resulting in low carbohydrate assimilation and reduced growth (Ellis et al., 1981). Most yield losses occur through infection of flower buds, reducing fruit set and overall plant vitality, with direct infection of fruits being rare (Urbanietz & Dunemann, 2005). Characteristic symptoms of powdery mildew include leaves and blossoms covered with a white, powdery mycelium coating, ultimately causing leaf deformation and reduced shoot size in the later stages (Crassweller et al., 2020).

2.2.1.3 Fireblight (*Erwinia amylovora*)

Fireblight is among the most devastating diseases facing apple production. It is a necrotic disease caused by the bacterial pathogen *Erwinia amylovora*, which causes infected blossoms, foliage, and fruits to appear water-soaked before turning black, giving them a scorched appearance (Steinberger & Beer, 1988; Oh & Beer, 2005). The inoculum source is a bacterial ooze that exudes from infected tissue as droplets (Zeng et al., 2020). The most destructive effects of the pathogen are the formation of cankers that girdle the trunk, branches, and rootstock, which can rapidly lead to the death of a tree (Aćimović et al., 2023).

2.2.1.4 Marssonina Blotch (*Marssonina coronaria*)

Marssonina blotch, also known as apple blotch, is a serious disease affecting apple orchards worldwide caused by the fungus *Marssonina coronaria* (Lee et al., 2011). Severe leaf infection causes premature defoliation, which weakens the physiological balance of the host, resulting in long-term reduced tree vigour and decreased yields (Wöhner & Emeriewen, 2018). The disease first appears as dark green circular patches on the upper surface of mature leaves in mid-summer. As the disease progresses, the leaf spots coalesce, black fruiting bodies develop on the affected surfaces, and the surrounding tissue becomes chlorotic (Crassweller et al., 2020).

2.2.1.5 European Canker (*Neonectria ditissima*)

European canker is a destructive disease caused by the fungus *Neonectria ditissima* that has a major impact in Northern Europe (Garkava-Gustavsson, 2013). European canker affects yields by reducing tree vigour through the deterioration of tree architecture and branching (Delgado et al., 2022). Infections are observed as cankers on trunks and branches, which become girdled, leading to the death of all tissue distal to the infection site and, in severe cases, the entire tree (Weber & Børve, 2021). Furthermore, the pathogen also causes direct yield losses in fruit through storage rots (Weber, 2014). *N. ditissima* is identifiable by characteristic red pustules developing within cankers (Weber & Børve, 2021).

2.2.1.6 Frogeye Leaf Spot and Black Rot (*Botryosphaeria obtusa*)

The saprophytic fungus *Botryosphaeria obtusa* causes frogeye leaf spot on leaves and black rot on fruit (Phillips et al., 2007). Frogeye leaf spot is a significant disease in North America, with most losses occurring through fruit rot and limb cankers (Biggs, 2004). The initial symptoms of frogeye leaf spot are small purple circles appearing on leaves, which enlarge and turn brown in

the centre. Black rot appears at the calyx of the fruit, developing into a rotting area that increases as a series of concentric bands, with decayed flesh remaining firm and leathery (Crassweller et al., 2020).

2.2.1.7 Cedar-Apple Rust (*Gymnosporangium juniperi-virginianae*)

Cedar-apple rust is a major demicyclic rust disease in North America, caused by the fungal pathogen *Gymnosporangium juniperi-virginianae*. Red cedar (*Juniperus virginiana*) and apple are alternate hosts of the pathogen (Aldwinckle et al 1977; Chen & Korban, 1987). Cedar-apple rust initially presents as small, yellow spots on the leaf surfaces that enlarge, changing colour to orange-red, with small black fruiting bodies becoming visible. Severe infections cause tree defoliation, reduced fruit size and quality, or deformation (Crassweller et al., 2020).

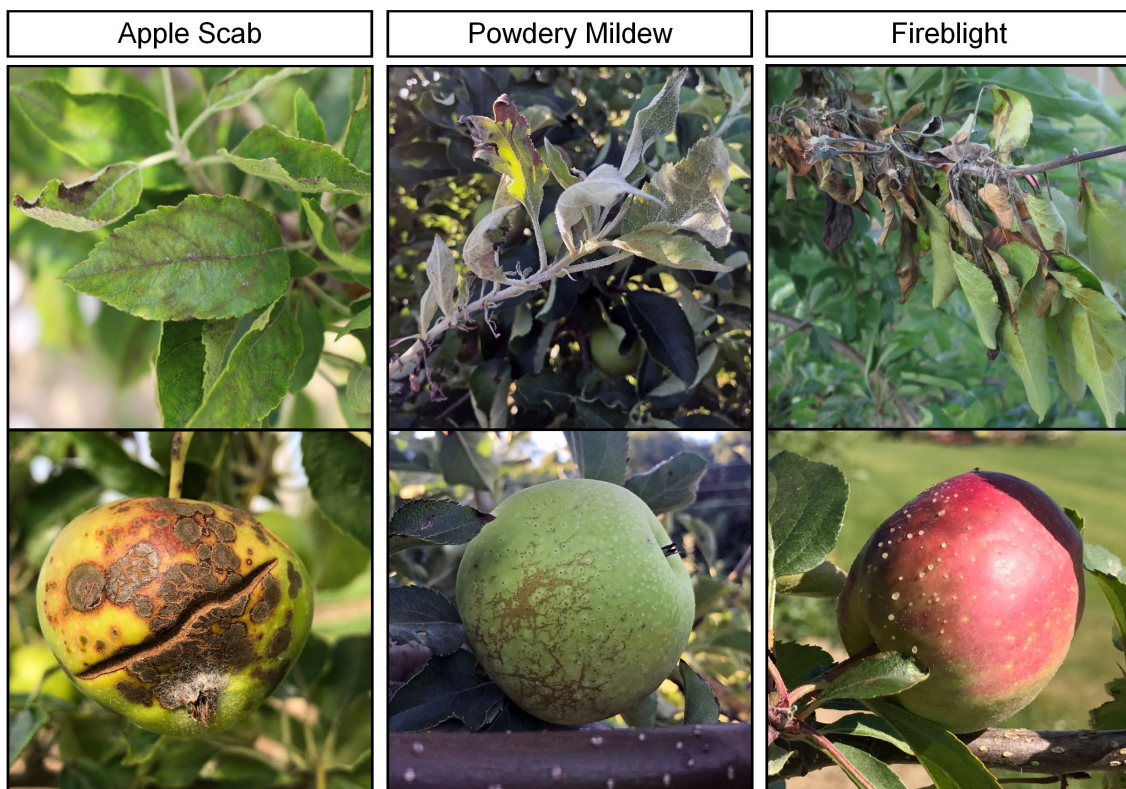


Figure 2.3 Severe foliar and fruit symptoms of apple scab, powdery mildew and fireblight (adapted from Ayer et al., 2020; Strickland et al., 2020; Wallis et al., 2020)

2.2.2 Conventional Methods of Disease Monitoring

Integrated Pest and Disease Management (IPM) combines monitoring, cultural and biological management, and tactical pesticide use (Jacobsen, 1997). IPM offers significant economic benefits by reducing overall pesticide costs and potentially increasing yields through healthier

crops. Additionally, IPM provides environmental benefits by reducing pesticide runoff, thus minimizing its impact on non-target species and contributing to biodiversity conservation (Tudi et al., 2021). Despite being considered the best practice for disease protection in orchards, the labour-intensive demands of disease monitoring limit the practical use of IPM in most commercial orchards (MacHardy, 2000). The most common technique for disease monitoring involves visual assessment by crop scouts (Ray et al., 2017). Crop scouting is low-throughput and expensive, and the lack of experienced individuals able to perform these tasks means full coverage and regular monitoring are limited. Although detailed guidelines for characteristic pathogen symptoms and assessment standards have improved accuracy and reliability, the technique remains subjective and may lead to biased assessments (Bock et al., 2020). Furthermore, it is difficult to detect the early stages of the disease through visual assessment, especially in their latent, presymptomatic stages (Bock et al., 2010). Advanced disease assessments can be achieved through serological, molecular, and biomarker-based methods, which can provide objective, accurate assessments of disease in crops, even in presymptomatic stages. However, these advanced methods are laborious, destructive, and require specialised equipment and elaborate preparation procedures that are not feasible for real-time, on-site diagnosis (Sankaran et al., 2010; Fang et al., 2015; Martinelli, 2015). Current disease monitoring methods can be improved by enabling widespread coverage and rapid early detection of diseases within orchards. There is an urgent need for disease detection, classification, and monitoring techniques to provide rapid, objective assessments of epidemics with appropriate coverage (Mahlein, 2016).

2.3 Remote Sensors for Disease Detection

2.3.1 Leaf Optical Properties

Remote sensors are powerful, cost-effective methods for rapid, large-scale, non-invasive assessments for plant disease detection in agriculture. Remote sensing for plant pathology uses non-contact measurements of electromagnetic radiation (Figure 2.4) interactions with plant and pathogenic material (Mulla, 2013). Leaf optical properties are characterised by reflectance, transmittance, absorbance, and emission of electromagnetic radiation, which are determined by biochemistry and physiology (Jacquemoud & Ustin, 2001). Plant pathogens may be directly present or cause significant changes to leaf structure and morphology, transpiration, and pigment concentrations, all of which can be detected by remote sensing systems. There is a suite

of remote sensing systems available, each capable of detecting disease symptoms based on certain influences symptoms have on foliar biochemistry and physiology (Zhang et al., 2019a).

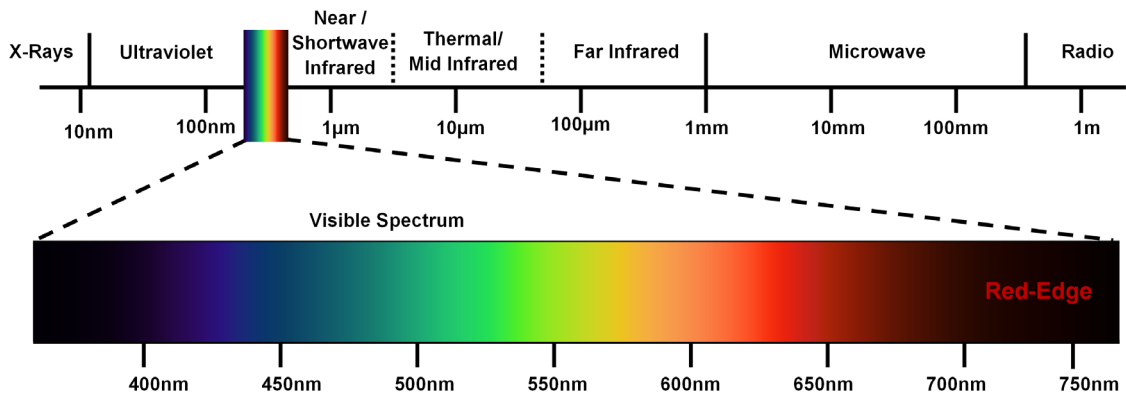


Figure 2.4 The electromagnetic spectrum (excluding Gamma Rays)

Leaf reflectance characteristics are valuable for diagnosing tree health and detecting disease presence. Plant pathogens affect the photosynthetic process and damage plant tissue cell structure, thereby modifying the interaction between vegetation and electromagnetic radiation (Bock et al., 2020). These impacts manifest as changes in leaf and canopy reflectance due to alterations in pigmentation, water content, cellular structure degradation, and hypersensitive reactions (Mahlein et al., 2018). Reflectance of vegetation is typically observed in three distinct spectral domains: visible (VIS, 400 to 700 nm), near-infrared (NIR, 700 to 1100 nm), and short-wave infrared (SWIR, 1100 to 2500 nm) (Prabhakar et al., 2012; Mahlein et al., 2012; Gogoi et al., 2018).

The visible domain is where the main light-absorbing pigments are chlorophylls (chlorophyll a and chlorophyll b), carotenoids, xanthophylls, and polyphenols (Jacquemoud & Baret, 1990). Healthy leaves are green due to the high absorption in blue and red wavelengths by chlorophyll in palisade cells (Gitelson et al., 2003). However, during senescence, as chlorophyll levels decline, increasing reflectance in red and blue bands causes yellow-brown colours to develop in visible images (Blackburn, 1998b; Mulla et al., 2013). Beyond the visible domain, more information regarding leaf physiology can be used to determine health and identify potential signs of stress. The red edge is a key region observed in plant health monitoring. The red edge is a spectral phenomenon for chlorophyll-producing plants, defined as a significant increase in reflectance at 700 nm at the border between red and NIR (Bock et al., 2010). Stressed leaves exhibit a downward shift in this rapid rise in reflectance toward the red region of the spectrum, known as a blue shift of the red edge (Horler et al., 1983). In the NIR domain, absorption within leaves is low, and reflectance and transmittance reach their maximum values due to internal scattering at

the air-cell-water interactions within the leaves, providing information on leaf and cell structure (Jacquemoud & Ustin, 2001; Slaton et al., 2001). In the shortwave infrared domain, water absorption bands are found, allowing reflectance in this region to estimate leaf water content (Ceccato et al., 2001; Jacquemoud & Ustin, 2001). Beyond the shortwave infrared lies the thermal infrared domain (TIR: 6.0 - 14.0 μm). Thermal infrared measures radiation emitted from surfaces, enabling the characterisation of plant tissue health based on changes in the transpiration rate and water content, which may indicate stress (Ishimwe et al., 2014; Khanal et al., 2017).

The following section provides an in-depth review of various sensor technologies that have potential applications in the early detection of apple diseases. These technologies include visible-band RGB sensors, multispectral sensors, hyperspectral sensors, fluorescence imaging, thermal imaging, and 3D imaging sensors. Each sensor type offers unique capabilities for identifying disease symptoms at different stages. This review will discuss the principles behind each technology, the specific disease indicators they can detect, examples of their use in detecting apple diseases, and their strengths and limitations.

2.3.2 Colour Cameras (RGB Imaging)

Colour cameras, produce visible-spectrum imagery and are the most common instruments used in agriculture for sensing plant parameters (Olsen & Anderson, 2021). Most colour cameras use silicon-based charge-coupled device (CCD) or, more commonly, complementary metal-oxide semiconductor (CMOS) sensors with arrays of three colour photosensors (red, green, and blue) to obtain reflectance values, which are used to estimate the true colour of each pixel in the visible domain. RGB imagery extracts colour components of hue, saturation, and intensity (Pallotino et al., 2019). This imagery can identify colour, texture, and shape parameters to aid diagnosis based on specific features of disease symptoms, including biomass variation, wilts, and pathogen bodies (Bock et al., 2010; Behmann et al., 2015). Assessments from RGB imagery are objective, accurate, and reliable, equivalent to those obtained by visual estimation. However, unlike manual inspection from in-field crop scouting, assessments from RGB imagery can have higher throughput and be less prone to subjective errors, making them useful in quantifying disease severity (Bock et al., 2020).

Due to their similarity to visual assessments, there are few studies that directly assess the use of RGB imagery for the early detection of diseases in apple orchards. However, RGB imagery has

been effectively used to quantify the severity of fireblight infections by measuring shoot senescence. The reflectance intensity for each of the three individual bands was calculated to measure the senescence on blighted shoots, determining the proportion of healthy green tissue to infected tissue to identify and quantify infection severity (Jarolmasjed et al., 2019). Chandel (2021) found that high-resolution RGB imagery was sufficiently capable of detecting and mapping powdery mildew from an unmanned aerial vehicle (UAV) platform in apple orchards. Histograms in the blue channel showed an ability to distinguish and segment powdery mildew-infected leaves from healthy leaves and other background objects, enabling high classification accuracy (Chandel et al., 2020). These RGB methods have been applied to apple diseases that significantly influence canopy reflectance, with considerable distinctions between healthy and infected tissue colour. However, they may prove less effective when symptoms are much smaller, and there is limited contrast between healthy and infected tissue, such as with the olive-green lesions of symptomatic apple scab.

Despite the lack of disease detection capability studies in orchards, RGB imagery is extensively used for training and testing deep learning convolutional neural network (CNN) models. These studies utilise the imagery of various plant diseases acquired in controlled laboratory and real-world environments. RGB imagery containing apple diseases is available in public datasets such as PlantVillage (Hughes & Salathe, 2015) and PlantPathology (Thapa et al., 2020), with the latter featuring imagery acquired under varying illumination conditions, leaf angles, and symptom variance (Figure 2.5). Unlike the orchard studies by Jarolmasjed et al. (2019) and Chandel et al. (2021), these images are localised on single leaves containing known late-stage symptoms. They are captured using handheld devices in the absence of strict acquisition protocols, which make scaling up coverage for full orchard monitoring difficult. This image acquisition step is important, and it is recommended that standardised imaging procedures be adopted to maintain uniform focus, sharpness, and illumination, as well as to control the angle and distance between the sensor and plant to avoid biases in classification (Mahlein, 2016). The camera and hardware settings play a major role in ensuring suitable image quality for assessment. Having appropriate camera sensors and lenses, along with optimal exposure settings (aperture, shutter speed, ISO levels), is essential to provide clear imagery for detecting diseases (O’Conner et al., 2017).

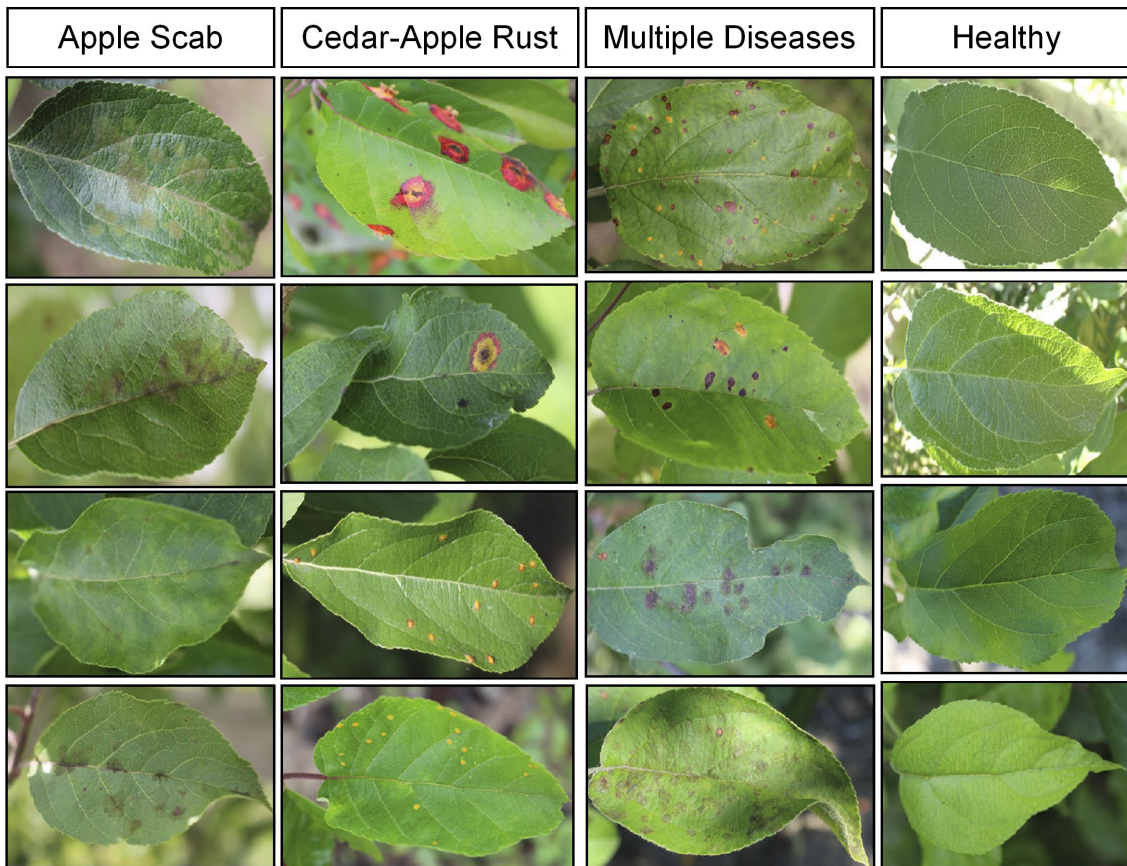


Figure 2.5 RGB imagery displaying the symptom variance of late-stage apple diseases (adapted from Thapa et al., 2020)

RGB imagery is an objective way to diagnose diseases from symptoms and quantify severity, but its major limitation is the inability to detect diseases pre-symptomatically, potentially limiting its use as a standalone sensor for disease management. However, RGB imaging has several key benefits over other sensing methods. Colour cameras are generally low-cost, easily accessible, and highly suited to field studies due to their lightweight, robust design, high-quality light sensitivity, and acquisition rates. Furthermore, the resolution of these commercial cameras is significantly better than that of other sensing methods discussed in remote sensing of plants, enabling the detection of plant disease symptoms at small scales. RGB imagery is a well-established method for quantifying severity and diagnosing late-stage diseases. It is currently used as a tool for aiding crop scouting, developing assessment aids, and analysing pathogen effects over time and across species (Bock et al., 2010). The accessibility and simplicity of colour cameras for growers mean they will likely continue to play a vital role in disease assessments of orchards well into the future.

2.3.3 Hyperspectral Sensing

Hyperspectral imaging is a powerful sensing tool for the presymptomatic detection of plant diseases, providing detailed information on the spatial and spectral variability of an object. Hyperspectral imaging offers increased continuity, range, and resolution of spectral reflectance measurements over colour cameras and multispectral imagers. These sensors measure the reflectance of an object in narrow wavebands (~10 nm) over a wide spectral range (350-2500 nm), effectively acting as a fingerprint to characterise the composition of each pixel (Mulla, 2013). In hyperspectral imaging, hundreds of these narrowband images are captured, providing both spatial and spectral data of a target subject, which are combined into a three-dimensional block of data known as a hypercube (Figure 2.6). This hypercube enables the visualisation of the biochemical and structural composition of the imaged sample (Gowen et al., 2007). The interactions between pathogens and plants induce changes in leaf physiology and biochemistry as complex processes govern the appearance and progression of disease symptoms. During pathogenesis, these interactions cause variations in reflectance by altering the physiological and biochemical states of the plant. Each host-pathogen interaction exhibits unique spatial and temporal dynamics, affecting reflectance at different wavelength ranges through various stages of the disease (Mahlein et al., 2018). Hyperspectral imagery can be used to sense crop characteristics such as water content and transpiration, chlorophyll, carotenoids, cellulose, cellular structure, leaf area index, and crop biomass (Mulla, 2013). Hyperspectral imaging captures subtle variations in these parameters, making it a valuable tool for early disease detection and detailed plant health analysis.

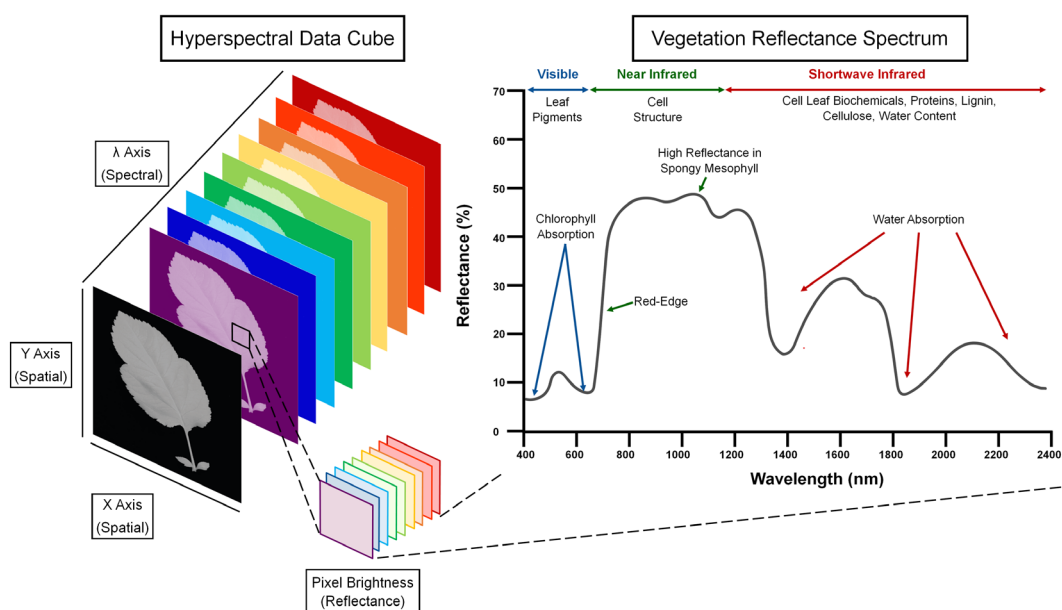


Figure 2.6 Simplified diagram of a hyperspectral imaging hypercube and vegetation reflectance spectrum

The high spectral resolution and sensitivity of hyperspectral data allow for the monitoring of subtle changes in reflectance patterns indicative of early stress symptoms. However, the entire spectrum is not always necessary, and spectral bands can be highly correlated, leading to redundancy in information (Delalieux et al., 2009a; Mahlein et al., 2012). Single wavebands are good indicators of biochemical features but are subject to variability from environmental factors and redundancy issues. Narrowband vegetation indices help reduce data dimensionality and enable more computationally efficient data processing and analysis (Kuska et al., 2018). Although many standardised narrowband indices are available, it is common to trial hyperspectral imagery in controlled settings to identify optimal wavebands and develop novel indices suited to specific diseases in different plants and phenological stages.

Non-imaging hyperspectral spectroscopy has successfully been used to detect apple scab disease at presymptomatic stages of infection (Delalieux et al., 2007). Narrow wavebands in the SWIR region between 1500-2250 nm, which are strongly associated with leaf water content, were found to be the most appropriate and applicable for detecting apple scab at early infection stages (Delalieux, 2009b). Specifically, reflectance at 1460 nm and 1940 nm showed effective discrimination potential for apple scab identification. These wavebands are the main water absorption bands, and a decreased spectral reflectance indicates an increase in leaf water content post-infection (Delalieux, 2009a). These results were validated in later hyperspectral imaging studies of early apple scab infections, displayed in Figure 2.7 (Nouri et al., 2018; Gorretta et al., 2019). Leaf phenology also plays an important role in leaf water content and reflectance at these stages, which could easily be misrepresented as early-stage scab infections (Delalieux et al., 2009a). At developed scab stages, vegetation indices such as R_{440}/R_{690} (where R_{440} indicates reflectance at 440 nm and R_{690} indicates reflectance at 690 nm) and R_{695}/R_{760} , as well as the chlorophyll a-related Pigment Specific Simple Ratio (PSSRa) R_{800}/R_{680} developed by Blackburn (1998a), exhibited superior distinction between non-infected and infected leaves (Delalieux et al., 2009b).

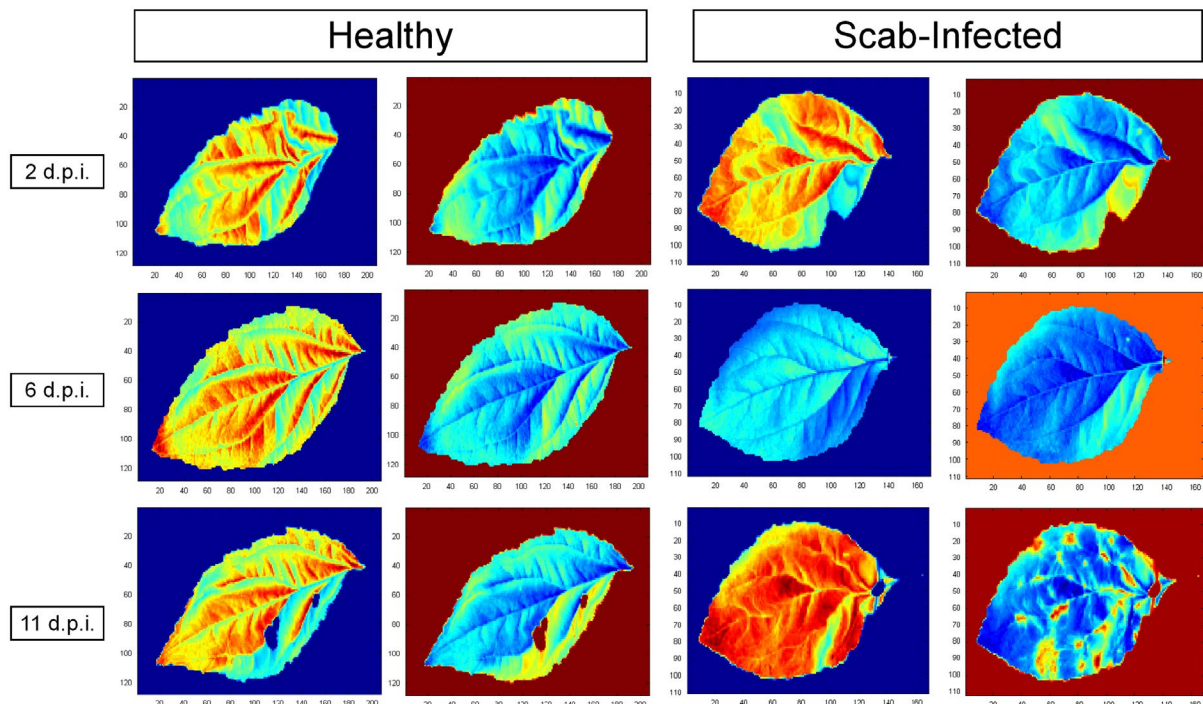


Figure 2.7 Hyperspectral imaging principal component analysis scores for healthy and apple scab- infected (adapted from Nouri et al., 2018)

Hyperspectral spectroscopy has also been extensively used to detect fireblight infection. Skoneczny et al. (2020) found that the indices Anthocyanin Reflectance Index (ARI), Modified Simple Ratio (MSR), and the novel indices $QF_{1450} (R_{1600}-R_{1450})/(R_{1600}+R_{1450})$ and $QFI_{1910} (R_{1600}-R_{1910})/(R_{1600}+R_{1910})$ could differentiate between healthy and fireblight-infected leaves. Jarolmasjed (2019) also used hyperspectral spectroscopy and found the red edge band, along with the 1170 nm band and novel vegetation indices (R_{1170}/R_{1320}) and (R_{1420}/R_{1880}) , to be most significant. As with apple scab observations, variations in the SWIR region, attributed to changes in leaf water content, were responsible for detecting fireblight infection in the early stages. Hyperspectral imaging has been used in many other applications to detect powdery mildew (Nagy et al., 2014; Shadrin et al., 2020), apple mosaic virus (Ban et al., 2019; Liu et al., 2024), and Marssonina blotch (Park et al., 2018; Shuaibu et al., 2018). In these studies, chlorophyll-related pigment indices in the visible spectrum and water content in the SWIR range showed the greatest capacity for disease detection.

The majority of studies using hyperspectral techniques have been conducted in laboratory environments with non-imaging sensors, limiting their potential for outdoor application. Of the studies discussed, only Jarolmasjed et al. (2019) applied spectroscopy in the field; however, this was a low-throughput technique used on a select number of trees. Non-imaging sensors do not provide spatial information; they average spectral information over a determined area, which may include both healthy and infected leaves, reducing the sensitivity and specificity of

observations and their applicability to real-world agricultural environments (Mahlein et al., 2018; Bock et al., 2020; Oerke et al., 2020). Imaging sensors are more widely applicable for disease detection as they can detect heterogeneous variations and patterns in observed surfaces. They also allow precise delineation of measurement areas and the elimination of background areas in an image (Deery et al., 2014). However, the practicalities of translating hyperspectral imagery to field settings are challenging. Hyperspectral imagers are often extremely expensive, with poor spatial resolutions, slow image acquisition, and limited fields of view, making adequate coverage of orchards unfeasible. While some studies have applied hyperspectral imagers to airborne systems for monitoring plant pathogens in citrus (Garcia-Ruiz et al., 2013; Abdulridha et al., 2019), their application in apple orchards is limited, aside from measuring nitrogen content (Ye et al., 2020; Li et al., 2022).

While hyperspectral cameras have great capabilities for detecting presymptomatic stress for a range of apple diseases, they have yet to be successfully applied to orchard environments. The large quantities of data pose significant computational challenges, as time series experiments can contain several gigabytes to terabytes (Fahlgren, 2015; Kersting et al., 2016). Orchard monitoring would likely require many thousands of images per day for adequate coverage, with each image requiring the extraction of reflectance signatures pixel by pixel. Information derived from controlled-environment studies could be used to identify specialised wavebands to develop optimal filters for multispectral imaging systems. The development of improved hyperspectral imaging systems, with greater portability, resolution, and acquisition speeds, can make hyperspectral imaging an effective practical tool in agriculture and plant phenotyping in the future (Behmann et al., 2018; Kuska et al., 2018). Until their effectiveness can be demonstrated in large-scale field studies, their use may be constrained to phenotyping studies in controlled environments.

2.3.4 Multispectral Cameras

Multispectral imaging systems are currently used in a wide range of precision agriculture applications, providing more detailed information on crop health than standard visible band imagery by incorporating data from red, green, blue, and additional NIR bands (Mahlein, 2016). Multispectral imagery can be assessed based on individual band imagery or combined to create false-colour composites (Figure 2.8). The interaction of NIR light with plant tissue is particularly useful for phenotyping changes in plant structure and leaf water content (Fahlgren et al., 2015). Although multispectral sensors often provide less data complexity and information content than

hyperspectral imaging, making them less preferred in early disease detection studies, they offer several key advantages. Multispectral imaging systems are generally lower in cost, lighter in weight, and have higher resolutions and fields of view than hyperspectral systems (Huang et al., 2010). These practical benefits make multispectral sensors commonly used in airborne applications for crop monitoring and various precision agriculture tasks (Deng et al., 2018).

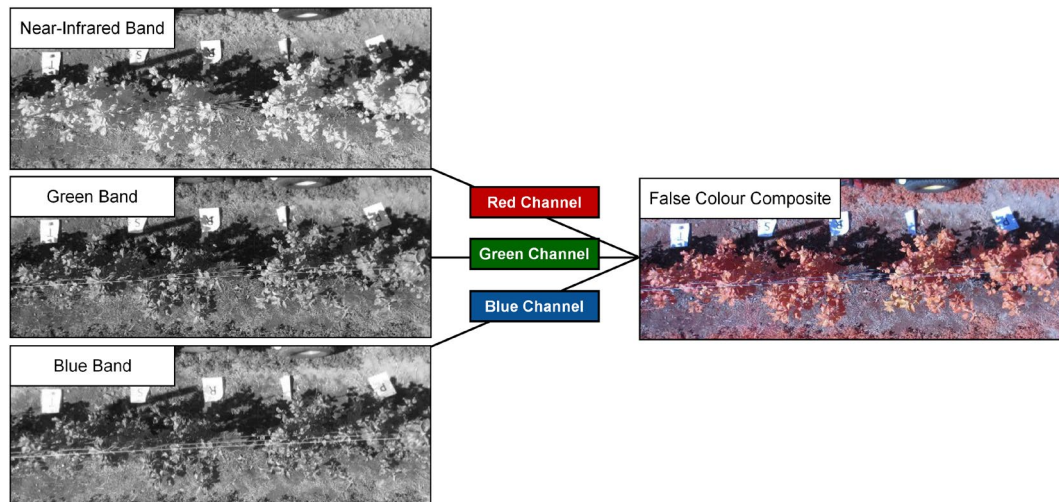


Figure 2.8 Multispectral imaging (component bands and false colour composite) of apple trees in an orchard (adapted from Jarolmasjed et al., 2018)

Numerous off-the-shelf multispectral cameras are available for agricultural purposes and are commonly installed on UAV platforms for precision agriculture management (Deng et al., 2018; Assmann et al., 2019). Commonly used systems include the MicaSense RedEdge (MicaSense, Seattle, USA) by Mamaghani et al. (2019) and the Parrot Sequoia (Parrot Drone SAS, Paris, France) by Olsson et al. (2021). Consumer colour cameras can also be modified into near-infrared sensors by removing the infrared 'hot mirror' filter, providing a low-cost, high-resolution multispectral imaging method (LeBourgeois et al., 2008). These modified multispectral systems have already demonstrated success in detecting plant stress within apple orchards (Jarolmasjed et al., 2018). Multispectral cameras utilise broadband vegetation indices developed from the reflectance characteristics of plants and spectral algorithms correlated to specific plant parameters, providing a more purposeful estimation of biophysical parameters than single bands alone. Standardised Difference Vegetation Indices (SDVIs), such as NDVI and NDRE (Gitelson & Merzlyak, 1994), are commonly used in multispectral imagery because they reduce the effects of spectral variations caused by surface topography and sun elevation. Modified multispectral cameras are also capable of deriving these vegetation indices (Anderson et al., 2016; Berra et al., 2017). However, SDVIs have seen limited success in disease detection studies, as the optimal information on the physiological status of plants does not often correlate ideally with the regions being studied (Delalieux et al., 2009a).

In the study of powdery mildew in apple orchards, Chandel et al. (2021) used a UAV-based multispectral camera (MicaSense) to measure nine vegetation indices that have the potential to characterise variations in canopy pigments due to the disease. The Modified Simple Ratio-Red (MSR_{Red}) index, Modified Simple Ratio-Blue (MSR_{Blue}) index, and Optimised Soil Adjusted Vegetation Index (OSAVI) showed the highest contrast, with lower values for infected leaves compared to healthy ones. These indices represent variations in chlorophyll, anthocyanin, and carotenoid pigments (Vescovo et al., 2012; Kyrtzis et al., 2017). Similarly, Jarolmasjed et al. (2019) employed two multispectral camera methods alongside RGB imagery and hyperspectral spectroscopy measurements. These included a dedicated multispectral camera (MicaSense) observing GNDVI, NDVI, and NDRE indices and a modified colour camera with the red channel detecting NIR reflectance (680-800 nm). All these indices typically detect variations in chlorophyll and water content of leaves (Abdulridha et al., 2020), making them effective at detecting leaf wilting and chlorosis caused by fire blight infections. Both multispectral cameras showed a significant correlation between these indices and disease severity ratings, indicating they could detect differences between healthy and infected tissue and potentially map disease spread in orchards. While these systems effectively detected powdery mildew and fireblight infections in high-density orchard environments on practical mobile acquisition platforms, neither demonstrated potential for early detection. These studies focused on quantifying the severity of late-stage infections rather than identifying early stress symptoms.

Aside from the aforementioned studies, the application of multispectral cameras for detecting apple disease in orchards is limited, with most focus on symptoms of abiotic water stress in canopies (Gomez-Candon et al., 2014; Virlet et al., 2015). However, multispectral sensors have been used to detect diseases in other tree crops, such as citrus (Garcia-Ruiz et al., 2013; DadrasJavan et al., 2019). Multispectral sensing has also been used for early detection of *Erwinia amylovora* infections in pear trees (Bagheri, 2020). By developing a multispectral camera system to measure vegetation indices previously found to be discriminative in hyperspectral analysis (Bagheri et al., 2018), fireblight infections, nutrient deficiencies, and healthy samples could be distinguished from UAV imagery.

Notably, apple scab detection using multispectral imagery has not been performed in either controlled or uncontrolled conditions. This may be attributed to the low resolution of these cameras and their intended operational height, making them unsuitable for apple scab detection. The dedicated multispectral cameras discussed in this section have a sensor resolution of 1.2 MP (1280x720 pixels). Chandel et al. (2021) used a 1.2 MP sensor, which, when flown over an orchard at a 15 m distance, had a resolution of 11 mm/pixel. Scab lesions typically reach a

maximum radius of 10 mm (Bowen et al., 2011). The ground sampling distance at these operating heights is too coarse to detect scab symptoms in all but the most severe infections. Multispectral cameras that contain high-resolution sensors may be capable of the detection of apple scab infections on leaves.

2.3.5 Chlorophyll Fluorescence Imaging

Chlorophyll fluorescence provides information on the photosynthetic performance of a leaf by quantifying light emitted from the chlorophyll under abiotic and biotic stresses (Chaerle & Der Streaten, 2000). Chlorophyll fluorescence imaging is an active sensing method that measures leaf fluorescence. This technique involves exciting the leaf with a red-far light source to assess photosynthetic electron transfer (Baker, 2008). Fluorescence imaging uses multispectral CCD sensors to detect the light emitted from plants in the blue, green, red, red-edge, and NIR bands, using multispectral imaging sensors (Sankaran et al., 2010). Chlorophyll fluorescence is valuable because it provides insights into the photosynthetic performance of a leaf by quantifying light emitted from the chlorophyll under stress conditions. This energy absorbed by chlorophyll can either be utilised in photosynthesis, released as heat, or emitted as chlorophyll fluorescence. Since these processes compete with one another, chlorophyll fluorescence data offer valuable insights into the efficiency of photosynthesis and heat dissipation (Maxwell & Johnson, 2000). Divergence in chlorophyll fluorescence measurements often precedes the appearance of visible symptoms, with changes in chlorophyll function occurring before changes in chlorophyll content (Konanz et al., 2014; Shakoor, 2017).

Chlorophyll fluorescence has been utilised in a limited capacity for early apple scab detection and has not been applied to other apple diseases. Delalieux (2009a) used light-adapted fluorescence imaging alongside hyperspectral spectroscopy to detect early symptoms of apple scab. The quantum efficiency of Photosystem II (Φ_{PSII}) photochemistry was derived from fluorescence imagery of leaves under light-adapted conditions. Due to their lower Φ_{PSII} quantum efficiency compared to control leaves, scab infection could be detected before the onset of visible symptoms. However, young apple leaves also show lower Φ_{PSII} quantum efficiency than mature leaves, making it difficult to distinguish young leaves from infected leaves without the simultaneous use of a spectral sensor. Furthermore, as apple scab infections developed and caused tissue damage, the observed Φ_{PSII} values increased. It was recommended that while there was some potential, accurate identification of scab infections could only be achieved with the simultaneous use of hyperspectral sensors. Belin et al. (2013) also performed early detection of apple scab in a comparative study between dark-adapted chlorophyll fluorescence and

thermography. While fluorescence imaging detected apple scab infections 1–2 days before the appearance of visible symptoms, the use of thermal imaging sensors was found to be superior.

The practicalities of chlorophyll fluorescence imaging limit its application for disease monitoring in the field. This active sensing method uses time-of-flight emission and detection of light, which restricts the operating speed of an acquisition platform (Deery et al., 2014). Furthermore, the sample preparation necessary for adequate fluorescence and the high-power requirements of the sensors limit their use outside controlled laboratory settings (Mahlein et al., 2012; Bauriegel & Herppich, 2014). Additionally, chlorophyll fluorescence has limited diagnostic potential, as its measurements are similar for a range of diseases and are sensitive to many other factors affecting the photosynthetic performance of leaves (Simko et al., 2016). While chlorophyll fluorescence imagery has shown potential for early detection of foliar diseases in controlled environments, previous reviewers agree that fluorescence imaging, especially when used independently, is unsuitable for disease detection in field environments (Fang et al., 2015; Mahlein, 2016).

2.3.6 Thermography

Thermography is a method of detecting the emissivity of a surface in the thermal infrared range (TIR: 3.0 - 14.0 μm) of the electromagnetic spectrum (Oerke & Steiner, 2010). Thermal infrared measurements can characterise tissue health, as pathogens influence the transpiration rate and, consequently, the water content of plants, indicating stress (Ishimwe et al., 2014; Khanal et al., 2017). Thermography is highly suited for disease detection because increasing leaf temperature correlates with a decrease in transpiration rate due to the active regulation of stomatal aperture (Chaerle & Der Straeten, 2000; Jones & Schofield, 2008). The spatial and temporal heterogeneities in thermal images of leaf tissue can indicate presymptomatic infection by a pathogen, with local temperature changes resulting from pathogen activity or plant defence mechanisms (Mahlein et al., 2012).

Thermography has demonstrated considerable potential for the early detection of apple scab infections, as well as for quantifying severity, resistance of host tissue, and differences in the aggressiveness of *V. inaequalis* isolates infecting plants with apple scab (Oerke et al., 2011). Thermography visualised presymptomatic apple scab detection through areas of localised cooling before the onset of visual symptoms and extended beyond these regions in the later stages of infection. These regions of localised cooling indicated an increased cuticular

transpiration rate around scab lesions (Oerke & Steiner, 2024). The maximum temperature difference (MTD) increased with the development of the scab and strongly correlated with the infection site size and overall disease severity. The use of MTD as an effective parameter for disease detection was also found in studies by Lindenthal et al. (2005) and Oerke et al. (2006). In the late stages of the disease, the MTD became less pronounced as senescence across the whole leaf reduced the overall transpiration rate (Oerke et al., 2011). Belin et al. (2013) also demonstrated the effectiveness of thermal imaging for apple scab detection, observing early signs of stress up to three days before the onset of visible symptoms. Thermal imaging was shown to be capable of early scab detection in TIR regions 3-5 μm (Belin et al., 2013) and 8-12 μm (Oerke et al., 2011), demonstrating the robustness of the method.

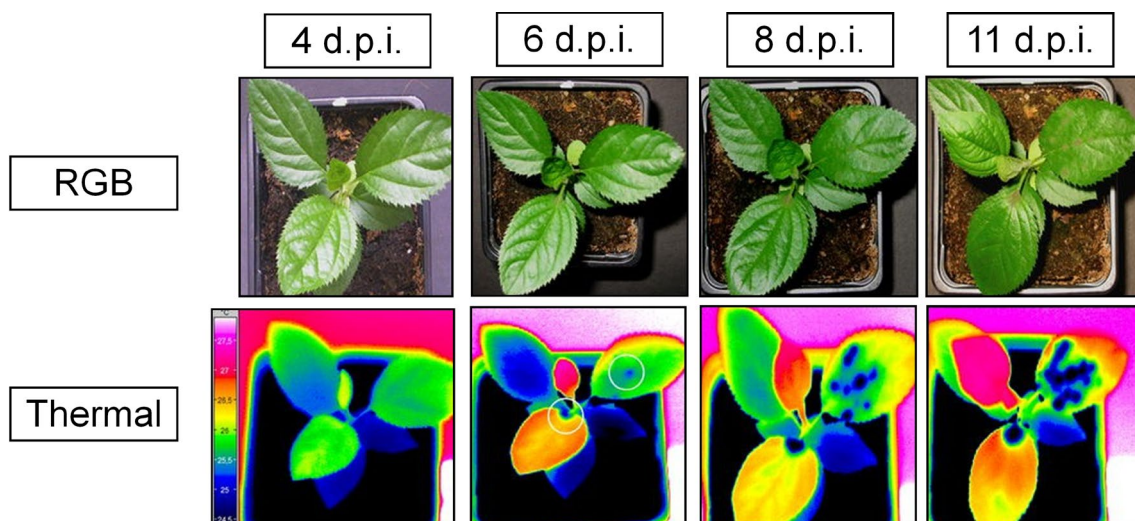


Figure 2.9 Thermal assessment of apple scab progression where white circles denote initial symptom development (adapted from Oerke et al., 2011)

Aside from these studies, there is limited application of thermal imaging for the early detection of apple diseases. Although MTD and the Crop Water Stress Index (CWSI) are often applied in the thermography of fruit crops (Gonzalez-Dugo et al., 2014; Lee, 2019), the diagnostic potential of thermal imaging is limited, as many plant diseases lead to similar effects on leaf transpiration (Pineda et al., 2020). Both thermal studies of early apple scab detection were performed in highly controlled environments. There are major practical limitations in applying thermal imagery in field environments. Thermal images are sensitive to noise and environmental factors such as ambient temperature, sunlight, rainfall, or wind speed. In a preliminary assessment of the potential of apple flower stigma temperatures for fireblight prediction, it was found that temperature was mainly influenced by solar radiation (Rougerie-Durocher et al., 2020). The ideal conditions for capturing thermal images include keeping leaves out of direct sunlight, dry and unobscured, and taking images against the sun, although this is challenging to achieve in real-world orchards. Additionally, thermal cameras have low sensor resolutions, making sub-leaf

assessments for apple scabs difficult as pixel values become mixed with background soil and canopy height variations. While thermal imaging has the potential to provide early warnings of tree stress in orchards, numerous issues must be addressed to improve its effectiveness. Nonetheless, thermography can play an effective role in disease risk prediction by measuring environmental conditions favourable for infections by phytopathogens, such as leaf wetness and surface temperature, to be used in models quantifying disease risks (Lindenthal et al., 2005).

2.3.7 3D Imaging Systems

3D imaging is a more recent sensing technique that allows for the evaluation of structural changes in a plant that could be linked to plant stress. Changes in plant structure and biomass can provide important information regarding plant health, as regions of stunted growth or deformation of leaves, fruit, and shoots can indicate disease (Paulus et al., 2014). While architectural traits can be estimated with 2D imagery, several photogrammetric solutions are available to produce 3D models of plants that offer different characteristics in terms of cost, field of view, and accuracy (Martinez-Guanter et al., 2019). For plant phenotyping purposes, 3D imaging generally uses either triangulation methods (Structure-from-Motion, Stereovision, Structured Light) or time-of-flight methods (LiDAR) to produce coordinates in a 3D space as a point cloud (Paulus et al., 2019). The only instance of 3D imagery being used for disease detection was through data fusion to improve early apple scab detection via thermal imagery (Chéné et al., 2012). 3D imaging excels in its ability to segment images based on depth, which can be extremely useful in separating leaves from the background in both RGB and thermal imagery, particularly in scenarios with complex or low-contrasting backgrounds.

Although there are no other studies using 3D imaging for disease detection, these systems have been widely applied in apple orchards for various management purposes. LiDAR scanning systems are the most common method for reconstructing tree canopy properties in orchards. LiDAR has been shown to generate reliable measurements for determining plant geometry and structural parameters, enabling targeted pruning of apple trees (He & Schupp, 2018; Murray et al., 2020). The quantification of structural parameters such as Leaf Area Index (LAI) also allows these sensors to inform Variable Rate Spray (VRS) technologies to optimise pesticide application based on canopy sizes (Maghsoudi & Minaei, 2014; Berk et al., 2020). LiDAR operates by creating point clouds based on the measurement of travel time from a laser transmitter to a target, effectively modelling the structural complexity of trees in apple orchards to inform orchard management.

LiDAR can assess the structural characteristics of plants with high accuracy but lacks colour information, which can limit its practical effectiveness for plant phenotyping (Lin, 2015). Colour or further reflectance information may be added through texture mapping with spectral sensor data, but this process can be laborious and inaccurate (Omasa et al., 2007; Martinez-Guanter et al., 2019). RGB-Depth (RGB-D) sensors are low-cost methods increasingly adopted in plant phenotyping research. A review of four low-cost RGB-D sensors found that an active stereoscopy sensor outperformed similar time-of-flight, structured light, and passive stereoscopy sensors for field phenotyping in outdoor lighting (Vit & Shani, 2018), in agreement with previous assessments by Kazmi et al. (2014). These low-cost RGB-D sensors were also utilised to aid thermography for apple scab detection (Chéné et al., 2012).

The operation of remote sensors in outdoor environments is essential for practical application. While these sensors display sensitivity to illumination variations in field conditions, they are typically applied to measure apple plant parameters in real-world orchards. 3D imagery is becoming an increasingly important addition to plant phenotyping studies; however, its use within disease detection studies has not been fully realised. There may be potential for quantifying diseases such as fireblight, powdery mildew, or abiotic stresses that influence the wilting of shoots and leaves, but these applications may only be effective in later stages of infection. There may be limited applicability of 3D sensors alone for disease detection, but incorporating 3D data through fusion with other sensing methods could provide valuable information on crop health.

3D imagery provides ancillary data to precision agriculture systems that can aid autonomous monitoring of orchards, such as collision detection systems for autonomous platforms (Petiteville et al., 2018) and informing variable rate spray technologies (Berk et al., 2020). Furthermore, regular monitoring through 3D imaging could be used to understand the impact of repeated infections on the growth and productivity of trees in orchards over time. The application of 3D imaging sensors is likely to become increasingly prevalent in future orchard monitoring systems, and further research into their potential for disease detection should be considered.

2.3.8 Sensor Selection

The selection of appropriate sensors for the early detection and identification of diseases in apples is crucial for informing targeted control measures. Although considerable research has been conducted on using RGB, hyperspectral, multispectral, fluorescence, thermal, and 3D imaging, no single sensor has demonstrated the capability for widespread early detection in commercial orchards (Table 2.1). Both hyperspectral and thermal imaging have shown great potential for detecting presymptomatic signs of stress from apple diseases, with hyperspectral imaging exhibiting significant diagnostic potential across various disease sources. However, these techniques have only been effectively demonstrated in controlled laboratory conditions, and there are inherent drawbacks to their use for appropriate coverage in orchards. In contrast, RGB imagery has been widely applied in real-world environments with notable diagnostic potential. However, these systems have only proven effective during the late stages of infection, when considerable damage has already occurred to apple trees, limiting their utility for early detection. Multispectral cameras have seen limited application for disease detection in apple orchards, often used alongside RGB imagery for detecting late-stage diseases. Despite this, there is evidence that these systems are capable of rapid in-field detection of early disease symptoms in other crops, such as wheat (Nguyen et al., 2023), tomato (Xu et al., 2006; Fahrentrapp et al., 2019), and trees including pear (Bagheri, 2020), olive (Castrignano et al., 2020), and pine (Yu et al., 2021). Further research is recommended to investigate the potential for multispectral imaging systems to detect early signs of apple diseases in real orchard environments.

The early detection and accurate classification of apple disease using individual sensors can be challenging, as they often study a limited range of responses which can have a weak linkage to the causative agent or be mistaken for another stress factor due to similar symptoms. A multimodal approach combining several sensors can produce more consistent and useful information than any individual data source, leading to improved classification accuracies in data analysis (Busemeyer et al., 2013). The aim of a multimodal sensor approach is to obtain a lower detection error probability and higher reliability by acquiring more relevant information (Castanedo et al., 2013). There are examples of large field-scanning platforms that utilise all the sensors reviewed here to achieve maximum information output for phenotyping crops (Kirchgessner et al., 2016; Virlet et al., 2016). However, the downside of implementing numerous sensors simultaneously is the drastic increase in cost, weight, and power requirements of the acquisition routine, limiting potential mobile platforms. Additionally, challenges arise from the different spatial and temporal resolutions of each sensor and the complexity and redundancy of the acquired data (Pallotino et al., 2019).

Sensor	Disease	Parameters	Early Detection	Diagnostic	Field Use	Reference
RGB	Powdery Mildew	Shape, texture, texture colour features; Greenness indices		x	x	Chandel 2020, 2021
	Fireblight			x	x	Jarolmasjed et al., 2019
	Multiple Diseases			x	x	Thapa et al., 2020
Hyperspectral	Apple Scab	Visible-SWIR reflectance; narrowband reflectance, narrowband indices	x	x		Delalieux et al 2007 ; Delalieux et al, 2009a ; Nouri et al., 2018 ; Gorretta et al., 2019
	Apple Mosaic Virus		x	x		Ban et al., 2014 Liu et al., 2024
	Fireblight		x	x		Jarolmasjed et al., 2019 ; Skoneczny et al, 2020
	Powdery Mildew		x	x		Nagy et al., 2014 ; Shadrin et al., 2020
	Marssonina Blotch		x	x		Park et al., 2018 ; Shuaibu et al 2018
Multispectral	Powdery Mildew	Blue, green, red, red-edge, near-infrared reflectance; broadband vegetation indices		x	x	Chandel et al 2020 ; Chandel et al 2021
	Fireblight			x	x	Jarolmasjed et al., 2019
Fluorescence	Apple Scab	Photosynthetic Change	x			Delalieux et al., 2009b ; Belin et al., 2013
Thermography	Apple Scab	Temperature; Transpiration	x			Oerke et al., 2011 ; Belin et al 2013

Table 2.1 Remote sensors utilised in literature for the detection of apple diseases

2.4 Classification Techniques for Disease Identification

2.4.1 Traditional Machine Learning Classification

Manual classification of remotely sensed imagery by expert operators familiar with disease symptoms can accurately distinguish between complex disease presences under various conditions and is easy to implement, requiring no sophisticated equipment (El Jarroudi et al., 2014). However, monitoring diseases within orchards would require the analysis of a large number of images, and the time-consuming nature of manual assessments is too labour-intensive and subject to human errors to be implemented at a large scale (Bock et al., 2020). Plant disease detection through remote sensing relies heavily on powerful data analytics to identify plant diseases through supervised and unsupervised machine learning methods (Behmann et al., 2015; Shruthi et al., 2019). Traditional methods of disease detection based on machine learning algorithms typically involve four steps: pre-processing, segmentation, feature extraction, and classification (Singh & Gupta, 2016; Prakash et al., 2017; Li et al., 2021). Pre-processing techniques enhance image quality. Segmentation methods isolate areas of interest.

Feature extraction techniques aim to identify and quantify relevant disease characteristics. Finally, classification algorithms categorise these extracted features into disease classes. A range of techniques is available for each step (Table 2.2), each with inherent benefits and limitations regarding processing time, ease of use, and accuracy (Iqbal et al., 2018).

Phase	Technique
Preprocessing	Colour Transformation Structure
	Image Enhancement
	Noise Reduction
Segmentation	K-means Clustering* (<i>Segmentation</i>)
	Thresholding
	Colour Segmentation
	Edge Detection
Feature Extraction	Texture
	Colour Segmentation
	Shape
	Vegetation Indices (Vis)
	Partial Least Squares (PLS)
	Analysis of Variance (ANOVA)
Classification (Supervised)	Support Vector Machine (SVM)
	Spectral Angle Mapper (SAM)
	Tree-based Modelling
	Artificial Neural Network (ANN)
	Convolutional Neural Network (CNN)
	K-nearest Neighbour (KNN)
Classification (Unsupervised)	K-means Clustering* (<i>Classification</i>)

Table 2.2 Key image analysis phases and techniques used in plant disease detection studies

The pre-processing, segmentation, and feature extraction stages are essential as they provide crucial data to the machine learning classification algorithms. However, the classification step is the most critical phase of the analysis process, as it correlates image-extracted information to biologically relevant traits to determine disease-infected tissue. Supervised classification, which requires learning from annotated training data, is the most commonly used technique for apple disease classification. Support vector machines (SVMs) are widely used classifiers in plant disease detection studies (Liu et al., 2017). However, they have only been implemented to classify fireblight (Jarolmasjed et al., 2019) and apple mosaic virus (Liu et al., 2023) from hyperspectral data. Unsupervised learning aims to determine key patterns in data without additional manual input of training data, allowing an algorithm to act on supplied information unsupervised. K-means clustering, an unsupervised technique, was used to effectively classify infected regions pertaining to apple powdery mildew in RGB imagery (Chandel et al., 2021). It

has also been used to segment trees from background soil in multispectral imagery before further analysis of fireblight infection (Jarolmasjed et al., 2019). Many remaining studies, notably thermography assessments (Oerke et al., 2011; Belin et al., 2013), have relied mainly on manual assessments and simple statistical analyses of results.

Machine learning classification techniques can achieve high levels of accuracy in test conditions but are heavily dependent on the preceding pre-processing, segmentation, and feature extraction steps, any of which can introduce errors or artefacts. These techniques are more suitable for investigative studies of sensor feasibility in detecting certain diseases. They often succeed only in controlled environments, requiring uniform lighting, high contrast from the background, and minimal noise to achieve useful results, which are not feasible in field environments (Zhong & Zhao, 2020; Li et al., 2021). Classification of plant pathogens through traditional machine learning methods can be highly accurate in most studies but is often restricted to diagnosing single diseases (Barbedo et al., 2016). The limitations of traditional machine learning algorithms can make them unsuitable for large-field operations, especially when tasked with diagnosing early symptoms of diseases in the complex conditions of real-world commercial orchards.

2.4.2 Deep Learning Convolutional Neural Network Models

In recent years, deep learning Convolutional Neural Networks (CNNs) have been widely implemented for various precision agriculture tasks (Kamilaris & Prenafeta-Boldú, 2018), with specific focus on disease detection studies (Boulet et al., 2019). CNNs are a class of feed-forward artificial neural networks popular in plant disease classification due to their high performance in classifying diseases in complex scenarios (Hasan et al., 2020). CNN models consist of multiple layers of image filters and feature maps within convolutional layers, along with pooling and fully connected layers representing learned features from the data (Yamashita et al., 2018). A simplified diagram of a CNN model is displayed in Figure 2.10. CNNs learn filter weights, fully connected layer weights, and biases directly from training datasets to solve classification problems through each of these layers. This autonomous learning process involves adjusting the weights of convolutional filters to detect features, tuning the weights of neurons in fully connected layers for final decision-making, and optimising biases for better model fitting. Unlike traditional machine learning techniques that rely on hand-crafted feature extraction, this enables CNN models to solve complex classification problems more quickly, efficiently, and with a lower error rate (Toda & Okura, 2019; Iqbal et al., 2018; Li et al. 2021).

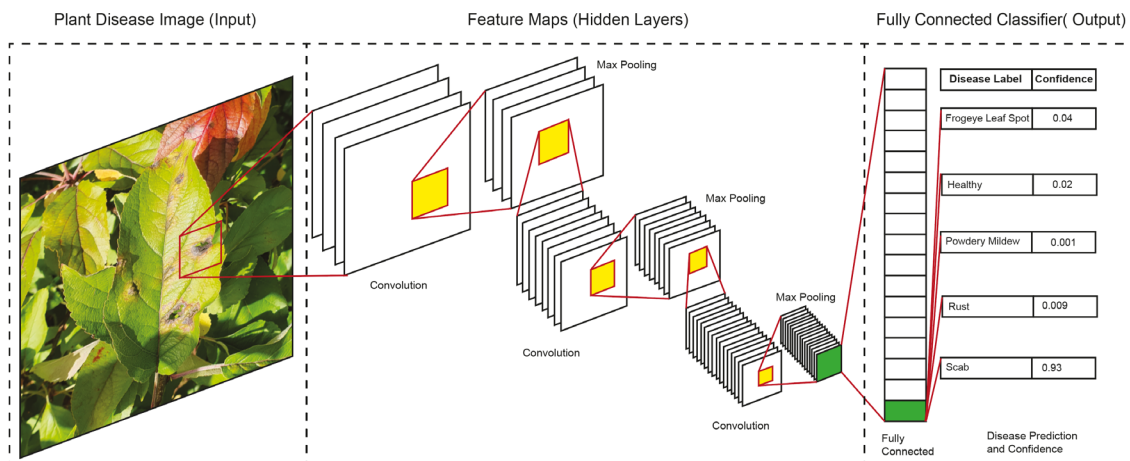


Figure 2.10 The basic structure of a CNN for apple disease classification (adapted from Liu & Wang, 2021)

Numerous CNN model architectures are utilised for disease detection, differing based on the number and arrangement of layers and additional processing units (Alzubaidi et al., 2021; Taye, 2023). CNNs are effective at early detection of plant diseases using various remote sensing techniques (Golhani et al., 2018), including Marssonina blotch with hyperspectral imaging (Park et al., 2018). As previously discussed in Section 2.3.2, RGB imagery has been widely used for the detection and classification of numerous apple diseases with high accuracies (Table 2.3). CNNs offer practical analysis options, enable real-time identification of apple diseases (Jiang et al., 2019) and provide severity estimates of these diseases in trees (Zhong & Zhao, 2020; Liu et al., 2022). They have been used to classifying numerous apple diseases accurately from imagery captured at various developmental stages of infection, in the presence of multiple diseases, and from multiple acquisition angles (Thapa et al., 2020). Many CNN classification studies promote the effectiveness of their custom-designed CNN architectures (Jiang et al., 2019; Chao et al., 2020; Wang et al., 2021; Chao et al., 2021; Li & Li, 2022; Li et al., 2022; Turkoglu et al., 2022; Yadav et al., 2022), sometimes without accurate manual interpretation of the disease imagery (Bansal et al., 2021).

Many CNN architectures are readily available and have been previously trained on millions of annotated images from ImageNet (Deng et al., 2009). These pre-trained CNN models can serve as the basis for new classification models with less data required for the new training stage, reducing training time and alleviating overfitting through a technique called transfer learning (Zhuang et al., 2020). Fine-tuning, a key transfer learning method, involves using the weights of a pre-trained model to initialise a new model before retraining on the target training set (Boulent et al., 2019). Fine-tuning significantly improves adaptation to new datasets compared to the direct application of a pre-trained network (Radenović et al., 2018).

Source	Model	Dataset	Conditions	Diseases Classified	Accuracy	F1 Score
Mohanty et al. (2016)	GoogleNet	PlantVillage	Controlled	38 various crop diseases including AS, CAR, FLS, H	99.34%	0.9935
Jiang et al. (2018)	VGG-INCEP	Unique	Mixed	ALS, MB, AMV, GS, Pucciniaceae glue rust	97.14%	
Chao et al. (2020)	XDNet	Unique	Mixed	ALS, AMV, AS, BS, GS, H	98.82%	
Li & Li, (2020)	ConViT	Unique	Mixed	ALS, AMV, BS, CAR, GS	95.21%	95.1900
Zhong & Zhao (2020)	DenseNet-121	PlantVillage	Controlled	AS (General), AS (Serious), CAR (General), CAR (Serious), FLS, H	92.29%	0.9270
Chao et al. (2021)	SE_Xception	Unique	Mixed	ALS, AMV, BS, CAR, GS, H	99.40%	99.1000
Turkoglu et al. (2021)	MLP-CNNs	Unique	Outdoors	AS, BS, Woolly Apple Aphid, Green Apple Aphid	99.20%	
Wang et al. (2021)	CA-Enet	Unique	Outdoors	AMV, AS, FLS, H Japanese Maple Rust, Glomerella Leaf Spot, Apple Litura Moth, Apple Leaf Mites	98.92%	0.9880
Li et al. (2022)	MCNN	Unique, PlantVillage	Controlled	ALS, AMV, AS, CAR, FLS,	95.31%	
Yadav et al. (2022)	AFD-Net	Plant Pathology 2020, Plant Pathology 2021	Outdoors	AS, CAR, FLS, H, PM, Multiple Disease	98.00%	0.8900
Vishnoi et al. (2023)	Deep CNN	PlantVillage	Controlled	AS, CAR, FLS	98.00%	0.9700

Table 2.3 Previous studies utilising CNN models for apple disease classification (ALS – Alternaria Leaf Spot; AMV – Apple Mosaic Virus; AS – Apple Scab; BS –Brown Spot; CAR – Cedar-Apple Rust; FLS – Frogeye Leaf Spot; GS – Grey Spot; H – Healthy; MB – Marssonina Blotch; PM – Powdery Mildew)

CNNs are a supervised learning method, and to achieve superior classification capabilities, large quantities of training data are required (Tajbakhsh et al., 2016). The lack of adequate labelled samples for training and fine-tuning poses a major challenge for deep learning studies, especially for multispectral and hyperspectral imagery (Saleem et al., 2019; Hasan et al., 2020). The collection and annotation of large quantities of foliar disease imagery are labour-intensive processes that constrain the development of classification models. Public datasets such as PlantVillage (Hughes & Salathe, 2015) and PlantPathology (Thapa et al., 2020) provide useful resources (Figure 2.11). One major limitation of the PlantVillage dataset is that it contains images of individual leaves with homogenous backgrounds. Despite high classification accuracies, these images do not accurately represent true orchard scenarios (Mohanty et al., 2016; Vishnoi et al., 2023). Applying models trained purely on these datasets may decrease accuracy when applied directly to orchard images. Deep learning algorithms trained from images captured in the field, with a natural background, provide significantly more accurate models than those trained in laboratories (Chao et al., 2020). Images captured in a natural growing

environment enable deep learning models to detect diseases better in real-world scenarios. Additionally, the collection and annotation of plant disease imagery from non-RGB sources are recommended to enable the early detection of infections through novel remote sensing applications.

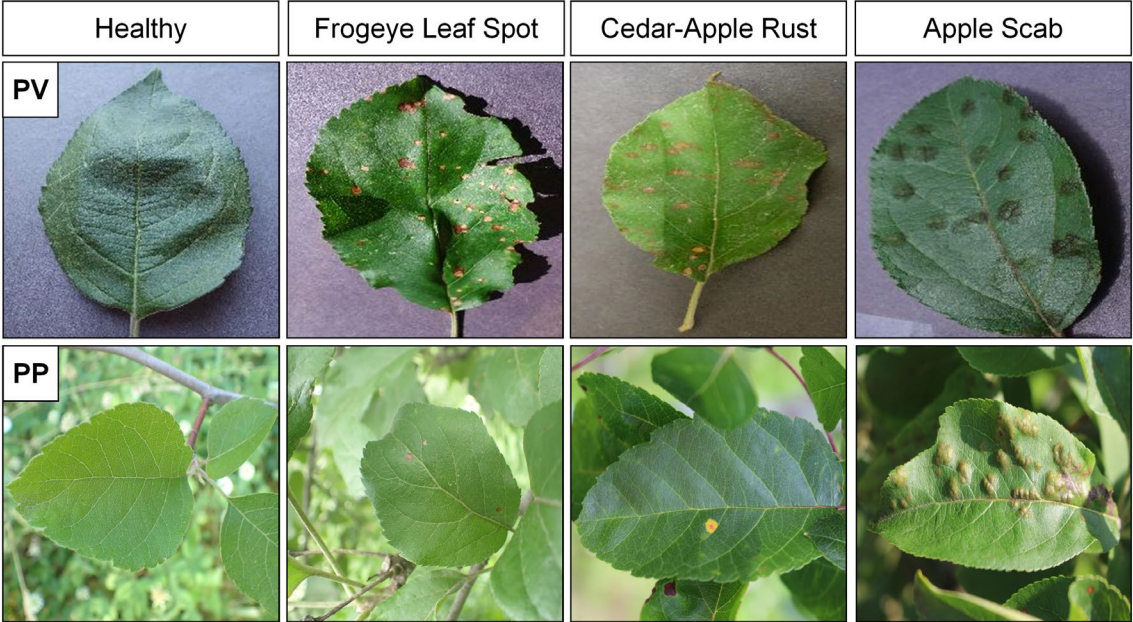


Figure 2.11 Example imagery of apple foliar diseases from public datasets. PV – PlantVillage (Hughes & Salathe, 2015); PP - PlantPathology2020 (Thapa et al., 2020)

2.4.3 Classification Model Selection

Automated classification by deep learning CNNs has largely overtaken traditional machine learning as the method of choice for disease diagnosis. Their ability to accurately classify multiple diseases concurrently, under various symptom displays, and in complex acquisition conditions without extensive pre-processing requirements opens up the possibility of automated monitoring of apple orchards on a large scale. Future research should focus on improving the robustness of these models by incorporating diverse datasets and exploring the integration with alternative sensing methods, such as colour cameras, to enhance early disease detection and classification accuracy.

2.5 Acquisition Platforms for Orchard Monitoring

2.5.1 Requirements for Acquisition Platforms in Orchards

The selection of an appropriate sensing platform is crucial for the effective acquisition of remotely sensed data in precision agriculture-based monitoring systems. Many early disease detection studies were conducted in controlled settings, using proximal imaging from fixed structures to optimise image and information quality. Transitioning from these controlled environments to real-world settings for disease detection experiments introduces new challenges in monitoring disease in apple orchards. Scaling imagery to orchard-wide monitoring will require the use of mobile platforms, which will introduce further complexities to detection, classification, and quantification tasks. Due to the novelty of apple disease detection, there are limited examples of mobile platforms within the context of the study. This section expands on research into potential technologies that have been applied in apple orchards for other precision management tasks or disease detection in other tree crops.

Mobile platforms range from ground-based to spaceborne (Figure 2.12), with increased imaging distance bringing a trade-off between spatial coverage and minimum pixel size (Shakoor et al., 2017). Platforms that offer larger spatial coverage per image are beneficial as they can observe whole orchards rapidly and capture more plants in a single image, both of which help maintain better consistency in environmental conditions that may influence measurements. Achieving rapid full coverage of an orchard is necessary to accurately map and quantify disease severity and inform reactive, site-specific treatment decisions. However, wide coverage is often achieved by increasing imaging distances, which comes at the expense of spatial resolution by reducing the ground sampling distance or the area covered by each pixel (O'Connor et al., 2017). Poor spatial resolution implies large pixels containing averaged information, making it difficult to distinguish infected tissue from non-infected tissue and background characteristics (Mulla, 2013). Many apple disease symptoms are localised entirely within individual leaves rather than affecting the whole canopy, especially during the early stages of infection. To effectively detect many apple diseases in the early stages of infection, ground sampling distance must achieve millimetre-scale observations. Each sensing platform has strengths and weaknesses for early detection and large-scale monitoring of plants on an epidemic hierarchical scale, i.e., region > field > foci > plant > symptom (Oerke et al., 2020). A compromise between rapid coverage and ground-pixel resolution must be made, informed by the optimal localisation scale for early disease symptoms and the limitations of sensing hardware (Mahlein et al., 2012).

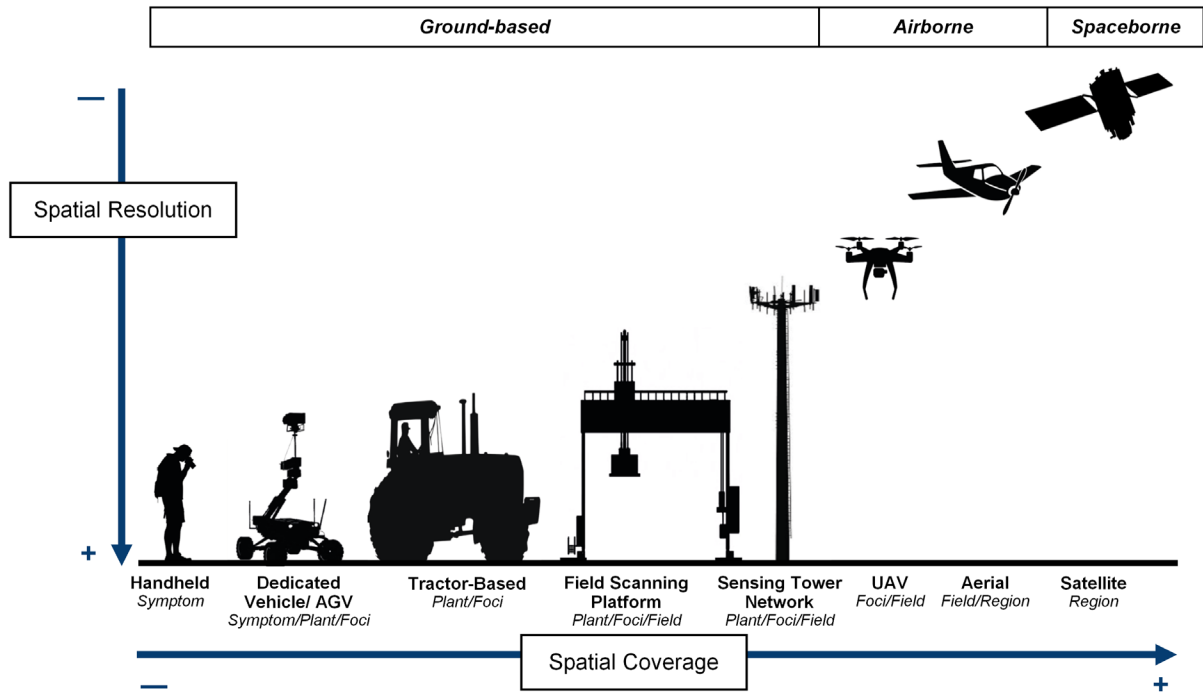


Figure 2.12 Remote sensing platforms for agricultural applications (adapted from Shakoor et al., 2017)

2.5.2 Ground-based Sensing Platforms

Ground-based sensing platforms, which operate directly in fields, can be used to acquire high-resolution imagery of disease symptoms. Handheld sensing is the most readily available approach to crop sensing. Most colour, modified multispectral, and thermal cameras are designed for handheld use, with select hyperspectral cameras also available (Behmann et al., 2018). Handheld platforms allow for close-up imaging of specific foci, providing high-resolution data crucial for detecting early disease symptoms. These platforms are versatile and can be used to detect disease in various parts of apple trees across orchards. Additionally, handheld sensing devices are generally cost-effective and user-friendly, making them accessible to a wide range of users. However, handheld methods are low-throughput and labour-intensive, offering little improvement in orchard coverage over traditional scouting methodologies (Deery et al., 2014). The strength of handheld platforms lies in the dexterity of the human operator, who can image infection in areas difficult to access, such as the lower canopy and the abaxial surface of leaves. These factors give handheld platforms a significant advantage in the early detection of many diseases.

Dedicated vehicles offer improved functionality compared to handheld sensors, providing a system of acquisition designed for use in the field for phenotyping tasks. The simplest of these is a hand-pushed cart, which offers an advantage over handheld methods by allowing heavier sensors to acquire imagery at consistent heights and angles while maintaining some of the

flexibility of human-adjusted viewing angles. Simple hand-pushed carts provide advantages in cost, simplicity, and flexibility, as well as the ability to maintain imaging height and angles and use multiple sensors. For example, the Phenocart developed by White & Conley (2013), used a bicycle-frame design and was mounted with an infrared thermometer, multispectral sensor, RGB camera, global navigation satellite system, and laptop. This setup has been used by Thompson et al. (2018) and Lima et al. (2020). While these methods are still heavily reliant on manual labour and can be difficult to use for sensing tree canopies, they offer an economical method for in-orchard observations of apple disease. More complex, dedicated phenotyping vehicles are available as manned buggies or Autonomous Ground Vehicles (AGVs). Manned buggies such as the Phenomobile (Deery et al., 2014) and Breedvision (Busemeyer et al., 2014), equipped with multiple sensors, have been developed for field phenotyping studies of arable crops. AGVs, such as the Thorvald II agricultural robotic platform (Grimstad & From., 2017), are commercially available options and are being used in some capacity for sensing fruit crops (Kirk et al., 2020). AGVs can theoretically provide continual observation of orchards with limited labour requirements; however, the upfront cost and maintenance of these technologies are extremely high, making them unlikely to be feasible for application in commercial farms in the near future.

Tractor-based platforms are a useful method for orchard monitoring as they are both widely accessible to most orchards and regularly utilised for various monitoring tasks. Sensors can be attached to these tractors with limited modifications, providing both side and aerial views of leaves while travelling at a moderate pace through orchards. These systems also have fewer concerns over the power and weight requirements of sensing methods. Tractor-mounted sensors have been used in the multispectral detection of fireblight (Jarolmasjed et al., 2019) and Huanglongbing in citrus orchards (Sankaran et al., 2013). Additionally, tractor-mounted sensors can measure tree area (Polo et al., 2009) and enable the real-time adjustment of pesticide applications alongside Variable Rate Spray (VRS) technology (Berk et al., 2020). One key issue with tractor-based platforms is the negative impact on image quality from vehicle vibrations or visibility reduction from pesticide spray and vehicle emissions. However, tractor-based platforms remain a potential option for low-cost crop monitoring, utilising systems readily available to apple growers.

Field scanning platforms provide a mobile acquisition method that can be automated for crop sensing with high levels of precision and reliable positioning for continual, precise monitoring of crop stress. These systems support heavy payloads, enabling them to carry numerous high-resolution sensors, including RGB, hyperspectral, fluorescence, thermal, and 3D imaging sensors. The automation capabilities of these platforms allow for continuous monitoring of crop stress.

Notable examples include the Rothamsted Field Scanalyzer (Lemnatec GmbH) (Virlet et al., 2016) and the Field Phenotyping Platform at ETH Zurich (Kirchgessner et al., 2017), which have been valuable for phenotyping studies in field crops. However, due to their expensive infrastructure, these systems are typically employed only for high-investment phenotyping studies. These systems have been designed for use with arable crops, and their implementation for monitoring tree crops would be challenging. Despite their strong capabilities for early stress detection, they are unsuitable for practical application in monitoring disease in current commercial orchards.

Fixed towers operate similarly to tractor booms but are stationary, enabling continuous monitoring and reducing noise from vibrations. The permanency of fixed towers would necessitate multiple units to achieve full coverage in an orchard, which can be costly and potentially disruptive to other orchard management activities. The cost, coverage, and resolution of towers depend on their height, but their design supports high weights and power requirements, allowing for fine spatial resolutions. Fixed sensing towers can monitor fine spatial and temporal variations in crops to inform site-specific management (Ahamed et al., 2012). They facilitate phenotyping with a spatial and/or temporal resolution that surpasses what traditional UGV and airborne approaches can achieve and can operate continuously (Shafiekhani et al., 2017). Although these fixed towers require significant infrastructure investments and the use of multiple sensors throughout orchards, they do offer an optimal trade-off between widespread coverage and high resolution.

The main limitations of ground-based sensors include the extended time required for monitoring single orchards and the challenges in standardising image acquisition due to plot size, soil compaction, and vibrations from motors or uneven terrain surfaces. Ground-based sensors also face difficulties in transportation between locations and may not be capable of generating real-time surface maps or measuring plant parameters from multiple trees simultaneously (Sankaran, 2015). Despite these limitations, ground-based systems offer significant advantages. They can support high-quality sensors with higher power requirements, facilitating real-time classification and even treatment applications due to their increased weight capacity, which further supports the use of advanced computational hardware.

2.5.3 Aerial Sensing Platforms

Airborne platforms offer significant advantages over ground-based sensing by enabling rapid coverage of large areas, facilitating swift management decisions. Unmanned Aerial Vehicles (UAVs), also known as drones or unmanned aerial systems, have become increasingly employed as remote sensing platforms for near-ground agricultural observations. UAVs are the most commonly used platform to acquire RGB and multispectral imagery for disease detection studies in fruit crops. These platforms have been successfully used to detect diseases in apples (Jarolmasjed et al., 2019; Chandel et al., 2021), citrus (Garcia-Ruiz et al., 2013; Abdulridha, 2019), pears (Schoofs et al., 2020; Bagheri et al., 2020), and grapes (Albetis et al., 2017). The most commonly used categories of UAVs include multi-rotor (rotocopters), fixed-wing, hybrid UAVs, and unmanned helicopters (Zhang & Zhu, 2023). Other types, such as parachute and blimp UAVs, are also available (Chawade et al., 2019). Multi-rotor UAVs are preferable due to their ability to hover and provide improved control, allowing for higher-quality data acquisition with better resolution and reduced blurring compared to fixed-wing UAVs, which can be affected by their speed (Sankaran et al., 2015). Several factors should be considered when selecting a UAV for agricultural applications, including platform stability, autonomy, battery resources, and operational altitude range (Barbedo, 2019b). Minimum operational heights are often determined by flight regulations, which can result in pixel sizes unsuitable for leaf disease detection (Stöcker et al., 2017; Barbedo, 2019b). Additionally, UAV systems have limitations in payload capacity and power supply, which can restrict the feasibility of using high-quality sensors and lenses or multiple sensing systems simultaneously. Despite these limitations, the integration of UAV systems into mainstream agricultural operations presents a significant opportunity for the remote sensing of crop diseases. UAV technology is now well-developed, making it a viable option for the widespread implementation of remote sensing-based disease monitoring in orchards.

2.5.4 Platform Selection

Ultimately, there is a trade-off between a platform's ability to acquire high-resolution imagery for detecting early symptoms of infections and its capability to monitor orchards rapidly, providing accurate assessments of the location and severity of infections. Currently, UAV systems offer the greatest opportunity for monitoring disease. These systems are modest in price, easy to operate, widely used, and capable of automating imaging routines. However, UAV systems face weight, power, and legal restrictions that may affect imaging capabilities (Duggal et al., 2016). Therefore,

it is essential to identify systems that are lightweight yet capable of capturing fine spatial resolution features on leaves. Alternatively, handheld operation remains the most readily applicable method, with the advantage of human dexterity allowing for the earliest possible detection and real-time identification of diseases on apple trees. Despite this, handheld methods are labour-intensive and may not significantly improve orchard coverage compared to traditional scouting methodologies. There is still a significant level of research required to transition remote sensing systems from controlled environments to practical field applications for the early detection of disease in apple orchards. While selecting an appropriate platform at this stage might be of low priority, understanding the best method of acquisition will aid in the selection, design, and development of optimal remote sensing systems

2.6 Potentiality and Practicalities of Remote Sensing for Disease Monitoring

2.6.1 Recommendations for Remote Sensing System Technologies and Opportunities for Further Research

An operational system that rapidly covers an orchard and precisely maps disease before epidemics spread could facilitate reactive pesticide application, resulting in significant chemical savings. The ability to detect and quantify apple scab, the most significant apple disease, would offer the greatest immediate benefit to apple production. Despite extensive research demonstrating early detection of apple scab using hyperspectral and thermal imagery, these systems have proven challenging to implement in real-world orchard conditions. It is imperative to investigate the feasibility of using other sensors to detect early signs of apple scab stress in uncontrolled, non-laboratory environments. RGB imagery has shown considerable potential for detecting apple scab infections in real-world environments; however, early detection remains challenging, particularly for high-throughput monitoring. Multispectral sensors have successfully been used in real-world environments to detect plant pathogens but have yet to be applied specifically to apple scab infections. Further research into the potential of multispectral imaging for the early detection of apple scab is recommended.

Deep learning CNN classification techniques have been successful in diagnosing multiple diseases in apple orchards. These models have primarily been applied to RGB images acquired from handheld devices, capturing information on apple disease symptoms in mature stages of

infection. There is considerable potential for utilising CNNs for widespread, automated classification and severity estimation of apple disease imagery from remotely sensed systems. For effective classification of apple scab infections, CNNs must identify apple scab symptoms from early to late stages of infection and from low to high severities (Figure 2.13). Additionally, they must distinguish these features from other plant pathogens present in real-world orchards under natural illumination conditions. Once the capabilities of early detection and classification of apple scab infections are proven, they can be applied to commercial orchards. UAV systems show the greatest promise for the regular, automated monitoring of orchards, necessitating the design of remote sensing systems capable of apple scab detection at high spatial resolutions. In the meantime, handheld and fixed platform acquisitions can be employed to assess feasibility and develop sensor designs for practical testing and trials of imaging and classification systems.

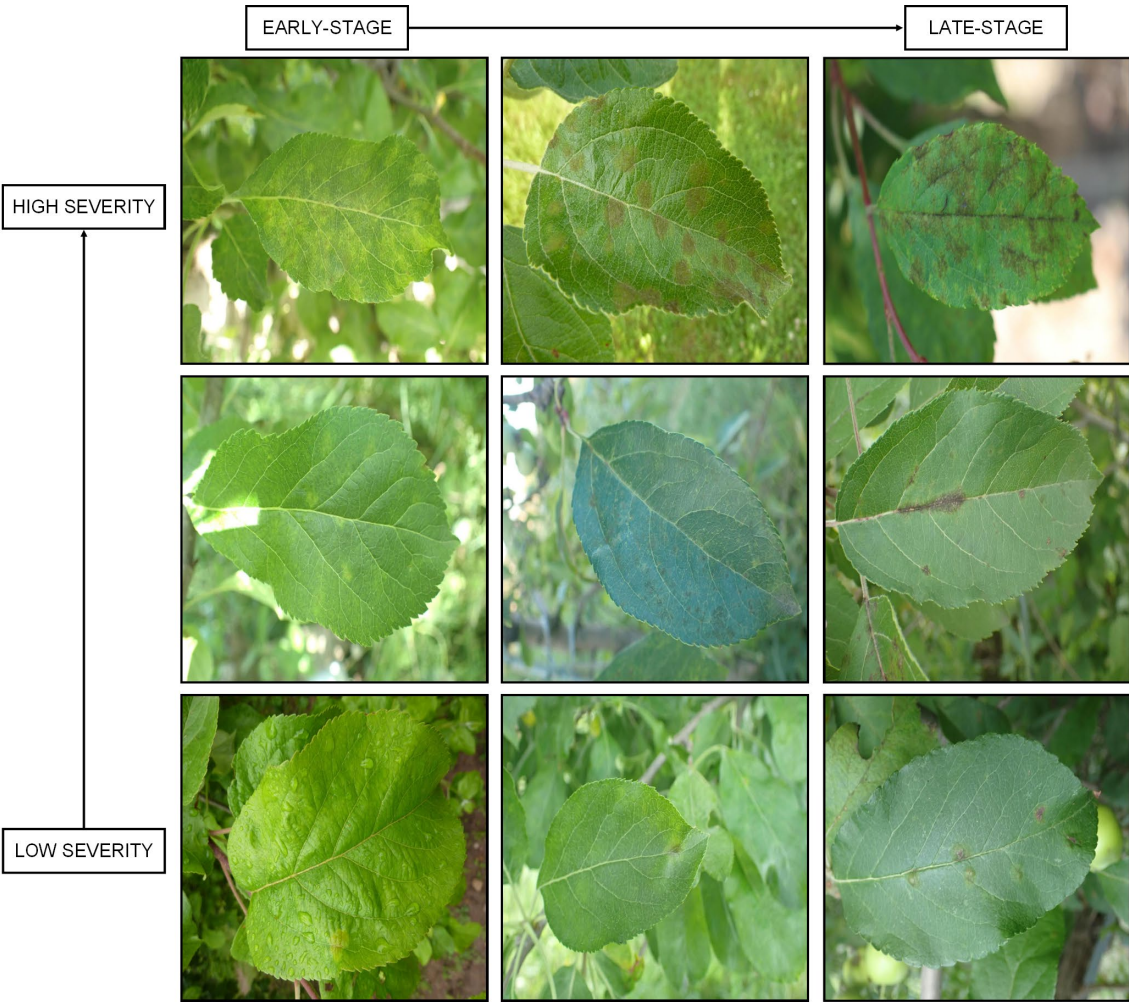


Figure 2.13 Apple scab symptom variation with stage and severity (adapted from Thapa et al., 2021)

2.6.2 Practical Considerations for Orchard Use

The complex and heterogeneous outdoor environments of orchards make the early detection of plant diseases extremely challenging. Both extrinsic and intrinsic factors of plant disease imagery significantly impact the accuracy of plant disease classification (Barbedo, 2019a). Extrinsic factors arise from physical issues encountered while acquiring imagery in uncontrolled environments (Figure 2.14). These include the presence of shadows, solar illumination angle, specular lighting, and bidirectional reflectance distribution function, all of which can affect reflectance values and vegetation indices. Aerial image capture can cause occlusions and shadows due to overlaying branches and leaves, masking regions of interest (Barbedo, 2013; Bock et al., 2020). The influence of these extrinsic factors can be reduced by optimising the acquisition platform and timing of monitoring, thereby improving classification accuracies.

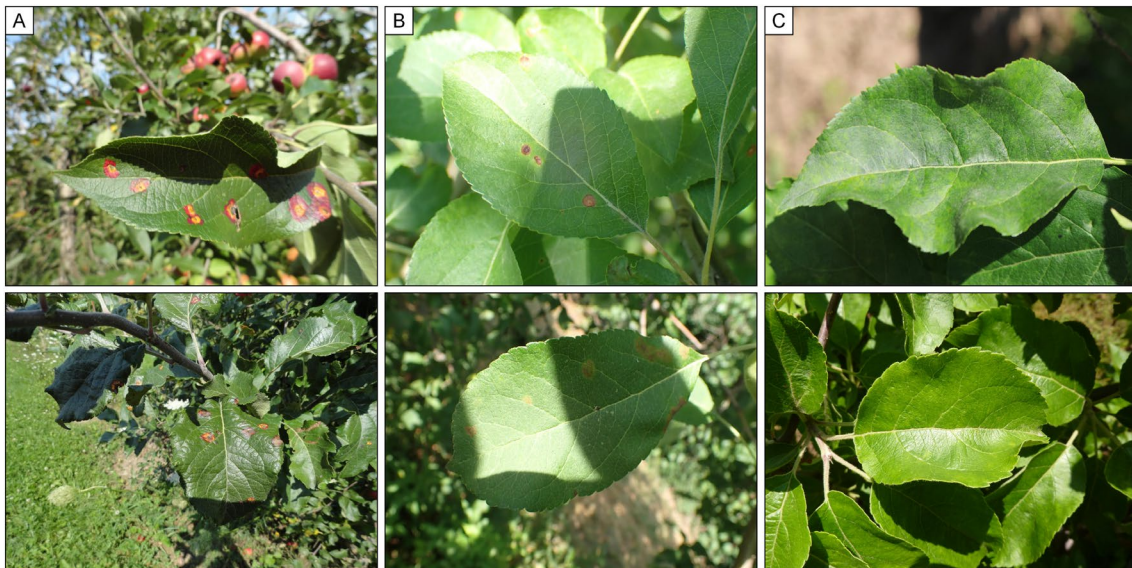


Figure 2.14 Extrinsic factors influencing accurate disease classification. Column A) Presence of strong shadows. Column B) Strong illumination and specular lighting. Column C) Occlusion of leaves by overlaying foliage. (Adapted from Thapa et al., 2021)

Intrinsic factors are more difficult to control as they result from the inherent variability of symptom presence within agricultural environments (Barbedo et al, 2016). There are three major intrinsic factors that can impact the accurate diagnosis of plant diseases (Figure 2.15). Firstly, a single disease can produce a wide range of symptoms depending on the phenological stage of the leaf or pathogen. Secondly, many pathogens and stress causes result in similar symptom expressions, increasing the difficulty in identifying the causative factor. Finally, multiple diseases are often present simultaneously, with symptoms of several diseases displaying on individual leaves. Classification models must be capable of accurately diagnosing individual apple diseases under these circumstances. Utilising highly varied apple disease

training datasets containing annotated images of a range of symptom expressions can enable CNNs to effectively generalise across the multitude of symptom displays (Thapa et al., 2020). Additionally, CNNs can employ a multi-label classification method to identify the component diseases in leaves exhibiting multiple symptoms (Ji et al., 2020).

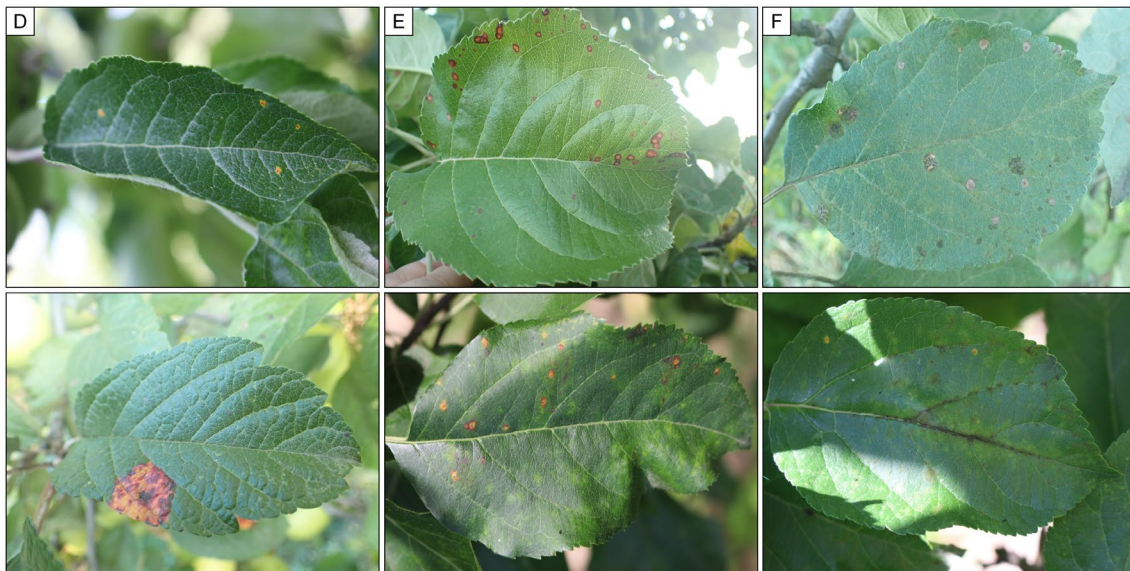


Figure 2.15 Intrinsic factors influencing accurate disease classification. Column D) Differing symptom presence from the same pathogen. Column E) Similar symptom presence from differing pathogens. Column F) Multiple pathogens present on individual leaves (adapted from Thapa et al., 2021)

2.6.3 Prospective Applications of Disease Monitoring Systems

The majority of the studies reviewed in this chapter employed remote sensors in controlled environments, primarily for phenotyping purposes. Phenotyping is a critical component of crop improvement, assessing the relative effects of genetic and environmental factors, as well as their interaction, on production traits such as yield potential and stress tolerance (Fiorani & Schurr, 2013; Sankaran et al., 2015). Remote sensors are highly effective for phenotyping as they enable non-destructive monitoring of plant parameters, thereby increasing experimental capacity for different genotypes and treatments by reducing the need for replicate sampling sets (Fahlgren et al., 2015; Araus & Kefauver, 2018). Numerous repetitions with varying genotypes and treatments must often be evaluated, considering both morphological and physiological plant traits, which increases the complexity and dimensionality of the data produced (Chawade et al., 2019). Information on plant stress tolerance gathered through these methods can be instrumental in breeding disease-resistant cultivars of apples (Papp et al., 2020). Given the controlled environmental conditions in phenotyping studies, remote sensing applications have been notably successful compared to the time-consuming visual assessments of disease (Mahlein, 2016).

For precision agriculture purposes, large-scale monitoring and timely plant protection measures are essential. Utilising an effective combination of sensors, classification models, and platforms can facilitate automated, rapid monitoring of orchards, providing a viable alternative or supplementary method to the labour-intensive traditional crop scouting. This approach enhances the implementation of Integrated Pest Management (IPM) strategies. Precise and accurate disease estimates are crucial for predicting yield loss and forecasting epidemics. An accurate understanding of disease incidence allows growers to estimate yields, inform labour needs, and assess the risk of storage rots to determine optimal marketing times. Disease forecasting models, such as ADEM (Xu & Butt, 1995; Berri & Xu, 2003) and RIMPro (Aćimović & Rosenberger, 2019), issue warnings to growers about the risks of apple scab, powdery mildew, European canker, and fireblight, enabling timely fungicide applications. These models rely on meteorological information, cultivar susceptibility, and regional inoculum levels to forecast disease risk (MacHardy, 2000). Providing more objective assessments of disease severity in orchards can improve the accuracy of these models' disease risk predictions.

The ultimate aim of an orchard monitoring system is to reduce pesticide use through site-specific application. Integrating remote sensing systems with Variable Rate Spray (VRS) technologies (Maghsoudi et al., 2014; Berk et al., 2020) can enable real-time adjustments of pesticide applications based on disease incidence and severity. The benefits of implementing a precision agriculture-based approach to disease monitoring are threefold. First, it can improve the economic cost-efficiency of apple disease management, especially for major diseases such as apple scab. Targeted pesticide application can significantly reduce input costs while maintaining or improving disease control. The site-specific precise application of pesticides minimises pesticide wastage, reducing overall expenditure on chemicals. Second, reducing pesticide use will have widespread benefits for ecosystems surrounding commercial orchards. Excessive pesticide application in orchards has contaminated surrounding soil and water bodies. Judicious use of pesticides reduces the contamination effects on these ecosystems due to excessive chemical runoff. Finally, a precision management approach to disease control aims to reduce crop losses, thereby increasing marketable yields. Accurate and timely detection of diseases can prevent the spread of infections, leading to higher fruit quality and yield quantity. Achieving increased yields through efficient and effective pesticide use would significantly contribute to the sustainable intensification of agriculture.

2.7 Conclusion

Remote sensors, classification models, and acquisition platforms are key precision agriculture technologies that offer the potential to improve disease monitoring in orchards compared to traditional labour-intensive crop scouting techniques. These technologies can be used for the early detection, identification, and quantification of plant pathogen infections in orchards, informing targeted pesticide spraying and other Integrated Pest Management (IPM) strategies. Despite considerable research into the use of different remote sensing technologies for apple disease detection, there have yet to be practical applications capable of commercial use. This review is the first to collate previous research on these precision agriculture technologies specifically for apple disease detection. It presents the requirements for disease monitoring in orchards, the current use of sensors, classification models, and acquisition platforms for apple monitoring, and recommendations for further research.

This review identified numerous options for early detection, including thermal and fluorescence imaging, with hyperspectral sensing being the most widely implemented for early apple disease detection. However, all these early detection studies were successful in part due to the controlled environmental and acquisition conditions in which they were performed. For practical application in orchards, remote sensors must demonstrate effectiveness in real-world conditions. Apple scab is largely considered to be the most important apple disease, receiving the largest quantities of fungicides. Developing a remote sensing strategy for apple scab monitoring would provide the most widespread benefit. Thermography has considerable potential for presymptomatic stress detection due to apple scab but may have difficulty operating under the influence of natural illumination and weather conditions. RGB imagery and multispectral imagery have been widely applied to numerous apple and other tree crop diseases, but the latter has seen limited investigation into its potential for apple scab detection.

While many methods of classifying diseases are available, deep-learning CNNs show the greatest promise for rapid, accurate identification tasks. They consistently demonstrate high classification accuracies when classifying apple diseases in laboratory and orchard conditions. Although several datasets are publicly available, they are mostly focused on RGB imagery of individual leaves displaying late-stage symptoms. Further research is needed to evaluate the accuracies of different sensors and to classify apple diseases in the early stages of infection. To achieve this, a large dataset must be collected. Acquisition platforms will be essential for implementation in orchards, providing adequate coverage while simultaneously offering high resolution to identify the smallest symptoms. UAVs have the greatest potential for orchard-wide surveys, but handheld devices may be the most readily available for use by crop scouts.

While there are many solutions available for research in laboratories, the technologies must also be scalable to orchards and demonstrate effectiveness in real-world environments. CNN models and UAVs are currently available solutions that have successfully been applied at scale for acquiring and classifying remotely sensed imagery for stress detection in field and orchard crops. The key limiting factor is the use of an appropriate imaging sensor. As it stands, only RGB imagery and multispectral imagery show potential for practical implementation in commercial orchards, but the latter has attracted notably little research for apple scab detection. It is recommended that future research investigates the capabilities of multispectral imaging systems for the early detection of apple diseases, specifically apple scab, in real-world conditions. The early detection of apple scab in orchards is challenging due to the variety of symptom variations, natural illumination conditions, tree physiologies, and other stress factors. Enabling early detection through multispectral imaging can improve the efficiency of disease control in apple orchards and reduce losses due to diseases. This review offers a step toward developing a precision agriculture approach to the sustainable intensification of apple production, improving the environmental impacts and increasing yields in commercial apple orchards.

3 Feasibility of Detecting Apple Scab Infections using Low-Cost Sensors and Interpreting Radiation Interactions with Scab Lesions

Abstract

Apple scab is a major crop disease caused by the fungus *Venturia inaequalis*. Apple scab can spread rapidly throughout orchards, diminishing tree productivity and causing huge losses in marketable fruit. Efficient orchard reconnaissance and early detection of infections can inform fungicide applications for effective disease control, and a range of new low-cost sensors offer a means of imaging orchards as the basis for scab detection. This study evaluates the potential contribution of three imaging devices: a multispectral (VIS-NIR), thermal, and 3D camera for detecting apple scab on young apple plants. In a controlled experiment, apple seedlings were infected with apple scab, and disease progression was imaged daily under natural illumination conditions in a glasshouse with minimal image processing. Whilst the thermal and 3D imaging was deemed unsuitable for scab detection, the high-resolution multispectral imagery was exceptionally effective, specifically the near-infrared (NIR) band (800-1000 nm). NIR imagery permitted the earliest scab detection due to the substantially lower reflectance of the fungal structures of *V. inaequalis* relative to healthy leaf tissue. Due to the novelty of multispectral imaging for scab detection, this chapter offers a model of near-infrared radiation interactions between the pathogen and leaf to explain the reflectance characteristics of scab lesions throughout the growth cycle of the pathogen. The simple, low-cost remote sensing approach developed here holds considerable promise for providing timely information on tree infection to improve the efficiency of apple scab disease management routines.

3.1 Introduction

Apple scab is considered the most important disease facing apple production due to the high disease susceptibility of most popular cultivars, widespread presence, and the economic cost of control (MacHardy et al., 2001). Epidemics of apple scab rapidly spread throughout orchards causing huge losses of marketable fruit and long-term reductions in tree productivity. The pathogen occurs in all commercial growing regions, with the most devastating effects occurring in countries with cool, moist springs and high summer rainfall (MacHardy, 1996). Current disease protection methods require abundant preventative fungicide applications that have a significant effect on production costs and negative impacts on the ecology, environment, and human health surrounding orchards (Papp et al., 2020). Responsive infection control strategies, informed by early detection of the presence of pathogens, could potentially reduce fungicide use significantly as part of an integrated pest management strategy (MacHardy, 2000). Detecting apple scab infection on leaves early, before the disease becomes infectious, could improve the efficiency of chemical treatment strategies through the timely application of curative fungicides and reduce crop losses. This smart farming strategy could lessen the economic and environmental impacts of scab treatment over current approaches.

The lifecycle and epidemiology of apple scab is well-defined. Apple scab, caused by the ascomycete fungus *V. inaequalis*, begins its lifecycle overwintering in leaf litter as ascospore-containing pseudothecia, which are responsible for the primary infection phase (Figure 3.1). Rainfall and the presence of sunlight promote the ejection of ascospores from the pseudothecia, which are spread by wind to trees up to 200 metres away (Belete & Boyraz, 2017). Germination occurs when ascospores land on young leaf tissue and penetrate through the cuticle via germ tubes, with high humidity and free water on the leaf surface required for germination (Bowen et al., 2011). Temperature determines the hours of continuous leaf wetness required before germination occurs, known as the Mill's infection period (MacHardy & Gadoury, 1989; Stensvand et al., 1997). In spring, the lower surfaces of leaves are the first to become exposed, with the first scab symptoms developing here. Once leaves are fully unfurled, symptoms appear on both the abaxial (lower) and adaxial (upper) surfaces. No penetration of the epidermal cell layer occurs. Instead, the pathogen develops subcuticular runner hyphae from the germ tubes, and melanoproteins create a nutrient transport system that diverts solute flow towards the site of infection (Delalieux et al., 2007; Jha et al., 2009). Sexual reproduction of *V. inaequalis* occurs within this subcuticular space as the hyphae develop into stromata, producing dense accumulations of conidia. As the conidia mature, they penetrate through the cuticle and become exposed, to then be released by rain and splash-dispersed to surrounding leaves and fruits.

Infection by splash dispersal acts as a secondary infection cycle that repeats until the end of the growing season (Bowen et al., 2011).

Young leaves are most susceptible to secondary infection, becoming more resistant as they mature until the cuticle cracks and the leaf is susceptible again. Once the fungus ruptures the cuticle, the disease symptoms become visible macroscopically. The thick mass of conidia gives lesions a velvety texture, and the melanin pigments contained within cells produce a distinctive olive-brown colour (Oerke et al., 2011). The diffuse, circular lesions that develop on the upper surface increase in size, raise and darken as the infection matures, ultimately leading to leaf senescence. Fruits are extremely vulnerable to scab after petal fall, especially during long, warm periods of high humidity. Symptomatic olive-brown lesions occur on the apple fruit skin that grow, darken, and coalesce, eventually developing a corky texture as both pathogen and apple flesh become necrotic. Symptoms occasionally occur on shoots as light-brown swellings or reddish-brown spots but are rarely scouted for in disease assessments (MacHardy, 1996). These visible symptoms provide the basis for apple scab diagnosis by agronomists.

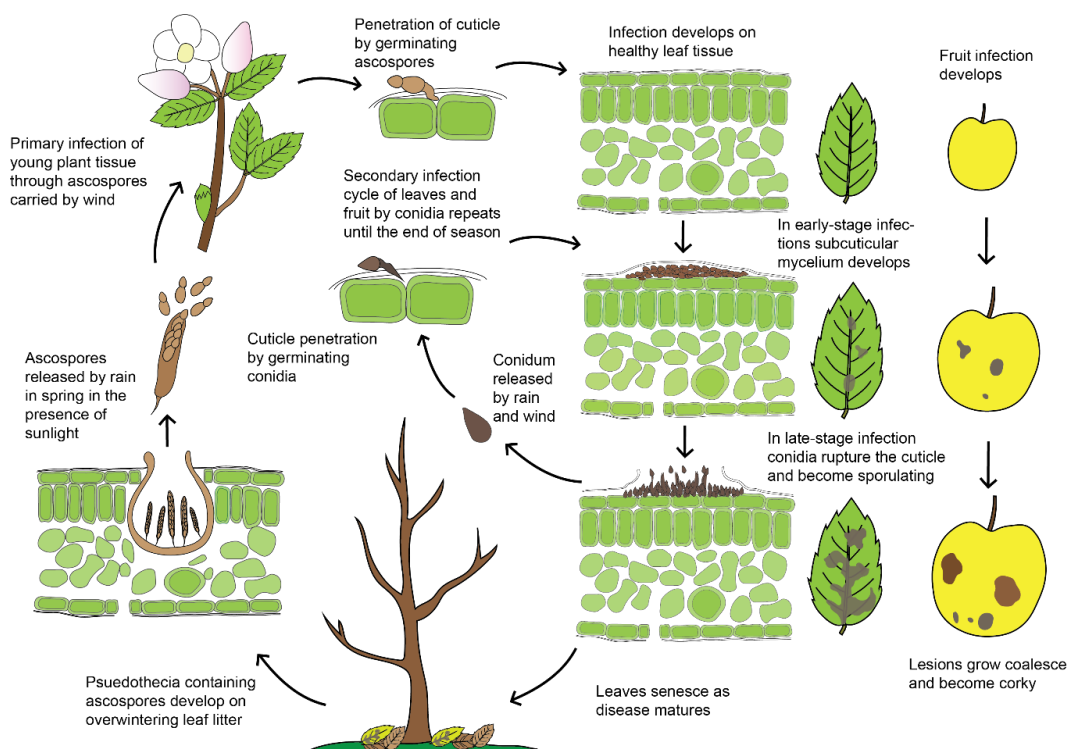


Figure 3.1 The lifecycle of the hemibiotrophic fungus *V. inaequalis* on apple trees.

Several studies have utilised remote sensing systems for the detection of apple scab on young plants, based not only on the visible symptoms but also the effect on the spectral and thermal properties of leaves to diagnose early infection. Delalieux et al. (2007) demonstrated that spectroscopy could detect scab infection early before the onset of visible symptoms through

variations in the reflectance characteristics of leaves and their impact on ratio indices. Shortwave infrared wavebands associated with water content between 1350–1750 nm and 2200–2500 nm could distinguish infected and non-infected leaves at an early stage, especially as a ratio index (R_{1480}/R_{2135}) (Delalieux et al., 2009b). The chlorophyll-related Pigment Specific Simple Ratio (PSSRa = R_{800}/R_{680}) (Blackburn, 1998a) was also capable of detecting scab at a later stage of infection. Hyperspectral sensing can be effective at detecting apple scab disease early through the stress response of plants although their utility for orchard use is challenged by their high costs, complex acquisition requirements, and large volumes of data produced.

Thermographic imaging of leaves infected with *V. inaequalis* displayed concentric spots of lower leaf temperature 1 to 3 days before the appearance of visible scab symptoms due to increased rates of leaf transpiration (Oerke et al., 2011). Areas of decreased leaf temperature exceeded that of the scab lesions by up to 80% when the first symptoms became visible, which indicated that the extent of infection and scab colonisation greatly exceeded the macroscopic lesion size. Another strong indication of stress from leaf infection was the maximum temperature difference across a single leaf, which would be expected to remain homogenous across healthy leaf tissue, with higher differences occurring where the transpiration rate was affected due to lesions. Measurements of maximum temperature difference are a well-established method for determining leaf infections (Lindenthal et al., 2005; Oerke et al., 2006; Jafari et al., 2017). A major drawback of these thermal imaging methods is the lack of diagnostic potential, as many biotic and abiotic stress factors display similar effects on transpiration (Oerke et al., 2011). A further study of scab infection found thermal sensing to be effective at displaying symptoms earlier than that of fluorescence imagery (Belin et al., 2013). Infected leaves showed a decrease in Photosystem II quantum efficiency, but this is similar to that of young leaves, and the protocols required for fluorescence imaging are unsuitable for use on tree crops (Delalieux et al., 2009a). 3D imaging has been used in past research as a way of segmenting thermal images, which can be difficult to distinguish from backgrounds, to detect scab, as well as to determine leaf curvature, orientation and growth rate that are all affected by scab infection (Chéné et al., 2012). There has been no further research into the use of 3D sensors for apple scab detection in plants, likely due to the limited structural influence of scab on young plants and the negligible height of lesions on leaves in the early stages of infection.

While the initial research demonstrated the potential for the early pre-visual detection of apple scab in controlled laboratory settings, further progress towards operational techniques has stalled, likely due to the requirements for specialist equipment. The previous examples of spectrometry, thermography and fluorescence imagery are unsuited for detecting disease on

leaves in complex orchard settings because they need controlled illumination sources, complex optics and computational hardware that increase the bulk and power necessary to run such systems (Lopez-Ruiz et al., 2017). Such sensors are also expensive and delicate, and they require significant training to acquire and analyse data, making them unlikely to achieve widespread adoption as a solution in real-world orchards. However, there have been numerous breakthroughs in low-cost sensors used for plant phenotyping over the past decade, including thermal imaging (Acorsi et al., 2020; Vagelas et al., 2021), 3D imaging (Vit & Shani, 2018; Paulus et al., 2014) and multispectral sensing (Kitić et al., 2019). These low-cost sensors are lightweight and designed for ease of use and may lend themselves to imaging in orchard environments. In this context, the simultaneous deployment of many low-cost sensors has enabled the scaling up of measurements to facilitate the rapid imaging of large numbers of plants.

Off-the-shelf systems for low-cost thermal and 3D imaging are readily available from suppliers, whereas finding a low-cost spectral imager is more challenging. Hyperspectral cameras (Behmann et al., 2018) and multispectral cameras used in agriculture and research, including Parrot Sequoia+ and MicaSense RedEdge, exist (Assman et al., 2018), yet these systems cost £1,000s, and they are primarily designed only for use with UAV systems which further increases costs. A well-established method in plant phenotyping is to convert digital cameras into visible and near-infrared sensitive (VIS-NIR) cameras, as their CCD and CMOS sensors can detect wavelengths between 400-1000 nm (Verhoeven, 2008; LeBourgouis et al., 2008; Morales et al., 2020). These systems do not compute radiance data as calibrated reflectance values, but they do provide high-resolution near-infrared imagery that can display features through monochromatic brightness values. In general, commercially available digital RGB (red-green-blue) cameras are low-cost, lightweight, durable sensing systems designed for ease of use. These cheap, high-resolution camera systems could provide greater benefits than current expensive, low-resolution, off-the-shelf multispectral cameras for detecting apple scab.

A low-cost sensing approach holds promise for establishing a practical method for the widespread survey of orchard trees for scab infections. As the first stage in developing this method, this study evaluated a range of low-cost (below £1,000) sensors for the early detection of apple scab under natural illumination conditions. Apple seedlings were artificially inoculated with *V. inaequalis* before images were acquired daily using a novel, low-cost, high-resolution multispectral (RGB, red-edge and NIR wavebands), thermal and 3D cameras. Images were visually interpreted for symptoms to track disease development throughout the experiment. The purpose of this paper is to provide descriptive evaluation on the suitability for each individual sensor to detect apple scab from the early to late stages of infection. The use of the high-

resolution multispectral camera is a novelty for the detection of scab infection, and so the physical processes underpinning the results will be discussed. The overall aim is to determine which low-cost sensors display the potential for the early scab detection in apple orchards.

3.2 Methodology

3.2.1 Plant Material and Inoculation

Young apple plants were propagated from the seeds of the economically important and highly susceptible cultivars of Gala and Braeburn in an uncontrolled glasshouse at Lancaster University (Lancaster, UK) that simulated the natural illumination environment of an orchard. A total of 45 seedlings were grown in individual, uniform 500 ml pots filled with young plant compost containing slow-release fertiliser and irrigated when required. All plants had been actively growing for three months and contained at least four unfurled leaves. Seedlings were selected as test subjects due to the simplicity of their structures and their lack of exposure to other potential sources of stress and infection. The young plants were artificially inoculated with apple scab in order to image daily from the known point of infection. *V. inaequalis* is well-suited to artificial inoculation, and standard practice is to use conidia as these spores are abundant, easy to harvest and prepare, and suspend well in water, unlike ascospores (Moore, 1964). An amalgamation of techniques was used to develop a novel, low-cost, in-situ inoculation method.

Inoculum was gathered from infected leaves in commercial orchards of Jazz and Jonagold varieties in Herefordshire (UK) during October 2020. Infected samples were identified by assessing leaves that contained freshly sporulating lesions, which correlated to those in the literature and orchard production guides (MacHardy, 1996). Harvested leaves were placed in a paper bag to minimise condensation and frozen at -20 °C in a sealed container, a common method of storing scab conidia (Szkolnik, 1978). The inoculum suspension was produced by shredding 20 infected leaves, mixing with 100 ml of distilled water and shaking vigorously, a method adapted from disc-cutting methods by Barbara et al. (2008) and Xu et al. (2008). An application of 5 ml of vegetable juice was added to help stimulate the fungal growth (Szkolnik, 1978). The suspension was then immediately applied to leaves, which avoided the need to germinate spores on agar plates. Two methods of inoculum application were trialled.

The first round of experiments utilised a drip method with a pipette, as used by Oerke et al. (2011), to produce scab lesions in precise locations that could help indicate if infection spread to other leaves. However, this method caused excessive runoff down the midrib of leaves,

displacing most of the inoculum applied and resulted in development on only 2 of the initial 20 plants with a bias towards development along the midrib. The second method applied inoculum via an atomiser, with inoculum evenly sprayed across all leaves until their surfaces were saturated (Delalieux et al., 2007). The spray method proved more successful, with 17 of the remaining 25 plants developing infections. Each pot was individually covered with a transparent polythene bag to maintain a high humidity that promoted germination (Xu et al., 2008). They were then carefully transferred to a warm, dark room, avoiding displacement of the inoculum from the leaves, and incubated for 48 hours. After the incubation period, each pot was transferred to the glasshouse, where illumination, temperature and relative humidity were left uncontrolled. The environmental conditions recorded within the experimental glasshouse are provided in Appendix A.

3.2.2 Low-Cost Sensing Setup

3.2.2.1 *Multispectral Camera Setup*

Multispectral imaging was achieved using two co-aligned Raspberry Pi-based CMOS sensors with the infrared-cut filter removed from one (Figure 3.2). Each sensor was fitted with a 16 mm telephoto lens and was capable of capturing 12.3 MP images with a 1.55 μm pixel pitch. This setup provided high-resolution sensing with adjustable focus and aperture. External bandpass filters (Midwest Optical Systems, Palatine, USA) covering the red-edge band (680-720 nm) and NIR band (800-1000 nm) were fitted to the sensors so that the multispectral camera system delivered RGB, red-edge and NIR wavebands. Both sensors were operated through a Raspberry Pi Compute Module 4 and I/O Board (Raspberry Pi Foundation, Cambridge, UK), which enabled simultaneous dual-camera image acquisition. The approximate cost of the setup was £500.

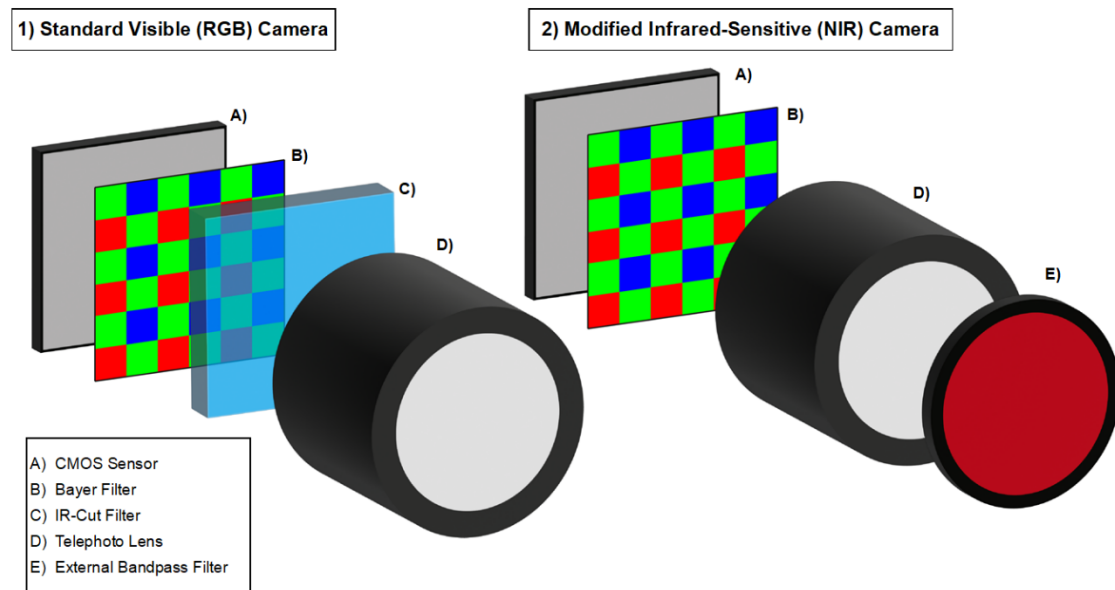


Figure 3.2 Low-cost, high-resolution stereoscopic multispectral camera

3.2.2.2 Thermal Camera Setup

Thermal and 3D imagery was acquired using cheap, off-the-shelf options. Thermal images were acquired with a CAT S60 smartphone featuring a FLIR lepton sensor (FLIR Systems, Inc., Wilsonville, USA), with a spectral sensitivity of 8-14 μm and a thermal sensitivity of 50 mK. The cost of the CAT S60 smartphone was approximately £299.

3.2.2.3 3D Camera Setup

3D data was acquired with an Intel Realsense d435i stereoscopic camera (Intel Corporation, Santa Clara, USA) which processed a 3D model from dual NIR imagery aided by structured NIR light at a cost of £299, although this does not include the computational hardware required to acquire imagery, which would increase the price-point. 3D point clouds had an RGB texture overlay generated by the onboard camera to provide a true colour model.

3.2.2.4 Acquisition Procedure

All three imaging systems were fixed to a variable friction arm and clamped to a platform directly above the imaging surface for nadir-view imagery (Figure 3.3). The multispectral camera and 3D sensors were positioned 750 mm above the imaging surface, and due to differences in field-of-view, resolution and focal length, the thermal camera was positioned 300 mm above the surface. While this arrangement of sensors led to different imaging geometries between sensors, this was acceptable for the purposes of this study, where precise image co-

registration was not required. The images from the three sensors were ultimately interpreted manually rather than through a quantitative procedure. Moreover, this variability in geometry is similar to that anticipated when using an array of different sensors in the field setting for operational scab detection. Images were taken between 11 am and 3 pm from 7-35 days post inoculation (d.p.i.) After both sets of experiments, over 9000 images were taken from multispectral, thermal and 3D cameras. Information on the camera specifications and acquisition methods of the imaging system are displayed in Table 3.1



A	B	C	D	E	F
Raspberry Pi CM4	RGB Camera	VIS-NIR Camera with External Bandpass filter	Intel RealSense D435i Stereoscopic 3D Camera	CAT S60 with FLIR Lepton Thermal Camera	Variable Friction Arm

Figure 3.3 Low-cost image acquisition setup consisting of a multispectral camera, thermal camera, and 3D imager on a variable friction arm

Imaging System	Multispectral Camera	Thermal Camera	3D Camera
Spatial Resolution	4056 x 3050 pixels	80 x 60 pixels	848 x 480 pixels
Field of View	45° x 34°	46° x 36°	87° x 58°
Approximate Cost	£500	£300	£299
Image format	JPEG	JPEG	PLY
Acquisition Software	Linux (Raspberry Pi OS)	MyFLIR	Intel RealSense Viewer

Table 3.1 Low-cost camera specifications

3.2.3 Disease Assessment

Apple scab incidence and severity were assessed through visual interpretation of the seedling images by a single trained individual to maintain consistency. Diagnosis of apple scab was based on the symptoms listed in the Penn State Tree Fruit Production (Crassweller et al., 2020), and in the works of MacHardy (1996). This method of manual interpretation of symptoms is equivalent to scouting performed by agronomists as a ground-truth. Disease severity was graded on an ordinal scale, a widely-used descriptive method of classifying disease based on the intensity of symptoms present (Bock et al., 2010).

The symptoms to be observed were derived from the production guides and previous literature that used sensors to detect apple scab. The multispectral images were checked for spatial variability in reflectance intensity in Adobe Photoshop Software (Adobe Inc., San Jose, USA). Thermal images were searched in FLIR Tools for regions of localised cooling. Models acquired through 3D imaging were assessed for signs of deformation and stunting of leaves and to determine the span of leaves and plants to the nearest 5 mm in the open-source software MeshLab.

Each image was examined alongside a corresponding RGB image where scab could be identified based on the colour, shape, and texture of lesions. Disease progression was assessed retrospectively from the most recent to the oldest images, which allowed scab infections to be traced back to the initial location with greater accuracy. Infection severity was assessed daily using an ordinal scale (Figure 3.4). Early detection of apple scab was taken to mean detection of lesions before they become sporulating, in terms of the ordinal scale provided, this is at stages of low severity and earlier.






Asymptotic	No symptoms		Moderate Severity	Multiple larger lesions on multiple leaves	
Initial Symptoms	Small lesion on a single leaf		High Severity	Extensive disease with most leaf surfaces infected with scab	
Low Severity	Small lesions across multiple leaves				

Figure 3.4 Ordinal scale of categorical apple scab infection severities and example RGB imagery.

3.3 Results

3.3.1 Multispectral Imagery

Preliminary observations revealed that high-resolution multispectral images had by far the greatest potential for detecting scab at any stage. NIR imagery, in particular, displayed symptoms of scab earlier, clearer and to a greater extent than any other image type. Symptoms in the NIR band were characterised by dark lesions contrasted against asymptomatic leaf tissue of high brightness. Although similar symptoms could be observed in red-edge images, they were much less pronounced, likely due to the narrower spectral bandwidth than the NIR, which allowed less light to enter the sensor (Figure 3.5). Reflectance in the red-edge was also influenced by pigment concentrations unrelated to scab. For the remainder of this section of the paper, to demonstrate the ability of low-cost multispectral imagery to provide information on scab infection, only multispectral NIR band images will be compared against RGB, which are representative of the view of a human observer.

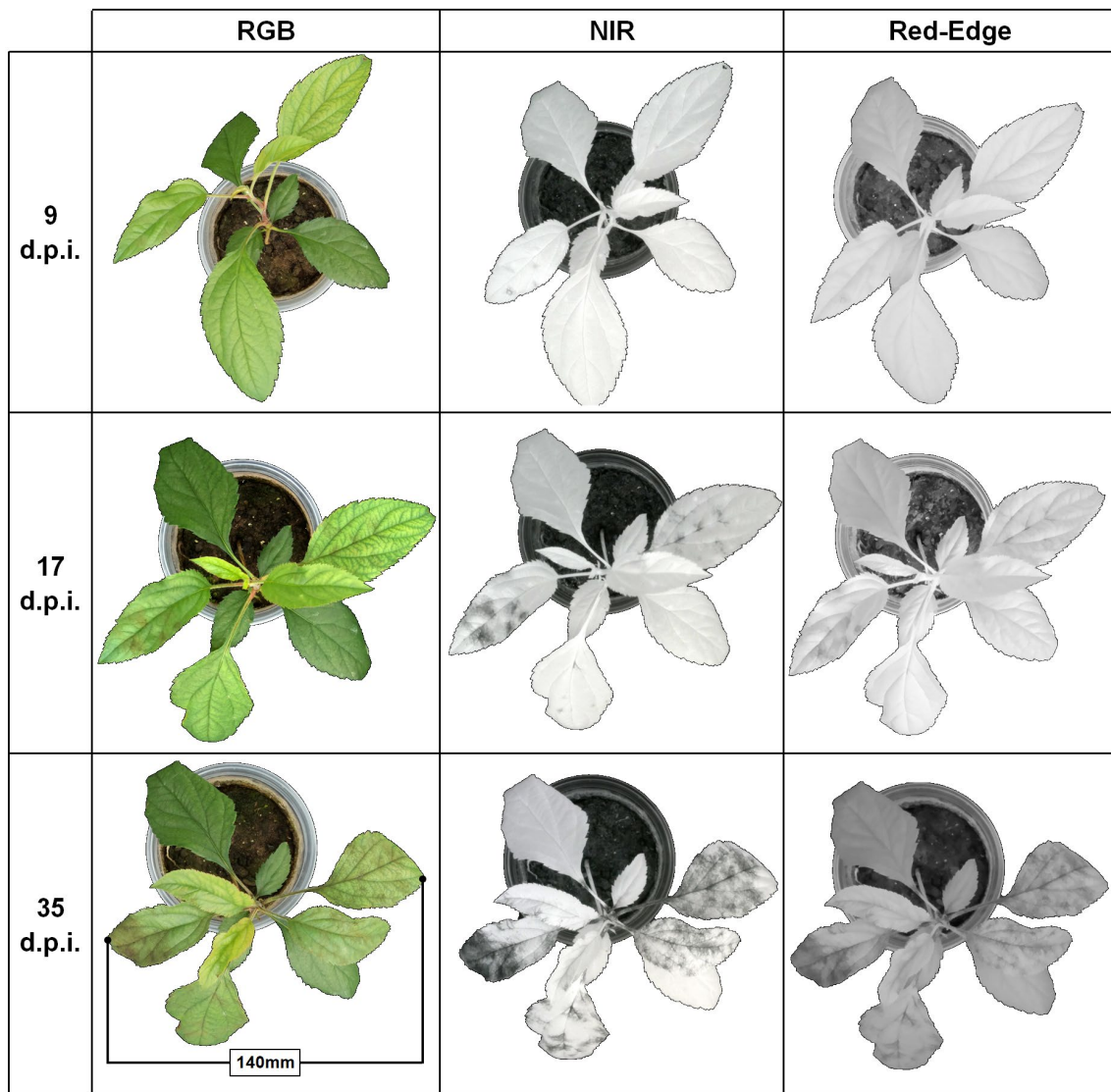


Figure 3.5 The progression of apple scab from low to severe infection in RGB, NIR and red-edge imagery over the experiment with imagery acquired at 9 (low severity), 17 (moderate severity), and 35 (high severity) days past inoculation (d.p.i.).

The NIR imagery provided information based on pixel brightness that was sensitive to scab symptoms from initial symptoms to high-severity infections. Infected tissue had a much lower brightness than healthy tissue, making it easy to locate scab infections and distinguish them from other leaf features. At the initial symptom stage, infection points were difficult to identify visually through RGB imagery, appearing as small, dark-green points along leaf veins roughly two weeks after inoculation. Infection sites would have been difficult to distinguish without contextual information of infection sites from the time series and cross-referencing between multispectral image types. This allowed lesion growth to be tracked backwards from late-stage infections to the initial sites of infection (Figure 3.6). Initial symptoms would remain as small points for several days after first detection until rapid growth would occur, indicating that the lesions were sporulating. It was at this stage of moderate severity that infection could be identified by the naked eye if inspected, but the determination of size and location of lesions was

still challenging with RGB imagery. An example of the full-time series imagery for a plant sample is provided in Appendix D.

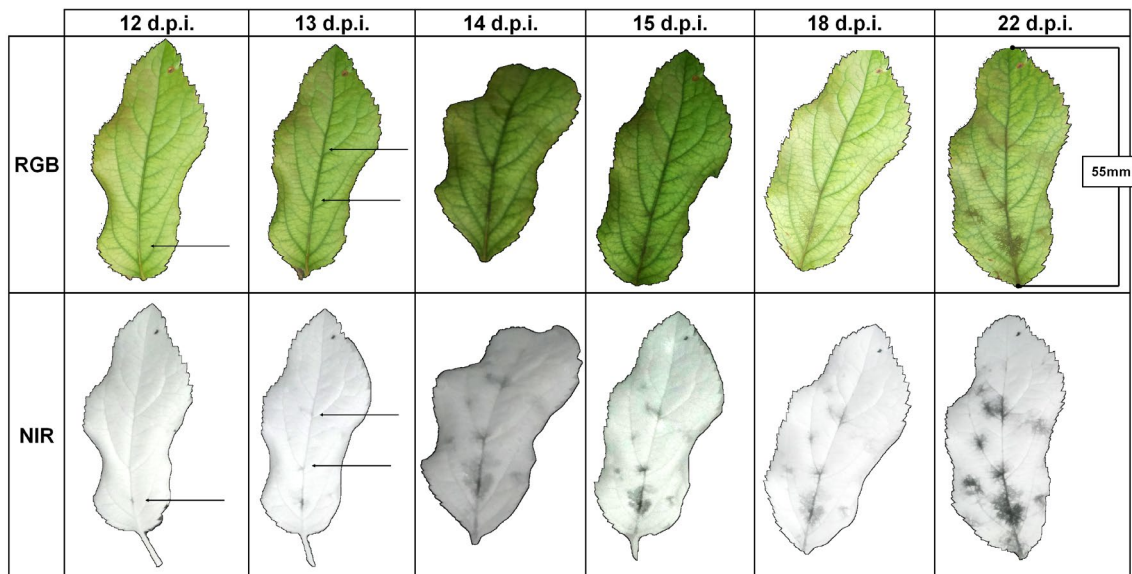


Figure 3.6 The progression of apple scab symptoms on a single leaf from initial symptoms at 12 d.p.i. to moderate severity at 22 d.p.i. Arrows indicate initial infection locations identified through retrospective analysis.

The high-resolution multispectral imagery provided great levels of detail on the colour, shape, and texture features of scab lesions on leaves and their development throughout disease progression (Figure 3.7). Symptomatic lesions at low severity were small, light-brown, circular, and with a fuzzy texture with clearly separate points of origin. When focusing on the full pixel resolution, the circular lesions appeared more diffuse, expanding from a central point along a main vein in a web-like pattern and growing along venules with green leaf tissue visible in between. The lack of contrast between olive lesions and green tissue, and diffuse borders made it difficult to determine the extent of lesions without image enhancement. In mature infections the network of fungal structures broadened, leaving little-to-no green tissue visible within lesions. As the mass of mycelium increased in mature lesions, they developed dark-brown and grey colours (Figure 3.5). The symptoms discussed were clearly detectable in otherwise healthy leaves, but in leaves that had suffered damage due to abnormally high glasshouse temperatures that resulted in brown, necrotic tissue, it was more difficult to determine scab lesion location and extent (Figure 3.8, Figure 3.9, and Figure 3.10).

NIR imagery was sensitive to scab infection from pre-visual symptoms to late-stage infections. In the early stages of infection, apple scab can be observed as a dark point along the midrib or vein of a leaf, three to six days before it is detectable in RGB. The central point of infection had a significantly lower pixel brightness than the diffuse edges, where the fungal structures are at their least dense (Figure 3.7). Symptomatic fungal structures appeared similar to those in RGB imagery but were more defined and covered a greater proportion of leaf tissue. Throughout the visual assessment of disease severity, NIR imagery would consistently rank infections at a higher severity than that of RGB images on the same day. Large areas of asymptomatic tissue remained within infected leaves, and no subcuticular mycelium was detectable in both RGB and NIR imagery. As scab lesions grew and merged, over half of the leaf tissue would display fungal symptoms and eventually begin to senesce due to the stress caused by the disease.

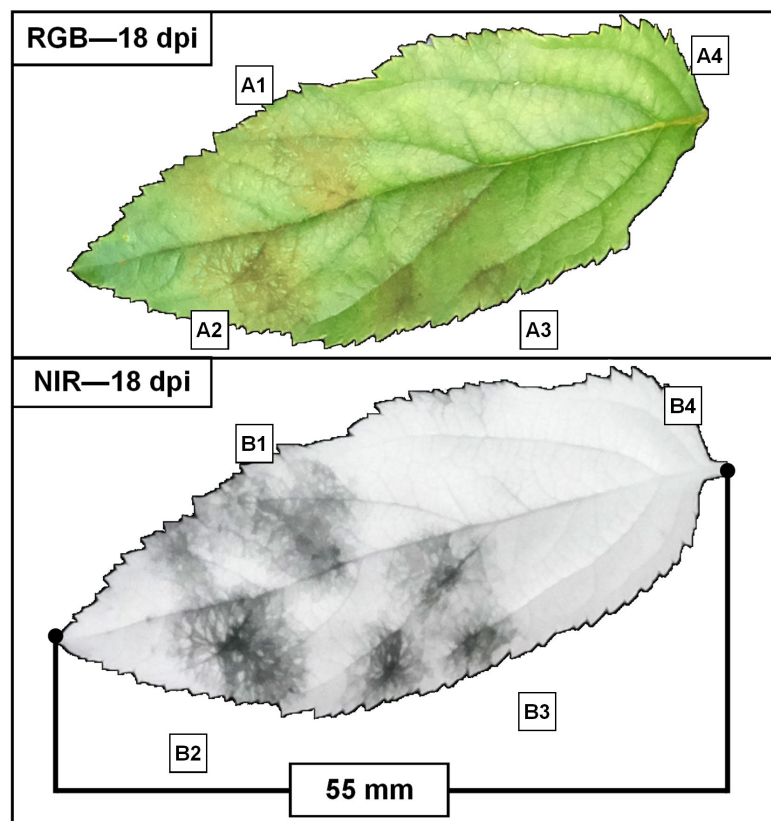


Figure 3.7 A single apple leaf with moderate-severity infection in A) RGB and B) NIR imagery at 18 days post inoculation. Features labelled include: 1) mature coalesced lesions, 2) large circular lesions growing along venules, 3) small lesions with individual points of infection on main veins 4) asymptomatic leaf tissue

The ambient light environment had a major impact on the visibility of scab lesions on leaves in NIR imagery and, to a lesser extent, RGB (Figure 3.8). Early detection of apple scab infection was easiest to detect under shade or cloud cover on bright days as this gave the largest contrast between healthy and infected tissue and the greatest detail on leaf features as colour and texture information. Overcast days were also useful as light was diffuse so healthy, and infected tissue

could be clearly determined. Under stormy conditions, less light reached the plants, resulting in dimmer images with lower levels of detail (Figure 3.8). Direct sunlight was a major challenge; specular light reflected from the leaf surface which reduced the detail of the leaf texture in both RGB and NIR imagery, making it difficult to detect lesions underneath. Shadows cast across leaves also increased the difficulty of identifying scab lesions due to the reduced contrast between dark lesions and dark leaf tissue. Disease severity assessments of leaves under direct sunlight may be incorrectly attributed as having a lower severity compared to the same leaves imaged under shade earlier in the time series.

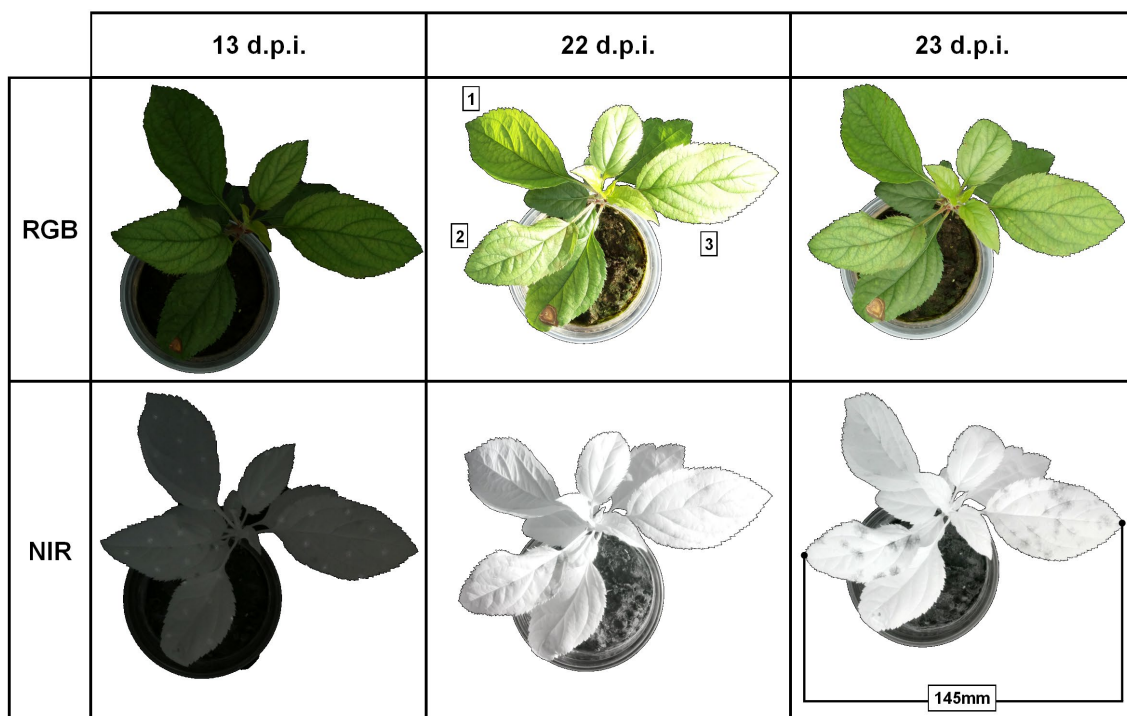


Figure 3.8 Influence of ambient light environment on the perception of scab. Irradiance was measured at 13 d.p.i. as 0.048 kW/m^2 , at 22 d.p.i. as 0.353 kW/m^2 , and at 23 d.p.i. as 0.149 kW/m^2 . Observe the influence of shadow on infected leaf 1, and specular light on infected leaves 2 and 3. Bright spots in NIR imagery at 13 d.p.i. are an artefact from the NIR structured light from the 3D camera.

3.3.2 Thermal Imagery

The early detection of apple scab from thermal imagery was inconclusive due to the difficulty in distinguishing temperature changes from the plants stress response against external environmental influences of sunlight. In optimal imaging conditions of diffuse light, thermal infrared emission measured regions of cooling by $1\text{-}2 \text{ }^\circ\text{C}$ in regions where scab symptoms were developing, although this could only be identified by using multispectral images to locate infected regions beforehand (Figure 3.9). Temperature variance due to leaf stress was often significantly lower than compared to regions that were influenced by shading, direct sunlight, and the background material (Figure 3.10). Furthermore, the thermograms were low resolution

and compression into JPEG format further degrading image quality. The coarser image resolution for thermography compared to multispectral imagery, made it extremely difficult to detect symptoms, especially during the early stages of infection when spatial temperature variations are small. Acquiring higher-resolution thermal imagery for the specified low-cost price-point was unachievable.

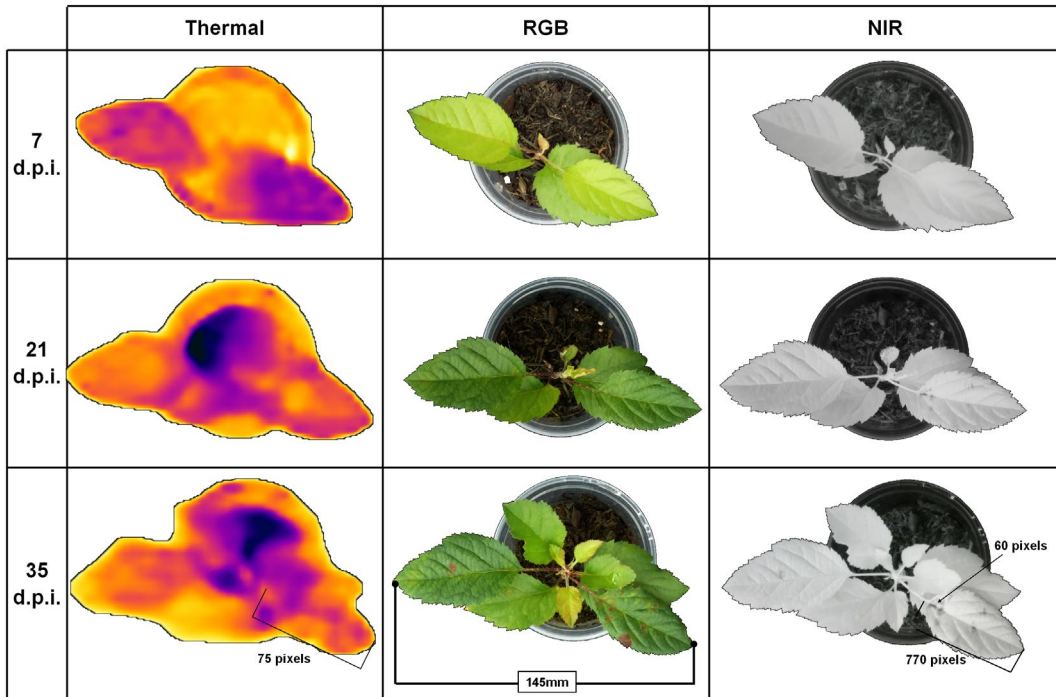
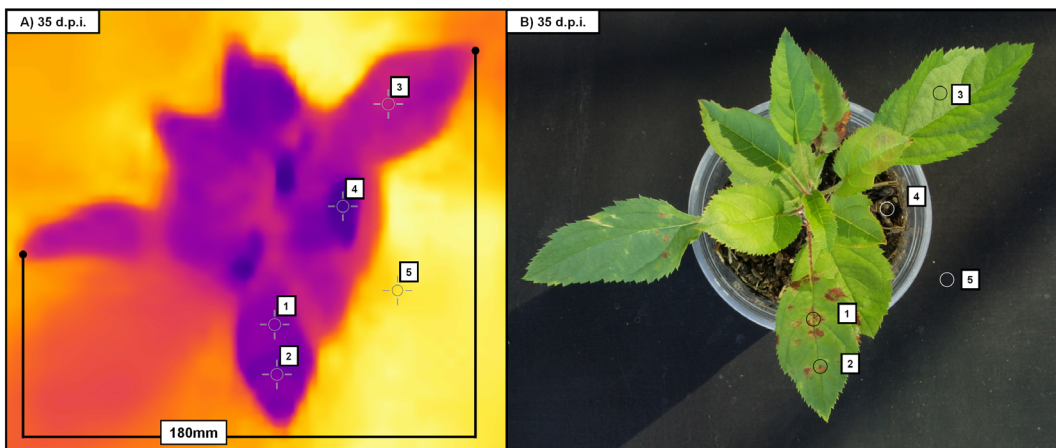


Figure 3.9 Progression of apple scab infection in Thermal, RGB and NIR imagery over a 28-day period from 7 d.p.i. to 35 d.p.i.. Length of leaf in pixels from base to tip of a 50 mm leaf, and diameter of a 4 mm scab lesion included to highlight difference in image resolution between thermal and multispectral systems.



Label	Feature	Temperature °C
1	Fungal structure on leaf	29.5
2	Infected green leaf tissue	29.5
3	Healthy leaf (in sun)	30.6
4	Potting soil	28.0
5	Imaging surface	33.7

Figure 3.10 Temperature variation across different features of a A) thermogram and corresponding B) RGB

3.3.3 3D Imagery

The results of 3D modelling of young plants were mixed. During the early stages of infection, there were no discernible changes to plant architecture or leaf structure that would indicate scab infection. In some cases of severe infection leaf deformation occurred after 50% of the surface was covered with fungal symptoms. Symptomatic lesions could be observed in the RGB texture overlays of the point clouds, but as with thermal imaging, the low resolution provided little benefit (Figure 3.11). There were several artefacts commonly observed in the 3D models that affected the model quality, which was attributed to the coarse depth resolution. An NIR texture overlay could be registered to the generated point cloud at finer depth measurements, which helped improve model quality. The 3D imaging did not provide the ability to detect scab infections at the early stages but did provide a benefit as a supplementary sensor for measuring the sizes of leaves and lesions during assessment.

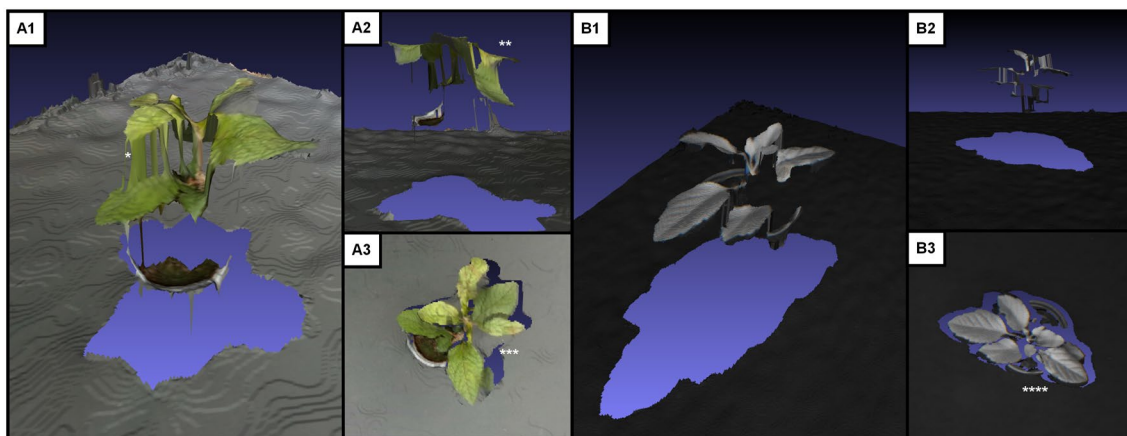


Figure 3.11 3D models of young apple plants with an A) RGB texture overlay and B) NIR texture overlay observed from 1) isometric viewpoints, 2) side viewpoints 3) top-down viewpoints. Artefacts labelled include *overlay stretching between different depths, ** flattening of plant height, *** incorrect background depth between leaves, **** gaps in models due to shadowing from leaves

Overall, the results clearly demonstrated that multispectral imaging is the superior method to thermal and 3D imaging for detecting apple scab from early to late stages through subjective visual interpretation. Of the three multispectral bands used, NIR-based imagery displayed the greatest promise for detecting scab lesions on young plants at early stages under natural illumination. Low-cost thermal imaging did not provide suitable data and is not recommended for further use for early detection of disease in real-world conditions. There may still be potential for 3D imaging to aid research in developing a scab detection system by acting as an ancillary technology supporting multispectral assessment through generating 3D models and spatial measurements of plants, leaves, and lesions, but it cannot be used alone to detect early symptoms of scab, only at late stages of the disease through the onboard RGB and NIR cameras.

3.4 Discussion

3.4.1 Radiation Interaction with Scab Lesions

Reflectance characteristics of leaves in the VIS-NIR range show the greatest potential for detecting scab infection on apple plants. The visible domain is where the light-absorbing pigments, specifically chlorophyll in the palisade cells, have the greatest influence on healthy leaf tissue reflectance. The melanin pigments in conidia have low reflectance in blue wavelengths, increasing exponentially towards red, giving a brown-coloured reflection. This colour does not contrast significantly against the chlorophyll in green leaf tissue, making it difficult to differentiate early symptoms from leaf tissue at early stages and to determine the extent of scab lesions in later stages.

In healthy leaves, only a small fraction of NIR radiation is absorbed by cells, with the majority being reflected back through the upper surface or transmitted down through the leaf (Woolley, 1971). Multiple scattering of photons causes reflectance to be much greater than the reflectance of visible light, where absorption of pigments results in single scattering processes (Ustin & Jacquemoud, 2020). The reflectance of NIR light in leaves is determined by the internal cellular structure, especially in the spongy mesophyll layer at the cell membrane and air interfaces where light is reflected and refracted (Gausman & Allen, 1973). NIR reflectance increases with an increase in number of intercellular air spaces because light is scattered in passing from hydrated cell walls with a higher refractive index than that of intercellular air and is much less likely to be absorbed (Allen et al., 1970). In scab lesions the dense accumulation of subcuticular conidia has a significantly lower volume of air cavities than the mesophyll layer that reduces the penetration into the spongy mesophyll of the leaf and instead interacts with the subcuticular matter. Lesions contain masses of individual cells where near-infrared light undergoes similar cell wall interactions and scattering. Unlike the spongy mesophyll layer, there is little intercellular air space, increasing the likelihood of scattered light being absorbed within the conidia (Curran, 1989). The scattering and absorption of NIR light results in little radiation being reflected up through the surface and appears as regions of low brightness in NIR imagery and reduced transmission through to the mesophyll layers (Figure 3.12). The symptoms visible in NIR imagery are a result of the fungal structures themselves reducing reflection rather than a physio-chemical plant response to disease as *V. inaequalis* does not penetrate the epidermal layer or damage underlying cells in a way that would affect mesophyll layer structure (Bowen et al., 2011; MacHardy, 1996). Due to the novelty of the method and the limited research on the

absorbance, reflectance, and refractive characteristics of phytopathogenic fungi at NIR wavelengths, further study into the interactions of *V. inaequalis* with NIR radiation is recommended

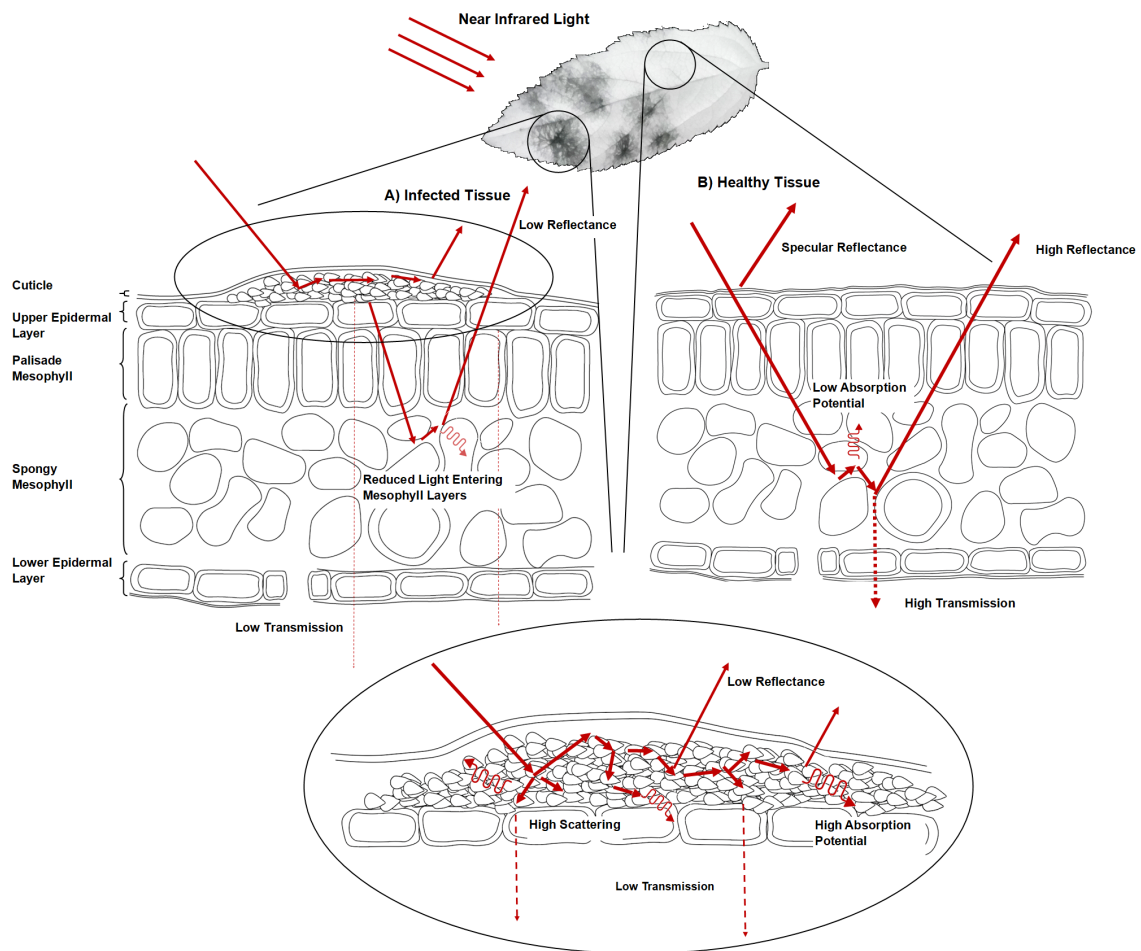


Figure 3.12 Interaction of NIR light with infected and asymptomatic leaf cross-sections

3.4.2 Apple Foliar Sensing Requirements

Only high-resolution multispectral imagery from converted digital cameras was found to be effective at detecting scab on seedlings from initial symptoms to high-severity infections. Low-cost thermal imagery was less effective despite well-documented research into leaf temperature changes caused by scab (Oerke et al., 2011) and other fungal diseases (Lindenthal et al., 2005; Jafari et al., 2017). Previous experiments were performed under controlled environmental and illumination conditions, using expensive, specialist equipment that could accurately measure temperature changes at a higher spatial resolution than the FLIR lepton. While these studies provide useful insights into the thermal properties and transpiration of scab-infected plants, it would not be feasible to implement them in commercial orchards for early disease detection. The low resolution and major influence of sunlight on the results would create major challenges

when imaging adult trees from a greater distance, further influenced by weather and other stress factors. Furthermore, proprietary software was required for advanced analysis of the FLIR thermal images, which restricted the ability to determine maximum temperature difference features in this study. If developments in thermography technologies further reduce the price of thermal imaging cameras with high resolutions, there may be scope to review the recommendation for use in certain circumstances. 3D imagery had not previously been utilised in the detection of scab based on deformation scab indices on leaves but had been used as an ancillary technology to aid the segmentation of leaves (Chéné et al., 2012) and to provide point clouds for 3D spectral modelling. There may still be potential for 3D sensors as an ancillary technology in tree-level scales, where models can be acquired from a greater distance. Although the Intel RealSense was selected based on the recommendations of outdoor use by Vit & Shani, (2018), other methods may be found to be more suitable, and as with thermal imaging further developments in the near future may improve the feasibility of use. Of the three low-cost sensors applied for early detection of apple scab, high-resolution multispectral imaging has the greatest potential for successful application in commercial orchards.

3.4.3 Directions for Future Research

Modifying digital cameras can open disease detection up to growers of small and large orchards in both developed and developing nations as they are cheap, robust and easy to operate. The concept of converting RGB cameras into multispectral imaging systems would work for most commercial digital cameras but not all have the adaptability of the Raspberry Pi based system. One important factor to consider is the image resolution, as scab symptoms are several millimetres in diameter which can be challenging when using imagery acquired from a platform at a distance from trees. Another key factor is adequate control over the exposure settings that affect brightness, focus and clarity. The influence of specular reflectance of solar radiation has been significant detriment to thermal and 3D and has been shown to degrade clarity in multispectral images, this problem can be mitigated by reducing the light reaching the sensor through shorter shutter speeds and smaller apertures. Similarly control of focus is important and maintaining an appropriate shutter speed to achieve maximum detail in an image. In this experiment no post-processing took place as images were saved as JPEGs. Post-processing of RAW imagery could also help mitigate the effects of sunlight and shade in detecting scab symptoms on leaves. Automating the image acquisition process is necessary in order to capture data across orchards for disease detection rapidly and having a multispectral camera operating remotely and automatically adjust settings based on environmental conditions would achieve this.

A limitation of this study is the labour-intensive and subjective nature of severity ranking. Whilst appropriate at the current stage of comparing different sensing technologies, for larger trials on mature trees, a more objective approach of ranking disease severity based on the percentage of tissue infected would be preferable. Using machine learning rather than manual estimations can improve the objectivity of results. Several studies have devoted research to using RGB images from consumer cameras to identify apple scab and other diseases accurately in complex environments using machine learning (Chandel, et al., 2021; Jarolmasjed et al., 2019) and by extension deep learning methods (Chao et al., 2020; Jiang et al., 2019; Liu et al., 2017; Zhong & Zhao, 2020). Using machine learning to automate the identification, classification and quantification of apple scab could improve labour costs in data analysis to complement the low-cost sensors for a comprehensive, economical solution to Apple scab detection. To reliably detect scab early would require accurate annotating for training and testing classification models. This study demonstrates the ability of a crop scout to determine scab infection even at early stages of infection. One major challenge of remote sensing for disease detection in crops is the potential for multiple biotic and abiotic stresses to act concurrently upon plants, leading to large variations of symptoms displayed on leaves. Further study into the effect of other biotic and abiotic stresses on leaves and scab lesions would be required to improve classification confidence in real-world detection of apple scab.

3.5 Conclusion

The aim of this research was to identify a suitable low-cost sensing system for detecting apple scab disease on young apple plants. A sensing system consisting of a multispectral, thermal, and 3D camera was constructed to observe *V. inaequalis* progression on infected apple seedlings in a glasshouse. It was demonstrable that low-cost sensing of apple scab through multispectral imaging is not only feasible but ideally suited due to the unique epidemiology of *V. inaequalis*. NIR imagery clearly displayed the extent of fungal structures against the high brightness of asymptomatic leaf tissue, and the high-resolution provided insight into the growth of scab and diagnosis based on shape features. Low-cost thermal images were unsuitable for diagnosing scab at any stage due to the poor resolution, and 3D sensing did not provide significant benefit when used alongside multispectral imaging. This study displays the feasibility for low-cost detection of apple scab through the novel use of VIS-NIR-based multispectral imagery. There is a great scope for this technology to be utilised to improve the efficiency and economics of scab management strategies. To achieve its full potential, multispectral imagery must be scaled up for image acquisition and classification of apple scab on mature apple trees by developing methods of automating image acquisition and analysis.

4 Classifying Early Apple Scab Infections in Multispectral Imagery using Convolutional Neural Networks

Abstract

Multispectral imaging systems combined with deep learning classification models can be cost-effective tools for the early detection of apple scab (*Venturia inaequalis*) disease in commercial orchards. Near-infrared (NIR) imagery can display apple scab symptoms earlier and at a greater severity than visible-spectrum (RGB) imagery. Early apple scab diagnosis based on these NIR images may be automated using deep learning Convolutional Neural Networks (CNNs). CNN models have previously been used to accurately classify a range of apple diseases but have primarily focused on identifying late-stage rather than early-stage detection. This study fine-tunes CNN models to classify apple scab symptoms as they progress from the early to late stages of infection from multispectral (RGB-NIR) time series imagery.

A large Apple Disease Identification (ADID) dataset was created from publicly available, pre-existing disease datasets and a novel multispectral dataset. This ADID dataset contained 29,000 images of infection symptoms across six disease classes. Two CNN models, the lightweight MobileNetV2 and heavyweight EfficientNetV2L, were fine-tuned to identify each disease class in a testing dataset, with performance assessed through metrics derived from confusion matrices. The models achieved overall scab-prediction accuracies of 93.84% and 94.22% for MobileNetV2 and EfficientNetV2L, respectively, but only achieved accuracies of 77.14% and 77.64% for classifying scab within the multispectral imagery. These lower performance scores were attributed to a higher proportion of false-positive scab predictions in the multispectral dataset. Time series analyses revealed that the models could classify apple scab earlier than the manual classification techniques, leading to more false-positive assessments. CNN-based classification could accurately distinguish between healthy and infected samples up to 7 days post-inoculation for NIR imagery.

4.1 Introduction

Rapid and reliable diagnosis of plant pathogens is essential for sustainable disease management within apple orchards. Disease monitoring has traditionally been achieved through crop scouting, with tree health monitored through visual assessments of stress symptoms, followed by recommendations for appropriate disease management (Crassweller et al., 2020). Manual assessments also provide valuable information on inoculum presence for disease forecasting models and are used to evaluate the efficacy of disease management strategies objectively (Berrie & Xu, 2003). Crop scouts require extensive knowledge and training before becoming effective at orchard disease diagnosis; hence, scouting is time-consuming and expensive and fails to provide the coverage or frequency necessary to detect the earliest disease symptoms on trees. Furthermore, crop scouts struggle to diagnose presymptomatic infections, and their subjective decisions may lead to misdiagnoses (Mahlein, 2016; Bock et al., 2020). Orchard monitoring is an essential part of disease management, but the limitations of current strategies prevent the widespread adoption of site-specific control options. As a result, the standard disease control strategy relies on the regular mass spraying of protective pesticides throughout the season in order to limit pathogen germination and spread (Alaphilippe et al., 2013). This chemical-intensive approach has high economic and environmental impacts on commercial orchards and limited effectiveness at controlling the spread once symptoms are present (Simon et al., 2011).

Of all the pathogens that threaten annual apple production, apple scab (*Venturia inaequalis*) has the most significant economic impact. This fungal disease is present worldwide, but the effects are most severe in temperate regions with high rainfall that promotes the initial spreading and germination of the pathogen (MacHardy, 1996). Characteristic symptoms of the disease are the dark lesions that grow on leaves and fruit. Symptoms developing on fruits are the primary source of direct yield loss, although repeat infections of leaves can weaken plants and reduce bud formation limiting tree productivity. The conidia that form these lesions also act as the source of secondary infections throughout the season, making disease control difficult once these lesions form (Jha et al., 2009; Bowen et al., 2011). The polycyclic nature of *V. inaequalis* infections requires an average of 13 repeated fungicidal treatments throughout each growing season (Barbara et al., 2008), with detrimental environmental and economic effects on commercial orchards. This intensive fungicide use has increased the risk of *V. inaequalis* strains developing pesticide resistance (Chatzidimopoulos et al., 2020), reducing the efficacy over subsequent seasons. Disease forecasting models are critical to apple scab management (MacHardy, 2000). Epidemiological models such as ADEM (Berrie & Xu, 2003) and RIMpro (Aćimović & Rosenberger, 2018) require information on weather conditions, varietal susceptibility, and

inoculum levels from manual assessments, in order to forecast disease incidence and infection. These disease-forecasting models can reduce fungicide use by optimising spray timing, yet this can result in increased disease incidence (Berrie & Xu, 2003) or providing excess spray recommendations when unnecessary (Garofalo et al., 2019). Advancements in remote sensing technologies and classification models have made full-scale automated orchard disease monitoring feasible. These technologies have the potential to provide rapid, reliable, and repeatable disease monitoring across whole orchards. Early detection could aid site-specific treatment decisions. Targeted control measures could then be used to reduce pesticide use to reduce the overall economic and environmental impact caused by current fungicide usage while minimising the risk of severe epidemics.

There are numerous examples of remote imaging systems with the potential for early apple scab detection. Thermal imagery acquired in the 5-8 μm range has been shown to detect scab two days before visible symptoms develop, with areas of localised cooling of 1 $^{\circ}\text{C}$ caused by increased transpiration at infection sites (Oerke et al., 2011). These cooler areas extended up to 80% further than scab lesions once symptoms became visible. Other researchers have established reliable early detection through thermography, detecting symptoms up to three days earlier in the 3-5 μm range than in RGB imagery (Belin et al., 2013). However, despite the solid basis of early detection studies, thermal imagery has only been successful at close range under temperature- and illumination-controlled laboratory conditions. External influences of illumination and weather conditions within orchards would cause larger temperature fluctuations across leaves than those caused by varying transpiration rates. Thermal imaging systems have low resolution and can only sense the intra-leaf variability caused by early scab symptoms within proximal distances, limiting their practicality for imaging the many trees within commercial orchards. Bleasdale et al. (2022) demonstrated how multispectral imagery, specifically within the near-infrared waveband, could detect apple scab earlier at a greater sensitivity than RGB imagery under varying illumination levels in uncontrolled environmental conditions. The dark fungal structures of *V. inaequalis* contrast significantly against bright, healthy leaf tissue, even during the early stages of infection. Through manual assessment of the time series, they found that scab could be detected nine days after inoculation, between two to six days earlier than in RGB imagery. The main limitation of this study was the subjectivity and time-consuming nature of the manual classification process, and further research into the use of automated classification techniques on the multispectral dataset was recommended.

Deep learning Convolutional Neural Networks (CNNs) are a class of artificial neural networks popular in plant disease classification studies due to their high performance and limited pre-

processing requirements compared to traditional machine-learning classification methods. A comprehensive review of using CNNs for plant disease identification is presented by Boulent et al. (2019). In recent years, CNNs have been used to classify a variety of apple diseases from traditional RGB datasets (Jiang et al., 2019; Chao et al., 2021), including apple scab infection (Zhong & Zhao, 2020; Kodors et al., 2021; Turkoglu et al., 2022). Each study confirms that CNNs can rapidly classify diseases from images of leaves containing well-established symptoms. Two large apple disease datasets, PlantPathology2020 and PlantPathology2021 (Thapa et al., 2020), have recently provided researchers with many sample images to train CNNs for disease classification. Both datasets contain imagery of diseases at different levels of severity, including early symptoms, and under variable illumination conditions to improve training and allow CNNs to achieve high classification accuracies even under challenging orchard conditions (Yadav et al., 2022). Whilst these studies have shown considerable promise, more research on the ability of CNNs to detect apple diseases at their earliest stages is required as this rapid treatment is critical for appropriate disease management. Using CNNs to classify apple scab in multispectral RGB-NIR imagery could enable the rapid classification of early scab symptoms and be a valuable tool for providing disease incidence assessments.

This study evaluates the ability of CNNs to classify apple scab infection as it progresses from early-stage to large-stage in multispectral (RGB-NIR) imagery. Two pre-trained CNN models, MobileNetV2 and EfficientNetV2L, are fine-tuned and utilised to classify both scab-infected and healthy samples from a previously collected multispectral time series. Both models were trained on multispectral imagery and supplementary data from public sources that contain imagery of apple leaves across six disease classes. A multi-class classification strategy is used to identify scab from plant images containing symptoms under varying illumination conditions and increasing levels of severity. The trained models are validated through a performance analysis of class predictions from public datasets, where images and labels were previously independently verified. A time series analysis of the novel multispectral dataset is performed based on a heatmap of confidence of scab predictions. The differences in performance between the individual RGB and NIR component images are also assessed to determine the differences in capabilities of CNNs to classify apple scab in standard RGB and NIR-based multispectral data. This paper is the first to use CNNs to classify apple diseases using low-cost, high-resolution multispectral imagery and to determine the change in scab-classification capabilities with progression in symptom severity.

4.2 Methodology

This section describes the three main components developed for the study to achieve its aim: the datasets, the CNN models, and the analytical techniques. The first subsection covers the construction of the novel Apple Disease IDentification (ADID) dataset from annotated imagery within public and private datasets. The second subsection discusses the MobileNetV2 and EfficientNetV2L models and the code structure developed for a multi-class classification strategy. The final subsection describes the methods and metrics used to evaluate the overall performance of the models and their ability to predict apple scab from early to late stages in a multispectral time series.

4.2.1 Apple Disease Identification Dataset

4.2.1.1 *Multispectral Dataset Acquisition*

The primary data used in this research was a multispectral time series of images acquired from a previous study on the feasibility of using low-cost sensors for early apple scab detection (Bleasdale et al., 2022). Apple seedlings were grown in a glasshouse at Lancaster University (Lancaster, UK) and artificially infected using an inoculant containing conidia, a suspension of *V. inaequalis*. After incubation, each seedling was individually placed on a black surface and imaged from above from 7-35 days post-inoculation (d.p.i). All imaging occurred within the same glasshouse, where illumination, temperature, and relative humidity remained uncontrolled. Multispectral imagery was achieved by modifying digital cameras to be sensitive to near-infrared (NIR) light (Verhoeven, 2008; LeBourgouis et al., 2008). There were 45 seedlings photographed over the 28 days of the experiment, yielding 2,504 multispectral images at 12.3 MP resolution. The lead author manually classified each image as 'healthy' or 'scab' from the first visible sign of symptoms. The RGB and NIR time series imagery were classified independently, leading to differences in the datasets (Figure 4.1). Minor technical issues resulted in images not being acquired for some seedlings at 11, 17, and 27 d.p.i., coloured grey within the heatmap.

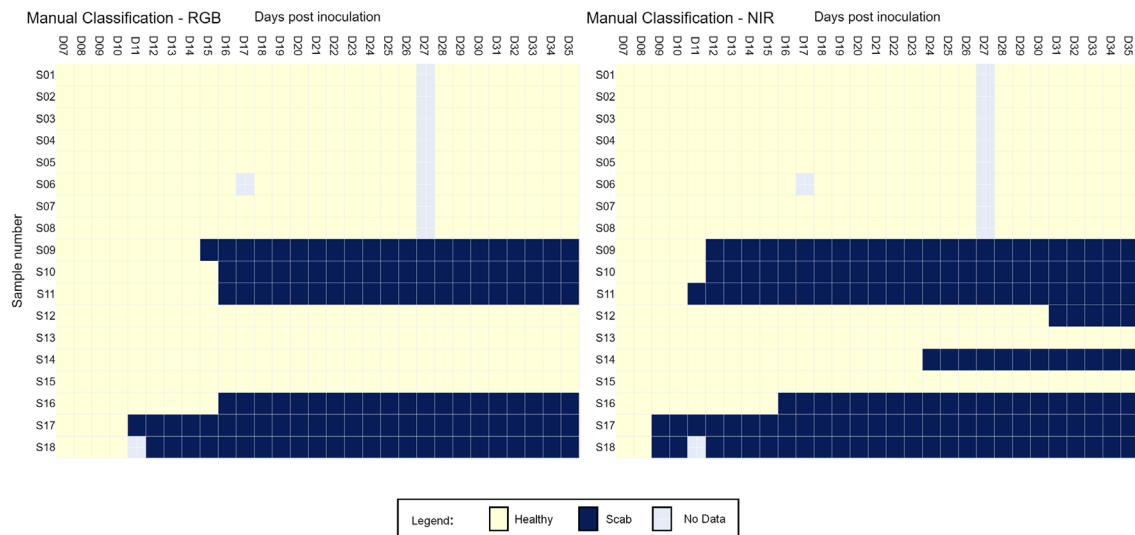


Figure 4.1 Manual classification results of the RGB and NIR time series datasets. Each cell represents a single image.

4.2.1.2 Supplementary Apple Disease Imagery

The primary multispectral dataset was supplemented with secondary publicly available datasets to create a large ADID dataset. CNNs require large, varied training datasets for robust classification under heterogeneous acquisition conditions and intra-class variability (Boulent et al., 2019). The primary multispectral time series contained a small number of samples with similar symptom features and approximately twice as many healthy samples as scab samples. When the size and diversity of the data are limited, CNNs can overfit and produce inaccurate classifications (Alomar et al., 2023). Four additional datasets were therefore incorporated into the ADID dataset: PlantPathology2020 (Thapa et al., 2020), PlantPathology2021 (Yadav et al., 2022), PlantVillage (Hughes & Salathe, 2015; Mohanty et al., 2016), and AppleScabLDs (Kodors et al., 2021). Images from these datasets contained a wide variety of late-stage symptoms that would increase the variance in the training data to minimise the risk of overfitting or bias toward healthy predictions. All the public datasets were downloaded from the Kaggle platform (<https://www.kaggle.com>). The final ADID dataset contained 29,000 images acquired from different RGB sensors with varying illumination effects, leaf backgrounds, and symptom severities (Figure 4.2). All images were resized via compression or expansion techniques to 900 x 1200 pixels.

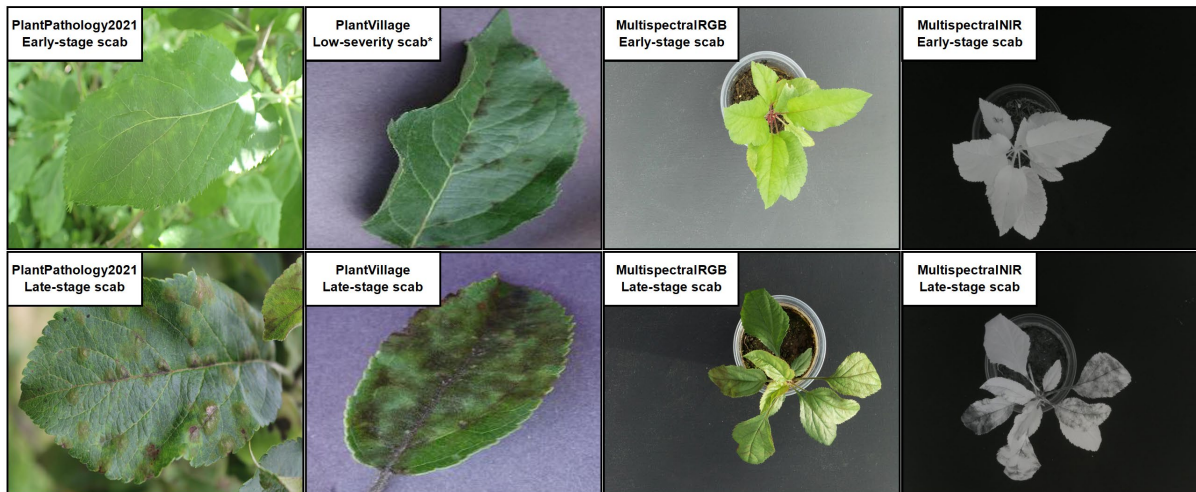


Figure 4.2 Example images of the variation of symptoms in the early and late stages of apple scab infection. *PlantVillage contains only well-established symptoms of scab, although this still includes variations in the stage and severity of lesions.

The ADID dataset contains six classes, including four fungal diseases: frog-eye leaf spot (*Botryosphaeria obtusa*), powdery mildew (*Podosphaera leucotricha*), cedar-apple rust (*Gymnosporangium juniperi-virginianae*) and apple scab (*Venturia inaequalis*), alongside a healthy and a complex class. The healthy class was defined as images showing no symptoms of biotic disease on leaves. The complex class was defined as images containing two or more diseases or symptoms that could not be reliably identified as one of the four fungal diseases. An example of each class is displayed in Figure 4.3. The annotation of images differed between datasets, with lead authors, plant pathologists, and agronomists providing assessments for PlantVillage (Hughes & Salathe, 2015), AppleScabLDs (Kodors et al., 2021), and for both PlantPathology2020 and PlantPathology2021 (Thapa et al., 2020). Two key amendments were made to the original annotations. In PlantPathology2020, the original class ‘multiple_diseases’ was relabelled ‘complex,’ in PlantPathology2021, all images containing two or more classes were also relabelled ‘complex.’ Grammatical formatting was performed to achieve consistent labelling between datasets. No further corrections were made to the annotations made in previous assessments. As the labels had been independently verified, they could be used as an unbiased data source to validate the performance of the model in classifying the test dataset. The composition of the final ADID dataset under a multi-class labelling strategy is summarised in Table 4.1

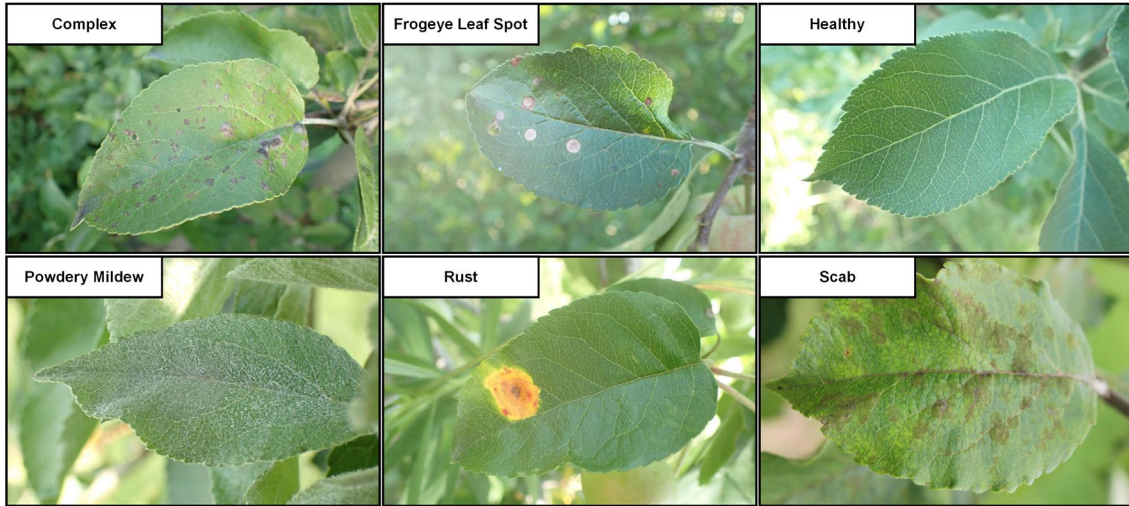


Figure 4.3 Example images of characteristic symptoms of each of the six classes from the PlantPathology2021 dataset

Dataset	Complex	Frogeye Leaf Spot	Healthy	Powdery Mildew	Rust	Scab	Total
PlantPathology2021	2956	3180	4623	1184	1859	4822	18624
PlantPathology2020	206	0	864	0	1380	1189	3639
PlantVillage	0	592	1606	0	253	594	3045
AppleScabLDs	0	0	206	0	0	982	1188
MultispectralRGB	0	0	875	0	0	377	1252
MultispectralNIR	0	0	784	0	0	468	1252
ADID	3162	3772	8958	1184	3492	8432	29000

Table 4.1 Composition of classes from the public and primary datasets of the 29,000 images used in the final ADID dataset

4.2.1.3 Dataset Partitioning

The final ADID dataset was partitioned with an 80:20 split into training and testing sets. Images from public datasets were split at random into training and testing datasets, as all plant samples and symptoms were independent. The multispectral dataset required a different approach due to the limited sample number and the acquisition as a time series rather than random sampling. The dataset split had to be determined manually, as having the same plant sample and infection occurring in both training and testing results could cause high bias and unreliably high accuracies. The division took place on a sample-by-sample basis, with all daily images for 26 seedlings used for training and 18 for testing the model. The multispectral data was split 60:40 between testing and training data, allowing more samples to be assessed in a time series. Samples (S) S01-S08 were inoculated but showed no apple scab symptoms during manual classification. The remaining samples S09-S18 developed characteristic scab lesions during the course of the experiment. No validation dataset was required as the CNN performance would be assessed from the annotated testing set. This helped preserve the number of multispectral

images used to train the model. Table 4.2 displays the final distribution of classes for the 23,200 training and 5,800 testing images in the ADID subsets.

Image Set	Complex	Frogeye Leaf Spot	Healthy	Powdery Mildew	Rust	Scab	Total
Training	2542	3081	6930	961	2907	6779	23200
Testing	620	691	2028	223	585	1653	5800

Table 4.2 The distribution of class labels for the training and testing datasets

4.2.2 Fine-Tuning Convolutional Neural Networks

4.2.2.1 The MobileNetV2 and EfficientNetV2L CNN Models

Two pre-trained CNN models to classify the ADID dataset, MobileNetV2 (Sandler et al., 2018) and EfficientNetV2L (Tan & Le, 2021), were selected due to their differing architectures and resource requirements. Both models were compared against each other to demonstrate that the classification of multispectral imagery can work regardless of the architecture. The MobileNetV2 and EfficientNetV2L models were readily available from the Keras library, having already been pre-trained on the millions of annotated images on ImageNet (Deng et al., 2009). These models were fine-tuned on the ADID testing set. Fine-tuning uses the weights of these pre-trained models to initialise them before retraining all or part of these weights on the target training set (Boulet et al., 2019). This process significantly enhances the ability of the CNNs to adapt to the target classification set compared to using a pre-trained network directly (Radenović et al., 2018; Dhaka et al., 2021). A large amount of annotated data is required to train CNNs for optimal classification. The limited variation in the multispectral data put the model at risk of overfitting, especially for the NIR images. Several augmentation techniques were applied to all training images to improve the final accuracy further. Data augmentation is a standard method of artificially expanding databases by simulating changes in acquisition conditions (Alomar et al., 2023). Seven geometric augmentations were applied randomly to all images within the training dataset: horizontal flips, vertical flips, shearing, zooming, width shifts, height shifts, and rotations. For this study, all pre-trained model weights were frozen except for the final fully connected layer. This layer remained unfrozen and was retrained on the training set to produce fine-tuned MobileNetV2 and EfficientNetV2L models for apple scab classification. The entire CNN training and testing process is presented in Figure 4.4.

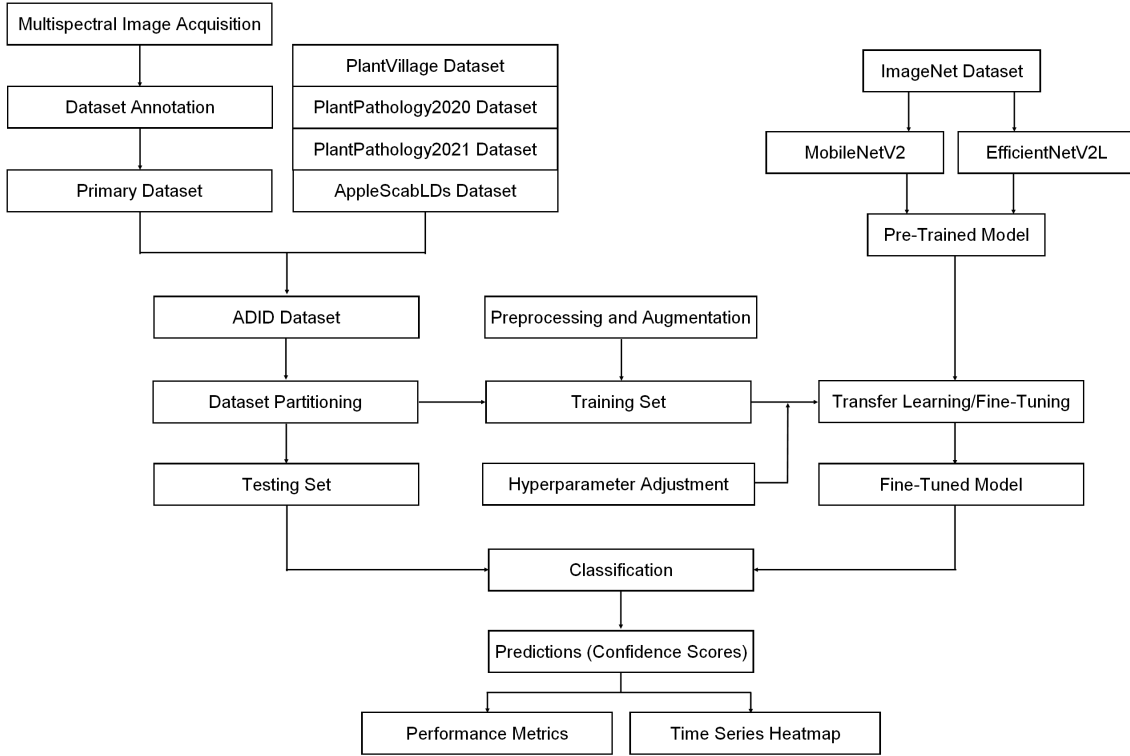


Figure 4.4 Flow diagram of the ADID Dataset multi-class classification process

4.2.2.2 Model Training Environment

Appropriate hyperparameters are essential for optimal CNN model training. Consistency was maintained to enable fair comparisons between MobileNetV2 and EfficientNetV2L models. All hyperparameter adjustments for both models were tuned based on the validation accuracies and performance of models measured from previous validation runs. Each model was trained past convergence for 20 epochs, using an incremental learning rate with the Softmax activation function, Adam optimisation and a CategoricalCrossentropy loss function, defined as:

$$CrossEntropy Loss = - \sum_i^c t_i \log(s_i) \quad (1)$$

Where t_i is the probability of the ground truth, and s_i is the probability of the target class (CNN confidence score) for each class C . The ideal batch sizes for the hardware were 60 and 6 for MobileNetV2 and EfficientNetV2L, respectively (Table 4.3).

Configuration Parameters	
CPU	AMD Ryzen 7 5800H 3.2GHZ
GPU	Nvidia GeForce RTX 3070 Laptop GPU (8Gb)
RAM	64Gb
Hard Disk	1Tb
Operating System	Windows 11 Home OS Build 22000.1455

Table 4.3 The hardware and software environment of the experiment

4.2.3 Performance Assessment

After each model had completed training and classification, results were recorded in a spreadsheet, attributing a confidence score to each of the six classes per image. Being a multi-class strategy, the confidence scores distributed across the six classes were equal to 1.00. A confidence score of 0.33 provided a boundary threshold for the model to provide positive predictions for a maximum of three disease labels. Full-scale and individual-label confusion matrices were generated via the model, with the prediction labels from the latter used to analyse the accuracy of each model.

		Class	
		0	1
True Label	0	TN	FP
	1	FN	TP
		0	1
		Predicted Label	

Where:

True Negative (TN): Correctly identified absence of labelled leaf class

False Negative (FN): Incorrectly identified absence of labelled leaf class

False Positive (FP): Incorrectly identified labelled leaf class

True Positive (TP): Correctly identified labelled leaf class

These values were used to assess the performance of each CNN model classification using the formulas provided below.

Accuracy – Evaluation of the overall performance of the model:

$$Accuracy = \frac{TP + TN}{TP + TN + FP + FN} \quad (2)$$

Recall/Sensitivity – Evaluation of the performance of performance of the model in predicting true-positive cases:

$$Recall = \frac{TP}{TP + FN} \quad (3)$$

Specificity – Evaluation of the performance of the model in predicting true-negative cases:

$$Specificity = \frac{TN}{TN + FP} \quad (4)$$

Precision – The accuracy of the positive predictions made by the model:

$$Precision = \frac{TP}{TP + FP} \quad (5)$$

F1 Score - A consistency mean of recall and precision where there is an imbalance between the false positive and negative samples within the class:

$$F1\ Score = \frac{2 (Recall \times Precision)}{(Recall + Precision)} \quad (6)$$

The confidence scores attributed to apple scab for each day were used for the time series analyses. These scores were then used to generate a heatmap, where the value of each cell represents one image on one day, as with the manual classification time series (Figure 4.1). Yellow cells indicated low confidence in containing apple scab, with colours developing from aqua to dark blue as confidence increases. The heatmaps for each model were then assessed and compared against each other. Key features of these assessments included discrepancies between model and manual classifications, the earliest points of detection, the confidence scores, and the presence of noise or significant errors in classification.

4.3 Results and Discussion

The first subsection of the results assesses the overall performance of the ADID-trained CNNs by demonstrating the ability to accurately classify each of the six classes in the publicly available data subset. The second subsection investigates the model performance on the experimental multispectral dataset and the discrepancies between the performance metrics and the time series analysis. The third subsection further examines the classification of apple scab by comparing the results of RGB and NIR imagery against each other. The final subsection reviews the limitations of the experiment and provides recommendations for further research.

4.3.1 Model Training and Convergence

Training MobileNetV2 and EfficientNetV2L on the ADID dataset proved successful, with minimal indication of overfitting or bias throughout the epochs from Training Accuracy and CategoricalCrossentropy Training Loss metrics (Figure 4.5). Both models achieved high performance when classifying images across the entire ADID dataset, validating the capability of both CNNs to classify late-stage apple disease images. The final models achieved training accuracies of 97.49% and 99.33% for MobileNetV2 and EfficientNetV2L, respectively, although the latter required a significantly longer training time (Appendix C).

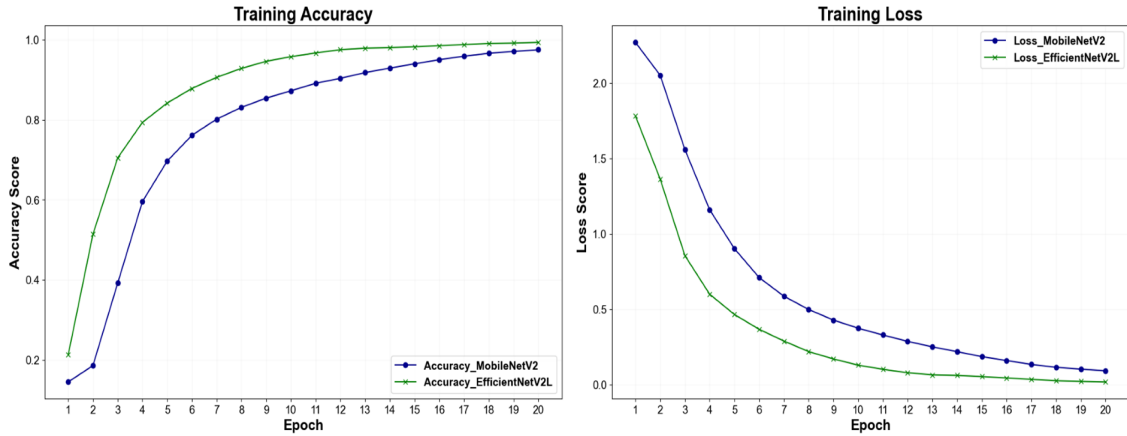


Figure 4.5 Graphs displaying the convergence speed for training accuracy (left) and loss (right) for both MobileNetV2 and EfficientNetV2L models

Model	Training Time	Avg time per epoch	Training Accuracy	Training Loss	Testing Time	Testing Accuracy
MobileNetV2	7815s	390s	0.975	0.093	95s	0.969
EfficientNetV2L	25111s	1256s	0.993	0.018	123s	0.971

Table 4.4 CNN model training and testing metrics for the MobileNetV2 and EfficientNetV2L models. Training and testing accuracy and training loss were recorded after Epoch 20.

4.3.2 Classification Performance on the ADID Dataset

The full-scale confusion matrices for all six classes are illustrated in Figure 4.6, and performance metrics are presented in Table 4.5. The overall test accuracies of 96.99% and 97.13% are comparable to the highest overall prediction accuracies of 97.14% achieved by Jiang et al. (2019) and 98.82% by Chao et al. (2020). Direct comparison is difficult due to the different disease classes and the novelty of the multispectral dataset. The performance results for all six classes show that overall, the EfficientNetV2L model slightly outperforms MobileNetV2. The models perform exceptionally well when classifying ‘frogeye leaf spot’, ‘healthy’, ‘rust’, and ‘powdery mildew’ classes. Classification of ‘powdery mildew’ consistently ranks best, most likely due to the uniqueness of symptoms and the small batch of test samples. Both models perform weakest for the ‘complex’ class across all metrics, yet they still outperform the prediction accuracy of 51% in Thapa et al. (2020) and the F1-score of 0.56 in Yadav et al. (2022) for the equivalent ‘multiple-disease’ class in PlantPathology2020. These results demonstrate a clear limitation of the ‘complex’ class, potentially attributed to the broad definition of ‘complex’, encompassing all images displaying symptoms of more than one disease. CNNs are highly effective at generalising, often correctly labelling diseases under novel circumstances. The ‘complex’ class is for images containing symptoms from multiple diseases, and there is the potential for CNNs to classify the individual causative diseases rather than the combination as a whole. Furthermore, including the ‘complex’ class may adversely affect the training of the model

weights against diseases with severe symptoms. The ‘complex’ class should be removed in future studies in place of a multi-label classification strategy (Wei et al., 2014).

The ‘scab’ class has the second weakest performance of the six, achieving F1-scores of 0.896 and 0.899 and performing worse than the 0.97 F1-score achieved by Yadav et al. (2022). These results are heavily influenced by the novel multispectral time series data, accounting for 10.0% of the training and 17.5% of the testing images. MobileNetV2 had more true-positive predictions of apple scab than EfficientNetV2L and more false-positive and fewer false-negative predictions, which may be more desirable to inform spray decisions as they reduce the risk of missing an infection that can quickly spread. The following sections examine the scab class in greater detail by exploring the influence of multispectral time series imagery on the classification results.

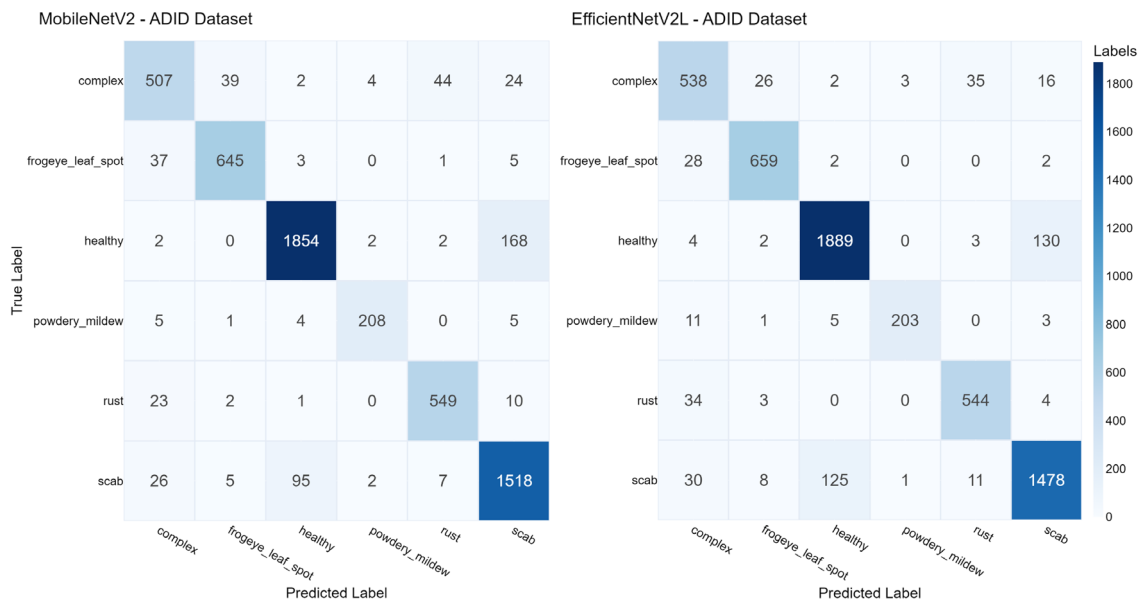


Figure 4.6 Confusion matrices of CNN predictions for each of the six classes in the ADID dataset for the MobileNetV2 and EfficientNetV2L models.

Model	Metric	Complex	Frogeye Leaf Spot	Healthy	Powdery Mildew	Rust	Scab	Total
MobileNetV2	Accuracy	0.9631	0.9845	0.9536	0.9960	0.9840	0.9384	0.9699
	Recall	0.8500	0.9479	0.9295	0.9372	0.9504	0.9310	0.9260
	Specificity	0.9766	0.9894	0.9666	0.9984	0.9877	0.9414	0.9787
	Precision	0.8133	0.9238	0.9373	0.9587	0.8968	0.8636	0.8970
	F1 Score	0.8312	0.9357	0.9334	0.9475	0.9228	0.8961	0.9113
EfficientNetV2L	Accuracy	0.9655	0.9872	0.9519	0.9964	0.9845	0.9422	0.9713
	Recall	0.8855	0.9638	0.9354	0.9279	0.9487	0.9062	0.9262
	Specificity	0.9751	0.9904	0.9608	0.9991	0.9885	0.9566	0.9803
	Precision	0.8097	0.9315	0.9276	0.9763	0.9024	0.8927	0.9039
	F1 Score	0.8459	0.9474	0.9315	0.9515	0.9250	0.8994	0.9149

Table 4.5 Performance metric scores for each of the six classes for the MobileNetV2 and EfficientNetV2L models.

4.3.3 Apple Scab Classification from the Multispectral Time Series

4.3.3.1 Classification Performance

The classification results were divided into test images from multispectral sources and those from public datasets to examine the capability of early apple scab prediction from multispectral imagery. The confusion matrices and the performance metrics for the multispectral data are displayed in Figure 4.7 and Table 4.6, respectively. The performance of both models to classify apple scab from within the multispectral dataset is considerably lower than their classifying ability on publicly available data. Despite the lower performance, the F1 scores of 0.665 and 0.630 demonstrate that MobileNetV2 and EfficientNetV2L can correctly identify scab in most circumstances. MobileNetV2 outperforms MobilenetV2, yet only marginally compared to the training time and computational cost. MobileNetV2 has more instances of true-positive and fewer false-negative scab predictions yet has more false-positive classifications than EfficientNetV2L.

There are numerous reasons why both models perform poorer when classifying apple scab from the primary multispectral subset than from the full ADID dataset. Images from public datasets account for 91.4% of total images within the ADID dataset, with most of these containing localised images of leaves with large and well-defined, late-stage symptoms of diseases (Thapa et al., 2020). By contrast, the primary multispectral dataset contains images of whole plants, as seedlings, with an extensive background area. The early symptoms displayed in the multispectral dataset cover a much smaller area both on the leaf and within the entirety of the image itself, unlike the public images, which could prove more difficult for the CNNs to identify accurately. The training dataset for the primary multispectral imagery is also much smaller and less varied, increasing the likelihood of biases toward certain image features that may adversely affect classification accuracies. Furthermore, the multispectral dataset contains symptoms of leaves due to heat and drought stress, which was caused by hot weather in July 2021. These symptoms have been ignored for the study but may have influenced model training and predictions. Further analysis of the multispectral data as a time series provides a greater understanding of the CNN capabilities to classify early apple scab.

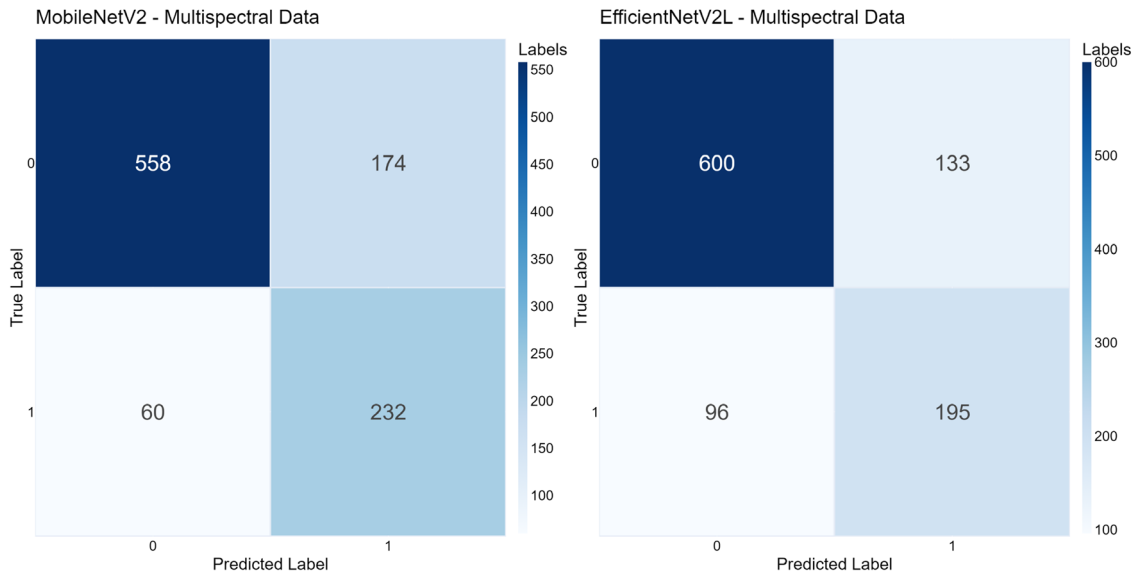


Figure 4.7 Confusion matrices of the scab category in the multispectral dataset for the MobileNetV2 and EfficientNetV2L models. 0 indicates negative labels (healthy) and 1 positive labels (scab)

Model	Metric	Score
MobileNetV2	Accuracy	0.7714
	Recall	0.7945
	Specificity	0.7623
	Precision	0.5714
	F1 Score	0.6645
EfficientNetV2L	Accuracy	0.7764
	Recall	0.6701
	Specificity	0.8186
	Precision	0.5945
	F1 Score	0.6300

Table 4.6 Performance scores for the scab classifications in the multispectral imagery by the MobileNetV2 and EfficientNetV2L models

4.3.3.2 Time Series Assessment

The time series heatmaps of confidence outputs from all models (Figure 4.8) show that apple scab is detected earlier and in more samples than the manual classification described earlier in Section 4.2.1.1 (Figure 4.1). The results are consistent between models, with most samples retaining a positive scab classification after first detection. MobileNetV2 consistently classifies ‘scab’ earlier and in more plant samples compared to EfficientNetV2L. Furthermore, these scab predictions in the former have much higher confidence scores than the latter. Sporadic noise increases over time, with samples on individual days containing false positives and negatives, with little indication that illumination and acquisition conditions or specific samples are the cause.

Several key differences exist in the time series predictions between CNN models and the manual classification. The earliest detection of apple scab by CNN classification occurred at 7 d.p.i. in

Samples S09 to S12, S17, and S18; these results were 5 to 25 days before visible symptoms were detected. These early apple scab classifications are comparable to the earliest symptoms detected in thermal imagery at 6 d.p.i. (Oerke et al., 2011). Samples S01 to S08 were manually classified as healthy but showed sporadic classification of scab by the CNNs in the late stages of the experiment. These samples had been inoculated, but through visual inspection, it was assumed that the pathogen had not germinated. It cannot be determined whether these results are false positives, and it is recommended that a control set is used in future research. A potential cause of false-positive scab predictions is the presence of numerous lesions due to heat damage on the leaves. This may have influenced the model into classifying abiotic lesions or masked scab symptoms during manual assessment. Samples S13 and S15 were classified as scab by the CNNs instead of healthy under manual assessment. Conversely, samples S14 and S16 have been labelled as containing scab in the manual classification but show no signs of scab in the CNN predictions.

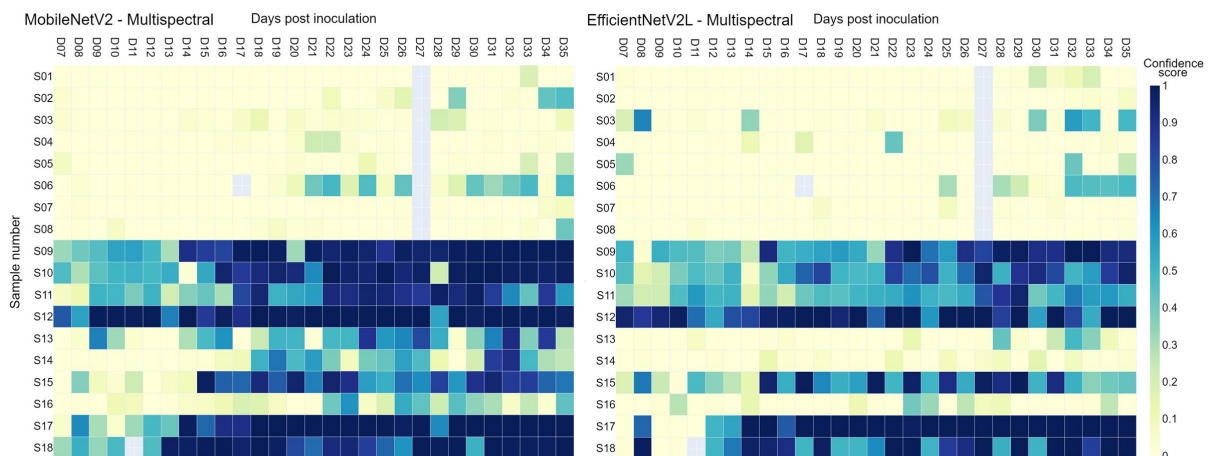


Figure 4.8 Heatmap of the scab prediction confidence in the multispectral time series classification for the MobileNetV2 (left) and EfficientNetV2L (right) models. Each cell represents the confidence score output for an individual image.

4.3.4 Comparing Classification Performance on RGB and NIR Imagery

The individual RGB and NIR components of the multispectral imagery were investigated separately to reveal the differences and influences each had over the final multispectral results. Classification performance was consistently better in NIR imagery than in RGB imagery, with classification performance higher in all categories except specificity (Table 4.7). Classification of NIR imagery produced more true-positive ‘scab’ predictions, displayed higher confidence scores, and classified ‘scab’ earlier than RGB imagery (Figure 4.9). The NIR time series features more stable ‘scab’ predictions on infected samples, with less noise and false negatives, especially in the latter half of the experiment when scab symptoms had progressed from early to late stages. The NIR time series contains more examples of positive predictions in samples S01 to S08 than in

RGB; these samples were manually classified as healthy. The results show that CNNs reliably classify early and late-stage apple scab in NIR imagery, even with limited training data; the classification of RGB images should have been more robust due to the similar features found in the RGB images of the public datasets. As previously discussed, prediction results may be negatively influenced by errors in manual classification, as well as limited quantity and variation in training samples. Numerous instances of noise exist across all four of the time series, with little correlation between them, suggesting limited influence from the acquisition procedure or plant physiology on these outliers.

Model	Metric	RGB Score	NIR Score
MobileNetV2	Accuracy	0.7871	0.7559
	Recall	0.7462	0.8333
	Specificity	0.8010	0.7200
	Precision	0.5607	0.5794
	F1 Score	0.6403	0.6834
EfficientNetV2L	Accuracy	0.7754	0.7773
	Recall	0.5000	0.8025
	Specificity	0.8691	0.7657
	Precision	0.5652	0.6132
	F1 Score	0.5306	0.6952

Table 4.7 Performance scores for the scab classifications in the RGB and NIR imagery by the MobileNetV2 and EfficientNetV2L models.

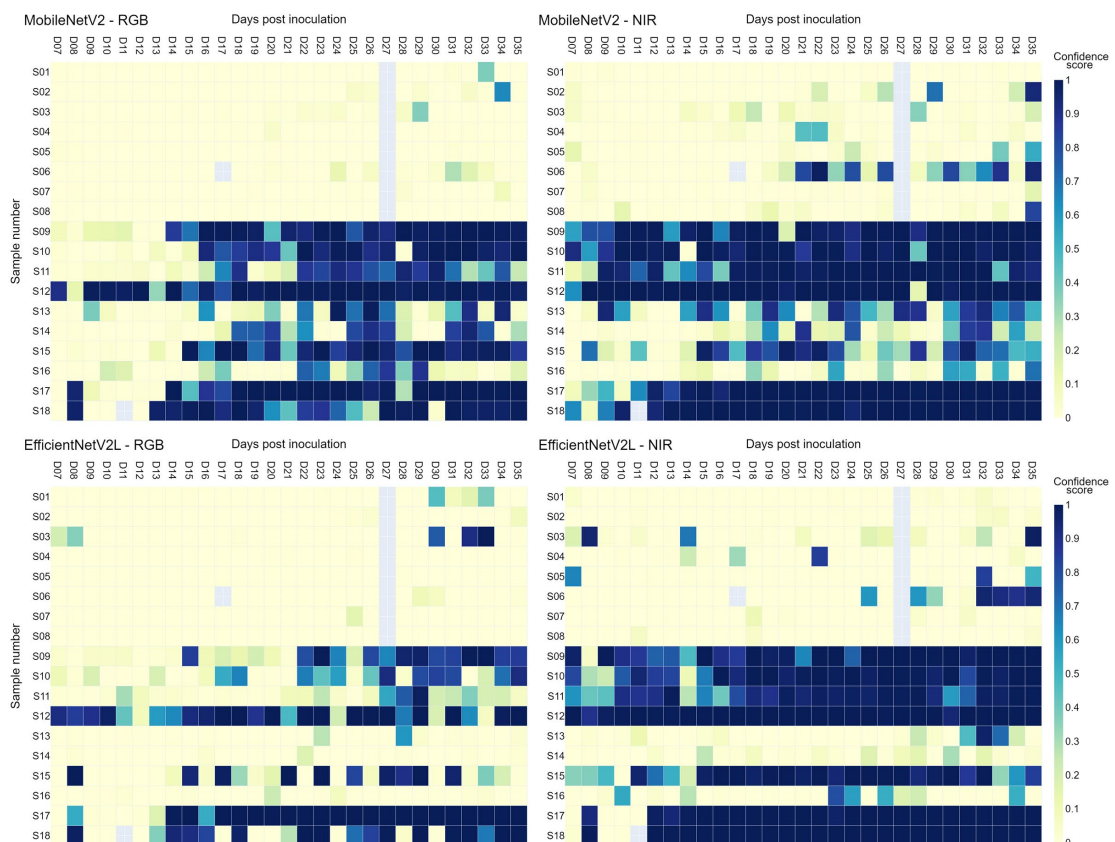


Figure 4.9 Above) Heatmap of the scab prediction confidence in the RGB (left) and NIR (right) time series imagery for the MobileNetV2 model. Below) Heatmap of the scab prediction confidence in the RGB (left) and NIR (right) time series imagery for the EfficientNetV2L model. Each cell represents the confidence score output for an individual image.

The results demonstrate the potential for using NIR imagery for the early detection of apple scab and through to the late stages of infection. The high confidence of early-stage predictions is attributed to the high contrast of scab symptoms on leaf tissue in the NIR imagery. Issues regarding poor performance in the multispectral data may be solved by increasing the training data with more significant variations of symptoms, plants, and acquisition conditions. While NIR imagery can be more helpful in detecting apple scab earlier than RGB imagery, further research is required to determine the viability of usage within commercial orchards.

4.3.5 Experimental Limitations and Recommendations for Further Research

The study reveals that CNN models can classify apple scab infections in multispectral imagery quicker, earlier, and more objectively than manual techniques. However, the CNNs were considerably more effective in classifying late-stage symptoms on publicly available secondary datasets compared to the primary dataset. Several improvements could help demonstrate the benefits these technologies can provide. CNN training requires a large quantity of data to yield reliable results. In the present study, only 1,252 NIR images were acquired on simple seedling samples, leading to a limited selection of symptoms despite dataset augmentation. More NIR images, with a greater range of early apple scab symptoms, would provide a more robust classification model.

This research and previous studies show the strength of CNNs in diagnosing diseases from multiple sources within RGB (Jiang et al., 2018; Chao et al., 2021; Yadav et al., 2022). No equivalent multispectral datasets currently exist containing frog-eye leaf spot, powdery mildew, and cedar-apple rust symptoms. Acquiring and labelling NIR images of these diseases would enable researchers to determine the diagnostic capabilities in realistic orchard settings. Furthermore, this would improve the robustness of model training and the reliability of scab disease predictions in orchards. Multi-label classification techniques are recommended as these have an advantage in field assessments, as several stresses are often present concurrently. Further experiments should consider removing the complex category as this can not only adversely affect training models but provide no further information on the disease and, therefore, potential treatment options. Countless stress symptoms occur on leaves and fruits from pest and abiotic sources. The generalisation capabilities of CNNs allow for detecting diseases in the presence of non-pathogenic symptoms if the models are trained to ignore them as background information. Increasing the training data by including diseases in the presence of other stresses could improve diagnostic capabilities within real-world scenarios.

The earliest that CNN models can classify scab infection is 7 d.p.i., one day later than from manual observation in thermal imagery (Oerke et al., 2011). The author collected the first images of the experiment at 7 d.p.i., so it may be possible that the models could detect scab even earlier. Future experiments should begin preferably from the day after inoculation to remove any doubt on the earliest detection of initial symptoms. An area that could be further explored is the earliest point at which scab infection should be labelled and the influence this may have on the training of the models. It can be assumed that as soon as *V. inaequalis* germination has occurred, the sample is infected, but the current labelling method was based on manual classification from the earliest date of visual detection. Providing training data containing initial symptoms based on retrospective assessments could create a bias toward scab predictions, as these initial symptoms are often featureless dark points (Bleasdale et al., 2022). A more rigorous assessment of false positives must occur. High numbers of false positives reduce model precision and, at an orchard scale, may lead to incorrect estimations of scab severity, which would inevitably lead to the over-spraying of pesticides. Classification experiments using a control set could improve the validity of performance metrics and the ability of CNNs to distinguish between healthy and early-stage infections. Time series imagery of healthy plants alongside those with present or latent scab symptoms can be used to confidently identify false positives. Additionally, it may aid investigations into acquisition settings or plant physiologies that may influence 'scab' predictions.

This chapter showed CNNs to be effective at classifying disease regardless of model architecture with minimal difference in performance. Model selection should be determined by computational and time resources available. EfficientNetV2L provided marginally higher performance but at the cost of a major increase in training time and resource requirements against MobileNetV2. Lightweight CNNs, including MobileNetV2, could enable greater accessibility to this technology and rapidly assess orchard health in many regions worldwide. Multispectral imagery combined with CNN-based classification can identify early-stage and well-developed apple scab symptoms on seedlings. This research provides a step toward full-scale apple scab detection within orchards that could be used to inform site-specific spraying and scab forecasting models. Further development of the technologies, with suitable acquisition platforms and processing environments, could create a powerful tool for growers to have regular updates on disease and crop health, with less reliance on the schedule of crop scouting set by agronomists.

4.4 Conclusion

This study successfully achieved the aim of automating the detection of early apple scab infection by using CNNs to classify a time series of multispectral imagery. CNN models consistently classified early-stage and late-stage scab infections in RGB and NIR imagery and distinguished these from other diseases in public datasets. Time series analyses have demonstrated that apple scab could be detected earlier and more often in CNN-based classification than by manual classification. The results confirmed that using NIR imagery to detect apple scab was superior to RGB as predictions occurred earlier and with greater accuracy overall. Despite this, overall predictions from both NIR and RGB imagery within the multispectral dataset were less accurate than predictions made in publicly available datasets, where images focused on late-stage symptoms on specific leaves. Future research should investigate the earliest possible detection point with earlier imaging and determine a reliable precision metric using control samples.

The current method of scouting for disease in orchards is sporadic, infrequent, and expensive, which limits targeted control strategies and promotes mass pesticide spraying. Fine-tuning CNN models with multispectral imagery can allow for the early detection of apple scab infection using high-resolution multispectral sensors. Applying these methodologies to commercial orchards could better inform scab forecasting models and enable site-specific spray decisions across whole orchards, reducing the spread of disease epidemics, pesticide use, and yield losses. The success of the lightweight MobileNetV2 models and the low-cost multispectral imaging technique indicated that this technology would be accessible to orchards worldwide, potentially leading to widespread environmental and economic benefits.

5 Monitoring Apple Scab Progression from Visible and Near-Infrared Time Series Imagery with Convolutional Neural Networks

Abstract

Apple scab (*Venturia inaequalis*) and other fungal pathogens are major threats to apple production. Early disease detection can inform effective and efficient control measures, but rapid, accurate assessments are challenging when monitoring tree health within real-world conditions. High-resolution near-infrared (NIR) imaging has the potential to detect apple scab earlier than visible (RGB) imagery under natural illumination. Classification of this multispectral imagery can be automated accurately and rapidly through Convolutional Neural Network (CNN) models. The aim is to study the effectiveness of CNNs in classifying apple scab through the early-to late stages of infection from a large time series dataset containing RGB and NIR imagery.

105 apple plants were cultivated from seed, and experimental samples were artificially inoculated with apple scab. Images were acquired daily to produce a large primary dataset of RGB and NIR time series imagery. Secondary data was used to supplement training and validate model classification abilities. Three CNN models, MobileNetV2, InceptionResNetV2, and EfficientNetV2L, were fine-tuned, and a training set of primary and secondary data was used to classify healthy and scab-infected samples, as well as other common apple diseases using a multi-label classification strategy. EfficientNetV2L was the best-performing model, achieving an overall accuracy of 98.6% in the secondary validation data and 85.4% in the primary multispectral data. Further investigation revealed that infection severity, specifically the ratio of healthy-to-infected leaves on a sample, caused a bias towards healthy predictions. Adjusting the testing set to localise imagery around infection symptoms improved the overall accuracy of classifying both RGB imagery (90.3%) and NIR imagery (95.4%). All CNN models consistently classified apple scab earlier, more accurately and with a greater precision and recall in NIR imagery than in RGB imagery.

5.1 Introduction

Accurate monitoring of crop diseases is fundamental for effective and sustainable crop protection. Early detection of plant pathogens can improve the efficiency of disease control by facilitating site-specific management strategies through targeted fungicide application and sanitation techniques. Remote sensors offer a powerful, cost-effective method for rapid, large-scale, non-invasive assessment of plant disease detection in agriculture (Mahlein, 2017; Khanal, 2017). Remote sensing for plant pathology uses non-contact measurements of electromagnetic radiation interactions between plant tissue and pathogenic material (Mulla, 2013). The most commonly used sensing methods in disease detection studies are RGB, multispectral, hyperspectral, chlorophyll fluorescence, and thermal imaging, which enable the characterisation of different plant parameters to identify early signs of stress (Li et al., 2014; Mahlein, 2016; Zhang et al., 2019). Demonstrating early disease detection capabilities is a key objective of remote sensing studies. However, achieving early detection can be difficult in the field due to complex environmental interactions and external influences from acquisition conditions (Kuska et al., 2018). Additionally, plant pathogens in the early stages of infection are often heterogeneously distributed throughout the field, so remote sensors need to be able to detect small symptoms at low severities while also providing wide coverage in order to implement site-specific treatment effectively (Oerke et al., 2020).

Apple scab is widely considered to be the most important disease of apples, where losses impact entire orchards if left untreated (MacHardy, 1996). Apple scab causes substantial losses of yield and income due to the presence of lesions on fruit, rendering them unmarketable. Apple scab infections develop in spring from the pathogen overwintering on leaf litter, infecting young apple leaves. Symptomatic scab lesions on leaves and fruits act as secondary sources of infections, which continue to infect and spread rapidly throughout the orchard during the growing season and develop on fruits in storage (Bowen et al., 2011). Due to the polycyclic nature of the pathogen, an average of 13 fungicidal sprays are applied to orchards each season, approximately every 10 days (Berrie & Xu, 2003; Ridley et al., 2024). This intensive fungicide application accounts for a significant portion of production costs, with total scab fungicides accounting for up to 50% of the total chemical costs (MacHardy, 2000). Furthermore, the widespread application of large quantities of fungicides for apple scab control has adverse consequences on terrestrial and aquatic ecosystems (Hamed et al., 2022). Detecting apple scab earlier can increase the efficiency of fungicide application and sanitation treatments, improving the sustainability and reducing the economic cost of disease management (Delalieux et al., 2007).

Numerous sensors have been utilised in studies of early scab infection. Thermography (Oerke et al., 2011), hyperspectral sensing (Delalieux et al., 2007; Delalieux et al., 2009a; Gorretta et al., 2019), and fluorescence imaging (Delalieux et al., 2009b.; Belin et al., 2013) have previously been shown to discriminate between scab-infected and healthy samples in the early stages of the disease. Despite the successes of these studies, they have not been transferred to field environments because they require large, specialist equipment operating within controlled environments to detect diseases accurately. Bleasdale et al. (2022) demonstrated the feasibility of using low-cost sensors under natural illumination conditions, showing that high-resolution multispectral (VIS-NIR) imaging, specifically near-infrared (NIR) imagery, could be used to discriminate between healthy and scab-infected samples, with NIR imagery displaying scab symptoms as dark lesions comprising conidial structures against bright, healthy leaf tissue. The significant contrast between infected and healthy tissue under natural illumination allowed for reliable identification in NIR imagery up to three days before RGB-based assessments. These multispectral sensors show great potential for application in orchards due to their ability to detect early symptoms under a range of natural illumination conditions.

Deep learning Convolutional Neural Networks (CNNs) are a class of feed-forward artificial neural networks popular in plant disease classification studies due to their high performance and limited pre-processing requirements compared to traditional classification methods (Hasan et al., 2020). They display far superior classification speeds and accuracies in real-world illumination conditions, with considerable symptom variance and do so without requiring time-consuming preprocessing, feature selection or background removal steps. CNNs have been widely implemented for various agricultural tasks (Kamilaris & Prenafeta-Boldú, 2018), with specific attention dedicated to disease detection studies (Boulent et al., 2019). CNNs comprise image filters and feature maps within convolutional layers, along with pooling and fully connected layers representing learning features from the data (Yamashita et al., 2018). CNNs solve classification problems by learning directly from training datasets through these layers, unlike traditional machine learning techniques that rely upon hand-crafted feature extraction (Toda & Okura, 2019). Numerous CNN model architectures are available, differing from each other depending on the number and arrangements of layers and additional processing units utilised (Alzubaidi et al., 2021; Taye, 2023). CNNs have previously been used to accurately classify apple scab from numerous other pathogens (Turkoglu et al., 2019; Zhong & Zhao, 2020; Kodors et al., 2021; Yadav et al., 2022); however, these studies largely use RGB imagery of individual leaves showing late stages of the disease. Applying CNNs to multispectral data could enable the classification of plant diseases much earlier in their life cycle (Hasan et al., 2020). Furthermore, disease symptoms change as the infection progresses and increases in severity,

and CNNs should be capable of accurately classifying these symptoms at all infection stages (Saleem et al., 2019). Despite previous research dedicated to classifying apple scab, neither early detection from multispectral imaging nor performance assessments of infections within a time series have been undertaken.

Chapter 4 demonstrated that it was possible to use CNNs to classify NIR imagery, providing promising results when CNNs were used to monitor early-to-late scab symptoms on seedlings within a multispectral time series. The results showed that it was feasible to classify both RGB and NIR imagery concurrently and that scab could be classified earlier and more accurately with NIR imagery rather than RGB imagery. The performance of these CNNs in classifying multispectral imagery was considerably lower than the results published in previous literature. This was attributed to several experimental limitations, including the size and the degree of symptom variation within the NIR training set and the robustness of CNN fine-tuning. CNNs require a large quantity of varied samples to be trained to reduce the risk of underfitting or overfitting predictions, but obtaining training data can be time-consuming and expensive. Large datasets of apple diseases are publicly available, including PlantVillage (Hughes & Salathe, 2015) and PlantPathology (Thapa et al., 2020), but these only contain RGB images of late-stage diseases focussing on specific leaves or organs. There is currently an absence of spectral image datasets for plant disease studies (Wang et al., 2021). Furthermore, due to the experiment being based on a time series, the imagery of individual plants used in training and testing data had to be completely separated, leading to a limited number of test samples to analyse.

The experiment performed in Chapter 4 relied on time series imagery for training and testing CNN models. Due to the novelty of the data, a high proportion of the imagery was dedicated to CNN training, leaving few plant samples to assess for early detection of apple scab. Initial results suggested that CNNs were superior to manual classification techniques, detecting apple scab earlier and in more samples than those manually labelled, leading to low accuracy and precision metrics. This study lacked the use of control samples, which made it difficult to determine bias towards positive scab predictions in the absence of visible symptoms. To successfully demonstrate the potential of CNNs to classify and monitor scab progression over time, longer experiments with multispectral imaging beginning earlier and acquired from control and experimental samples are needed to provide the necessary training and testing data.

The aim of this chapter is to investigate the effectiveness of NIR and RGB imagery, classified using fine-tuned CNN models, to monitor apple scab infections over time. To achieve this, a high number of control and artificially-inoculated experimental apple plants are imaged daily with

RGB and NIR imaging sensors to acquire a large time series dataset covering presymptomatic, early and late stages of infection. Three pre-trained CNN architectures, MobileNetV2, InceptionResNetV2, and EfficientNetV2L, are then fine-tuned on the primary multispectral dataset, and supplementary data from secondary sources. A multi-label classification approach is then used to identify apple scab alongside four further distinct disease classes: frog-eye leaf spot, healthy, powdery mildew, and cedar-apple rust. The classification capabilities of CNNs are then assessed based on their confidence score outputs across each class. These confidence scores are then used to generate confusion matrices and calculate performance metrics. Variability in confidence score is also assessed over time through time series analysis. Further investigation into the acquisition, illumination and plant physiological conditions influencing classification accuracy provides recommendations for future practical use.

5.2 Materials and Methods

5.2.1 Apple Plant Material

5.2.1.1 *Apple Cultivation*

For robust training and testing of CNN models for apple scab detection, a wide range of plant physiologies and symptom variance was necessary, which required a large number of apple plants to image. All plant material was cultivated within two glasshouses at Hazelrigg field station at Lancaster University (Lancaster, UK). The illumination, humidity, and temperature conditions were uncontrolled, aside from the use of extractor fans for ventilation and to constrain extreme temperatures. For the experiment, 105 apple saplings of various ages were cultivated from the seeds of commercially important apple varieties (Gala, Braeburn, and Cox), although seedlings these were genetically distinct from these parent plants. Each seedling was grown in a standard potting mix and transplanted into larger pot sizes corresponding to age. Plants over two years old were grown in large (4 L) pots, plants aged between one and two years were grown in medium (3 L) pots, and the remaining younger plants were grown in small (2 L) pots. Plants received minor pruning during dormancy to develop various structural shapes. By the time of the experiment, plant heights ranged from 0.3 m to 1.2 m while still actively growing. Tall, top-heavy plants were supported using 0.9 m green plastic stakes.

During the apple cultivation period, actions were taken to control powdery mildew (*Podosphaera leucotricha*) infections which developed in the conducive environment of the glasshouses. These control measures included sanitation by the physical removal of infected tissue from the growing

environment and the application of fungicidal sprays. The application of fungicides ended the month prior to scab inoculation. At the start of the experiment, the plants were actively growing new leaves, and no symptoms of powdery mildew were visible at that time, although pesticide residue could be observed on some leaves. The 105 apple saplings were proportionally divided into control and experimental samples at a ratio of 1:3, with 27 control and 78 experimental samples (Table 5.1)

Plant Size	Control	Experimental
Small	16	45
Medium	3	9
Large	8	24

Table 5.1 Quantity of each plant size across control and experimental samples

5.2.1.2 Apple Scab Inoculation Procedure

Experimental plants were artificially inoculated with apple scab using a suspension of *V. inaequalis* conidia. Inoculum was harvested from infected leaves gathered from commercial orchards in Herefordshire, UK, in October 2020 (see Chapter 3.2.1). All collected leaves were placed in a paper bag to minimise condensation and frozen at -20 °C in a sealed container (Szkolnik, 1978). The inoculum suspension was produced by shredding 50 g of infected leaves and placing them in a container with 500ml of distilled water and shaking vigorously, a simplified approach adapted from the methods used by Barbara et al. (2008) and Xu et al. (2008). This suspension was then immediately applied to leaves, which avoided the need to germinate conidial spores on agar. The inoculum was applied via an atomiser, homogenously spraying the suspension across all leaves until their surfaces were saturated (Delalieux et al., 2007). Due to the size and number of the plants, as well as the location of the experiment, control over humidity, temperature, and illumination was limited. The inoculant was sprayed abundantly on all apple plants after sunset during a prolonged period of wet weather occurring on 23rd August 2023. These environmental conditions allowed free water to remain on leaves with temperature and humidity conditions conducive to scab germination over the following 36 hours. The weather conditions recorded during the experiment are provided in Appendix A. After three weeks, only ten samples displayed initial symptoms of apple scab, indicating a potential low inoculation success rate. To increase the number of experimental samples with scab symptoms for training and testing, a second round of artificial inoculation was conducted at 21 d.p.i. By 56 d.p.i., 43 plants developed visual symptoms of scab, demonstrating a 54% inoculation success rate. Throughout the experiment, control samples were manually inspected for scab infection. All control samples remained scab-free during the experiment until leaf drop in December 2023.

5.2.2 Multispectral (VIS-NIR) Time Series Imagery

5.2.2.1 Multispectral (VIS-NIR) Imaging System

High-resolution multispectral imaging was achieved by modifying commercial digital cameras to become sensitive to NIR wavelengths (Verhoeven, 2008; LeBourgouis et al., 2008). The technique was developed from the stereoscopic VIS-NIR multispectral sensor utilised in Bleasdale et al. (2022). Two Canon EOS RP cameras (Canon Inc., Tokyo, Japan) with 26.2 MP full-frame CMOS sensors (5.75 μm pixel pitch) were fitted with short focal length 50 mm lenses. While one camera retained standard RGB Recall, the second was converted by removing the internal infrared filter and replacing it with an external infrared longpass filter (Midwest Optical Systems, Palatine, United States) that enabled near-infrared detection between 800-1000 nm (see Chapter 3.2.2.1). Both sensors were co-aligned and fixed 200 mm apart on a stereoscopic camera bracket. Both sensors had their exposure settings manually adjusted via remote operation through EOS Utility Software (Canon Inc., Tokyo, Japan) and were operated simultaneously through a wireless shutter release remote control.

5.2.2.2 Time series Acquisition Procedure

The primary dataset collected in this study was a time series of RGB and NIR imagery for each individual plant from 1 d.p.i. to 56 d.p.i. Individual plants were placed in the centre of a black imaging surface two metres below the stationary multispectral camera system. Each camera was manually calibrated at the beginning of the experiment on a mid-sized reference plant, adjusting the exposure and focus according to the illumination conditions. A low aperture setting was used to achieve a deep depth of field and keep most leaves within the image in focus, although this did result in darker imagery overall. The camera settings were not readjusted and remained constant for the remainder of the daily imaging regardless of plant size or illumination condition. Imaging occurred daily, between 10 am and 2 pm, for 56 days. All images were acquired within the experimental glasshouse, with illumination conditions varying over time.

Images were taken directly above the plants to recreate a nadir perspective. Control plants were always imaged first, brought into the experimental environment individually and then swiftly removed to minimise exposure to *V. inaequalis*. Due to unforeseen circumstances, images could not be acquired at 44 d.p.i. After 56 days of imaging, 5775 RGB and 5775 NIR (JPG format) images were collected. The time series imagery captured the growth of apple plants and the

development of apple scab over the course of the experiment (Figure 5.1). Examples of the full-time series imagery for large, medium and small plants are provided in Appendix D.

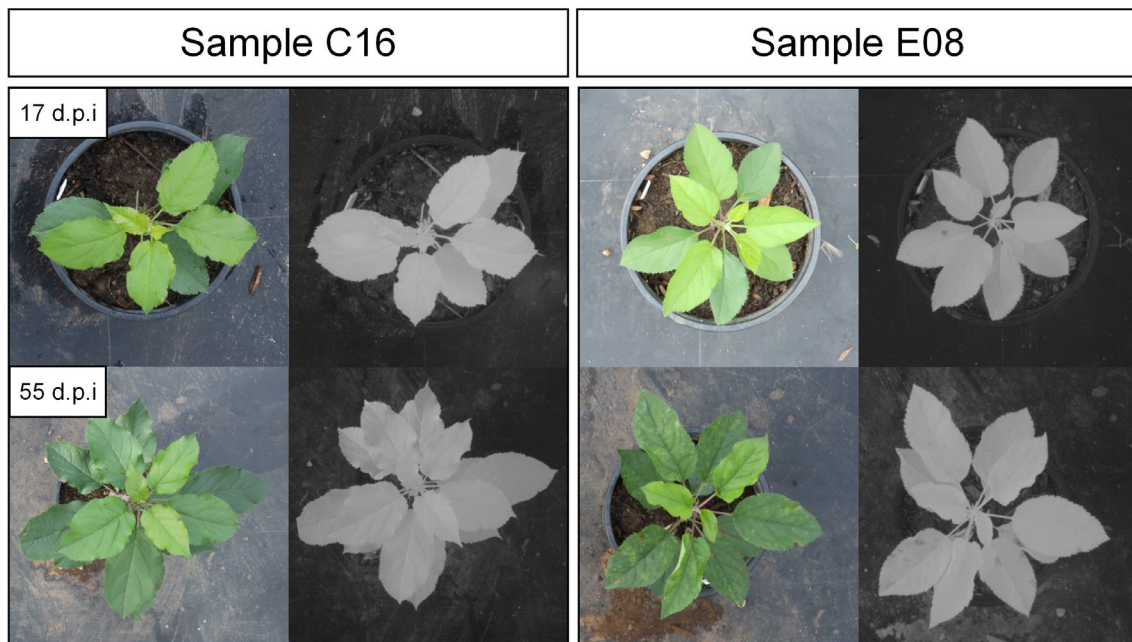


Figure 5.1 RGB and NIR time series imagery displaying examples of control (C16) and experimental (E08) samples at an early and late stage of the experiment.

5.2.3 Apple Disease Dataset

5.2.3.1 Primary Multispectral Data

A total of 11,550 images were acquired as the primary dataset for the experiment, which required preprocessing and annotating for training and testing the CNN models. All images were manually cropped into a 1:1 frame around the entire plant and scaled to 1500x1500 pixels via compression and expansion methods. NIR images were converted to monochrome to display NIR reflectance as overall brightness rather than across individual red, green, and blue bands. The imagery was organised by plant sample number, date of acquisition and waveband (RGB or NIR) to produce 210 individual time series. The lead author manually annotated each time series, tracking infection backwards from 56 d.p.i. to the earliest point of infection. Scab in RGB imagery was identified by the characteristic olive-brown lesions present on the leaves (Belete & Boyraz, 2017). Scab in NIR imagery was identified by the dark lesions on healthy white tissue, indicative of infection (Bleasdale et al., 2022), which was then cross-referenced against RGB imagery to identify known sites of infection. It was assumed that once the scab had been detected in the earliest image, all subsequent imagery was considered scab-infected, irrespective of symptom absence. RGB and NIR time series imagery were classified independently of each other due to

apple scab symptoms presenting earlier in the NIR time series than in RGB, previously demonstrated through manual identification (see Chapter 3.3.1) and CNN-based classification (see Chapter 4.3.4). Other signs of stress from abiotic factors, such as heat, drought, and mechanical damage, were ignored. All images were annotated using a multilabel classification approach, attributing a class label of 'HEALTHY', 'SCAB', and 'MILDEW' to the corresponding filename in a CSV workbook. Due to the multi-labelling strategy, images could contain both 'SCAB' and 'MILDEW' concurrently, but 'HEALTHY' remained independent (Table 5.2).

Labels	HEALTHY	MILDEW	SCAB
RGB	4717	1035	1103
NIR	4725	0	1095

Table 5.2 Quantity of 'HEALTHY', 'MILDEW' and 'SCAB' label classes in the RGB and NIR imagery in the primary dataset

5.2.3.2 Secondary Supplementary Data

The use of supplementary data was necessary as CNNs require a large amount of training data to be capable of providing accurate, unbiased predictions of disease classes. Secondary data from publicly available sources provided image classes of multiple disease categories with varied symptom presence and acquisition conditions. These images were used to improve training robustness by introducing multiple potential diseases, thus reducing biases caused by the imbalance of 'HEALTHY' and 'SCAB' samples in the primary data. Additionally, the secondary data provided independently annotated images that could be used to validate CNN model performance on standard RGB apple disease imagery. The secondary, publicly-available datasets obtained were PlantVillage (Hughes & Salathe, 2015), PlantPathology2020, PlantPathology2021 (Thapa et al., 2020), and AppleScabLDs (Kodors et al., 2020). These datasets contained localised imagery of multiple apple diseases in controlled (PlantVillage) and real-world orchard environments (PlantPathology2020, PlantPathology2021, AppleScabLDs) which, when combined, produced a highly varied dataset with varying image qualities, illumination conditions, and viewing angles.

These secondary data images are intended to supplement the primary dataset imagery for CNN training, enhancing generalisation capabilities in classification tasks. The secondary data covered five disease classes 'FROGEYE' (*Botryosphaeria obtusa*), 'HEALTHY', 'MILDEW' (*P. leucotricha*), 'RUST' (*Gymnosporangium juniperi-virginianae*), and 'SCAB' (*V. inaequalis*), as well as leaves containing combinations of symptoms from these pathogens (Figure 5.2). All datasets contained RGB imagery, localised on unique apple leaves containing well-defined symptoms of

the diseases. Further supplementary multispectral data of apple scab on seedlings, previously acquired by Bleasdale et al. (2022), was also used. This provided an extra 1,600 images of healthy and scab-infected seedlings from high-resolution RGB and NIR sources.

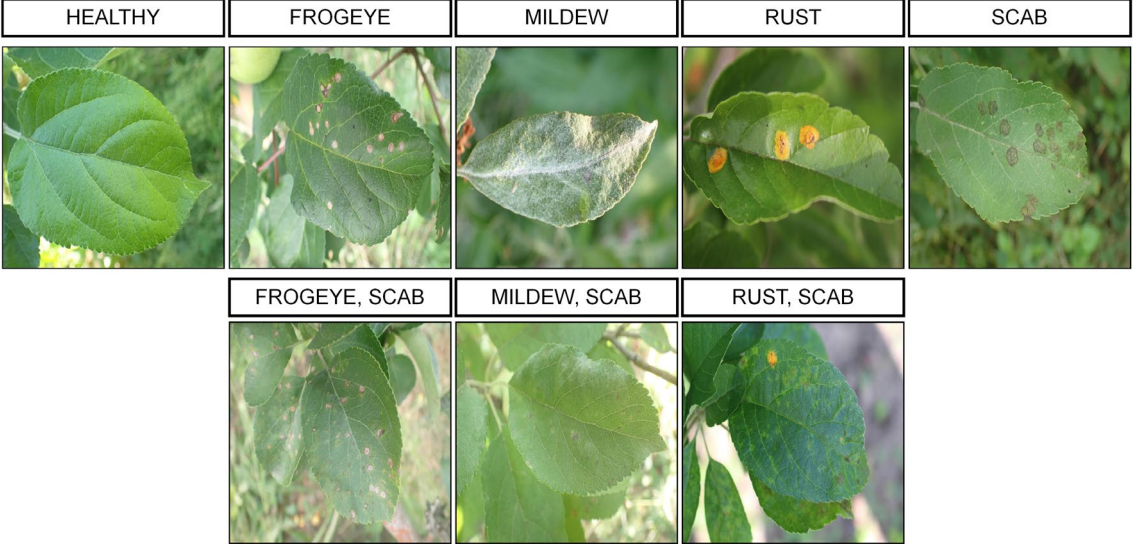


Figure 5.2 Example imagery for each disease class from the secondary validation (public - PlantPathology2021) data. The three lower images display examples of multiple diseases occurring within a single leaf.

5.2.3.3 Training and Testing Set Partition

The fully annotated primary and secondary datasets had to be divided into separate test and training sets. As all primary dataset images were obtained from time series, randomly dividing the dataset was not feasible. If the same plant were included in both training and testing sets, the physical similarities of plant and symptom features between days would introduce unfair biases towards correct classification. All plant samples in the testing set had to be completely independent of the training set. For the purposes of the performance assessment, all experimental samples selected displayed symptoms of scab by the end of the experiment; no samples that may have had latent infections were tested. As only 43 of the 78 plants developed infection, a reduced number of testing plants had to be compromised to achieve a sufficient training set. An approximate 60:40 split between training and testing sets was used. For the testing set, 20 control samples and 20 experimental samples were selected, with variations in pot size, plant physiology, and symptom severity. This produced a total of 4,400 testing images, 2,200 RGB, and 2,200 NIR evenly split between control and experiment samples. To validate the models and compare performance to previous literature, an equal quantity of secondary data from public sources was used, with the 4,400 images selected randomly among the five classes. The most challenging issue for CNN training is the lack of adequate training samples with annotations, so augmentation is often used to solve these dataset limitations (Hasan et al., 2020).

The primary dataset displayed considerable variation in plant structure and physiology, symptom size, shape and severities, and illumination conditions. Despite these variabilities, the stationary imaging angle, homogenous black background, and similarity of symptoms day-to-day would increase the likelihood of CNN overfitting, especially within the NIR time series. The primary training set was artificially inflated by dividing imagery into multiple locations containing symptom features to add a greater diversity of scab symptoms used for training. This helped address the imbalance between 'HEALTHY' and 'SCAB' samples that could lead to prediction biases (Wang et al., 2021). As with preprocessing, this localisation technique had to be performed manually. The low severity of the symptoms meant that automated localisation could miss key symptom features and introduce training errors (Alomar et al., 2023). The localisation method was not necessary for images from secondary sources, as they were mainly localised during acquisition and had a much greater diversity of disease symptoms.

Additional augmentation through geometric transformations was applied to all training images to enlarge the datasets for recognition and decrease the chance of overfitting. Geometric transformations alter the image to make the CNN invariant to changes in position and orientation (Taylor & Nitschke, 2018). These augmentations included random rotations, translations, zoom scaling, and inversions for data variation enhancement during training and to mitigate the risk of overfitting the test predictions. Multispectral images that could not be classified confidently, whether through the uncertainty of earliest infection date or lack of visible symptoms post infection, were not included in the training set. These could have introduced a bias towards scab in the early stages of infection and the control samples. The final training set contained a range of imagery for the 'HEALTHY' and 'SCAB' classes in both RGB and NIR imagery (Figure 5.3) as well numerous examples and combinations for 'FROGEYE', 'MILDEW', and 'RUST'.

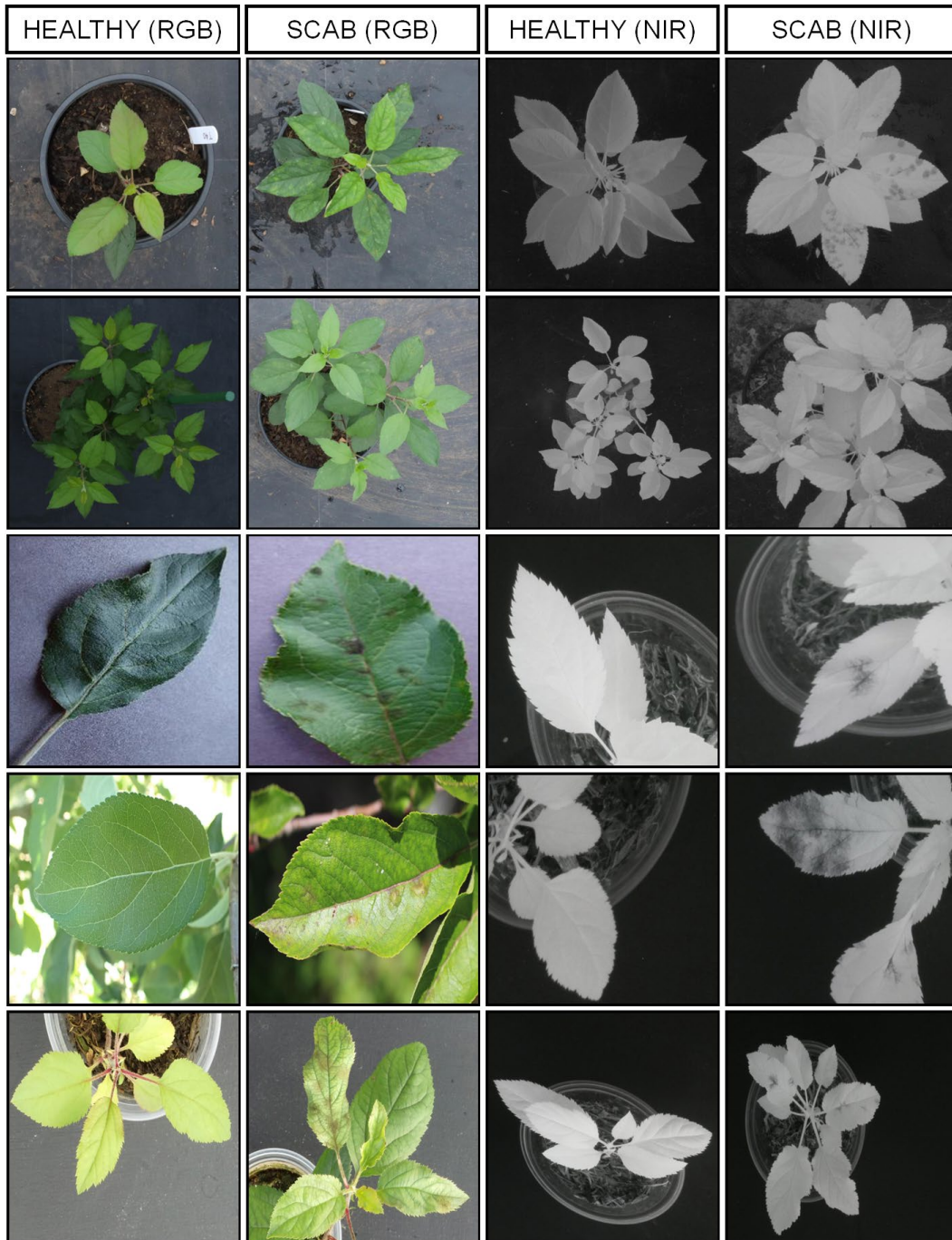


Figure 5.3 Example images within the training set from primary and secondary sources demonstrating the variance within the 'HEALTHY' and 'SCAB' classes in RGB and NIR imagery

All images in both sets were resized to 1200 x 1200 pixels, and their filenames were randomised to reduce further chances of bias. In total, 20,000 training images and 8,800 testing images were used in this study (Figure 5.4). These sets had a greater quantity of 'HEALTHY' samples than all other classes, followed by 'SCAB'. As both datasets were fully annotated for an in-depth performance assessment, no validation set was required; instead, all train set images were dedicated to training.

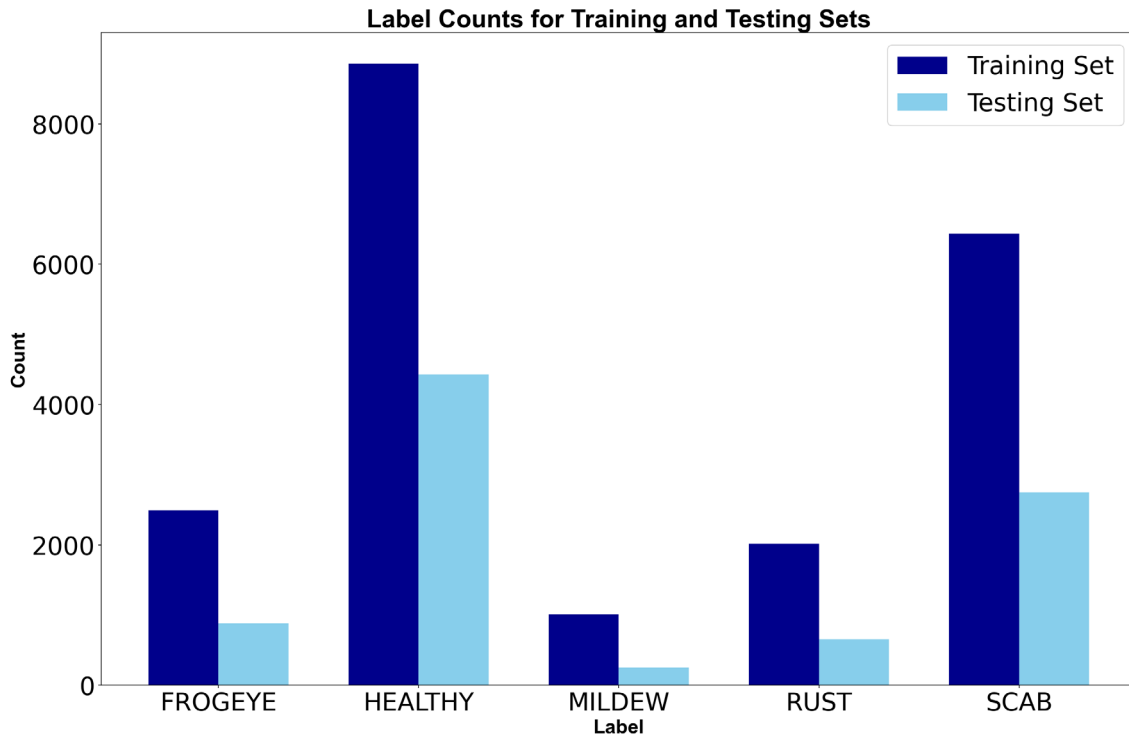


Figure 5.4 The class label distribution across the training and testing sets of the apple disease dataset

5.2.4 Convolutional Neural Networks

5.2.4.1 Fine-Tuning Convolutional Neural Networks

Three pre-trained models: MobileNetV2 (Sandler et al., 2018), InceptionResNetV2 (Szegedy et al., 2016), and EfficientNetV2L (Tan & Le, 2021) were fine-tuned to classify the testing set. As most of the CNN models used in previous apple disease classification studies have proven successful, they were adopted here based on their differing architectures and resource requirements. Each model could be compared against the others to establish which performed best and to ascertain whether the classification of multispectral imagery would work regardless of the architecture. Each model was fine-tuned on the primary and secondary data within the training set, until model convergence. Throughout the training, the output for training time, training accuracy and training loss were displayed per epoch. After training, each fine-tuned model and their weights were saved as hdf5 files. This allowed the fine-tuned models to be readily available for future classification without requiring retraining. Upon training, each model immediately classified the testing set, and provided a confidence score output for each training image in a CSV folder. The full fine-tuning and classification process is shown in Figure 5.5.

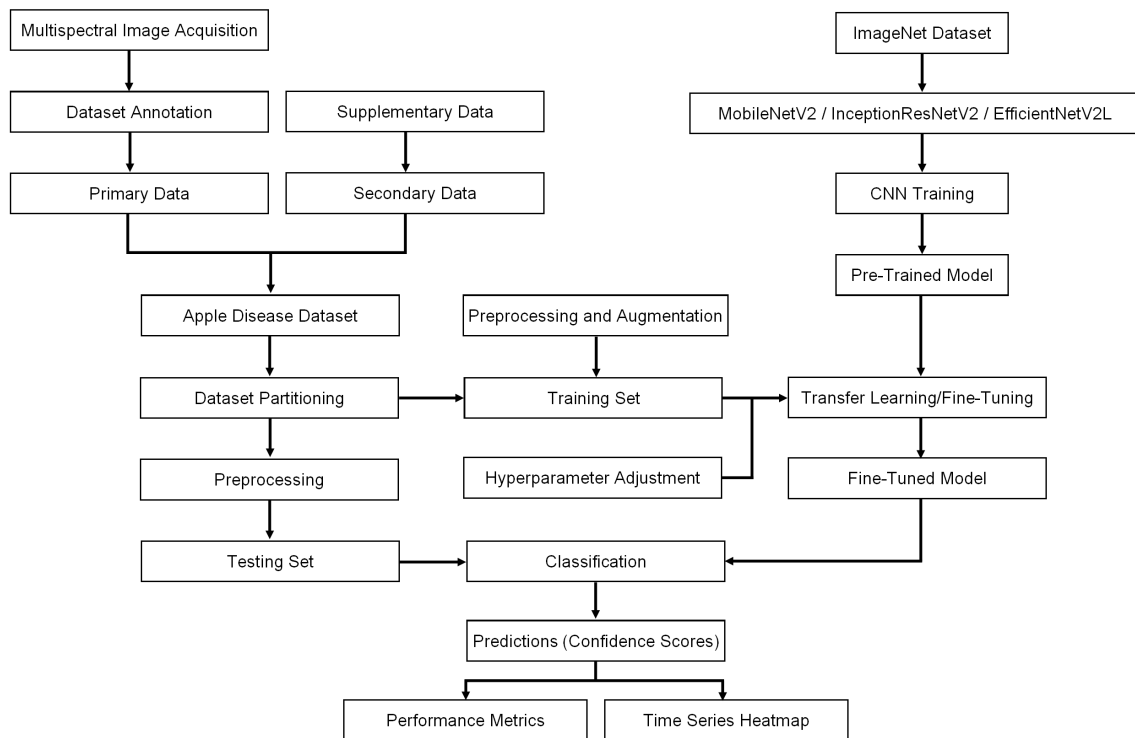


Figure 5.5 Flow diagram of the apple disease dataset multi-label classification process

All three models were downloaded from the Keras library, having already been pre-trained on millions of annotated images from ImageNet (Deng et al., 2009). Transfer learning is a technique that leverages the knowledge of a pre-trained model as the foundation for a new classification model, requiring less data for the new training phase, thereby reducing training time and mitigating overfitting (Zhuang et al., 2019). Fine-tuning, a key transfer learning method, involves using the weights of a pre-trained model to initialise the model before retraining either all or part of these weights on the target training set (Boulent et al., 2019). This approach significantly enhances the adaptability of a CNN classifier compared to the direct application of a pre-trained network (Radenović et al., 2018; Dhaka et al., 2021). For this study, all model weights were frozen except for the final fully connected layer, which remained unfrozen and was retrained on the training set to produce three fine-tuned CNN models for apple scab classification (Figure 5.6).

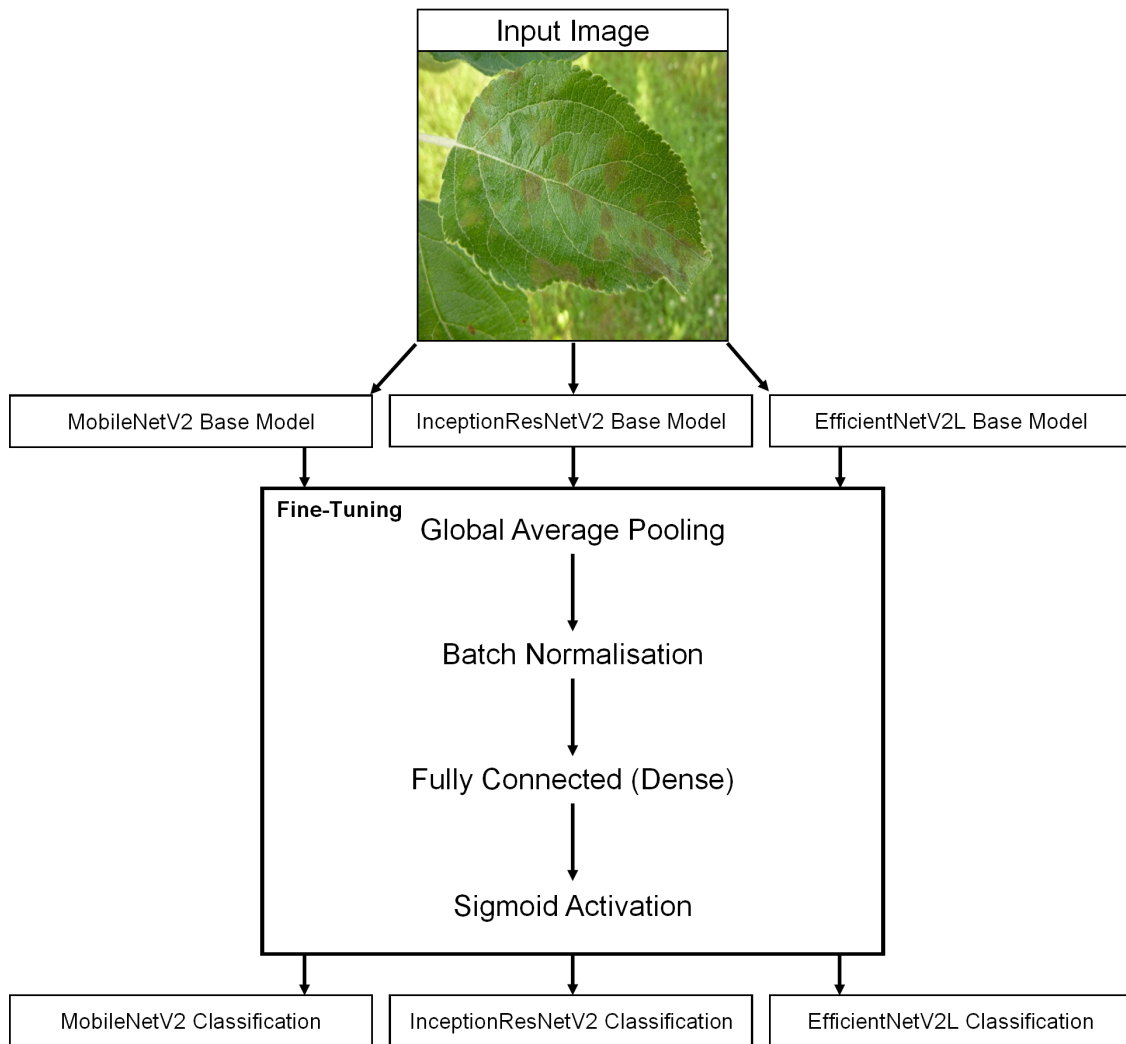


Figure 5.6 Process of fine-tuning the final fully-connected layer of the pre-trained MobileNetV2, InceptionResNetV2, and EfficientNetV2L models

5.2.4.2 Operational Environment and Hyperparameter Adjustment

For optimal training and classification, CNN architectures must use appropriate hyperparameters that balance high performance with hardware utilisation and training times (Ang et al., 2023). Hyperparameter adjustments for each model were tuned based on the hardware resources available (Table 5.3) and the performance assessment of the validation testing set. All CNN models were trained and classified in Python on the PyCharm IDE. Each model was trained until convergence at epoch 12 with a decremental learning rate for each epoch. For the computing resources available, batch sizes of 40, 30, and 6 were optimal for MobileNetV2, InceptionNetV2, and EfficientNetV2L. For multi-label classification, the Sigmoid activation function and BinaryCrossentropy loss function were most appropriate. The complete model fine-tuning and classification code has been provided in Appendix B.

Hardware Configuration Parameters	
CPU	AMD Ryzen 7 5800H 3.2GHZ
GPU	Nvidia GeForce RTX 3070 Laptop GPU (8Gb)
RAM	64Gb
Hard Disk	1Tb
Operating System	Windows 11 Home OS Build 22000.1455

Table 5.3 Hardware configuration parameters

5.2.5 CNN Classification Performance Evaluation

The performance of each CNN model was assessed in terms of their confidence score outputs for each disease class, specifically 'SCAB'. Due to the presence of multiple diseases in the dataset, which is also a common occurrence in real-world orchards, a multilabel classification approach was adopted. This multilabel approach means that CNN classification output predictions for each individual class can have a maximum confidence score of 1.00. A threshold score of 0.5 was used, and values over this threshold were considered a positive prediction for that class. As a leaf could not be both healthy and infected simultaneously, prediction outputs that contained a disease class alongside 'HEALTHY' had the latter class ignored. Individual-label binary confusion matrices were used as the basis for performance assessments, with true and false positives and negatives based on the manually annotated labels. From these confusion matrices generated, metrics for accuracy, recall (sensitivity), specificity, precision, and F1 Score were calculated for each model (see Chapter 4.2.3). The performance assessments of multispectral data were focused only on 'SCAB' classifications. These assessments were made on the overall dataset of RGB and NIR imagery on a sample-by-sample basis.

For the time series analyses, the confidence scores attributed to the 'SCAB' class for each day were used. These scores were used to generate a heatmap using the Plotly graphing library in Python, where the value of each cell represents the confidence score for one image of one plant on one day. The heatmaps for RGB and NIR time series were assessed and compared against each other to determine the key features, trends, and discrepancies from the manual classification. These include the earliest points of detection, the presence of noise, and plant physiology or illumination conditions that may influence false results. To finalise the comparison of RGB and NIR imagery for scab detection, a time series of cumulative confidence was produced.

5.3 Results

5.3.1 CNN Model Training Convergence

The MobileNetV2, InceptionResNetV2, and EfficientNetV2L architectures underwent training until convergence was achieved at epoch 12. Following the final training epoch, the CNNs exhibited training accuracies of 0.9524, 0.9772, and 0.9740 with corresponding training losses of 0.0469, 0.0102, and 0.0176 for MobileNetV2, InceptionResNetV2, and EfficientNetV2L, respectively (Figure 5.7). These preliminary results suggested that InceptionResNetV2 had the best performance in classifying the training dataset. EfficientNetV2L incurred the longest training duration, taking 67.8% longer to train all 20,000 images than MobileNetV2. Despite the extended training duration, the classification of all 8,800 test images by EfficientNetV2L took only slightly longer than MobileNetV2 (Table 5.4). The training performance metrics, including training accuracy, training loss, and the training time recorded after each epoch, as well as overall classification (testing) time, are provided in Appendix C.

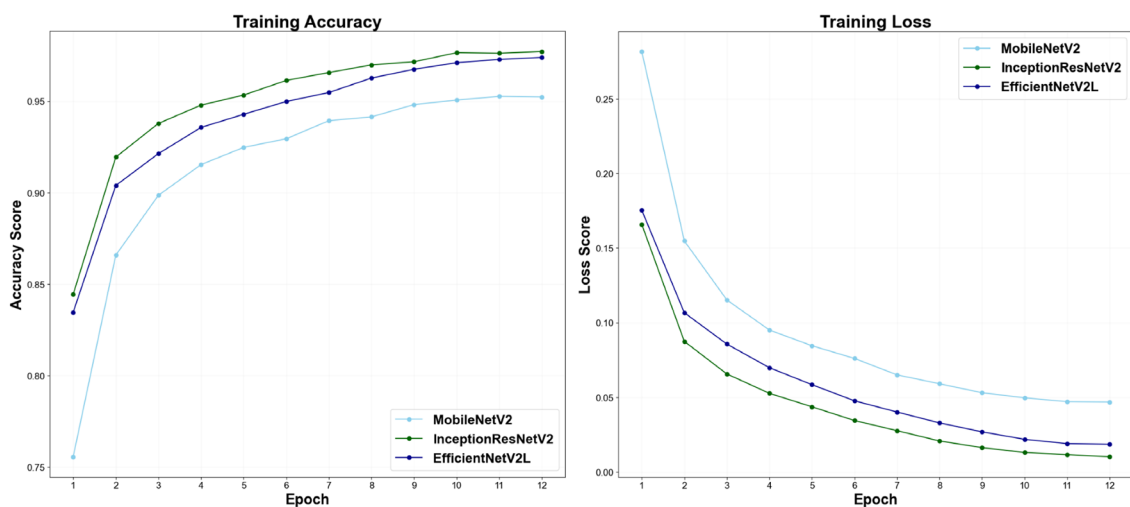


Figure 5.7 Convergence in training accuracy (left) and training loss (right) for MobileNetV2, InceptionNetV2 and EfficientNetV2L models

Model	Training Time	Time per Epoch	Testing Time
MobileNetV2	9159s	763s	336s
InceptionResNetV2	9500s	792s	331s
EfficientNetV2L	15370s	1281s	353s

Table 5.4 Training and testing runtimes for MobileNetV2, InceptionNetV2 and EfficientNetV2L models

5.3.2 CNN Classification Performance

5.3.2.1 Validating CNN Performance on Secondary Data

The three models were validated based on their classification performance for all five classes across the 4,400 images from the public sources in the secondary data. This validation approach was chosen due to the limited number of classes within the primary dataset, which exhibited a bias towards healthy samples and in which only binary classification would be feasible. Thus, potentially overlooking the CNNs discriminatory capabilities in classifying scab, among other diseases. The classification results derived from confusion matrices demonstrated strong performances across each model, with high accuracies maintained across all five classes (Table 5.5). The overall F1 Scores calculated were 0.9428, 0.9557, and 0.9662, with 'SCAB' class scores of 0.9528, 0.9516, and 0.9644 for MobileNetV2, InceptionResNetV2, and EfficientNetV2L, respectively. EfficientNetV2L exhibited the highest overall performance, demonstrating a modest 0.66% improvement over MobileNetV2 and 0.43% over InceptionResNetV2. This improvement was more pronounced in the 'SCAB' class, with a 1.45% and 0.89% increase in accuracy. The 'MILDEW' class received the highest validation accuracies, followed by 'RUST', with 'SCAB' receiving the lowest. This was attributed to the imbalance in class labels in the testing dataset, as accuracy measurements are greatly influenced by the number of true negative predictions. Investigation of the F1 Scores demonstrates high performance in both 'HEALTHY' and 'SCAB' classes, even with the influence of the RGB and NIR time series imagery in the training set. These results underscore the effectiveness of the CNNs and their ability to accurately identify multiple diseases even under challenging illumination conditions and combined disease symptoms.

Model	Metric	FROGEYE	HEALTHY	MILDEW	RUST	SCAB	Total
MobileNetV2	ACC	0.9789	0.9791	0.9923	0.9852	0.9611	0.9793
	REC	0.9421	0.9712	0.9150	0.9376	0.9393	0.9473
	SPE	0.9881	0.9823	0.9969	0.9936	0.9724	0.9877
	PRE	0.9518	0.9578	0.9456	0.9625	0.9463	0.9529
	F1	0.9469	0.9644	0.9300	0.9499	0.9428	0.9501
InceptionResNetV2	ACC	0.9777	0.9800	0.9966	0.9864	0.9675	0.9816
	REC	0.9432	0.9790	0.9636	0.9482	0.9367	0.9529
	SPE	0.9864	0.9804	0.9986	0.9931	0.9834	0.9892
	PRE	0.9454	0.9537	0.9754	0.9599	0.9670	0.9584
	F1	0.9443	0.9662	0.9695	0.9541	0.9516	0.9557
EfficientNetV2L	ACC	0.9827	0.9886	0.9930	0.9895	0.9757	0.9859
	REC	0.9705	0.9696	1.0000	0.9665	0.9653	0.9696
	SPE	0.9858	0.9965	0.9925	0.9936	0.9810	0.9902
	PRE	0.9448	0.9912	0.8885	0.9636	0.9634	0.9628
	F1	0.9574	0.9803	0.9410	0.9650	0.9644	0.9662

Table 5.5 CNN prediction accuracies for each class in the test set from secondary (public) data sources. (ACC – Accuracy, REC – recall, SPE – specificity, PRE – precision, F1 – F1 score)

Having assessed the ability of each CNN to classify imagery from public sources within the secondary data, it was possible to compare performance more broadly against similar metrics reported in earlier studies. All three CNNs outperformed the VGG_INCEP model (97.1%) the model developed by Jiang et al. (2018), as well as the InceptionResNetV2 model (88.6%) employed by Turkoglu et al. (2022). Only EfficientNetV2L achieved performance comparable to XDNet (98.4%) by Chao et al. (2020) and an EfficientNetV2 model (98.8%) by Xiao et al. (2023). The only model in the literature to surpass the EfficientNetV2L performance was an SE_Xception model (99.4%) trained by Chao et al. (2021). The results from the validation data suggest comparable performance with previous studies against previous research, although direct comparisons can be drawn against studies utilising the same public datasets: PlantVillage and PlantPathology datasets. For instance, Mohanty et al. (2016) achieved an accuracy of 0.99 through transfer learning on GoogleNet, while Vishnoi et al. (2023) achieved an accuracy of 0.98 and recall of 0.94 on scab with images from PlantVillage. While these studies show higher performance, the PlantVillage dataset was simple, localised entirely on individual leaves with late-stage symptoms under controlled illumination conditions with high-contrast black backgrounds.

The PlantVillage dataset presents ideal acquisition and classification conditions rather than the practical, real-world conditions this study chooses to replicate (Saleem et al., 2019). All models in our study outperformed the ResNet50 model used on PlantPathology2020, which attained a 97.0% accuracy (Thapa et al., 2020), and the AFD_Net model, which achieved an accuracy of 92.6% on PlantPathology2021 (Yadav et al., 2022). The performances of all three CNNs display a

marked improvement over the previous fine-tuned MobileNetV2 and EfficientNetV2L in Chapter 4, which achieved F1 scores of 0.911 and 0.914, respectively. This improvement in accuracy is attributed to adopting a multi-label classification approach instead of a multi-class approach. The inclusion of a multiple disease 'COMPLEX' class adversely impacted the training and classification of each individual disease within these class images. These comparative analyses highlight the effectiveness of CNN models trained on this study dataset to accurately distinguish late-stage apple scab and healthy leaves from other foliar diseases from localised leaf imagery under the challenging conditions encountered in real-world scenarios.

5.3.2.2 Scab Classification Performance on Multispectral Imagery

Having demonstrated the diagnostic abilities of CNNs to distinguish the 'HEALTHY' and 'SCAB' classes from other disease types, the same assessment methodology was applied to the 4,400 multispectral images in the primary dataset. Although overall accuracies showed that 'SCAB' predictions were statistically significant, there was a major drop in performance for this dataset compared to the validation data (Table 5.6). The high accuracies and specificities suggested minimal false positives in experimental or control samples. The F1 scores are not discussed because there were no true positive samples for the control set, which did not allow precision metrics to be calculated for these samples. The mean accuracy scores across NIR and RGB imagery were 0.807, 0.829, and 0.854 from MobileNetV2, InceptionResNetV2, and EfficientNetV2L, a significant improvement over the mean accuracies of 0.7714 and 0.7764 from MobileNetV2 and EfficientNetV2L reported in Chapter 4. However, the mean recall score, the proportion of true positives identified correctly, was significantly worse, with scores of 0.418, 0.486, and 0.607 from MobileNetV2, InceptionResNetV2, and EfficientNetV2L compared to scores of 0.795 and 0.670 presented in Chapter 4. MobileNetV2 and InceptionResNetV2 models misclassified 'SCAB' as 'HEALTHY' more often than correctly identifying them as infected. This indicates an overwhelming bias towards 'HEALTHY' when classifying the test data. Only EfficientNetV2 predicted true positives more often than false negatives to achieve a statistically significant recall score of over 50%.

The disparity between high accuracies and low sensitivities is caused by the imbalance between the 'HEALTHY' and 'SCAB' classes in the test dataset, where a bias towards the former can lead to high true negative classifications in the latter, skewing accuracy results. All models showed superior performance in classifying 'SCAB' when using NIR imagery compared to RGB. The overall accuracy of NIR imagery was 7.3% higher, and its recall was 23.1% greater than that of RGB imagery. As only EfficientNetV2L displayed a reliable classification of scab in both sets of

imagery, further classification performance assessments will only consider results from EfficientNetV2L going forward.

Labels	Accuracy		Recall		Scab Count	
	RGB	NIR	RGB	NIR	TP	FN
MobileNetV2	0.7827	0.8318	0.3650	0.4718	516	716
InceptionResNetV2	0.7968	0.8618	0.4206	0.5523	600	632
EfficientNetV2L	0.8236	0.8846	0.5696	0.6447	749	484

Table 5.6 Model prediction accuracy and recall for the 'SCAB' class for RGB and NIR imagery and the total count of 'SCAB' predictions (True Positives (TP) and False Negatives (FN))

Further assessment of the classification results by assessing the classification of each plant sample individually provided useful information on the sources of the poor sensitivities (Table 5.7). While overall performance in the experimental set was modest, the classification performance of control samples was high, with few instances of false positives across all 20 control samples in RGB and NIR imagery. The CNN specificity was calculated to be 0.9218 and 0.9800 for RGB and NIR, showing a greater ability to predict a true negative of scab within the latter imagery. It was noteworthy that other studies lack control samples for comparison purposes. For instance, Yadav et al. (2022) reported high specificities of up to 0.99 but did not include control samples. Similarly, the previous chapter lacked a well-defined control set but achieved specificities up to 0.8186, with higher specificities observed in RGB imagery than in NIR imagery. These results show that the risk of false positive predictions of scab is low, especially from NIR imagery.

Analysing the classification of scab on each individual plant revealed that even the best-performing and most stable EfficientNetV2L model exhibited notable performance variations in the cumulative predictions of experiment samples. Classification sensitivities ranged from 0.277 to 0.917 in RGB and 0.111 to 0.869 in NIR. There was no discernible correlation between the initial infection date and prediction recall despite the greater length of time for scab infections to mature and spread. In the NIR imagery, four of the five lowest-ranking accuracy and sensitivities occurred when classifying the oldest plants in large pots (E01 to E05). These samples were the largest plants classified, with the most complex structures. They were also the most resilient to scab infections due to their maturity and had low infection severities by the end of the experiment. There was a clear relationship between plant size and recall ability, with the larger plants influencing poorer 'SCAB' classification performance likely due to the lower infection severities compared to smaller, more susceptible plants with fewer leaves.

Control Labels	RGB	NIR	Experiment Labels	RGB		NIR	
	Accuracy	Accuracy		Accuracy	Recall	Accuracy	Recall
C01	1.0000	1.0000	E01 (12 d.p.i.)	0.4909	0.3636	0.5636	0.4545
C02	0.9636	0.9273	E02 (38 d.p.i.)	0.5091	0.5556	0.7091	0.1667
C03	0.9091	1.0000	E03 (33 d.p.i.)	0.6545	0.7391	0.7091	0.4348
C04	0.7273	0.9636	E04 (38 d.p.i.)	0.6545	0.2778	0.7091	0.1111
C05	0.9636	1.0000	E05 (34 d.p.i.)	0.7818	0.6364	0.7818	0.5652
C06	0.9636	1.0000	E06 (23 d.p.i.)	0.7636	0.6364	0.8909	0.8485
C07	0.8909	1.0000	E07 (12 d.p.i.)	0.7455	0.6744	0.8909	0.8636
C08	0.7818	0.9636	E08 (21 d.p.i.)	0.8182	0.7143	0.8364	0.8000
C09	0.8727	0.9636	E09 (19 d.p.i.)	0.7091	0.5556	0.9091	0.8649
C10	1.0000	1.0000	E10 (17 d.p.i.)	0.6182	0.4615	0.6000	0.4359
C11	1.0000	1.0000	E11 (33 d.p.i.)	0.7273	0.3478	0.8545	0.6522
C12	0.9455	1.0000	E12 (37 d.p.i.)	0.8727	0.7778	0.8727	0.6842
C13	1.0000	1.0000	E13 (14 d.p.i.)	0.7091	0.6000	0.7455	0.6667
C14	0.9818	1.0000	E14 (18 d.p.i.)	0.8364	0.7500	0.8364	0.7632
C15	1.0000	1.0000	E15 (32 d.p.i.)	0.7455	0.3913	0.9455	0.8696
C16	0.9636	0.9455	E16 (33 d.p.i.)	0.7091	0.3043	0.8364	0.6087
C17	0.9273	1.0000	E17 (13 d.p.i.)	0.7091	0.6279	0.8182	0.7674
C18	0.8727	0.8909	E18 (32 d.p.i.)	0.9455	0.9167	0.8727	0.7083
C19	0.9636	0.9636	E19 (19 d.p.i.)	0.6364	0.4118	0.7091	0.5946
C20	0.9074	0.9636	E20 (21 d.p.i.)	0.7273	0.5833	0.7091	0.5429
TN	996	1024	TP	348		401	
FP	75	23	FN	263		220	

Table 5.7 EfficientNetV2L prediction accuracy and recall for the 'SCAB' class for RGB and NIR imagery for each plant samples and the total count of 'SCAB' predictions (True Negative (TN), False Positives (FP), True Positives (TP) and False Negatives (FN))

5.3.3 Enhancing Classification Performance Through Localisation

5.3.3.1 Image Localisation Rationale and Methodology

A further qualitative investigation into the classification performance of each sample revealed two major trends affecting classification recall. First, larger plants with a greater number of leaves were misclassified more often, as well as images where symptoms were sparse with small lesions on a few leaves. Second, there was a clear influence of infection severity on the classification performance through all stages of apple scab progression. Plants with a lower percentage of leaf cover displaying symptoms were more likely to be misclassified as healthy. Even during early-stage infections, plants with scab lesions spread across numerous leaves had greater sensitivities than late-stage infections of single lesions. This offers a major explanation as to why the classification performance was higher in the validation data than in the multispectral data. In the secondary data, image acquisition was focused on individual leaves displaying the recognisable features of infection classes, with the clear aim of robust CNN training. The key difference between the secondary data and the primary data collected was that

in this study, whole plants were imaged, not just specific focal regions. This caused a higher ratio of healthy-to-infected tissue in ‘SCAB’ positive imagery, causing the bias towards ‘HEALTHY’ predictions. It was clear that the primary data within the testing set, containing multispectral images of whole plants, was unsuitable for accurately classifying apple scab, especially at early stages and low severities. Acquisition of more multispectral imagery to improve CNN training was unfeasible. The primary data within the testing set was therefore augmented by localising the images onto the regions displaying scab symptoms identified during the manual dataset annotation. Image localisation has previously been demonstrated to improve image classification (Barbedo, 2019a). Localisation of imagery was performed manually by cropping each training image labelled scab to zoom into smaller regions that contained symptoms and their surroundings. This technique reduced the ratio of healthy to scab-infected leaves within the multispectral images. This approach was somewhat subjective but aimed to maintain a combination of infected, healthy and background features within each image (Figure 5.8). As healthy samples did not contain scab symptoms, and the overall model performance on these images was acceptable, these images did not need to be localised. Cropping transformed the multispectral imagery to levels of localisation similar to those exhibited in the public datasets.

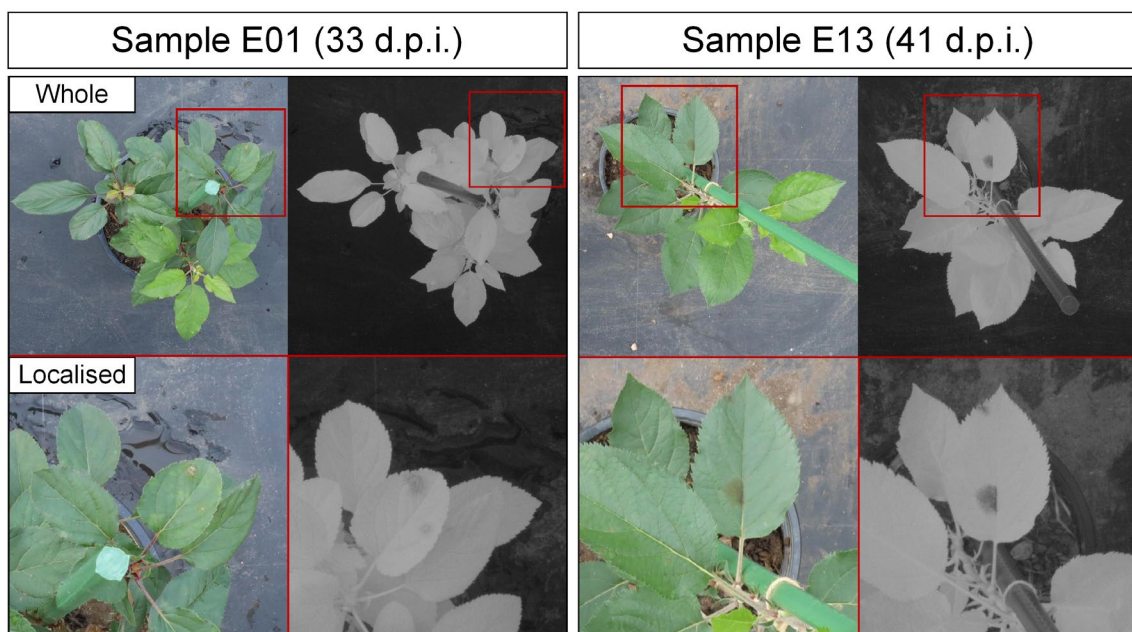


Figure 5.8 Example of whole-plant and localised images of experimental samples E01 and E13 in RGB and NIR imagery

5.3.3.2 Classification Performance on Localised Multispectral Imagery

The previously fine-tuned EfficientNetV2L model reclassified all images within the new localised testing set. This methodology significantly improved classification performance, with an overall 42.19% increase in true positives and a 34.5% decrease in false negatives compared to the

original whole-plant imagery in the testing set (Table 5.8). Recall scores ranged from 0.590 to 1.000 in RGB and 0.714 to 1.000 in NIR imagery. Again, NIR was superior to RGB, with 6.4% more true positives and 31.2% fewer false negatives, but the difference in performance was reduced as the RGB imagery experienced a greater overall improvement as a result of the manual localisation. All samples that had previously performed poorly, especially the larger plants and with low-severity infections, achieved greater ‘SCAB’ prediction sensitivities, with only 3 samples scoring below 0.8 in NIR imagery. These results demonstrated that the classification of apple scab was improved when localised imagery was used in preference to whole-plant imagery.

Experiment Labels	RGB		NIR	
	Accuracy	Recall	Accuracy	Recall
E01	0.8909	0.8636	0.8546	0.8182
E02	0.5818	0.9444	0.9818	0.9444
E03	0.8182	0.8696	0.8909	0.9565
E04	0.8909	1.0000	0.9818	0.9444
E05	0.9091	0.7727	0.9818	0.9565
E06	0.8909	0.8788	0.9818	1.0000
E07	0.9636	0.9535	1.0000	1.0000
E08	0.9091	0.8571	0.8909	0.8571
E09	0.9091	0.8611	0.9455	0.9189
E10	0.7091	0.5897	0.8909	0.8462
E11	0.9636	0.9130	0.9455	0.9130
E12	0.9091	0.9444	0.9636	0.8947
E13	0.8727	0.8250	0.8182	0.7619
E14	0.9091	0.8611	0.9818	0.9737
E15	0.8909	0.7826	1.0000	1.0000
E16	0.8546	0.6957	0.9273	0.8261
E17	0.9273	0.9070	0.9273	0.9070
E18	0.9636	0.9583	0.9273	0.8333
E19	0.8364	0.7647	0.8182	0.7568
E20	0.8546	0.7778	0.8182	0.7143
TOTAL	0.8727	0.8510	0.9264	0.8912
TP	516		549	
FN	95		72	

Table 5.8 Cumulative EfficientNetV2L prediction accuracies and sensitivities for the ‘SCAB’ class for RGB and NIR imagery and the total count ‘SCAB’ predictions (True Positives (TP) and False Negatives (FN))

To further reiterate the effectiveness of this localisation technique for enhancing classification accuracy, the pre-trained MobileNetV2 and InceptionResNetV2 models were also used to reclassify the new test set. Cumulatively, accuracies and recall scores were 13.3% and 53.0% greater than whole-plant imagery, despite an outlier in the low performance of InceptionResNetV2 classification of RGB imagery (Table 5.9). EfficientNetV2L still performed best of the three, achieving accuracies of up to 95.4% in the classification of ‘SCAB’ from NIR imagery comparable to accuracies achieved in previous literature. MobileNetV2,

InceptionResNetV2, and EfficientNetV2L achieved the final F1 scores in RGB of 0.6972, 0.7143, and 0.8245, respectively, and 0.8816, 0.8745, and 0.9150 in NIR imagery. After improving the classification of apple scab from multispectral imagery with three CNNs, the evidence shows that the classification of ‘SCAB’ is more accurate, sensitive, and precise from NIR images than RGB.

Labels	Accuracy		Recall		Scab Count	
	RGB	NIR	RGB	NIR	TP	FN
MobileNetV2	0.85318	0.93636	0.60884	0.83897	893	339
InceptionResNetV2	0.86909	0.92864	0.58920	0.88084	907	325
EfficientNetV2L	0.90273	0.95364	0.84452	0.88406	1065	167

Table 5.9 Model prediction accuracies and recall scores for the ‘SCAB’ class for cropped RGB and NIR imagery. The total count of ‘SCAB’ labels True Positives (TP) and False Negatives (FN) are also displayed.

5.3.4 Time Series Assessment

To assess the capabilities of the CNNs to monitor scab progression over time, heatmaps of scab predictions were produced for overall manual identification (Figure 5.9) and EfficientNetV2L classifications across the RGB (Figure 5.10) and NIR (Figure 5.11) time series. The heatmap of manually classified images shows the expected pattern to be observed. The manual classification was considered the ground truth, hence any classification of ‘SCAB’ predicted earlier than the first date of infection in the manual time series was considered to be a false positive in the predicted data. Control samples C01 to C20 in the top half of the heatmap should have a zero-confidence score for ‘SCAB’ throughout the 56 days of the experiment. The experimental samples display a large variation in earliest infection points, ranging from 12 to 38 d.p.i. This variation makes it difficult to determine the true earliest points of infection between NIR and RGB imagery and displays the inconsistency with inoculation and latency periods of scab infection across the test set samples.

The CNN-based confidence outputs for each image were used to convert the results to heatmaps. As EfficientNetV2 was consistently the most accurate, only results from this model have been further assessed. The confidence threshold of 0.5 was maintained, with any value below considered a null classification. Apple scab was classified 1.4 days earlier in the NIR time series than in RGB, on average. Out of the 20 experimental samples, ‘SCAB’ was classified on the same day in RGB and NIR imagery in 12 plants, with samples E13 and E14 being detected two days earlier and E19 detected three days earlier in the NIR time series. Plant sample E20 was an outlier, being the only sample manually classified earlier in RGB than in NIR by one day. Of all the plants, E01 and E07 had the earliest detection date, at 12 d.p.i. Overall, NIR matched manual classifications better, being detected on the date of manual classification in 17 samples, unlike

RGB, where only 10 samples achieved this. There was considerable variation in early classification between samples between the RGB and NIR datasets. The greatest difference occurred in E19, which was classified nine days earlier in NIR than RGB, followed by E10, being classified seven days earlier. E01, E16, E18 and E20 were classified one day earlier in RGB than NIR and E02, E03, E04 and E08 on the same day. The remainder of the samples classified ranged between one-to-three days earlier. These results provide further support to the classification performance assessments in the use of NIR imagery to detect apple scab.

These heatmaps can also be used to discriminate between extraneous noise and direct influences of misclassifications. In the RGB dataset, many false positives were predicted on the sample plant over consecutive days, indicating specific features that were not detectable in NIR imagery. Investigation into these causes revealed that these influences were largely the result of abiotic damage to leaves, occurring in both control and experimental imagery. There were also trends in false negatives occurring on specific days, at 31, 43 and 49 d.p.i. in RGB and 49, 51 and 53 d.p.i. in NIR. These can be attributed to the acquisition on the specific day of imaging, due to the sensor exposure settings not being fully optimised to the illumination conditions. These features were more pronounced in NIR imagery, where strong solar insolation directly on the leaf surface caused a higher likelihood of 'HEALTHY' predictions.

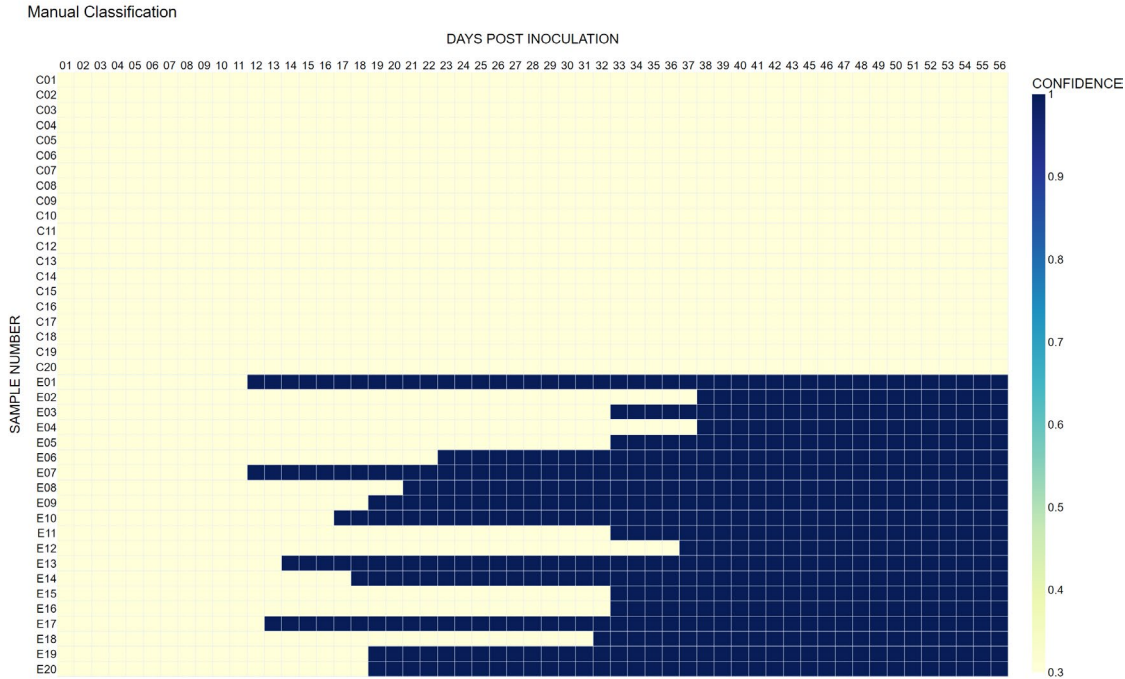


Figure 5.9 Time series of manually classified data (Yellow – Healthy; Aqua/Blue – Scab) for control (C01-C20) and experimental (E01-E20) samples

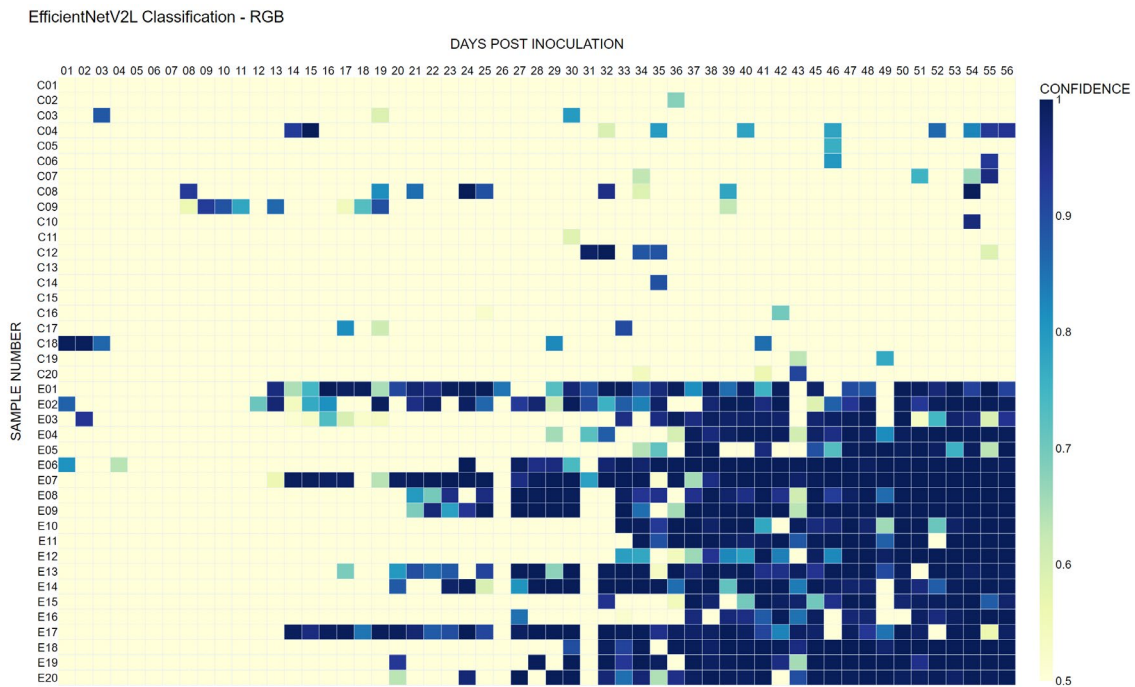


Figure 5.10 Time series heatmap of 'SCAB' confidence scores for RGB imagery. (Yellow – Healthy; Aqua/Blue – Scab) for control (C01-C20) and experimental (E01-E20) samples

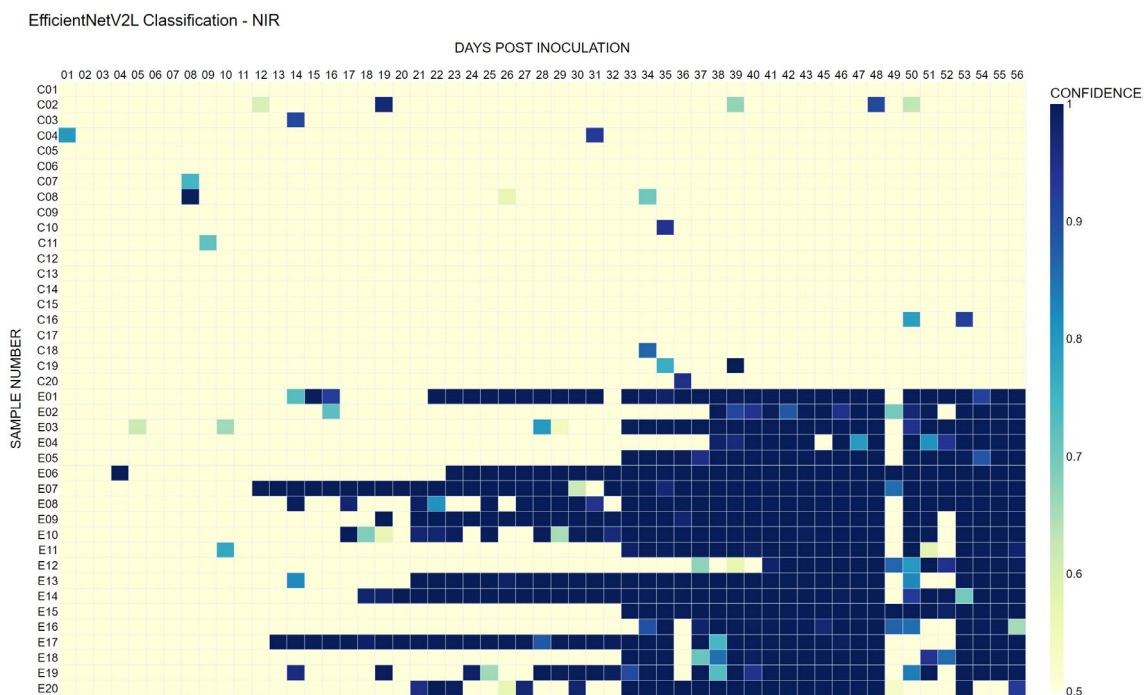


Figure 5.11 Time series heatmap of 'SCAB' confidence scores for NIR imagery. (Yellow – Healthy; Aqua/Blue – Scab) for control (C01-C20) and experimental (E01-E20) samples

Due to the inconsistencies in the dates of the initial infection, noise, and other influences from plant physiology and acquisition conditions, it was difficult to interpret the differences between RGB and NIR imagery for monitoring scab progression over the duration of the experiment. To reduce these effects, a 3-day smoothed time series of cumulative scores for the control and

experimental samples was produced (Figure 5.12). This time series displays the precision of scab detection across all samples over time, following the sum of confidence scores with minimal false positives across all 20 experimental samples. The model has high precision for apple scab predictions. For RGB imagery, the greatest overprediction of scab occurred on day 15, with a score of 4.76 rather than 4.00. There were no overall over-predictions in NIR imagery. The mean confidence difference for scab predictions was 12.12% for NIR and 19.49% for RGB. In the early stages and control samples, there are varying levels of specificity where confidence scores for 'SCAB' exist in the absence of symptoms. The specificity for control samples in the NIR imagery is lower and more stable, with less fluctuation than RGB imagery.

In the late stages of the disease, at 38 d.p.i., all 20 samples are infected, and a maximum confidence score of 20 can be achieved. Initially, NIR imagery performs better than RGB imagery, with a higher confidence score than RGB. However, a notable deviation occurred around day 48, attributed to higher illumination levels in the imagery from 49 d.p.i to 51 d.p.i., which brought down the mean confidence. This had a much greater effect on the NIR imagery, leading to cumulative accuracies between both image types being comparable in the late stages. The smoothed moving-mean time series analysis clearly illustrates that the EfficientNetV2L model classifies apple scab earlier and more confidently and with greater stability in NIR imagery than in RGB imagery under most natural illumination conditions.

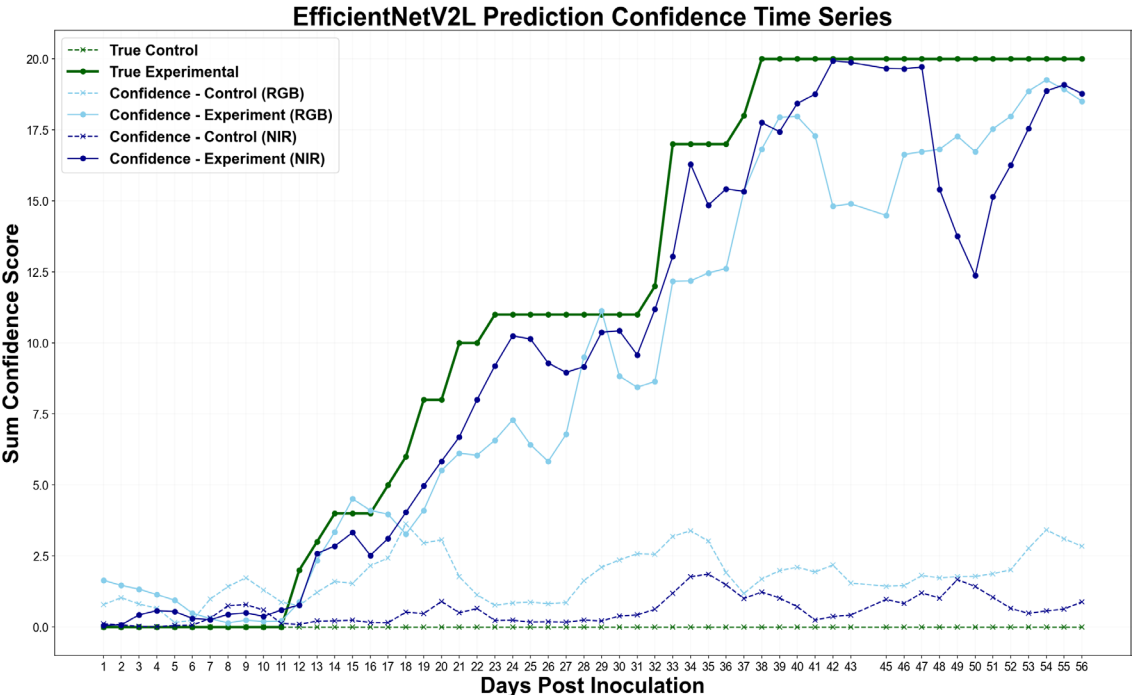


Figure 5.12 Smoothed 3-day moving mean time series of the sum of manual classification scores (green) and confidence scores of all 40 experimental and control samples in RGB (light blue) and NIR (dark blue) imagery from 1 to 56 days post-inoculation.

5.4 Discussion

5.4.1 CNN Classifiers for Apple Scab Monitoring

The aim of this study was to investigate whether NIR and RGB imagery could be used to reliably detect and monitor apple scab over a time series under natural illumination conditions. Three important results emerged from the assessment of the CNN-based classification. The first was that apple scab classification was superior in NIR imagery than in RGB imagery in almost every regard, with greater numbers of true predictions and fewer false predictions in both experimental and control samples. The second was that classifying apple scab on images of whole plants led to poor Recall of 'SCAB' predictions, but that classification performance could be enhanced by localising imagery on a smaller leaf area. This issue would be greater if the current acquisition method were scaled up to larger adult trees in orchards. The third and final result was that while NIR imagery outperformed RGB in most cases, strong direct sunlight could cause a bias towards 'HEALTHY' predictions if exposure settings are not optimised; these are circumstances where RGB imagery would be better suited.

Of all CNNs fine-tuned on multispectral data, the EfficientNetV2L model consistently performed best across primary and secondary data in the testing set. Despite a longer training time, the marginal difference in testing time, considering the improvements in precision and recall, makes EfficientNetV2L a recommended architecture for studies of this nature. While MobileNetV2 and InceptionResNetV2 had improved classification performance through localisation, their recall capabilities, specifically for RGB imagery, are not high enough to reliably monitor for scab. A key goal of this research was to provide an accurate estimation of scab that balances precision and recall so that few false positives would overinfluence spray or false negatives, leading to disease epidemics. This study used a confidence score of 0.5 as a reasonable threshold to achieve this balance. Practical use in orchards would likely be more risk-averse, preferring to over-spray than to chance epidemics; in these situations, reducing threshold values to 0.3 would reduce false negative healthy predictions and provide greater recall at a minor expense to overall precision. Conversely, if over-spraying must be avoided, increasing the threshold value can reduce the number of false positive scab predictions, improving overall precision. Multispectral imaging for apple scab monitoring within orchards would result in thousands of images acquired daily, with a proportion of these expected to produce false positive results. Ensuring high classification accuracy, coupled with methods to mitigate the influence of noise, will be

essential for providing appropriate disease management within orchards without risking widespread epidemics or overuse of fungicide sprays.

Chapter 4 recommended using a control set for future studies of apple scab detection, as there was uncertainty in numerous healthy samples where CNNs predicted scab. Due to the limitations of the experimental procedure, it was uncertain whether CNNs were detecting latent infections or whether these were false positives. The classification of control samples in this study demonstrates an extremely low false positive rate for control samples, especially when observed in near-infrared imagery. Furthermore, scab classification of experimental samples by EfficientNetV2L rarely occurred earlier than the manually classified time series, except in circumstances that could be attributed to noise. This is in contrast to the previous chapter demonstrated that CNNs could detect apple scab earlier than manual techniques. Based on the results of this study, it is unlikely CNNs would classify apple scab earlier than a manual assessment of both RGB and NIR time series that is performed thoroughly.

5.4.2 Multispectral Imagery for the Early Detection of Apple Scab

The detection of apple scab from NIR imagery was, on average, one day earlier than in RGB imagery, only a marginal improvement, unlike the earlier studies in Chapters 3 and 4. This is likely due to a reduction in the imaging scale caused by including larger plants at a greater imaging distance, reducing the relative pixel size between studies. Despite this, the automated detection of apple scab symptoms from NIR imagery was considerably more accurate compared to RGB imagery, especially in the early stages of infection. The superior detection sensitivity is due to the high contrast between symptomatic lesions and healthy leaf tissue. Direct sunlight exerted a major influence on the presence of scab in the imagery. Near-infrared wavelengths have a strong reflection in healthy leaf tissue, as the light is refracted through the spongy mesophyll layer with minimal absorption. The dense layers of conidia in scab lesions increase the absorption potential of the surface, resulting in a strong contrast between healthy and infected tissue (Bleasdale et al., 2022). When insolation is high, the reflectance difference between infected and healthy tissue is lower, causing lesions to fade and masking the key features used to classify scab (Figure 5.13). Specular lighting also caused some masking effects in RGB imagery, but the impacts on scab classification were less severe.

One explanation for the effects of strong insolation on classification results was the fixed exposure settings of the NIR camera. Modifying the commercial camera required removing the internal infrared filter and dust reduction system. The removal of these components affected the calibration between the lens and the sensor, affecting the autofocus and autoexposure

adjustment settings. All focus and exposure settings were set for the first plant sample; however, the weather conditions varied throughout the daily image acquisition phase. Changes in weather conditions and cloud cover led to certain images being under or overexposed. The effects of varying illumination conditions could be mitigated if exposure settings were adjusted automatically in real-time. Additional methods to reduce these impacts could include imaging earlier in the day for better lighting conditions or incorporating a greater quantity of high-exposure imagery into the training dataset. Direct sunlight had less influence over RGB-based classification so in cases where high exposure is unavoidable, RGB sensors may be used as an alternative.

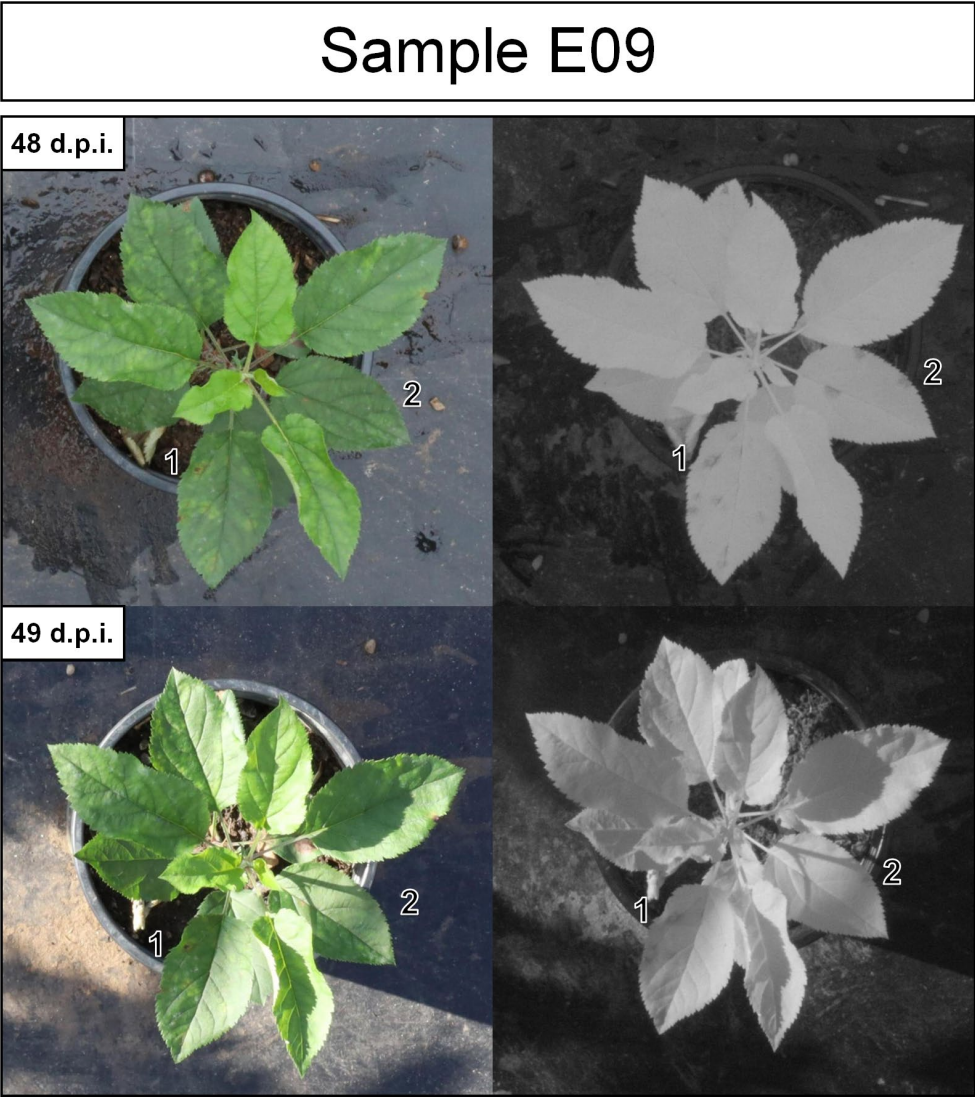


Figure 5.13 The influence of strong sunlight on apple scab prominence in sample E09. Lesions on leaves marked 1 and 2 become visible at 49 d.p.i. compared to the previous day

While apple scab could also be classified from RGB imagery, these classifications were less precise and sensitive than NIR imagery despite a more substantial training set from secondary data sources. A key difference revealed in the results was the trend of false positives in the

control samples. The main hypothesis for this was the presence of abiotic symptoms caused by heat damage within the glasshouses. Abiotic stress presented itself as dark brown areas of necrotic tissue (Figure 5.14). These symptoms, while not similar to apple scab, were distinct from most of the 'HEALTHY' labelled training images. Abiotic symptoms were ignored because they were not caused by fungal pathogens. However, this decision may have had an adverse impact on classification. One interesting finding is that these dark abiotic symptoms were much less severe in NIR imagery, which made the identification of scab more precise. These abiotic symptoms, either from heat stress, water stress, or mechanical stresses, would likely be present in all real-world conditions, and it is vital that these are not misclassified as a fungal disease as this would lead to incorrect management and spray decisions. Increasing the training dataset with more instances of healthy leaves containing abiotic symptoms could solve this issue, as could introducing a further 'ABIOTIC' category.

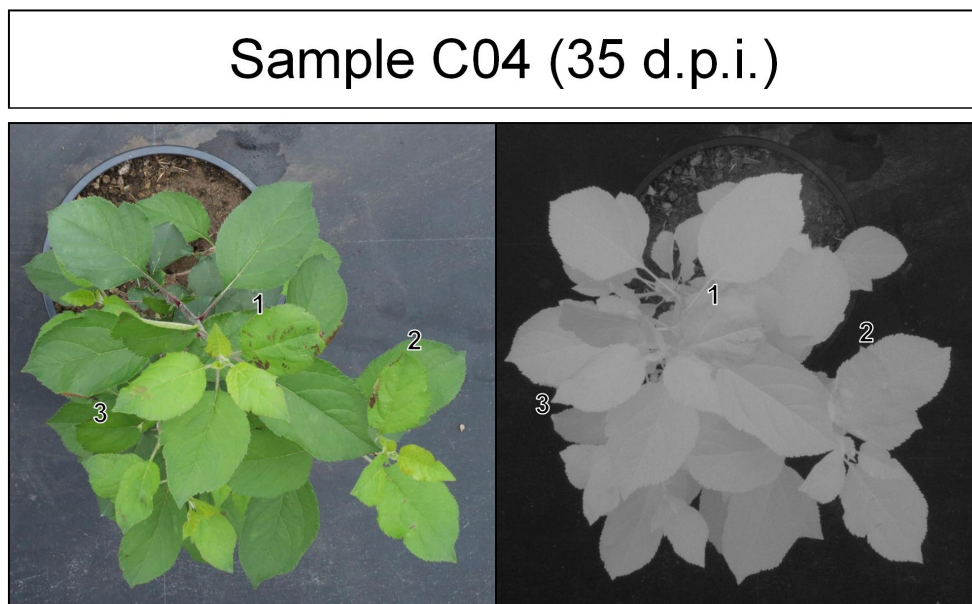


Figure 5.14 Example of abiotic (heat) stress on control sample C04 in RGB and NIR imagery. Characteristic symptoms of damaged leaf tissue are present on leaves marked 1, 2 and 3

Although efforts to control powdery mildew were made before the experiment, the environmental conditions under which experimental samples were kept caused symptoms to return at 12 d.p.i. until the end of the experiment. Assessment of the imagery revealed that powdery mildew could be clearly identified in the RGB imagery but was undetectable in NIR imagery (Figure 5.15). There were no changes in leaf brightness or texture that indicated the presence of powdery mildew, even in severe infections. Classification of the test dataset by EfficientNetV2L produced 'MILDEW' predictions in 231 RGB images but 0 NIR images. Furthermore, the presence of powdery mildew masked underlying scab lesions in RGB imagery but had little impact in NIR imagery. This finding has two important implications. Firstly, NIR

imagery can be used to detect apple scab in the presence of other diseases or stress symptoms, even when these symptoms cover the same leaf area. Secondly, it has revealed a limit to the diagnostic potential of fungal disease detection using NIR imagery. It is possible that NIR imagery may be capable of diagnosing other fungal diseases such as frog-eye leaf spot and cedar-apple rust successfully, as with apple scab, but not powdery mildew. Due to the novelty of near-infrared imaging for stress detection in apple scab, further investigation into the interactions between powdery mildew and heat-damaged leaves with near-infrared radiation should be performed.

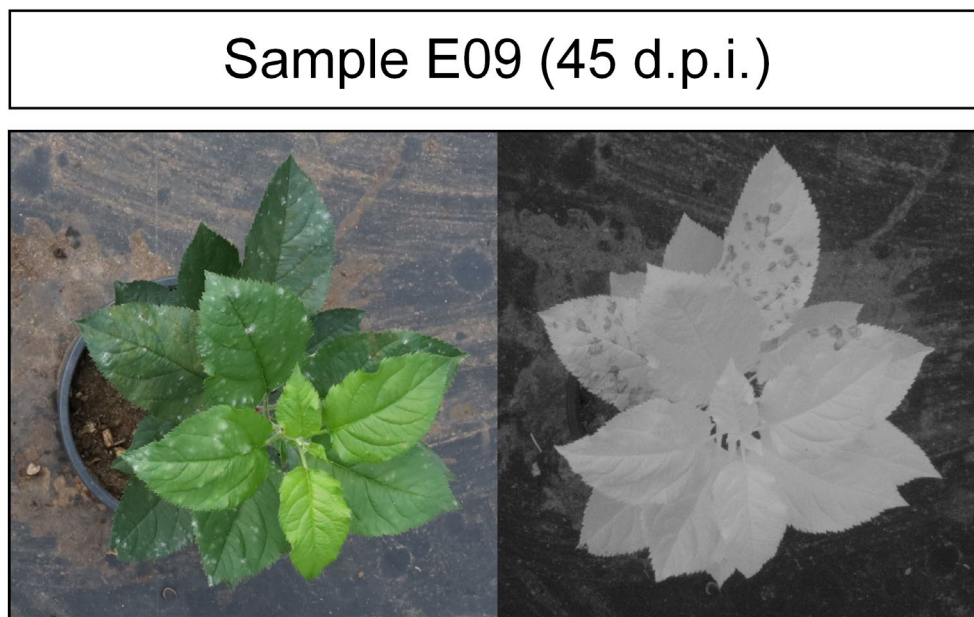


Figure 5.15 Example of powdery mildew (white fungal mycelium on leaf surface) and scab on experimental sample E09. While characteristic scab lesions are clearly visible in the NIR imagery, powdery mildew cannot be detected.

5.4.3 Experimental Challenges and Limitations

The semi-controlled nature of the experiment introduced numerous challenges to accurately monitoring apple scab progression from early to late stages using CNNs. Reliably determining the earliest point of detection was a desirable outcome of this research, as this could effectively demonstrate the use of multispectral remote sensing to inform disease control methods. Achieving this required a large number of plants of different physiologies to calculate the mean date of early detection robustly. The moderate (54%) success rate of inoculation reduced the quantity of plant samples for training and testing. In the earliest stages of the experiment, this success rate was much lower, with only 10% of experimental plants developing infection within the first 21 days. There was clearly an issue regarding the inoculation process that could be attributed to any of the four following causes. Firstly, the pathogen had been stored in a freezer for approximately three years. Although *V. inaequalis* could remain dormant in storage at these temperatures (Szkolnik, 1978), there was a risk that the conidia may have denatured, and that

the strength of the inoculum applied to leaves was lower than anticipated. Secondly, the experiment took place between late summer and early autumn when many of the leaves of the plants were mature. Mature leaves, with tougher cuticles, are much less susceptible to scab infection than younger leaves (Bowen et al., 2011), and it is possible that the conidia would fail to germinate in the subcuticular region. Thirdly, inoculation was carried out in a glasshouse under warm temperatures. The date of inoculation was intentionally selected due to the foreseen period of overcast, wet weather, as temperature, humidity, and illumination could not be controlled. The environmental conditions were warmer than the optimal inoculation conditions for scab germination according to the revised Mills criteria (MacHardy & Gadoury, 1989). The inoculum suspension may not have remained as free water on the surface for a sufficient length of time to develop a rapid onset of symptoms. Furthermore, a heatwave occurred between 9 and 17 d p.i, and the elevated temperatures could have adversely affected scab development. The fourth and final cause of poor inoculation could have been due to the control methods of powdery mildew prior to the experiment. Fungicidal sprays had been applied to treat powdery mildew in the months before the experiment, and despite all leaves being rinsed, this fungicide may have left residual protectant capabilities.

In plants that did develop scab symptoms, the rate of severity increase was also much lower than anticipated and, in some cases, even regressed. The glasshouse environment was not conducive to scab germination, and elevated surface temperatures during days with high sunshine likely affected its progression and spread. Management of powdery mildew during the experiment also affected scab presence. Active fungicidal treatment was avoided. Instead, a leaf wash was applied to reduce powdery mildew spored on the leaf surfaces. The intensive application of this leaf wash on certain plants further impacted scab development. The inoculation and disease development issues ultimately led to fewer, less varied multispectral images of scab than anticipated, causing a greater bias towards 'HEALTHY' samples and a reduced quantity of training and testing data. Future experiments should consider exercising greater control of the growing environment, especially during inoculation, to increase the success rate of scab infection and reduce the risk of plant stress from abiotic sources, or other plant pests and pathogens.

The low development of the scab also affected classification performance analysis as symptom presence and progression were inconsistent. Image annotation relied on tracing symptoms back to the earliest point of detection and considering all images after this to be infected. In reality, there were several instances where both RGB and NIR images labelled 'SCAB' contained no clear symptoms on a specific day, despite being present earlier in the time series. These cases were

ignored for plant imagery used in the training set due to the adverse effect on accurate 'HEALTHY' predictions. CNN predictions of these images occurring in the test set often manifest as false negatives. In the EfficientNetV2L predictions of the localised dataset, there were 167 false negatives: 95 for RGB imagery and 72 in the NIR imagery. A qualitative visual assessment was performed on the potential causes of these. While there were 14 cases of there being no discernible reason why the scab was not detected, most could be attributed to a potential cause by a lack of apple scab features. Occlusions were the greatest cause of misclassifications, where scab symptoms were masked by overlying leaves (Figure 5.16). The influence of direct sunlight was another common cause of misclassification. In some samples, scab severity was reduced, and symptoms became fainter over time due to the reduction of conidial density in the lesions, either due to adverse environmental conditions or the management of powdery mildew.

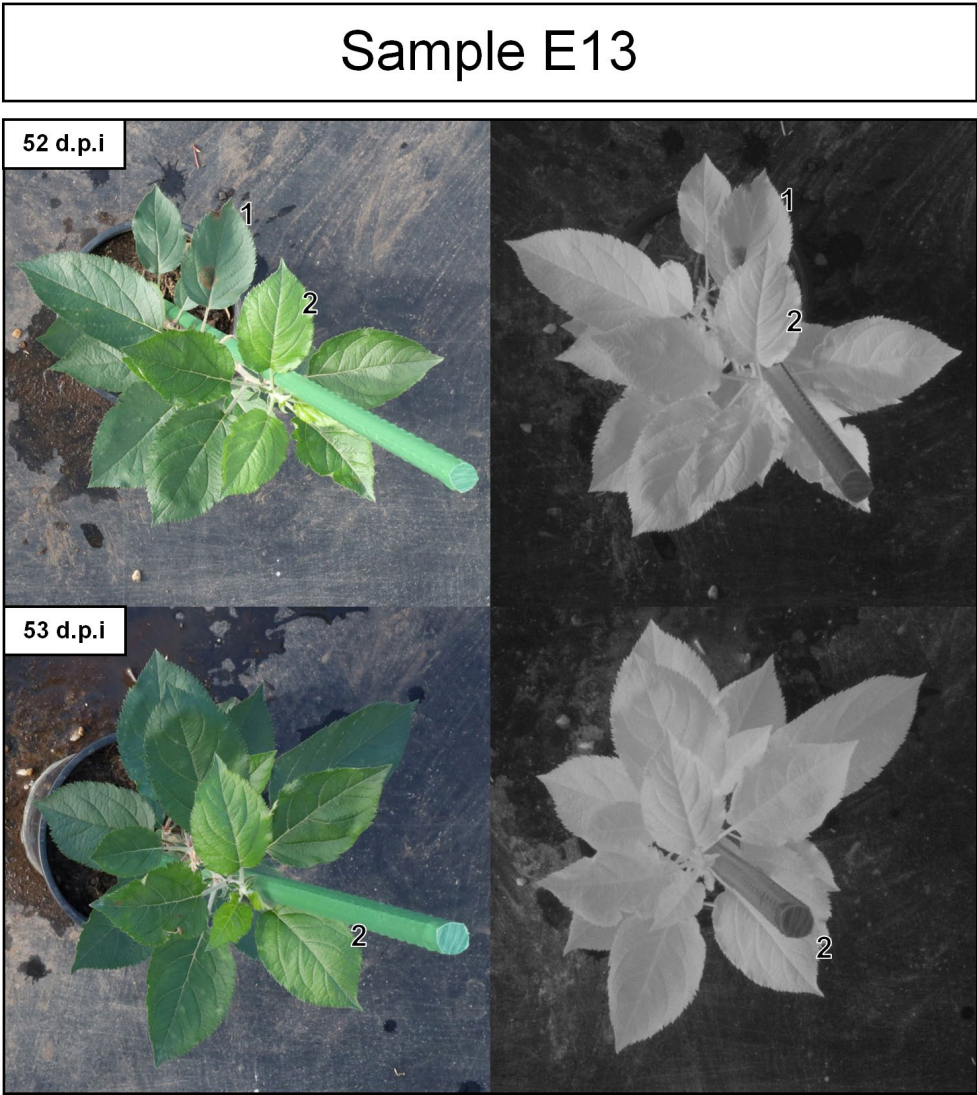


Figure 5.16 Occlusion of scab lesions on Sample E13 in both the RGB and NIR time series. Scab lesions on leaf 1 at 52 d.p.i. are masked by the overlying leaf 2 at 53 d.p.i., presenting no scab symptoms in the whole-plant imagery.

This discussion has identified the limitations and challenges of using CNNs to monitor apple scab. Recommendations for future experiments include exercising greater control over the growing environment, specifically the temperature and humidity during the inoculation period, which would have mitigated many of the adverse effects that influenced scab development. Furthermore, this would have reduced the risk of further stress from abiotic sources or powdery mildew disease. While these solutions may have allowed for earlier detection and higher classification accuracies, the imagery acquired under these conditions would not have demonstrated the potential of both multispectral imagery and CNNs to classify apple scab in complex scenarios. Commercial orchards will have inconsistent illumination, occlusions, concurrent symptom presence, unknown infection ages and disease management routines. Despite the challenges faced, the experiment produced varied multispectral datasets for robust training of CNNs to classify apple diseases and demonstrated the effectiveness of NIR imagery for classifying apple scab symptoms throughout all stages of infection.

5.4.4 Recommendations for Future Research

5.4.4.1 *Large Multispectral Dataset Acquisition*

In this study, a multispectral dataset of 28,800 images was created from public datasets containing five disease classes, and RGB and NIR time series imagery of healthy and scab-infected plants was captured in an experimental environment. This combined training set was sufficient for the study, as the primary data testing set had consistent acquisition angles and high-contrast backgrounds. However, to improve classification potential in commercial orchards, more multispectral imagery, specifically NIR imagery, is required. This imagery should be taken on adult trees in real-world conditions and of other diseases, specifically powdery mildew, frog-eye leaf spot and cedar apple rust. This dataset should reflect the aims of PlantPathology, where field scenarios were represented by leaf imagery taken at different maturity stages across varying sensor settings and with further variations arising from differences in plant physiology and acquisition conditions (Thapa et al., 2020).

The secondary public datasets trained and tested on images acquired under these conditions achieved more accurate classifications than those from the primary multispectral dataset despite consisting only of RGB imagery. The performance metrics used to assess CNN performance are not best suited to time series imagery; instead, having a large, varied dataset containing localised leaf symptoms in corresponding RGB and NIR imagery may lead to more

robust training and testing. Imaging additional diseases could help determine the diagnostic potential of NIR imagery. Performance assessments on a dataset of this nature could provide better comparisons to other CNN-based classifications in previous literature.

5.4.4.2 Automated Localisation, Segmentation and Quantification

Further research is needed into the classification of apple scab at different severities of infection in order to determine how this affects classification accuracy. The results showed that sensitivities were much lower in plants with high healthy-to-infected leaf ratios. Imaging individual leaves would likely provide the highest accuracy results, but the acquisition time and computational costs of imaging and classifying all leaves in an orchard would be unfeasible. A compromise between adequate coverage and accurate classification should be found by quantifying severity on an ordinal scale, either based on categorical intensity level (Rexhepi et al., 2018) or percentage area infected using standard area diagrams (Bock, 2020). Deep learning CNNs have demonstrated the potential to classify frog-eye leaf spot intensities based on infection stage categories (Wang et al., 2017) and other plant diseases (Ji & Wu, 2022) in PlantVillage. Utilising CNNs to calculate the percentage of infected areas covered (Gonçalves et al., 2021) would provide more detailed information for identifying the influence of severities.

The optimal pixel sizes and focal levels that accurately classify early apple scab symptoms at low severities must be determined. Understanding these will then allow for the automation of the localisation process, avoiding the need for labour-intensive manual techniques used in this study. These localisation methods may be as simple as random cropping or dividing by a grid-based system (Kodors et al., 2022) or the use of Mask R-CNNs for the automated segmentation of leaves (Yang et al., 2020; Storey et al., 2022). Automated localisation, segmentation and quantification could not only enable more accurate classification of apple scab but could be used to map infections and provide severity values for precision control techniques and threshold-based spraying methods.

5.4.4.3 Reliable Early Detection through Multispectral Time Series Assessment.

The recommendations provided throughout this discussion are intended to improve the experimental procedure, create a substantial multispectral training set, and provide an automated solution to quantifying disease progression. These will be vital for a large-scale study to determine the earliest detection of apple scab by NIR imagery. Understanding the extent of early detection from multispectral imagery is essential to determine the level of decision-making

that can be achieved by using multispectral imaging and CNN-based classification. This can provide an understanding of whether using curative fungicides in a reactive disease management method is feasible. Controlling the humidity, temperature, and illumination conditions, as well as the aggressiveness of scab isolates and strength of suspension, can provide information on the earliest detection points for imaging systems (Oerke et al., 2011). Furthermore, continual monitoring of infection progression at a shorter imaging frequency could provide real-time detection of diseases within orchards and smoothing the rate of false predictions per sample due to extraneous noise and illumination conditions of non-biotic stress symptoms.

5.5 Conclusions

This study aimed to investigate the effectiveness of apple scab monitoring in natural illumination conditions using CNN classification on RGB and NIR time series imagery. A large, multispectral time series dataset of scab infections was acquired across 105 plants daily from one day post inoculation for eight weeks. This generated a substantial training and testing set containing variations in symptom appearance, plant physiology, and illumination conditions. Supplementary images from secondary data sources were used to increase the number of disease classes for more robust training and validation of classification performance. Three CNNs, MobileNetV2, InceptionResNetV2, and EfficientNetV2L, were trained to classify apple scab from five distinct disease categories via a multilabel approach. The CNN performances were assessed by analysing the confidence of output predictions by label and over a time series. Further investigation showed that localising imagery down from whole plants to infected regions improved CNN classification of scab. The EfficientNetV2L model provided superior classification results to the other fine-tuned CNN models. Despite the long training times, the increase in classification performance is vital for appropriate use in commercial orchard applications.

CNNs consistently classified 'SCAB' in NIR imagery earlier and more confidently than in RGB imagery. NIR-based classification also received more true predictions and fewer false predictions overall, showing greater performance. This greater level of true predictions was due to the high contrast distinguishing between healthy and infected leaf tissue; however, the Recall was reduced in strong sunlight. RGB had more false positives, especially within the control set, likely caused by misclassifying abiotic symptoms of scab. Despite this, RGB could detect powdery mildew present in the dataset, unlike NIR. Further research was recommended to create a larger

multispectral dataset, including other diseases, to assess the diagnostic capabilities of NIR and determine whether this is scab-specific. Classification sensitivity was poor for whole-plant imagery but can be enhanced through manual localisation around detected scab symptoms. This was considered to be related to the ratio of healthy leaf tissue to infected leaf tissue. Detecting scab infection in the early and low severity stages is necessary for precision disease management to reduce pesticide use. Utilising the recommendations of a controlled inoculation procedure and a temperature-controlled environment while maintaining natural light conditions and CNNs trained on the current dataset would help achieve this. Determining the earliest point of infection by NIR imagery could let researchers know the decision-making level this technology could help achieve. Ultimately, this research has demonstrated the capability of multispectral imagery, specifically in the NIR band, when classified by CNNs, to provide rapid, accurate detection of apple scab infections throughout the developmental cycle on leaves.

6 General Discussion

6.1 Introduction

Early detection and accurate identification of plant pathogens are essential for precision agriculture systems to inform appropriate disease management strategies. Remote sensing and classification systems must be effective in complex environments where crops are grown, and multiple diseases proliferate. There has been significant previous research into the early detection of apple scab using remote sensors, however, these studies have been limited to seedlings cultivated and imaged in controlled laboratory environments with specialised imaging setups (Delalieux et al., 2007; Oerke et al., 2011; Belin et al., 2013). Recent studies on apple disease classification have demonstrated the capabilities of deep learning Convolutional Neural Networks (CNNs) to automate the identification of apple scab infections from RGB imagery acquired in commercial orchards (Thapa et al., 2020; Wang et al., 2021; Turkoglu et al., 2022). Although these studies achieved highly accurate identification, they were based on manually captured imagery localised on individual leaves on trees that displayed characteristic late stages of the disease. The aim of this thesis was to develop a remote sensing strategy capable of detecting and classifying early-stage apple scab symptoms under complex, real-world conditions where plant morphology, illumination, and additional stress factors are uncontrolled. To achieve this, a novel experiment was designed in which apple plants were cultivated in semi-controlled glasshouse environments, and multispectral (VIS-NIR) time series imagery was acquired under natural illumination conditions. CNNs were employed to rapidly and objectively classify apple scab-infected plants from healthy samples and other disease classes. The results presented in earlier chapters demonstrate the effectiveness of CNN-classified NIR-based multispectral imaging for the early detection of apple scab disease under natural illumination conditions.

This chapter provides a comprehensive discussion of the novelties, successes, challenges, and limitations of the methods and results encountered in achieving early detection of apple scab infections under natural illumination conditions. Each section addresses the key novel elements of the study. Section 6.2 evaluates the experimental environment, including the cultivation of apple plants and the inoculation procedure. Section 6.3 details the high-resolution multispectral imaging system and acquisition techniques. Section 6.4 evaluates the multispectral imagery dataset and the application of NIR imaging. Section 6.5 reviews the use of CNN models for classifying apple scab symptoms. Section 6.6 appraises the effectiveness of NIR imagery for the

early detection of apple scab infections. Finally, Section 6.7 synthesises the strengths and weaknesses of the research methodology to provide clear recommendations for further work.

6.2 Apple Plant Samples

A total of 150 apple plants were cultivated for the purpose of this study. Grown from seedlings over three years, these plants exhibited a wide range of structural characteristics and physiologies. When inoculated, these plants produced a wide range of scab symptoms that could be used to assess the early detection and classification capabilities of the remote sensing strategy. All apple plant material was cultivated at Hazelrigg field station at Lancaster University (Lancaster, UK). To provide a semi-controlled environment for the experiment, two SolarDome glasshouses were utilised: one experimental, where samples were grown, inoculated and imaged and the second, where control, storage, and management activities took place (Figure 6.1). The ambient air temperatures within the glasshouses were consistently higher than temperatures recorded outdoors at Hazelrigg field station year-round (Table 6.1). The cool, wet spring months in Lancaster caused consistently high humidity within the SolarDomes, which, when combined with limited airflow and closely spaced plants, caused environmental conditions that were conducive to powdery mildew infestations. During summer, the elevated ambient air temperatures, surface temperatures, and low humidity promoted drought and heat stress in apples, causing damage to leaf tissue. Conditions recorded inside and outside the SolarDome glasshouses during the experiments are provided in Appendix A. Maintaining greater control over temperature, airflow, and illumination during the cultivation period would have made cultivating healthier, stress-free plants easier. Despite this, the glasshouses satisfied the wind protection, illumination, and power requirements necessary to monitor the apple plants.

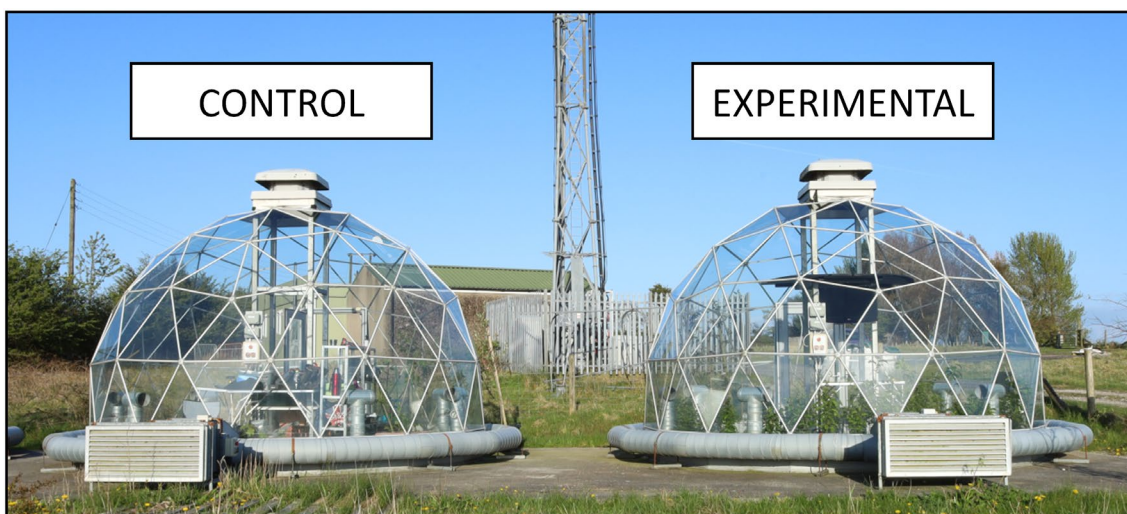


Figure 6.1 Control and Experimental SolarDome Glasshouses

Temperature	JAN	FEB	MAR	APR	MAY	JUN	JUL	AUG	SEP	OCT	NOV	DEC
Outdoor (°C)	5.3	4.7	6.8	6.6	9.8	14.7	17.1	15.3	15.4	11.4	7.5	5.9
Indoor (°C)	7.2	8.7	12.8	20.4	17.3	23.5	24.8	24.0	21.2	14.3	9.9	6.7

Table 6.1 Average monthly temperatures over 2021 recorded at Hazelrigg Field Station (Outdoor) and SolarDome (Indoor)

Due to space and cost constraints of the project, apple plants were grown from seeds of commercially important, scab-susceptible cultivars (Gala, Braeburn, and Cox). Unlike grafted apple trees traditionally cultivated in commercial orchards, seed-born apple trees are genetically distinct from their parents (Jensen et al., 2010). Each seedling exhibited unique physiological characteristics, influencing its morphology, heat and drought tolerance, and disease resistance. Growing these apple plants from seed resulted in unique branching structures, creating visually distinct plant material that would improve generalisation when used to train CNNs. This approach led to significant variation in plant tissue and apple scab features within the multispectral dataset. However, it also resulted in some plants being less tolerant to heat stress, more susceptible to powdery mildew, or more resistant to apple scab, which introduced additional stress symptoms and slowed the progression of scab development. Conducting experiments on grafted plants of economically important, highly susceptible cultivars, such as Gala and Braeburn, could provide further insights into plant disease development in commercial varieties. This method would likely yield more consistent and relevant data for practical applications in commercial orchards.

To determine the effectiveness of remote sensors for the early detection of apple scab, apple plants were artificially inoculated with a suspension of *V. inaequalis* conidia. Given the scale of the experiment involving a large number of sizable apple plants, inoculation was carried out in situ within the experimental glasshouse. A novel inoculation method was developed based on methodologies from previous studies (Szkolnik, 1978; Delalieux et al., 2007; Xu et al., 2008; Oerke et al., 2011). The inoculant was prepared by placing infected leaf tissue directly into distilled water and applying it immediately to the apple plants, thereby avoiding the need for complex in vitro cultivation of *V. inaequalis* conidia (Barbara et al., 2011). This inoculation approach achieved a moderate success rate, with a 56% infection rate in the large-scale Experiment 2 (Chapter 5). As discussed in Section 5.4.3, several factors may have contributed to the lower-than-expected infection rate. Firstly, the inoculant concentrations and aggressiveness might have been lower than anticipated. Additionally, the potential ontological resistance of apple leaves, due to maturity or unknown resistance characteristics (Bowen et al., 2011), may have reduced infection germination. Secondly, the environmental conditions within the glasshouses were not consistently conducive to apple scab development; high temperatures, low

humidity, and long daylight hours during the experiment may have hindered conidial germination and development. Moreover, the treatment of powdery mildew may have negatively impacted apple scab development. The management of powdery mildew involved chemical control through active fungicidal sprays and sanitation through removing infected tissue, thinning foliage and sulphur burning. Although these measures reduced inoculum for several weeks prior, powdery mildew symptoms reappeared during the time series acquisition. To mitigate the severity of infections and to prevent significant foliar stunting and damage, leaves were regularly rinsed with a non-fungicidal leaf wash to reduce surface mycelium and germination. While this approach maintained powdery mildew severity at controllable levels, residual symptoms persisted. Additionally, this sanitation method may have inadvertently affected the germination and development of *V. inaequalis* on the leaves.

The number of plant samples and acquired images displaying apple scab symptoms was lower than anticipated in Experiment 2. CNN models require a large quantity of training data to classify new imagery accurately. To ensure a sufficient training set, a second round of inoculation was conducted at 21 days post-inoculation (d.p.i.), resulting in greater success. However, this issue led to fewer sample time series available for the final testing set, and the earliest detection dates were later than expected, especially compared to previous small-scale Experiment 1. Exercising greater control over the environmental and inoculation conditions is essential to enhance the overall health and infection rates in future studies. Conducting experiments in climate-controlled environments would mitigate the risk of abiotic stress and powdery mildew developing in situ. Maintaining optimal temperatures (17-23 °C) and high humidity with leaf wetness during inoculation, as recommended by the Mills' infection period table (Table 6.2), can improve germination likelihood, and reduce the time before initial symptoms develop. Additionally, testing earlier in the season on grafted plants with known traits can help observe pathogen development on susceptible and resistant cultivars (Papp et al., 2021). Furthermore, controlling inoculant concentrations through measurement with a Neubauer counting chamber (Delalieux et al., 2007) or a Fuchs-Rosenthal haemocytometer (Oerke et al., 2011), as well as specifying the isolates applied, would better inform the inoculation process. This would result in faster and more severe infections, creating a greater variance in symptoms for imaging data collection and training and testing CNN models for apple scab detection. Detailed information about these parameters would also benefit early detection tests, where differences between NIR, RGB, and human observation may be pronounced.

Average Temperature (°C)	Leaf Wetness (hours)	Lesion Appearance (days)
1	40.5	N/A
2	34.7	N/A
3	29.6	N/A
4	27.8	N/A
5	21.2	N/A
6	18	17
7	15.4	17
8	13.4	17
9	12.2	17
10	11	16
11	9	15
12	8.3	14
13	8	14
14	7	13
15	7	12
16	6.1	10
17 - 23	6	9 - 10
24	6.1	N/A
25	8	N/A
26	11.3	N/A

Table 6.2 Mills' infection period table showing temperature and hours of leaf wetness required for scab germination. (Adapted from Stensvand et al., 1997)

One of the main objectives of this research was to produce a large number of plant samples for reliable assessment of the early detection of apple scab. A low-cost, non-laboratory method for growing and inoculating was employed. This methodology resulted in a diverse array of apple plants with structural differences, various developmental stages, and distinct leaf physiologies. Additionally, the inoculation process induced various scab symptoms on the plants. This diversity provided extensive data for training, improving the generalisation of CNN models, and demonstrating the robustness of their predictions. However, the limitations of the study, such as plant stress and the resultant variability in scab development, ultimately led to a reduced number of scab images, complicating early detection studies and the training, and testing of CNN models. Nonetheless, the presence of powdery mildew and abiotic stress, common in commercial orchards, allowed for the demonstration of early detection capabilities despite these complexities. This further highlighted the effectiveness of the high-resolution multispectral sensors in real-world conditions.

6.3 High-Resolution Multispectral Sensing

This study revealed that high-resolution multispectral imaging, specifically NIR imaging, is an effective method for accurately detecting early apple scab symptoms under natural illumination conditions. Extensive research demonstrated that NIR-based imagery can detect apple scab earlier and more accurately than conventional RGB imaging, using manual and automated classification techniques. The imagery acquired over a time series showed that symptoms in NIR imagery could be clearly observed throughout the development cycle of apple scab. The high resolution of the imagery allowed for the observation of initial scab infections through well-defined symptoms, providing a detailed understanding of the spread of fungal mycelium within lesions (Section 3.4.1). This high-resolution multispectral imaging technique has been previously applied to monitoring fireblight in apple orchards. However, this study represents the first time such imagery has been utilised for the detection of apple scab in a way that could be practically scaled up for use in commercial orchards.

Previous studies have identified that hyperspectral, thermal, and fluorescence imaging sensors demonstrate potential for the early detection of apple scab. While these three types of sensors are capable of presymptomatic stress detection due to apple scab, successful detection has typically relied on controlled environmental conditions and specialist systems. Before this research, multispectral cameras had not been applied specifically to apple scab detection, although they have been widely used in agriculture for various purposes (Jameel et al., 2020). Multispectral imagery is extensively used in satellite, aeroplane, and Unmanned Aerial Vehicle (UAV) based remote sensing, offering significant benefits for crop health monitoring compared to conventional visible-spectrum imagery (Maes & Steppe, 2019). Rapid technological advances have increased the affordability and practicality of lightweight multispectral sensors for UAVs, such as the Parrot Sequoia and MicaSense Red-Edge, facilitating their use in real-world applications (Assman et al., 2018). These aerial imaging systems have also been applied to disease detection, providing valuable information on vegetation indices and other health factors for diseases such as fireblight in apple (Jarolmasjed et al., 2019) and other orchard crops like citrus (DadrasJavan et al., 2019; Pourazar et al., 2019). Despite being affordable options, these commercial multispectral cameras have limitations in terms of resolution and focal length (Cao et al., 2019; Fawcett et al., 2020). These systems are more suited to detecting tree crop diseases with symptoms that significantly affect the tree canopy. However, apple scab lesions, particularly in its early stages of infection, are only several millimetres in diameter, rendering these commercial multispectral systems unsuitable for early detection, especially via UAV-based acquisition.

Modifying digital camera systems to become NIR-sensitive presents an alternative approach to multispectral imaging for plant phenotyping (Lebourgeois et al., 2008). By removing the internal NIR filter overlaying the CMOS sensors, standard RGB cameras can be adapted to detect wavelengths up to 1000 nm. This technique has gained popularity in various studies due to its ability to provide low-cost, high-resolution near-infrared sensitive imagery (Nijland et al., 2020). It has been employed in orchards to monitor abiotic stress (Jarolmasjed et al., 2018) and fireblight (Jarolmasjed et al., 2019). Additionally, these modified multispectral sensors have been effectively integrated into UAV platforms, enhancing the capability for extensive monitoring coverage (Berra et al., 2020). For this study, a stereoscopic imaging approach was utilised for high-resolution multispectral imaging. One camera was modified by removing the internal NIR filter and replacing it with an NIR long-pass filter (+800 nm), enabling detection of reflectance in the NIR spectrum (800-1000 nm). This camera was used alongside a conventional RGB camera to capture information from blue, green, red, and near-infrared wavebands. While the methodology remained consistent, the technology used differed between the small-scale Experiment 1 and the large-scale Experiment 2.

The small-scale experiment utilised a low-cost, open-source system developed on a Raspberry Pi (Raspberry Pi Foundation, Cambridge, UK). Full details of the setup are provided in Section 3.2.2.1. Raspberry Pi-based systems are well-established as low-cost imaging solutions, with available information on calibration protocols for scientific studies (Pagnutti et al., 2017). These systems have been previously used for plant imaging and phenotyping studies (Tovar et al., 2018), with several solutions available for calibrating and converting them to multispectral imagers (Lopez-Ruiz et al., 2017; Valle et al., 2017). These multispectral systems are powered through low-cost microcomputers, which, when utilised within IoT frameworks, can allow for fixed, continual real-time monitoring in field environments. Furthermore, their low weight, customisation, and calibration capabilities have led to successful applications on UAV systems (Belcore et al., 2019; Barjaktarovic et al., 2024). Despite these benefits, these sensors require development by the end user before operation.

The time-consuming and labour-intensive nature of imaging, along with a lack of portability experienced in Experiment 1, necessitated an alternative imaging approach for larger-scale testing. The second method, employed for large-scale Experiment 2, used commercial Canon EOS RP digital cameras (Canon Inc., Tokyo, Japan) to provide easier operation and superior image quality. Full details of this sensing setup are provided in Section 5.2.2.1. The improvements in image quality and ease of operation came at the cost of higher expenses and increased weight.

The difference in CMOS sensors and overall system size between the open-source and commercial camera methods is presented in Figure 6.2. Despite the higher costs, similar commercial camera-based systems have also been applied to UAV platforms for plant health monitoring (Jewan et al., 2022).

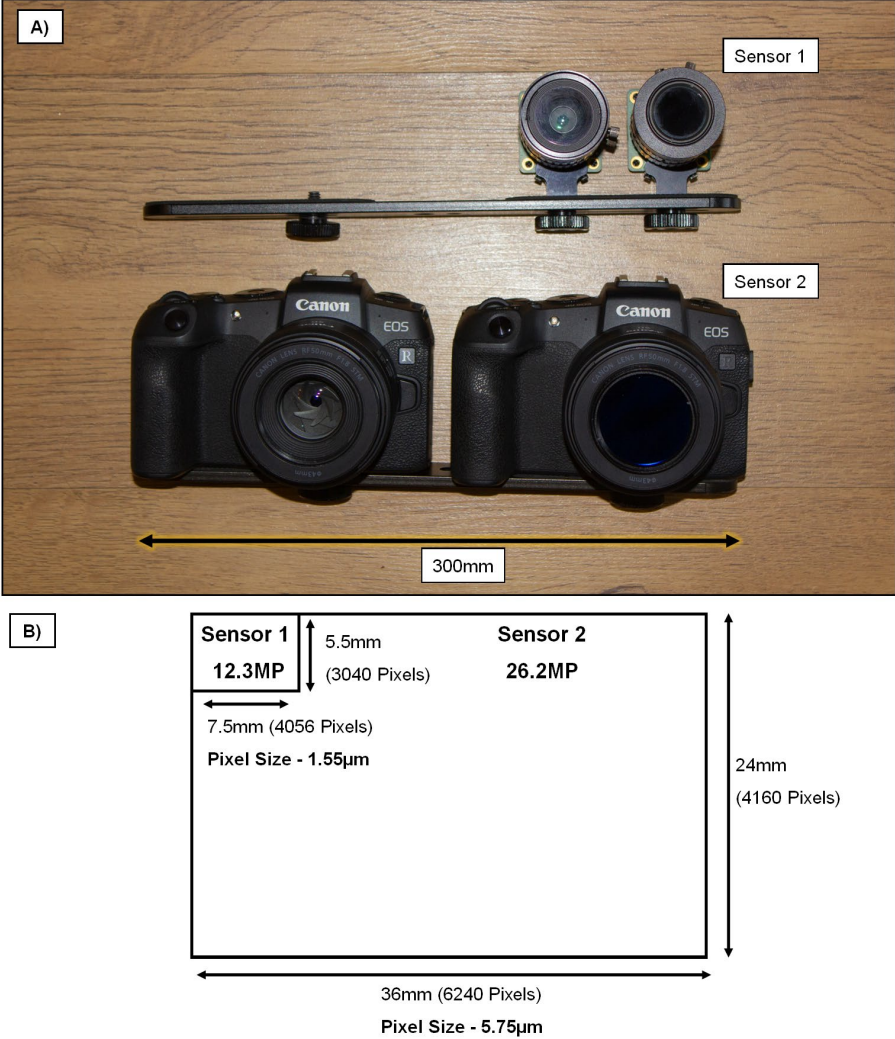


Figure 6.2 Comparison of sizes of Raspberry Pi (Sensor 1) and Canon (Sensor 2) systems. A) Size of stereoscopic sensing system. B) CMOS sensor size

The acquisition procedures used in this study were sufficient to collect the data necessary to demonstrate the potential of multispectral-based imagery. Full details of the image acquisition for Experiment 1 and Experiment 2 are presented in Section 3.2.2.4 and Section 5.2.2.2, respectively. The nadir-view nature of the imagery simulates aerial imagery that would be acquired from UAVs, providing extensive coverage of leaf areas that may display symptoms of apple scab despite potential occlusions of underlying leaves. It was observed in Section 3.3.1 and Section 5.3.4 that strong illumination reduces the visibility of scab symptoms in NIR imagery, leading to a bias towards healthy predictions. This issue arises due to overexposure of the

imagery, where bright and healthy leaf tissue masks critical scab symptoms. To address this, remote sensors must be developed to perform real-time adjustments of exposure settings (Figure 6.3) to optimise image acquisition under varying natural illumination conditions. Both appropriate exposure settings and camera hardware are essential for reliable image capture from aerial platforms (O'Connor et al., 2017). Since early apple scab symptoms can only be detected on a sub-leaf scale, the use of long focal length lenses and high-resolution CMOS sensors will be required to achieve this imaging scale.

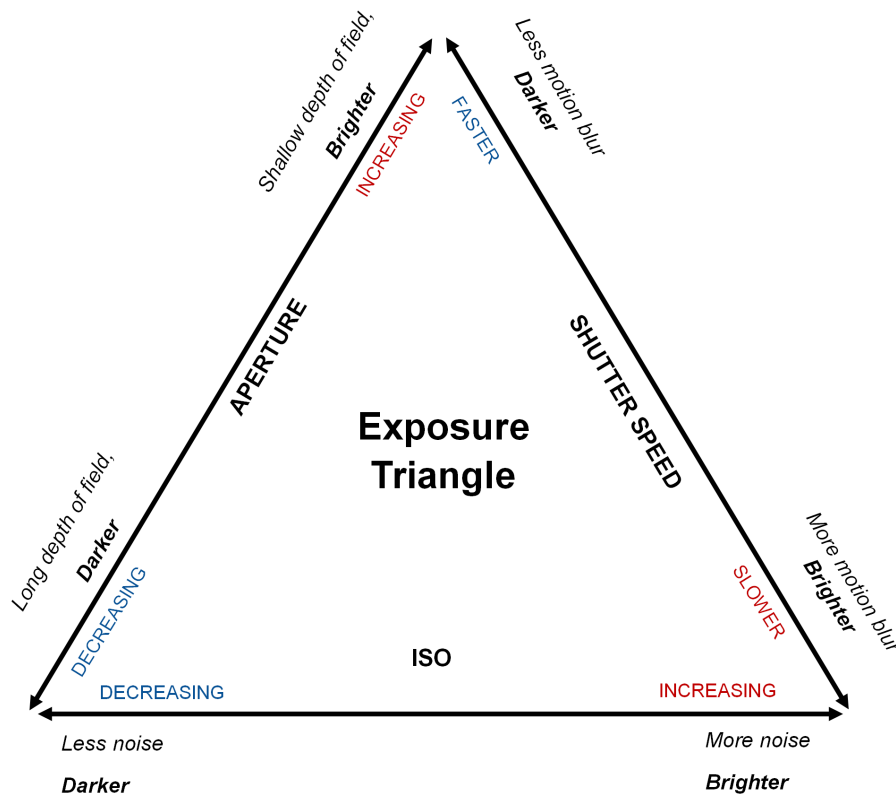


Figure 6.3 Exposure Triangle

Further research and development can enhance the performance and practicality of multispectral imagers, facilitating their application in orchards via UAVs or handheld devices. Advances in this area could enable simultaneous acquisition on a single sensor (Sadeghipoor et al., 2013), reducing weight and allowing the collection of vegetation indices. Commercial digital cameras hold the potential for widespread implementation in commercial orchards. Crop scouts could readily use handheld NIR imagery to aid early scab classification and collect training data for CNN models. For automated orchard monitoring, developing open-source methods that can be integrated into UAV-based platforms would be preferable. This study demonstrates that remote sensing systems, specifically those based on NIR imagery, have significant potential as a portable method for the early detection of apple scab under natural illumination conditions.

6.4 Multispectral Apple Disease Dataset

A large multispectral time series dataset, comprising 300 individual time series of each plant sample in RGB and NIR imagery, was acquired using the high-resolution multispectral imaging system. This dataset was novel in three significant ways: 1) It was the first study to use NIR imagery for apple scab detection. 2) It was the first study to achieve early detection of scab in uncontrolled settings. 3) It was the first study to image whole plants within a time series for training and testing CNNs to classify apple scab. All imagery was captured under semi-controlled conditions, with varying illumination, on apple plants exhibiting complex physiologies and a range of symptoms, including healthy apple scab and other stress features. Manual assessment and CNN-based classification of this dataset confirmed that the capability for early detection of apple scab was superior in NIR imagery compared to RGB imagery. The imagery included control samples, latent stages, early symptoms, and late-stage symptoms of apple scab at various severities. Additional stress features, such as abiotic and powdery mildew symptoms, were also observed. Due to the novelty of this dataset, this section aims to provide examples and descriptions of key health indicators featured in NIR imagery compared to RGB imagery.

NIR imagery was capable of strong detection due to the distinct differences observed between healthy and scab-infected tissue (Figure 6.4). Healthy green leaves typically display high brightness in NIR imagery, indicating the high reflectivity of the plant tissue. Within this imagery, key leaf texture features are discernible, with veins and venules visible. Other plant tissues, including petioles and stems, also appear white but are generally less bright than the foliar tissue. Inorganic matter in the background is considerably darker than the plant tissue in the foreground. Apple scab infections can be clearly identified in NIR imagery due to the high contrast between infectious lesions and healthy tissue. The conidial structures that cause the lesions have higher absorbance than healthy leaf tissue, causing a significant difference in the appearance of healthy and infected tissue. The distinct brightness, shape, and texture features of scab infections make detection through NIR imagery highly effective. These scab lesions have defined structures in NIR imagery and do not reduce leaf reflectance where *Venturia inaequalis* conidia are not present.

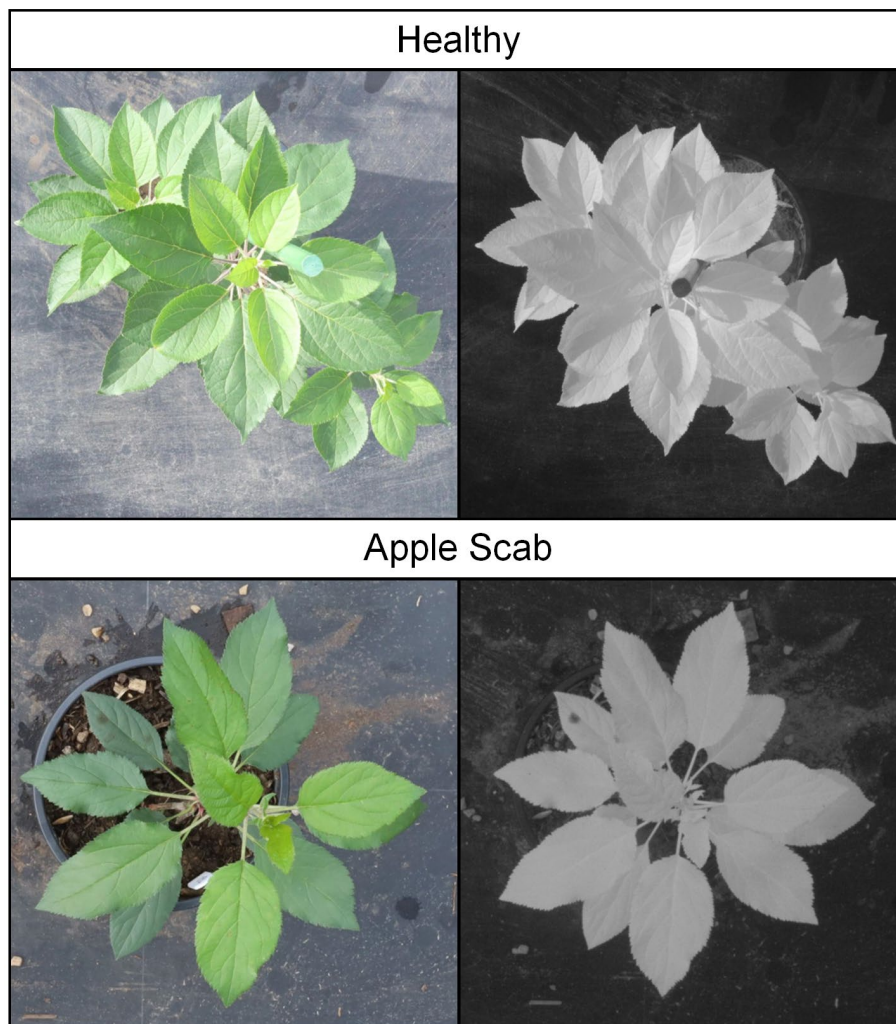


Figure 6.4 Above) Example of healthy image (Sample C07 at 47 d.p.i.). Below) Example of Scab imagery (Sample E13 at 30 d.p.i.)

Due to the uncontrolled temperature and humidity conditions in which the apple plants were cultivated, additional stress factors such as abiotic damage and powdery mildew were present in some of the time series imagery (Figure 6.5). The characteristics of these stress factors have not been fully explored. Abiotic tissue damage was common, particularly on mature leaves later in the time series. Heat stress typically caused brown necrotic tissue that contrasted heavily against green leaf tissue, leading to false positives in control samples. In NIR imagery, abiotic symptoms were much less pronounced, with only the damaged regions observable on severely stressed leaves. High-temperature stress can cause significant damage to mesophyll layers in leaves (Djanaguiraman et al., 2011), resulting in lower reflectance in these damaged tissues.

Biotic stress from powdery mildew was also present on experimental apple leaves during large-scale Experiment 2. The primary symptoms of the disease were observed as white, powdery mycelium accumulated on the leaf surfaces. Due to sanitation measures applied, this mycelium did not completely cover the leaves, and infected plants experienced only minor stunted foliar

growth. When observed through NIR imagery, there were no visible symptoms of the white fungus against the white leaf tissue, nor were there any discernible variations in leaf surface texture. These features were observed in 40 out of 150 plant samples that developed powdery mildew symptoms, indicating that NIR imagery has limited diagnostic capabilities for detecting powdery mildew.

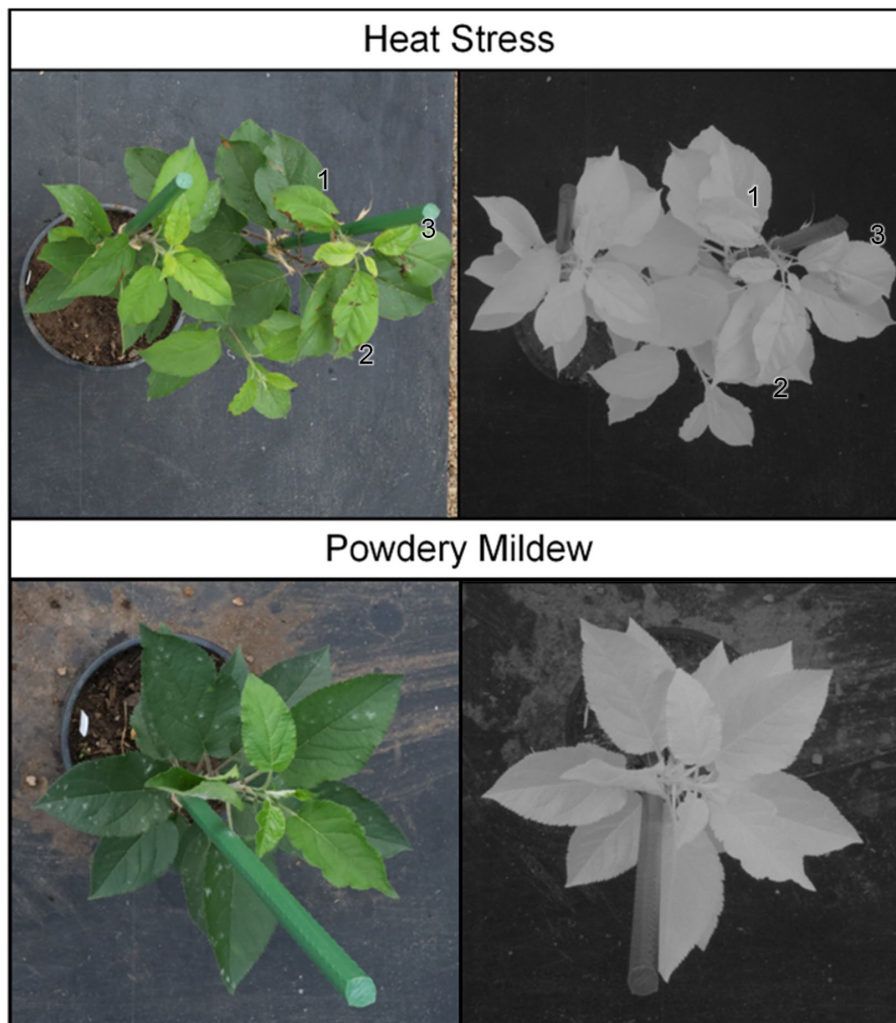


Figure 6.5 Above) Examples of brown necrotic tissue damage due to heat stress in the imagery, which are identifiable on leaves labelled 1, 2, and 3 (Sample C03 at 14 d.p.i.). Below) Examples of white fungal mycelium of powdery mildew in imagery (Sample T69 at 45 d.p.i.).

As the experiment progressed, powdery mildew and apple scab became increasingly prevalent, with distinct symptoms presented on individual leaves (Figure 6.6). Unlike powdery mildew, which develops on the leaf surface, apple scab develops in the subcuticular region of the leaf. Powdery mildew symptoms can overlay apple scab symptoms, posing a risk of masking them during visual assessments. Although this issue occurred in some RGB imagery, the extent of scab infections was clearly identifiable in NIR imagery. In orchards with both diseases, mapping apple scab and quantifying its severity would be much more precise using NIR imagery. The presence

of apple scab, powdery mildew, and other abiotic stress factors can exert significant stress on leaves. During the experiments, some plants displayed both symptoms along with extensive leaf damage. Despite the influence of multiple stress factors, individual lesions of apple scab were clearly visible. While both scab lesions and abiotic tissue damage impacted the reflectance of healthy leaves, the influence of scab lesions on reflectance was significantly greater than that of abiotic damage. In natural orchard conditions, where apple scab, powdery mildew, and abiotic stress factors often coexist, NIR imagery would likely provide more accurate assessments and precise quantification, as powdery mildew does not occlude lesion boundaries. This reduces the likelihood of misdiagnosis. The examples provided briefly discuss stress symptom features, which may aid in future image acquisition and dataset annotation. Further research into the impact of these stress factors on leaf structure and reflectance characteristics would be beneficial for future studies.



Figure 6.6 Above) Combination of apple scab and powdery mildew in imagery (Sample E08 at 45 d.p.i.). Below) Example of Apple Scab, powdery mildew, and heat stress (Sample T75 at 56 d.p.i.)

After both Experiment 1 and Experiment 2, the final dataset comprised 30,000 images, with 11,053 obtained from the primary experiments and the remainder from public sources (Figure 6.7). Although this final dataset contained many images from each category, the 'HEALTHY' and 'SCAB' classes were the most critical for this research. The final dataset included 9,923 'HEALTHY' and 7,990 'SCAB' images for RGB imagery, but only 3,775 'HEALTHY' and 1,632 'SCAB' images for NIR imagery. This dataset, enhanced via augmentation techniques, was effective enough for classification in semi-controlled settings but may be insufficient for applying CNN models trained on this data directly to orchards. The heterogeneity of orchard environments and the need for more accurate estimations necessitate a larger dataset. While this experiment provided greater variations in illumination conditions, plant morphology and symptom developmental stages, imaging angles and backgrounds were kept constant. One major limitation of training CNNs on simple imagery, such as that of the PlantVillage dataset, is that these individual leaves and homogenous backgrounds do not accurately represent true orchard scenarios (Mohanty et al., 2016). Applying models trained purely on the current dataset may result in decreased accuracy if applied directly to images collected via automated acquisition techniques in orchards.

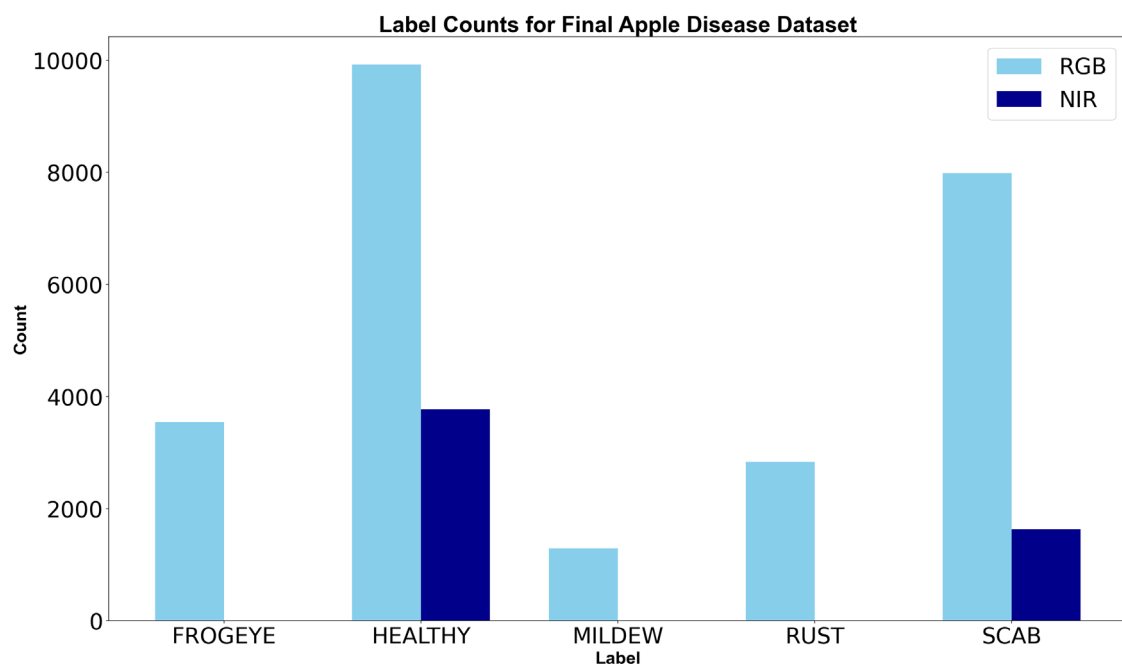


Figure 6.7 Label distribution in the Final Apple Disease Dataset generated over Experiment 1 and Experiment 2

More multispectral data should be collected to capture the variations in natural environments. Imaging leaves of different cultivars, colours, and morphologies, with various ages of infected tissues, image backgrounds, and illumination at different angles, is essential (Thapa et al., 2020). As previously stated, handheld-based acquisition methods are readily available for the current system and demonstrate considerable potential for detecting apple scab infections on leaves and

fruits in real-world environments (Figure 6.8). Additionally, collecting NIR imagery of disease symptoms can improve the diagnostic capabilities of CNNs. The collection of imagery from UAV platforms is recommended, as UAVs are the most likely platform for orchard monitoring using sensors. Understanding the capabilities of NIR imagery acquired from UAVs and training CNNs on these images is vital to ensure practical application and accurate monitoring in the future.



Figure 6.8 Apple scab symptoms on leaves and fruits in multispectral imagery acquired by handheld means from orchards around Lancaster, UK

6.5 Automated Classification of Apple Scab

Manual classification of remote sensing data is impractical to implement on a large scale due to the time-consuming nature of processing the high quantity of images collected. CNNs are now the most commonly used classification method in plant disease detection studies, demonstrating high accuracies and rapid diagnosis of diseases in both controlled and real-world environments (Jiang et al., 2019; Li & Li, 2020; Chao et al., 2021). In order for the practical application of NIR-based monitoring in orchards, CNNs must be capable of accurately detecting apple scab infections despite the presence of extrinsic and intrinsic factors that may affect accuracy (Section 2.6.2). Three pre-trained CNN models were fine-tuned on the multispectral training set for the classification of apple scab: MobileNetV2, InceptionNetV2, and EfficientNetV2L. These models were selected due to their high accuracies and differences in model size. Demonstrating effectiveness across three CNNs provides stronger support for the use of novel NIR imagery than relying on a single model. Due to the novelty of both multispectral imagery and time series data, the CNNs were validated by classifying apple diseases collected from secondary public datasets. The successful demonstration of CNNs to classify testing datasets with up to 0.986 accuracy, and F1 scores of 0.989 and 0.990 for the 'HEALTHY' and 'SCAB' classes respectively, placed the trained models on par with some of the best in existing literature. This demonstrated the effectiveness of classification across multiple symptoms and could be readily applied in real-orchard conditions.

For the primary multispectral datasets acquired in both Experiment 1 and Experiment 2, the results clearly showed that CNNs classified apple scab more accurately from NIR imagery than from RGB imagery. All performance metrics for the classification of imagery collected in Experiment 1 and Experiment 2 supported this conclusion. The initial use of CNNs, trained on a much smaller dataset and presented in Chapter 4, yielded some unforeseen results. The predictions from the MobileNetV2 and EfficientNetV2L models were comparable, though MobileNetV2 showed much greater performance with RGB data. Another key result was that the specificity of predictions in NIR imagery was lower, which was attributed to the detection of symptoms earlier and in more samples than were classified manually. It was recommended that a larger quantity of training data and control samples be used to enhance the reliability of testing. Implementing these recommendations clearly improved the training and analysis process. EfficientNetV2L proved to be superior to all other fine-tuned CNNs, detecting apple scab more accurately in both primary and secondary testing sets. The inclusion of a control category also demonstrated the high specificity of the models, with few false-positive scab predictions in

both RGB and NIR imaging but considerably fewer in NIR imaging. Applying a multi-labelling strategy, combined with a significantly larger multispectral training set, vastly improved overall performance. This approach allowed the models to better generalise and increased their classification accuracy. As noted, further studies should focus on expanding the training set to continue improving the generalisation capabilities and classification accuracies of CNN models. This would involve capturing more diverse and representative samples of apple scab and other stress conditions under various environmental conditions.

Unlike other studies, this study initially utilised whole-plant imagery rather than focusing solely on disease symptoms localised on leaves. While the classification of secondary data was comparable to other literature, this was not the case for multispectral imagery. This discrepancy was attributed to the use of whole-plant imagery rather than limitations in the training set for two reasons. Firstly, classification accuracies were poorer in RGB than in NIR data, despite the extensive quantity of RGB images of apple scab available in public datasets used to train the CNN models. Secondly, an evaluation of each plant sample revealed a correlation between larger plant samples and poorer classification scores. Larger plants had a higher ratio of healthy leaf tissue to infected tissue, resulting in lower percentage severities overall. To test this hypothesis and improve prediction performance, the primary testing set was augmented to localise imagery onto smaller regions where symptoms were present. The previously fine-tuned CNN models were then used to reclassify this data with much greater success. This finding underscores the need to further assess the impact of infection severity on apple scab prediction, as it significantly influences early disease monitoring in orchards. Additionally, there is a need to develop an automated method for localising imagery. The manual technique used in this study is unsuitable for widespread application in orchards, and an automated approach must be devised to appropriately divide imagery of a single tree, thereby reducing the risk of biased healthy predictions.

Alongside the low severity of imagery causing biases towards healthy predictions, capturing NIR imagery in direct sunlight also contributed to classification challenges. This issue primarily stems from overexposed imagery during the acquisition stage. Improving NIR image acquisition through real-time exposure adjustment would enhance the classification capabilities of CNNs in bright conditions. Additionally, increasing the amount of imagery acquired under these conditions in the training set would further improve performance. Due to the rapid spread of apple scab throughout orchards if untreated, practical applications of automated detection and classification methods must minimise false negative predictions as much as possible. For this experiment, a threshold confidence score of 0.5 was set to balance precision and recall, ensuring

overall accurate results. In scenarios where scab tolerance is lower and the risk of potential over-spraying is acceptable, lowering these threshold values can provide greater recall, albeit at the expense of a minor drop in overall accuracy (Table 6.3). Implementing these adjustments is crucial for enhancing the reliability and effectiveness of early disease detection systems in orchards. The ability to detect apple scab accurately in various lighting conditions and at different severity levels will significantly reduce the risk of undetected infections, ultimately protecting crop yields and reducing economic losses.

Labels	Whole-Plant Imagery				Localised Imagery			
	THRESHOLD (0.5)		THRESHOLD (0.3)		THRESHOLD (0.5)		THRESHOLD (0.3)	
	Accuracy	Recall	Accuracy	Recall	Accuracy	Recall	Accuracy	Recall
RGB	0.8859	0.7987	0.8809	0.8232	0.9027	0.8445	0.8905	0.8560
NIR	0.9482	0.8792	0.9432	0.8939	0.9536	0.8841	0.9505	0.8969
Total	0.9171	0.8390	0.9121	0.8586	0.9282	0.8643	0.9205	0.8765
TP	749		798		1065		1080	
FN	484		434		167		152	

Table 6.3 Impact of threshold value on classification performance of Chapter 5 dataset

Conversely, too many false positives would result in the unnecessary spraying of pesticides, negatively impacting the economic and environmental benefits of targeted site-specific control. Although specificities were low for RGB imagery and considerably lower for NIR imagery, these issues could lead to problematic levels of false positives if scaled up to commercial orchards. One method to reduce the rate of false positives is to combine the prediction results of both RGB and NIR data into a single multispectral image. Averaging the mean confidence reduces the impact of noisy false positive predictions in both the acquisition and classification of the imagery. Implementing this approach in the existing time series of Experiment 2 produces less noisy heatmaps and overall confidence levels that closely match manual classifications (Figure 6.9 and Figure 6.10).

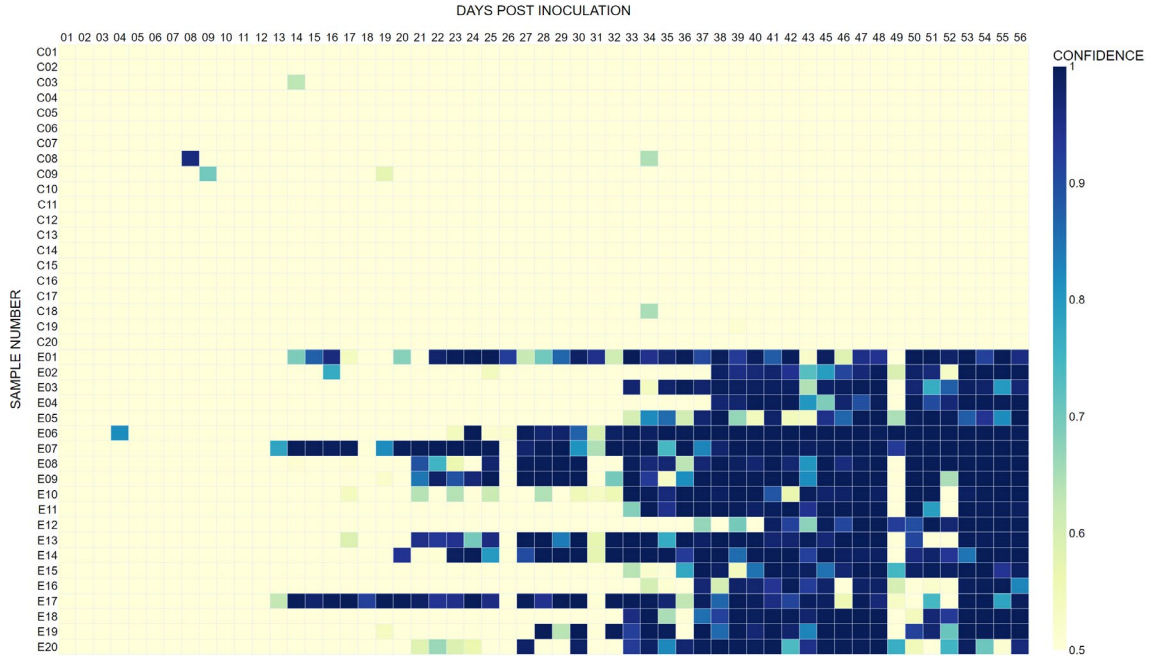


Figure 6.9 Heatmap of confidence prediction of combined multispectral (RGB+NIR) imagery

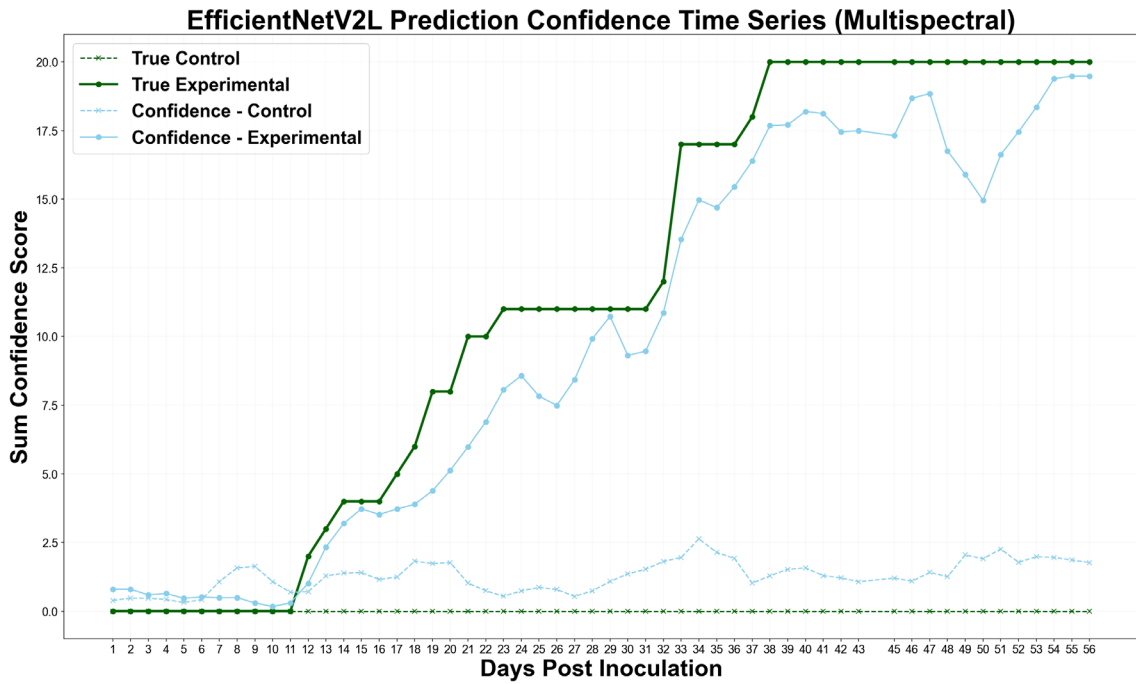


Figure 6.10 Smoothed 3-day moving mean time series of the sum of manual classification scores (green) and confidence scores of all experimental and control samples in combined multispectral (RGB+NIR) imagery

6.6 Early Detection of Apple Scab

This is the first study to use novel remote sensing systems to assess the early detection of apple scab symptoms under natural illumination rather than controlled laboratory conditions. Small-scale (Experiment 1) and large-scale (Experiment 2) trials were conducted to test the multispectral sensing and CNN-based classification methods for early detection. The results from both experiments were conclusive: NIR imagery allowed for easier and more reliable detection, both manually and through automated classification. Due to the semi-controlled nature of the experiments, there was significant variation in early detection (Table 6.4). In Experiment 1, where seedlings were imaged from a closer distance, early detection was achieved as early as 7 d.p.i., with an average detection range of 9-18 d.p.i. RGB imagery detected symptoms on average between 11-21 d.p.i. However, in Experiment 2, detection occurred later in general, with less difference between manual detection of scab using RGB and NIR time series (Figure 6.11). This delay is partially attributed to the challenges of inoculation discussed in Section 6.2, as well as the greater imaging distances, which reduced the resolution of initial symptoms. Nevertheless, when these time series were classified via CNNs, the models could detect apple scab earlier in NIR imagery than in RGB imagery, with a greater time difference between the two methods. This demonstrates the potential of NIR imagery and CNN-based classification for more effective early detection of apple scab infections in real-world orchard conditions.

Due to these issues, it is difficult to reliably determine the absolute earliest point of detection through RGB imagery, as the variation is too high between samples and dependent on many uncontrolled variables. A better understanding of early detection may help improve apple scab treatment in alternative ways. Decision-making based on multispectral imaging could determine whether curative spraying can be achieved. Additionally, it may be beneficial in plant phenotyping studies to breed resistant varieties or develop alternative control measures by clearly observing changes in fungal structures more accurately than in RGB imagery. Stronger assessments for early detection of apple scab infections should exercise greater control over environmental conditions and inoculant strength and image plants at a finer frequency than daily imaging.

Earliest Detection of Apple Scab (d.p.i.)					
Experiment 1			Experiment 2		
Sample	RGB	NIR	Sample	RGB	NIR
S5	19	16	E1	11	11
S7	19	16	E2	37	37
S22	15	12	E3	32	32
S23	14	10	E4	37	37
S24	16	12	E5	33	32
S25	16	11	E6	22	22
S26	21	18	E7	12	11
S29	16	10	E8	20	20
S31	17	17	E9	19	18
S34	30	32	E10	16	16
S35	11	7	E11	32	32
S36	16	18	E12	37	36
S38	16	16	E13	15	13
S39	16	11	E14	19	17
S40	19	17	E15	32	32
S41	13	11	E16	32	32
S42	11	9	E17	12	12
S43	12	9	E18	31	31
S44	14	11	E19	21	18
			E20	19	20
Mean	16.37	13.84	Mean	24.74	24.16

Table 6.4 The earliest detection dates of each positively tested plant sample in Experiment 1 and Experiment 2. The overall earliest date of detection is highlighted in yellow

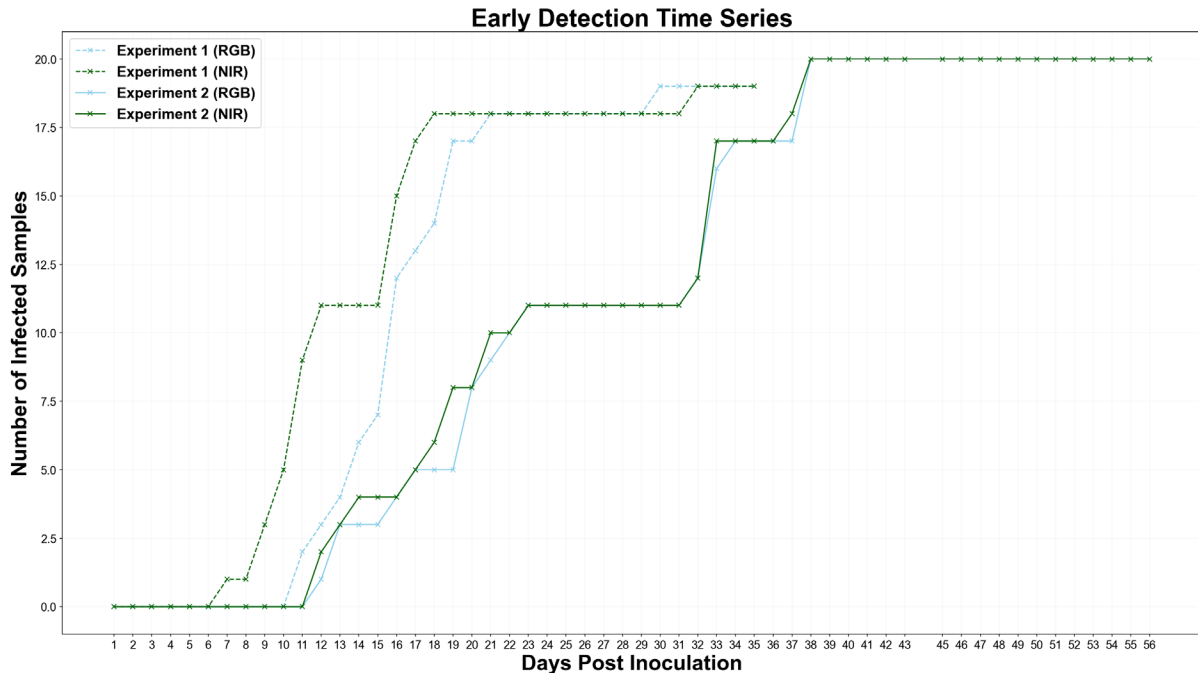


Figure 6.11 Early detection of scab time series from RGB and NIR imagery in Experiment 1 and Experiment 2

6.7 Recommendations for Further Work

Novel methodologies were applied throughout this study to achieve the early detection of apple scab: cultivation of plant material, development of a multispectral remote sensing system, generation and interpretation of a novel multispectral dataset, and classification using CNNs. The strengths, weaknesses, and numerous challenges faced within this research have been identified and discussed. Ultimately, this thesis clearly demonstrates that apple scab infections can be detected early using high-resolution multispectral imagery. Automated classifications of apple scab infection can be rapidly and accurately achieved based on NIR imagery. Classification under natural illumination conditions and scab severities is achievable and can be enhanced by optimising image acquisition. Further work is recommended to develop this system for practical application in commercial orchard settings. The following recommendations identify the key areas for the next stages of research.

6.7.1 Designing a Practical High-resolution Multispectral Imaging System

This experiment utilised two high-resolution sensing systems as a proof of concept that, while suitable for experimental analysis, would require further development before being operationalised within orchards. Whether the multispectral system is used via handheld acquisition or integrated onto UAV platforms, the following criteria are essential. The sensors must be high resolution, with a pixel area fine enough to detect apple scab symptoms from initial infection points. Using larger CMOS sensors with telephoto lenses may help achieve this. These sensors must also be lightweight, enabling portability and easy application onto mobile platforms. Finally, they must be capable of rapid, simultaneous RGB and NIR image acquisition and automated, real-time exposure settings adjustment. Using open-source, low-cost, lightweight technology from Raspberry Pi may be the most suitable hardware for developing this system.

6.7.2 Collecting and Annotating a Large Multispectral Apple Disease Dataset

Multispectral imaging is a novel approach to apple disease detection, and currently, there are no existing NIR datasets available to train CNN models. While this study acquired a large quantity of data, the homogeneous acquisition routine and time series nature of the experiment may have led to lower generalisation capabilities of the CNN, potentially limiting its direct application in orchards. Furthermore, this research has only demonstrated the capability of distinguishing apple scab from healthy tissue using NIR imagery, whereas RGB imagery has been used to diagnose five distinct disease classes. Therefore, collecting more varied training data from real-world orchards is recommended. Gathering and annotating data on apple scab and other disease symptoms in these conditions can improve CNN training and expand the diagnostic capabilities of CNNs beyond just apple scab detection.

6.7.3 Enhancing Apple Scab Classification Methods

Deep learning CNNs offer an accurate method for automating the classification of apple scab disease. As CNN-based classification performed better on localised imagery rather than whole-plant imagery, performing severity assessments on the testing dataset should be considered. This would quantitatively inform how CNN classification capabilities vary based on severity increase from initial symptoms to late stages of infection. While the CNNs used in this study were designed for simple classification across multiple classes, a greater range of features can also be applied. Several specific techniques can be employed to enhance CNN-based classification. Firstly, providing estimates of disease severity through categorical or percentage scales can help establish thresholds before fungicide application.

Techniques such as pixel-wise segmentation and object detection can be used to quantify the extent of infection on individual leaves, offering detailed severity metrics. Additionally, mapping disease hotspots can aid in the precise localisation of symptoms and visualise the spatial distribution of infections within an orchard, enabling targeted treatment. One major opportunity is to aid crop scouts in monitoring early apple scab through CNNs, which have the potential to provide real-time classifications from a live image feed. Furthermore, continual training using data captured in real-world conditions will likely improve classification accuracies. This approach can reduce the labour-intensive nature of crop monitoring and support rapid decision-making for crop treatment. Incorporating more detailed information into the classification process, such as performing severity assessments and spatial mapping, can enhance the overall effectiveness of CNN-based methods for disease detection and management in orchards.

6.7.4 Performing Controlled Early Detection of Apple Scab Assessments

NIR-based imagery was found to be effective for the early detection of apple scab in semi-controlled environmental conditions and natural illumination. This represents a step towards practical application, as previous research on early detection of apple scab was limited to laboratory environments. While the results successfully demonstrated early detection capabilities, the variability in the earliest feasible detection made it difficult to determine the potential benefits of targeted spraying. Implementing this technology in controlled laboratories for plant phenotyping may provide more detailed information on the differences. Continual monitoring of apple scab development and imaging at finer temporal resolutions, with greater control over environmental conditions and inoculant, could yield results comparable to those of previous studies. Furthermore, an in-depth analysis of NIR-based imagery could support the hypothesis of the absorption potential of scab and help determine the effectiveness of NIR imagery for detecting other stress symptoms, as well as understand why the diagnostic capabilities are absent for powdery mildew. Imaging within the controlled environments could also be used to calibrate and optimise sensors, exposure settings, and acquisition methods to ensure the earliest feasible detection of apple scab across a range of illumination conditions.

7 Conclusions and Future Research

7.1 General Conclusion

The early detection of plant pathogens is essential for sustainable disease control. Apples, one of the most extensively cultivated fruit crops, are associated with significant environmental impacts due to the intensive use of pesticides in disease management practices. Among all the diseases affecting apples, apple scab is the most critical, resulting in substantial yield losses, high control costs, and extensive fungicide application. Detecting apple scab symptoms in the early stages of infection can enhance decision-making in disease management, thereby reducing fungicide usage and mitigating yield losses. Despite the substantial body of research dedicated to remote sensing for early apple scab detection, existing solutions have been evaluated primarily in controlled environments, utilising specialist equipment impractical for deployment in real-world conditions.

The aim of this thesis was to develop a remote sensing strategy capable of detecting the early stages of apple scab under natural illumination conditions. Demonstrating detection capabilities from imagery acquired in semi-controlled environments represents a significant advancement toward developing a practical system for application in commercial orchards. To this end, a high-resolution multispectral imaging system was developed by modifying traditional RGB cameras to be sensitive to near-infrared (NIR) radiation. This system was highly effective for apple scab detection, displaying infections from the initial stages to well-developed symptoms under a range of illumination conditions. RGB and NIR time series datasets comprising 150 individual plants were acquired and manually classified, revealing that apple scabs could be detected several days earlier in NIR imagery than in RGB imagery. In NIR imagery, apple scab can be clearly identified by the lesions on infected tissue, which exhibit high absorbance potential, contrasting sharply with the high reflectance of healthy tissue. Consequently, this system demonstrated significant potential for the early detection of disease through manual assessment approaches in Chapter 3.

Manual assessments of disease, both in-field and in laboratory settings, are time-consuming and labour-intensive. Thus, the diagnosis of early apple scab from multispectral imagery necessitates rapid and accurate identification through automated classification techniques. Convolutional Neural Networks (CNNs) have previously been used to identify well developed symptoms of apple diseases from RGB imagery acquired in commercial orchards. This study applied three pre-

trained classification models to assess their ability to classify early stages of apple scab in NIR imagery: MobileNetV2, InceptionResNetV2, and EfficientNetV2L. Given the novelty of this problem, the CNNs were fine-tuned on a training set derived from the primary data containing multispectral time series imagery and secondary data from public sources. CNN performance was evaluated using metrics calculated from their prediction outputs and validated against secondary data from public sources. The classification of multispectral imagery proved successful in both Chapter 4 and Chapter 5, achieving rapid and accurate identification of early apple scab. Overall, the classification of apple scab was consistently superior in NIR-based imagery compared to RGB imagery, with the former detecting scab earlier and yielding fewer false positive and negative predictions. Ultimately, the heavyweight EfficientNetV2L showed the greatest performance of all three.

While the results of this study have clearly demonstrated that CNN-based classification techniques can be used to detect early apple scab on NIR imagery, several challenges affecting the performance of this system were identified. Although apple scab was precisely classified from early to late stages, CNNs struggled with low-severity infections spread across the plant. The ratio of healthy to infected tissue caused a bias towards healthy predictions by the classifiers. Classification performance improved significantly when the testing data was localised to smaller regions where apple scab symptoms were present. Successful classification was achieved under various illumination conditions; however, on days with high sunlight combined with sub-optimal acquisition settings, high-exposure images reduced the detection capabilities of both CNN and manual-based classification. In order to adapt to the highly variable weather conditions experienced within orchards, the real-time adjustment of exposure settings is crucial. Moreover, while NIR imagery effectively distinguished between healthy and scab-infected samples, it did not display symptoms of heat stress and powdery mildew clearly. Nevertheless, NIR imagery demonstrated a greater ability to distinguish apple scab infections from these symptoms than RGB imagery. Collecting more multispectral imagery from commercial orchards to train CNNs would inevitably improve their generalisation capabilities and help address the issues affecting classification performance.

The high-resolution multispectral imaging system, combined with the deep learning CNN classifiers developed in this thesis, offers a cost-effective and labour-saving solution for monitoring apple orchards for apple scab infections. This study is the first to demonstrate the effectiveness of NIR imagery for apple scab detection and to explore the capabilities of CNNs in classifying early-stage symptoms from a novel multispectral time series. This research serves as a proof of concept for the proposed sensing strategy and provides recommendations for further

development to facilitate the implementation of remote sensing-based disease monitoring in orchards. The goal is to provide ancillary technology to complement traditional crop scouting, thereby improving the frequency and coverage of disease monitoring. The information acquired can be used to inform site-specific management of apple scab epidemics, reducing reliance on costly and environmentally damaging mass spraying of fungicides, and improving the control of apple scab epidemics.

7.2 Future Research for Disease Monitoring in Orchards

The rationale behind this research was to enhance the efficiency of disease control in orchards, thereby contributing to the sustainable intensification of agriculture. This can be achieved by implementing precision agriculture technologies that enable site-specific control of apple scab infections. Central to precision agriculture methodologies are remote sensing systems capable of providing accurate information on crop health, even under the complex real-world conditions of orchards. This thesis successfully addressed the aim of early detection of apple scab infection under natural illumination conditions. In Section 6.7 four recommendations for further research were identified to improve the early detection of apple scab under natural illumination conditions. These include:

- (1) Develop an effective sensing system for image acquisition within orchards.
- (2) Build a large multispectral training set to enhance CNN training.
- (3) Improve the information output from automated CNN models for apple scab detection.
- (4) Establish the capabilities of early detection by NIR imagery in controlled environments

By following these recommendations, the high-resolution NIR-based imaging and classification strategy developed within this thesis can be enhanced in order to enable a practical disease-monitoring strategy for outdoor use. Applying these systems in commercial orchards will improve the sustainability of disease management. The final section of this chapter offers three opportunities for future research that may build upon the novel multispectral sensing system developed in this study for precision agriculture within commercial orchards for the sustainable intensification of apple production.

7.2.1 Assessment of Acquisition and Classification in High-Density Orchards

This research represents a significant step towards automated disease monitoring in orchards by transitioning early detection studies from controlled laboratory settings to semi-controlled environments. The next phase involves deploying the high-resolution multispectral sensor for detecting apple scab infections in commercial orchards. These sensing methods are particularly well-suited for deployment on UAV platforms, enabling aerial imaging of plants across extensive areas. However, classifying apple scab becomes increasingly challenging at greater imaging distances between the sensor and target, as symptoms appear smaller, and the presence of numerous healthy leaves can influence predictions. To address these challenges, field trials in scab-infested orchards must acquire additional training data and fine-tune CNN models. Furthermore, developing appropriate acquisition and classification procedures is crucial before commercial implementation. This process will involve scaling up the imaging from small plants to adult trees and entire orchards and determining an appropriate return frequency to monitor for apple scab throughout the season.

Accurate diagnosis of apple scab is crucial to prevent potentially devastating consequences from misdiagnosis, highlighting the need for safe, accurate, reliable, and robust field trials prior to adoption in commercial disease management practices. To ensure practical implementation, further research must establish strong connections with commercial agriculture and real orchard management. Understanding the capability of these systems to accurately monitor the early stages of apple scab across orchards is essential for their successful application in precision agriculture. This approach will ultimately enhance disease management, reduce chemical usage, and promote sustainable apple production.

7.2.2 Informing Integrated Pest and Disease Management Strategies

Integrated Pest Management (IPM) is regarded as the best practice for disease control in orchards; however, its effectiveness is constrained by the labour-intensive nature of orchard monitoring through crop scouting. The remote sensing system developed in this study has the potential for automation, enabling more frequent orchard monitoring during the intervals between scouting visits. Increased frequency and broader coverage of monitoring enhance decision-making capabilities for disease control. A significant benefit of this approach is the

potential for targeted pesticide application. Precise mapping and severity assessments of apple scab infections across individual trees can inform site-specific applications of curative fungicides based on the location and threshold levels of the pathogen. This targeted approach reduces the need for uniform spraying, decreasing fungicide volume while maintaining adequate disease protection. Additionally, continuous orchard monitoring provides critical data on the presence of *V. inaequalis*, which can be used to enhance existing scab risk models. Understanding the risk posed to specific orchard regions, based on scab presence in surrounding areas or historical data, can improve the accuracy of risk predictions. This information can better inform the use of protective fungicides based on risk assessments rather than routine, homogeneous sprays. Furthermore, site-specific spray adjustments can be made in real time by integrating this information with the variable rate spray technologies currently available.

Applying high-resolution multispectral imaging sensors with CNNs offers significant benefits for precision agriculture and supports low-cost, high-throughput phenotyping in laboratory and field settings. Monitoring plant responses to disease and abiotic stresses is crucial for characterising disease-resistant and abiotic-resistant varieties. Rapid acquisition and accurate classification of novel apple varieties can facilitate the identification of new cultivars with enhanced resistance to apple scab infection. Although this represents only a small part of the breeding process, it can significantly contribute to the introduction of scab-resistant cultivars into mainstream agriculture, thereby reducing the global volume of fungicides required.

7.2.3 Understanding the Impact on Sustainable Intensification of Apple Production

Throughout this research, the primary assumption has been that early detection of apple scab will contribute to the sustainable intensification of agriculture. Successful integration of this technology into commercial orchards will facilitate further exploration of its benefits, with field trials crucial for fully understanding and quantifying these potential advantages. Several key parameters should be investigated to assess the benefits of precision agriculture-based apple scab management. Research should focus on identifying the reduction in fungicide volume compared to conventional techniques, evaluating the impact of targeted pesticide application on epidemic severity, and studying the effects on marketable apple yields. This information will also contribute to assessing the cost-effectiveness of implementing these techniques. Ultimately, the aim of this research is to enhance the sustainability of apple production worldwide. Future studies should investigate how reducing pesticide applications can positively impact the environment and ecosystems surrounding commercial orchards.

8 References

Abdulridha, J., Ampatzidis, Y., Roberts, P., & Kakarla, S. C. (2020). Detecting powdery mildew disease in squash at different stages using UAV-based hyperspectral imaging and artificial intelligence. *Biosystems engineering*, 197, 135-148.

<https://doi.org/https://doi.org/10.1016/j.biosystemseng.2020.07.001>

Abdulridha, J., Batuman, O., & Ampatzidis, Y. (2019). UAV-Based Remote Sensing Technique to Detect Citrus Canker Disease Utilizing Hyperspectral Imaging and Machine Learning. *Remote sensing*, 11(11), 1373. <https://www.mdpi.com/2072-4292/11/11/1373>

Aćimović, S., & Rosenberger, D. (2018). An Introduction to the RIMpro Apple Scab Prediction Model. *Scaffolds Fruit Journal*, 27, 1-5.

Aćimović, S. G., Santander, R. D., Meredith, C. L., & Pavlović, Ž. M. (2023). Fire blight rootstock infections causing apple tree death: A case study in high-density apple orchards with *Erwinia amylovora* strain characterization [Original Research]. *Frontiers in Horticulture*, 2.

<https://doi.org/10.3389/fhort.2023.1082204>

Acorsi, M. G., Gimenez, L. M., & Martello, M. (2020). Assessing the Performance of a Low-Cost Thermal Camera in Proximal and Aerial Conditions. *Remote sensing*, 12(21), 3591.

<https://www.mdpi.com/2072-4292/12/21/3591>

Ahamed, T., Tian, L., Jiang, Y., Zhao, B., Liu, H., & Ting, K. C. (2012). Tower remote-sensing system for monitoring energy crops; image acquisition and geometric corrections. *Biosystems engineering*, 112(2), 93-107.

<https://doi.org/https://doi.org/10.1016/j.biosystemseng.2012.03.003>

Aktar, W., Sengupta, D., & Chowdhury, A. (2009). Impact of pesticides use in agriculture: their benefits and hazards. *Interdisciplinary toxicology*, 2(1), 1-12.

Alaphilippe, A., Simon, S., Brun, L., Hayer, F., & Gaillard, G. (2013). Life cycle analysis reveals higher agroecological benefits of organic and low-input apple production. *Agronomy for sustainable development*, 33(3), 581-592. <https://doi.org/10.1007/s13593-012-0124-7>

Albetis, J., Duthoit, S., Guttler, F., Jacquin, A., Goulard, M., Poilvé, H., Féret, J.-B., & Dedieu, G. (2017). Detection of Flavescence dorée Grapevine Disease Using Unmanned Aerial Vehicle (UAV) Multispectral Imagery. *Remote sensing*, 9(4), 308. <https://www.mdpi.com/2072-4292/9/4/308>

Aldwinckle, H. S., Lamb, R., & Gustafson, H. (1977). Nature and inheritance of resistance to *Gymnosporangium juniperi-virginianae* in apple cultivars. *Phytopathology*, 67, 259-266.

Allen, W. A., Gausman, H. W., Richardson, A. J., & Wiegand, C. L. (1970). Mean Effective Optical Constants of Thirteen Kinds of Plant Leaves. *Applied Optics*, 9(11), 2573-2577.

<https://doi.org/10.1364/AO.9.002573>

- Alomar, K., Aysel, H. I., & Cai, X. (2023). Data Augmentation in Classification and Segmentation: A Survey and New Strategies. *Journal of Imaging*, 9(2), 46. <https://www.mdpi.com/2313-433X/9/2/46>
- Alzubaidi, L., Zhang, J., Humaidi, A. J., Al-Dujaili, A., Duan, Y., Al-Shamma, O., Santamaría, J., Fadhel, M. A., Al-Amidie, M., & Farhan, L. (2021). Review of deep learning: concepts, CNN architectures, challenges, applications, future directions. *Journal of Big Data*, 8(1), 53. <https://doi.org/10.1186/s40537-021-00444-8>
- Anderson, H. B., Nilsen, L., Tømmervik, H., Karlsen, S. R., Nagai, S., & Cooper, E. J. (2016). Using Ordinary Digital Cameras in Place of Near-Infrared Sensors to Derive Vegetation Indices for Phenology Studies of High Arctic Vegetation. *Remote sensing*, 8(10), 847. <https://www.mdpi.com/2072-4292/8/10/847>
- Anderson, R., Bayer, P. E., & Edwards, D. (2020). Climate change and the need for agricultural adaptation. *Current Opinion in Plant Biology*, 56, 197-202. <https://doi.org/https://doi.org/10.1016/j.pbi.2019.12.006>
- Ang, K. M., Lim, W. H., Tiang, S. S., Sharma, A., Eid, M. M., Tawfeek, S. M., Khafaga, D. S., Alharbi, A. H., & Abdelhamid, A. A. (2023). Optimizing Image Classification: Automated Deep Learning Architecture Crafting with Network and Learning Hyperparameter Tuning. *Biomimetics*, 8(7), 525. <https://www.mdpi.com/2313-7673/8/7/525>
- Antal, G., Szabó, S., Szarvas, P., & Holb, I. J. (2024). Yield and cost-benefit analyses for apple scab sanitation practices in integrated and organic apple management systems. *Plants, People, Planet*, 6(2), 470-489.
- Araus, J. L., & Kefauver, S. C. (2018). Breeding to adapt agriculture to climate change: affordable phenotyping solutions. *Current Opinion in Plant Biology*, 45, 237-247. <https://doi.org/https://doi.org/10.1016/j.pbi.2018.05.003>
- Assmann, J. J., Kerby, J. T., Cunliffe, A. M., & Myers-Smith, I. H. (2019). Vegetation monitoring using multispectral sensors — best practices and lessons learned from high latitudes. *Journal of Unmanned Vehicle Systems*, 7(1), 54-75. <https://doi.org/10.1139/juvs-2018-0018>
- Auernhammer, H. (2001). Precision farming—the environmental challenge. *Computers and electronics in agriculture*, 30(1-3), 31-43.
- Ayer, K., Carroll, J., & Cox, K. (2020) Apple Scab. Retrieved February 5 2021, from <https://ecommons.cornell.edu/items/d71c5ea4-14a0-42bd-a4da-f5a3feb848ba>
- Bagheri, N. (2020). Application of aerial remote sensing technology for detection of fire blight infected pear trees. *Computers and electronics in agriculture*, 168, 105147. <https://doi.org/https://doi.org/10.1016/j.compag.2019.105147>
- Bagheri, N., Mohamadi-Monavar, H., Azizi, A., & Ghasemi, A. (2018). Detection of Fire Blight disease in pear trees by hyperspectral data. *European Journal of Remote Sensing*, 51(1), 1-10. <https://doi.org/10.1080/22797254.2017.1391054>

Baker, N. R. (2008). Chlorophyll Fluorescence: A Probe of Photosynthesis In Vivo. *Annual Review of Plant Biology*, 59(Volume 59, 2008), 89-113.

<https://doi.org/https://doi.org/10.1146/annurev.arplant.59.032607.092759>

Balasundram, S. K., Golhani, K., Shamshiri, R. R., & Vadamalai, G. (2020). Precision agriculture technologies for management of plant diseases. *Plant disease management strategies for sustainable agriculture through traditional and modern approaches*, 259-278.

Ban, S., Tian, M., & Chang, Q. (2019). Estimating the severity of apple mosaic disease with hyperspectral images. *International Journal of Agricultural and Biological Engineering*, 12(4), 148-153.

Bansal, P., Kumar, R., & Kumar, S. (2021). Disease Detection in Apple Leaves Using Deep Convolutional Neural Network. *Agriculture*, 11(7), 617. <https://www.mdpi.com/2077-0472/11/7/617>

Barbara, D. J., Roberts, A. L., & Xu, X.-M. (2008). Virulence characteristics of apple scab (*Venturia inaequalis*) isolates from monoculture and mixed orchards. *Plant Pathology*, 57(3), 552-561. <https://doi.org/https://doi.org/10.1111/j.1365-3059.2007.01781.x>

Barbedo, J. G. A. (2013). Digital image processing techniques for detecting, quantifying and classifying plant diseases. *SpringerPlus*, 2(1), 660. <https://doi.org/10.1186/2193-1801-2-660>

Barbedo, J. G. A. (2019a). Plant disease identification from individual lesions and spots using deep learning. *Biosystems engineering*, 180, 96-107. <https://doi.org/https://doi.org/10.1016/j.biosystemseng.2019.02.002>

Barbedo, J. G. A. (2019b). A Review on the Use of Unmanned Aerial Vehicles and Imaging Sensors for Monitoring and Assessing Plant Stresses. *Drones*, 3(2), 40. <https://www.mdpi.com/2504-446X/3/2/40>

Barbedo, J. G. A., Koenigkan, L. V., & Santos, T. T. (2016). Identifying multiple plant diseases using digital image processing. *Biosystems engineering*, 147, 104-116. <https://doi.org/https://doi.org/10.1016/j.biosystemseng.2016.03.012>

Barzman, M., Bàrberi, P., Birch, A. N. E., Boonekamp, P., Dachbrodt-Saaydeh, S., Graf, B., Hommel, B., Jensen, J. E., Kiss, J., Kudsk, P., Lamichhane, J. R., Messéan, A., Moonen, A.-C., Ratnadass, A., Ricci, P., Sarah, J.-L., & Sattin, M. (2015). Eight principles of integrated pest management. *Agronomy for sustainable development*, 35(4), 1199-1215. <https://doi.org/10.1007/s13593-015-0327-9>

Bauriegel, E., & Herppich, W. B. (2014). Hyperspectral and Chlorophyll Fluorescence Imaging for Early Detection of Plant Diseases, with Special Reference to *Fusarium spec.* Infections on Wheat. *Agriculture*, 4(1), 32-57. <https://www.mdpi.com/2077-0472/4/1/32>

Beckerman, J. L., Sundin, G. W., & Rosenberger, D. A. (2015). Do some IPM concepts contribute to the development of fungicide resistance? Lessons learned from the apple scab pathosystem in the United States. *Pest Management Science*, 71(3), 331-342.

<https://doi.org/https://doi.org/10.1002/ps.3715>

Behmann, J., Acebron, K., Emin, D., Bennertz, S., Matsubara, S., Thomas, S., Bohnenkamp, D., Kuska, M. T., Jussila, J., Salo, H., Mahlein, A.-K., & Rascher, U. (2018). Specim IQ: Evaluation of a New, Miniaturized Handheld Hyperspectral Camera and Its Application for Plant Phenotyping and Disease Detection. *Sensors*, 18(2), 441. <https://www.mdpi.com/1424-8220/18/2/441>

Behmann, J., Mahlein, A.-K., Rumpf, T., Römer, C., & Plümer, L. (2015). A review of advanced machine learning methods for the detection of biotic stress in precision crop protection. *Precision Agriculture*, 16(3), 239-260. <https://doi.org/10.1007/s11119-014-9372-7>

Belcore, E., Piras, M., Pezzoli, A., Massazza, G., & Rosso, M. (2019). RASPBERRY PI 3 MULTISPECTRAL LOW-COST SENSOR FOR UAV BASED REMOTE SENSING. CASE STUDY IN SOUTH-WEST NIGER. *Int. Arch. Photogramm. Remote Sens. Spatial Inf. Sci.*, XLII-2/W13, 207-214. <https://doi.org/10.5194/isprs-archives-XLII-2-W13-207-2019>

Belete, T., & Boyraz, N. (2017). Critical review on apple scab (*Venturia inaequalis*) biology, epidemiology, economic importance, management, and defense mechanisms to the causal agent. *J. Plant Physiol. Pathol*, 5(2), 2.

Belfanti, E., Silfverberg-Dilworth, E., Tartarini, S., Patocchi, A., Barbieri, M., Zhu, J., Vinatzer, B. A., Gianfranceschi, L., Gessler, C., & Sansavini, S. (2004). The HcrVf2 gene from a wild apple confers scab resistance to a transgenic cultivated variety. *Proceedings of the National Academy of Sciences*, 101(3), 886-890.

Belin, É., Rousseau, D., Boureau, T., & Caffier, V. (2013). Thermography versus chlorophyll fluorescence imaging for detection and quantification of apple scab. *Computers and electronics in agriculture*, 90, 159-163. <https://doi.org/https://doi.org/10.1016/j.compag.2012.09.014>

Berger, S., Sinha, A. K., & Roitsch, T. (2007). Plant physiology meets phytopathology: plant primary metabolism and plant-pathogen interactions. *Journal of Experimental Botany*, 58(15-16), 4019-4026. <https://doi.org/10.1093/jxb/erm298>

Berk, P., Stajko, D., Belsak, A., & Hocevar, M. (2020). Digital evaluation of leaf area of an individual tree canopy in the apple orchard using the LIDAR measurement system. *Computers and electronics in agriculture*, 169, 105158. <https://doi.org/https://doi.org/10.1016/j.compag.2019.105158>

Berra, E. F., Gaulton, R., & Barr, S. (2017). Commercial Off-the-Shelf Digital Cameras on Unmanned Aerial Vehicles for Multitemporal Monitoring of Vegetation Reflectance and NDVI. *IEEE Transactions on Geoscience and Remote Sensing*, 55(9), 4878-4886. <https://doi.org/10.1109/TGRS.2017.2655365>

Berrie, A., & Xu, X. (2003). Managing apple scab (*Venturia inaequalis*) and powdery mildew (*Podosphaera leucotricha*) using Adem™. *International Journal of Pest Management*, 49(3), 243-249.

Biggs, A. (2004). Relative Susceptibility of Selected Apple Cultivars to Fruit Rot Caused by *Botryosphaeria obtusa*. *HortScience: a publication of the American Society for Horticultural Science*, 39, 303-306.

Blackburn, G. A. (1998a). Spectral indices for estimating photosynthetic pigment concentrations: A test using senescent tree leaves. *International Journal of Remote Sensing*, 19(4), 657-675. <https://doi.org/10.1080/014311698215919>

Blackburn, G. A. (1998b). Quantifying Chlorophylls and Carotenoids at Leaf and Canopy Scales: An Evaluation of Some Hyperspectral Approaches. *Remote Sensing of Environment*, 66(3), 273-285. [https://doi.org/https://doi.org/10.1016/S0034-4257\(98\)00059-5](https://doi.org/https://doi.org/10.1016/S0034-4257(98)00059-5)

Bleasdale, A. J., Blackburn, G. A., & Whyatt, J. D. (2022). Feasibility of detecting apple scab infections using low-cost sensors and interpreting radiation interactions with scab lesions. *International Journal of Remote Sensing*, 43(13), 4984-5005. <https://doi.org/10.1080/01431161.2022.2122895>

Bock, C., Poole, G., Parker, P., & Gottwald, T. (2010). Plant disease severity estimated visually, by digital photography and image analysis, and by hyperspectral imaging. *Critical reviews in plant sciences*, 29(2), 59-107.

Bock, C. H., Barbedo, J. G. A., Del Ponte, E. M., Bohnenkamp, D., & Mahlein, A.-K. (2020). From visual estimates to fully automated sensor-based measurements of plant disease severity: status and challenges for improving accuracy. *Phytopathology Research*, 2(1), 9. <https://doi.org/10.1186/s42483-020-00049-8>

Boulent, J., Foucher, S., Théau, J., & St-Charles, P.-L. (2019). Convolutional Neural Networks for the Automatic Identification of Plant Diseases [Review]. *Frontiers in Plant Science*, 10. <https://doi.org/10.3389/fpls.2019.00941>

Bowen, J. K., Mesarich, C. H., Bus, V. G., Beresford, R. M., Plummer, K. M., & Templeton, M. D. (2011). *Venturia inaequalis*: the causal agent of apple scab. *Molecular plant pathology*, 12(2), 105-122.

Buja, I., Sabella, E., Monteduro, A. G., Chiriaco, M. S., De Bellis, L., Luvisi, A., & Maruccio, G. (2021). Advances in Plant Disease Detection and Monitoring: From Traditional Assays to In-Field Diagnostics. *Sensors*, 21(6), 2129. <https://www.mdpi.com/1424-8220/21/6/2129>

Busemeyer, L., Mentrup, D., Möller, K., Wunder, E., Alheit, K., Hahn, V., Maurer, H. P., Reif, J. C., Würschum, T., Müller, J., Rahe, F., & Ruckelshausen, A. (2013). BreedVision — A Multi-Sensor Platform for Non-Destructive Field-Based Phenotyping in Plant Breeding. *Sensors*, 13(3), 2830-2847. <https://www.mdpi.com/1424-8220/13/3/2830>

- Cao, S., Danielson, B., Clare, S., Koenig, S., Campos-Vargas, C., & Sanchez-Azofeifa, A. (2019). Radiometric calibration assessments for UAS-borne multispectral cameras: Laboratory and field protocols. *ISPRS Journal of Photogrammetry and Remote Sensing*, 149, 132-145. <https://doi.org/https://doi.org/10.1016/j.isprsjprs.2019.01.016>
- Cardim Ferreira Lima, M., Krus, A., Valero, C., Barrientos, A., del Cerro, J., & Roldán-Gómez, J. J. (2020). Monitoring Plant Status and Fertilization Strategy through Multispectral Images. *Sensors*, 20(2), 435. <https://www.mdpi.com/1424-8220/20/2/435>
- Castrignanò, A., Belmonte, A., Antelmi, I., Quarto, R., Quarto, F., Shaddad, S., Sion, V., Muolo, M. R., Ranieri, N. A., Gadaleta, G., Bartocchetti, E., Riefolo, C., Ruggieri, S., & Nigro, F. (2021). Semi-Automatic Method for Early Detection of *Xylella fastidiosa* in Olive Trees Using UAV Multispectral Imagery and Geostatistical-Discriminant Analysis. *Remote sensing*, 13(1), 14. <https://www.mdpi.com/2072-4292/13/1/14>
- Ceccato, P., Flasse, S., Tarantola, S., Jacquemoud, S., & Grégoire, J.-M. (2001). Detecting vegetation leaf water content using reflectance in the optical domain. *Remote Sensing of Environment*, 77(1), 22-33. [https://doi.org/https://doi.org/10.1016/S0034-4257\(01\)00191-2](https://doi.org/https://doi.org/10.1016/S0034-4257(01)00191-2)
- Chaerle, L., & Van Der Straeten, D. (2000). Imaging techniques and the early detection of plant stress. *Trends in Plant Science*, 5(11), 495-501. [https://doi.org/10.1016/S1360-1385\(00\)01781-7](https://doi.org/10.1016/S1360-1385(00)01781-7)
- Chandel, A. K., Khot, L. R., & C, B. S. (2021). Apple powdery mildew infestation detection and mapping using high-resolution visible and multispectral aerial imaging technique. *Scientia horticultrae*, 287, 110228. <https://doi.org/https://doi.org/10.1016/j.scienta.2021.110228>
- Chandel, A. K., Khot, L. R., & Sallato, B. C. (2020, 4-6 Nov. 2020). Towards rapid detection and mapping of powdery mildew in apple orchards. 2020 IEEE International Workshop on Metrology for Agriculture and Forestry (MetroAgriFor),
- Chao, X., Hu, X., Feng, J., Zhang, Z., Wang, M., & He, D. (2021). Construction of Apple Leaf Diseases Identification Networks Based on Xception Fused by SE Module. *Applied Sciences*, 11(10), 4614. <https://www.mdpi.com/2076-3417/11/10/4614>
- Chao, X., Sun, G., Zhao, H., Li, M., & He, D. (2020). Identification of Apple Tree Leaf Diseases Based on Deep Learning Models. *Symmetry*, 12(7), 1065. <https://www.mdpi.com/2073-8994/12/7/1065>
- Chatzidimopoulos, M., Lioliopoulou, F., Sotiropoulos, T., & Vellios, E. (2020). Efficient Control of Apple Scab with Targeted Spray Applications. *Agronomy*, 10(2), 217. <https://www.mdpi.com/2073-4395/10/2/217>
- Chawade, A., van Ham, J., Blomquist, H., Bagge, O., Alexandersson, E., & Ortiz, R. (2019). High-Throughput Field-Phenotyping Tools for Plant Breeding and Precision Agriculture. *Agronomy*, 9(5), 258. <https://www.mdpi.com/2073-4395/9/5/258>

Chen, H., & Korban, S. S. (1987). Genetic variability and the inheritance of resistance to cedar-apple rust in apple. *Plant Pathology*, 36(2), 168-174.

<https://doi.org/https://doi.org/10.1111/j.1365-3059.1987.tb02217.x>

Chéné, Y., Rousseau, D., Lucidarme, P., Bertheloot, J., Caffier, V., Morel, P., Belin, É., & Chapeau-Blondeau, F. (2012). On the use of depth camera for 3D phenotyping of entire plants. *Computers and electronics in agriculture*, 82, 122-127.

<https://doi.org/https://doi.org/10.1016/j.compag.2011.12.007>

Chiang, K.-S., & Bock, C. H. (2022). Understanding the ramifications of quantitative ordinal scales on accuracy of estimates of disease severity and data analysis in plant pathology. *Tropical Plant Pathology*, 47(1), 58-73. <https://doi.org/10.1007/s40858-021-00446-0>

Čirjak, D., Miklečić, I., Lemić, D., Kos, T., & Pajač Živković, I. (2022). Automatic pest monitoring systems in apple production under changing climatic conditions. *Horticulturae*, 8(6), 520.

Cox, K. D. (2015). Fungicide Resistance in *Venturia inaequalis*, the Causal Agent of Apple Scab, in the United States. In H. Ishii & D. W. Hollomon (Eds.), *Fungicide Resistance in Plant Pathogens: Principles and a Guide to Practical Management* (pp. 433-447). Springer Japan.

https://doi.org/10.1007/978-4-431-55642-8_27

Crassweller, R. M., T. A. Baugher, T. G. Ford, R. P. Marini, J. R. Schupp, D. Weber, G. Krawczyk, D. J. Biddinger, M. López-Uribe, J. Hopwood, K. A. Peter, B. L. Lehman, M. C. Brittingham, J. Johnson, E. Crow, E. Weaver, L. F. LaBorde, J. K. Harper, L. F. Kime, K. Kephart, R. H. Pifer, K. M. Kelley, L. He, P. Heinemann, C. Gregory and C. Jung (2020). 2020 - 2021 "Penn State Tree Fruit Production Guide." University Park, PA, USA, College of Agricultural Sciences; The Pennsylvania State University.

Curran, P. J. (1989). Remote sensing of foliar chemistry. *Remote Sensing of Environment*, 30(3), 271-278. [https://doi.org/https://doi.org/10.1016/0034-4257\(89\)90069-2](https://doi.org/https://doi.org/10.1016/0034-4257(89)90069-2)

DadrasJavan, F., Samadzadegan, F., Seyed Pourazar, S. H., & Fazeli, H. (2019). UAV-based multispectral imagery for fast Citrus Greening detection. *Journal of Plant Diseases and Protection*, 126(4), 307-318. <https://doi.org/10.1007/s41348-019-00234-8>

Damos, P., Escudero Colomar, L.-A., & Ioriatti, C. (2015). Integrated fruit production and pest management in Europe: the apple case study and how far we are from the original concept? *Insects*, 6(3), 626-657.

Deery, D., Jimenez-Berni, J., Jones, H., Sirault, X., & Furbank, R. (2014). Proximal Remote Sensing Buggies and Potential Applications for Field-Based Phenotyping. *Agronomy*, 4(3), 349-379.

<https://www.mdpi.com/2073-4395/4/3/349>

Delalieux, S., Auwerkerken, A., Verstraeten, W. W., Somers, B., Valcke, R., Lhermitte, S., Keulemans, J., & Coppin, P. (2009a). Hyperspectral Reflectance and Fluorescence Imaging to Detect Scab Induced Stress in Apple Leaves. *Remote sensing*, 1(4), 858-874. <https://www.mdpi.com/2072-4292/1/4/858>

Delalieux, S., Somers, B., Verstraeten, W. W., van Aardt, J. A. N., Keulemans, W., & Coppin, P. (2009b). Hyperspectral indices to diagnose leaf biotic stress of apple plants, considering leaf phenology. *International Journal of Remote Sensing*, 30(8), 1887-1912. <https://doi.org/10.1080/01431160802541556>

Delalieux, S., van Aardt, J., Keulemans, W., Schrevens, E., & Coppin, P. (2007). Detection of biotic stress (*Venturia inaequalis*) in apple trees using hyperspectral data: Non-parametric statistical approaches and physiological implications. *European Journal of Agronomy*, 27(1), 130-143. <https://doi.org/https://doi.org/10.1016/j.eja.2007.02.005>

Delgado, Á., García-Fernández, B., Gómez-Cortecero, A., & Dapena, E. (2022). Susceptibility of Cider Apple Accessions to European Canker—Comparison between Evaluations in Field Planted Trees and Rapid Screening Tests. *Plants*, 11(9), 1145. <https://www.mdpi.com/2223-7747/11/9/1145>

Deng, J., Dong, W., Socher, R., Li, L. J., Li, K., & Fei-Fei, L. (2009, 20-25 June 2009). ImageNet: A large-scale hierarchical image database. 2009 IEEE Conference on Computer Vision and Pattern Recognition,

Deng, L., Mao, Z., Li, X., Hu, Z., Duan, F., & Yan, Y. (2018). UAV-based multispectral remote sensing for precision agriculture: A comparison between different cameras. *ISPRS Journal of Photogrammetry and Remote Sensing*, 146, 124-136. <https://doi.org/https://doi.org/10.1016/j.isprsjprs.2018.09.008>

Dicks, L. V., Rose, D. C., Ang, F., Aston, S., Birch, A. N. E., Boatman, N., Bowles, E. L., Chadwick, D., Dinsdale, A., & Durham, S. (2019). What agricultural practices will most likely deliver “sustainable intensification” in the UK? *Food and Energy Security*, 8(1), e00148.

Dong, Y., Xu, F., Liu, L., Du, X., Ren, B., Guo, A., Geng, Y., Ruan, C., Ye, H., & Huang, W. (2020). Automatic system for crop pest and disease dynamic monitoring and early forecasting. *IEEE Journal of Selected Topics in Applied Earth Observations and Remote Sensing*, 13, 4410-4418.

Dong, Y., Xu, F., Liu, L., Du, X., Ye, H., Huang, W., & Zhu, Y. (2019). Monitoring and forecasting for disease and pest in crop based on WebGIS system. 2019 8th International Conference on Agro-Geoinformatics (Agro-Geoinformatics),

Duggal, V., Sukhwani, M., Bipin, K., Reddy, G. S., & Krishna, K. M. (2016, 16-21 May 2016). Plantation monitoring and yield estimation using autonomous quadcopter for precision agriculture. 2016 IEEE International Conference on Robotics and Automation (ICRA),

- Durand-Petiteville, A., Le Flecher, E., Cadenat, V., Sentenac, T., & Vougioukas, S. (2018). Tree Detection with Low-Cost Three-Dimensional Sensors for Autonomous Navigation in Orchards. *IEEE Robotics and Automation Letters*, 3(4), 3876-3883. <https://doi.org/10.1109/LRA.2018.2857005>
- El Jarroudi, M., Kouadio, A. L., Mackels, C., Tychon, B., Delfosse, P., & Bock, C. (2014). Disease severity assessment in epidemiological studies: accuracy and reliability of visual estimates of Septoria leaf blotch (SLB) in winter wheat. *Phytopathology*, 104(11), 37.
- Ellis, M., Ferree, D., & Spring, D. (1981). Photosynthesis, transpiration, and carbohydrate content of apple leaves infected by *Podosphaera leucotricha*. *Phytopathology*, 71(4), 392-395.
- Fahlgren, N., Gehan, M. A., & Baxter, I. (2015). Lights, camera, action: high-throughput plant phenotyping is ready for a close-up. *Current Opinion in Plant Biology*, 24, 93-99. <https://doi.org/https://doi.org/10.1016/j.pbi.2015.02.006>
- Fahrentrapp, J., Ria, F., Geilhausen, M., & Panassiti, B. (2019). Detection of Gray Mold Leaf Infections Prior to Visual Symptom Appearance Using a Five-Band Multispectral Sensor [Original Research]. *Frontiers in Plant Science*, 10. <https://doi.org/10.3389/fpls.2019.00628>
- Fang, Y., & Ramasamy, R. P. (2015). Current and Prospective Methods for Plant Disease Detection. *Biosensors*, 5(3), 537-561. <https://www.mdpi.com/2079-6374/5/3/537>
- Fawcett, D., Panigada, C., Tagliabue, G., Boschetti, M., Celesti, M., Evdokimov, A., Biriukova, K., Colombo, R., Miglietta, F., Rascher, U., & Anderson, K. (2020). Multi-Scale Evaluation of Drone-Based Multispectral Surface Reflectance and Vegetation Indices in Operational Conditions. *Remote sensing*, 12(3), 514. <https://www.mdpi.com/2072-4292/12/3/514>
- Fisher, M. C., Henk, D. A., Briggs, C. J., Brownstein, J. S., Madoff, L. C., McCraw, S. L., & Gurr, S. J. (2012). Emerging fungal threats to animal, plant and ecosystem health. *Nature*, 484(7393), 186-194. <https://doi.org/10.1038/nature10947>
- Food and Agriculture Organization of the United Nation (2024). FAOSTAT Crops and livestock products. Retrieved April 20, 2024 from <https://www.fao.org/faostat/en/#data/QCL>.
- Garcia-Ruiz, F., Sankaran, S., Maja, J. M., Lee, W. S., Rasmussen, J., & Ehsani, R. (2013). Comparison of two aerial imaging platforms for identification of Huanglongbing-infected citrus trees. *Computers and electronics in agriculture*, 91, 106-115. <https://doi.org/https://doi.org/10.1016/j.compag.2012.12.002>
- Garkava-Gustavsson, L., Zborowska, A., Sehic, J., Rur, M., Nybom, H., Englund, J. E., Lateur, M., Weg, W. E. v. d., & Holefors, A. (2013). Screening of apple cultivars for resistance to European canker, *Neonectria ditissima*. XIII Eucarpia Symposium on Fruit Breeding and Genetics, Warsaw, Poland,
- Garofalo, E. W., Clements, J. M., & Cooley, D. R. (2019). RIMpro and Apple Scab in New England: Accuracy and Grower Adoption. *FRUIT QUARTERLY*, 6(4).

Garrett, K. A., Nita, M., De Wolf, E. D., Esker, P. D., Gomez-Montano, L., & Sparks, A. H. (2021). Chapter 24 - Plant pathogens as indicators of climate change. In T. M. Letcher (Ed.), *Climate Change (Third Edition)* (pp. 499-513). Elsevier. <https://doi.org/https://doi.org/10.1016/B978-0-12-821575-3.00024-4>

Garthwaite, D., Barker, I., Laybourn, R., Huntly, A., Parrish, G., Hudson, S., Thygesen, H. and MacArthur, R. (2015) PESTICIDE USAGE SURVEY REPORT 265 ORCHARDS IN THE UNITED KINGDOM 2014

Garthwaite, D., Barker, I., Ridley, L., Mace, A., Parrish, G., MacArthur, R., and Lu, Y. (2018) PESTICIDE USAGE SURVEY REPORT 273 ORCHARDS IN THE UNITED KINGDOM 2016

Garthwaite, D., Hudson, S., Barker, I., Parrish, G., Smith, L. and Pietravalle, P. (2013) PESTICIDE USAGE SURVEY REPORT 252 ORCHARDS IN THE UNITED KINGDOM 2012

Gausman, H. W., & Allen, W. A. (1973). Optical Parameters of Leaves of 30 Plant Species 1. *Plant Physiology*, 52(1), 57-62. <https://doi.org/10.1104/pp.52.1.57>

Gautam, H. R., Bhardwaj, M. L., & Kumar, R. (2013). Climate change and its impact on plant diseases. *Current Science*, 105(12), 1685-1691. <http://www.jstor.org/stable/24099750>

Gessler, C., Patocchi, A., Sansavini, S., Tartarini, S., & Gianfranceschi, L. (2006). *Venturia inaequalis* Resistance in Apple. *Critical reviews in plant sciences*, 25(6), 473-503. <https://doi.org/10.1080/07352680601015975>

Gitelson, A., & Merzlyak, M. N. (1994). Spectral Reflectance Changes Associated with Autumn Senescence of *Aesculus hippocastanum* L. and *Acer platanoides* L. Leaves. Spectral Features and Relation to Chlorophyll Estimation. *Journal of Plant Physiology*, 143(3), 286-292. [https://doi.org/https://doi.org/10.1016/S0176-1617\(11\)81633-0](https://doi.org/https://doi.org/10.1016/S0176-1617(11)81633-0)

Gitelson, A. A., Gritz †, Y., & Merzlyak, M. N. (2003). Relationships between leaf chlorophyll content and spectral reflectance and algorithms for non-destructive chlorophyll assessment in higher plant leaves. *Journal of Plant Physiology*, 160(3), 271-282. <https://doi.org/https://doi.org/10.1078/0176-1617-00887>

Gogoi, N., Deka, B., & Bora, L. (2018). Remote sensing and its use in detection and monitoring plant diseases: A review. *Agricultural Reviews*, 39(4), 307-313.

Golhani, K., Balasundram, S. K., Vadamalai, G., & Pradhan, B. (2018). A review of neural networks in plant disease detection using hyperspectral data. *Information Processing in Agriculture*, 5(3), 354-371. <https://doi.org/https://doi.org/10.1016/j.inpa.2018.05.002>

Gomez-Candon, D., Labbé, S., Virlet, N., Jolivot, A., & Regnard, J.-L. (2014, 2014-05-21). High resolution thermal and multispectral UAV imagery for precision assessment of apple tree response to water stress. 2. International Conference on Robotics and associated High-technologies and Equipment for Agriculture and Forestry RHEA, Madrid, Spain

Gomiero, T. (2016). Soil Degradation, Land Scarcity and Food Security: Reviewing a Complex Challenge. *Sustainability*, 8(3), 281. <https://www.mdpi.com/2071-1050/8/3/281>

Gonçalves, J. P., Pinto, F. A. C., Queiroz, D. M., Villar, F. M. M., Barbedo, J. G. A., & Del Ponte, E. M. (2021). Deep learning architectures for semantic segmentation and automatic estimation of severity of foliar symptoms caused by diseases or pests. *Biosystems engineering*, 210, 129-142. <https://doi.org/https://doi.org/10.1016/j.biosystemseng.2021.08.011>

Gonzalez-Dugo, V., Zarco-Tejada, P. J., & Fereres, E. (2014). Applicability and limitations of using the crop water stress index as an indicator of water deficits in citrus orchards. *Agricultural and Forest Meteorology*, 198-199, 94-104. <https://doi.org/https://doi.org/10.1016/j.agrformet.2014.08.003>

Gorretta, N., Nouri, M., Herrero, A., Gowen, A., & Roger, J. M. (2019, 24-26 Sept. 2019). Early detection of the fungal disease "apple scab" using SWIR hyperspectral imaging. 2019 10th Workshop on Hyperspectral Imaging and Signal Processing: Evolution in Remote Sensing (WHISPERS),

Gowen, A. A., O'Donnell, C. P., Cullen, P. J., Downey, G., & Frias, J. M. (2007). Hyperspectral imaging – an emerging process analytical tool for food quality and safety control. *Trends in Food Science & Technology*, 18(12), 590-598. <https://doi.org/https://doi.org/10.1016/j.tifs.2007.06.001>

Granatstein, D., & Taylor, M. (2013). A cost comparison of organic and conventional apple production in the state of Washington. *Crop Management*. <https://doi.org/10.1094/CM-2013-0429-05-RS>

Grimstad, L., & From, P. J. (2017). The Thorvald II Agricultural Robotic System. *Robotics*, 6(4), 24. <https://www.mdpi.com/2218-6581/6/4/24>

Hamed, S. M., Okla, M. K., Al-Saadi, L. S., Hozzein, W. N., Mohamed, H. S., Selim, S., & AbdElgawad, H. (2022). Evaluation of the phycoremediation potential of microalgae for captan removal: Comprehensive analysis on toxicity, detoxification and antioxidants modulation. *Journal of Hazardous Materials*, 427, 128177. <https://doi.org/https://doi.org/10.1016/j.jhazmat.2021.128177>

Hasan, R. I., Yusuf, S. M., & Alzubaidi, L. (2020). Review of the state of the art of deep learning for plant diseases: A broad analysis and discussion. *Plants*, 9(10), 1302.

He, L., & Schupp, J. (2018). Sensing and Automation in Pruning of Apple Trees: A Review. *Agronomy*, 8(10), 211. <https://www.mdpi.com/2073-4395/8/10/211>

Heaven, T., Armitage, A. D., Xu, X., Goddard, M. R., & Cockerton, H. M. (2023). Dose-Dependent Genetic Resistance to Azole Fungicides Found in the Apple Scab Pathogen. *Journal of Fungi*, 9(12), 1136. <https://www.mdpi.com/2309-608X/9/12/1136>

Hines, C. J., Deddens, J. A., Jaycox, L. B., Andrews, R. N., Striley, C. A. F., & Alavanja, M. C. R. (2008). Captan Exposure and Evaluation of a Pesticide Exposure Algorithm among Orchard Pesticide Applicators in the Agricultural Health Study. *The Annals of Occupational Hygiene*, 52(3), 153-166. <https://doi.org/10.1093/annhyg/men001>

Holb, I. (2013). Apple powdery mildew caused by *Podosphaera leucotricha*: some aspects of biology. *International Journal of Horticultural Science*, 19(3-4), 19-23.

Holb, I., Abonyi, F., Buurma, J., & Heijne, B. (2017). On-farm and on-station evaluations of three orchard management approaches against apple scab and apple powdery mildew. *Crop Protection*, 97, 109-118.

Holb, I. J. (2007). Classification of apple cultivar reactions to scab in integrated and organic production systems. *Canadian Journal of Plant Pathology*, 29(3), 251-260. <https://doi.org/10.1080/07060660709507467>

Horler, D. N. H., Dockray, M., & Barber, J. (1983). The red edge of plant leaf reflectance. *International Journal of Remote Sensing*, 4(2), 273-288. <https://doi.org/10.1080/01431168308948546>

Huang, Y., Thomson, S. J., Lan, Y., & Maas, S. J. (2010). Multispectral imaging systems for airborne remote sensing to support agricultural production management. *International Journal of Agricultural and Biological Engineering*, 3(1), 50-62.

Hughes, D., & Salathé, M. (2015). An open access repository of images on plant health to enable the development of mobile disease diagnostics. arXiv preprint arXiv:1511.08060.

Iqbal, Z., Khan, M. A., Sharif, M., Shah, J. H., ur Rehman, M. H., & Javed, K. (2018). An automated detection and classification of citrus plant diseases using image processing techniques: A review. *Computers and electronics in agriculture*, 153, 12-32. <https://doi.org/https://doi.org/10.1016/j.compag.2018.07.032>

Ishimwe, R., Abutaleb, K., & Ahmed, F. (2014). Applications of thermal imaging in agriculture—A review. *Advances in remote Sensing*, 3(03), 128.

Jacobsen, B. J. (1997). ROLE OF PLANT PATHOLOGY IN INTEGRATED PEST MANAGEMENT. *Annual Review of Phytopathology*, 35(Volume 35, 1997), 373-391. <https://doi.org/https://doi.org/10.1146/annurev.phyto.35.1.373>

Jacquemoud, S., & Baret, F. (1990). PROSPECT: A model of leaf optical properties spectra. *Remote Sensing of Environment*, 34(2), 75-91. [https://doi.org/https://doi.org/10.1016/0034-4257\(90\)90100-Z](https://doi.org/https://doi.org/10.1016/0034-4257(90)90100-Z)

Jacquemoud, S., & Ustin, S. L. (2001). Leaf optical properties: A state of the art. 8th International Symposium of Physical Measurements & Signatures in Remote Sensing,

Jafari, M., Minaei, S., & Safaie, N. (2017). Detection of pre-symptomatic rose powdery-mildew and gray-mold diseases based on thermal vision. *Infrared Physics & Technology*, 85, 170-183.
<https://doi.org/https://doi.org/10.1016/j.infrared.2017.04.023>

Jarolmasjed, S., Sankaran, S., Kalcsits, L., & Khot, L. R. (2018). Proximal hyperspectral sensing of stomatal conductance to monitor the efficacy of exogenous abscisic acid applications in apple trees. *Crop Protection*, 109, 42-50.
<https://doi.org/https://doi.org/10.1016/j.cropro.2018.02.022>

Jarolmasjed, S., Sankaran, S., Marzougui, A., Kostick, S., Si, Y., Quirós Vargas, J. J., & Evans, K. (2019). High-Throughput Phenotyping of Fire Blight Disease Symptoms Using Sensing Techniques in Apple [Original Research]. *Frontiers in Plant Science*, 10.
<https://doi.org/10.3389/fpls.2019.00576>

Javaid, M., Haleem, A., Singh, R. P., & Suman, R. (2022). Enhancing smart farming through the applications of Agriculture 4.0 technologies. *International Journal of Intelligent Networks*, 3, 150-164.

Jensen, P. J., Makalowska, I., Altman, N., Fazio, G., Praul, C., Maximova, S. N., Crassweller, R. M., Travis, J. W., & McNellis, T. W. (2010). Rootstock-regulated gene expression patterns in apple tree scions. *Tree Genetics & Genomes*, 6(1), 57-72. <https://doi.org/10.1007/s11295-009-0228-7>

Jewan, S. Y. Y., Pagay, V., Billa, L., Tyerman, S. D., Gautam, D., Sparkes, D., Chai, H. H., & Singh, A. (2022). The feasibility of using a low-cost near-infrared, sensitive, consumer-grade digital camera mounted on a commercial UAV to assess Bambara groundnut yield. *International Journal of Remote Sensing*, 43(2), 393-423. <https://doi.org/10.1080/01431161.2021.1974116>

Jha, G., Thakur, K., & Thakur, P. (2009). The Venturia Apple Pathosystem: Pathogenicity Mechanisms and Plant Defense Responses. *BioMed Research International*, 2009(1), 680160.
<https://doi.org/https://doi.org/10.1155/2009/680160>

Ji, M., & Wu, Z. (2022). Automatic detection and severity analysis of grape black measles disease based on deep learning and fuzzy logic. *Computers and electronics in agriculture*, 193, 106718.
<https://doi.org/https://doi.org/10.1016/j.compag.2022.106718>

Jiang, P., Chen, Y., Liu, B., & Liang, C. (2019). Real-Time Detection of Apple Leaf Diseases Using Deep Learning Approach Based on Improved Convolutional Neural Networks. *IEEE Access*, 7, 59069-59080. <https://doi.org/10.1109/ACCESS.2019.2914929>

Jones, H., & Schofield, P. (2008). Thermal and other remote sensing of plant stress. *General and Applied Plant Physiology*, 34(1-2), 19-32.

Kamilaris, A., & Prenafeta-Boldú, F. X. (2018). Deep learning in agriculture: A survey. *Computers and electronics in agriculture*, 147, 70-90.

<https://doi.org/https://doi.org/10.1016/j.compag.2018.02.016>

Karunathilake, E., Le, A. T., Heo, S., Chung, Y. S., & Mansoor, S. (2023). The path to smart farming: Innovations and opportunities in precision agriculture. *Agriculture*, 13(8), 1593.

Kazmi, W., Foix, S., Alenyà, G., & Andersen, H. J. (2014). Indoor and outdoor depth imaging of leaves with time-of-flight and stereo vision sensors: Analysis and comparison. *ISPRS Journal of Photogrammetry and Remote Sensing*, 88, 128-146.

<https://doi.org/https://doi.org/10.1016/j.isprsjprs.2013.11.012>

Kersting, K., Bauckhage, C., Wahabzada, M., Mahlein, A.-K., Steiner, U., Oerke, E.-C., Römer, C., & Plümer, L. (2016). Feeding the World with Big Data: Uncovering Spectral Characteristics and Dynamics of Stressed Plants. In J. Lässig, K. Kersting, & K. Morik (Eds.), *Computational Sustainability* (pp. 99-120). Springer International Publishing. https://doi.org/10.1007/978-3-319-31858-5_6

Khaled, A. Y., Abd Aziz, S., Bejo, S. K., Nawi, N. M., Seman, I. A., & Onwude, D. I. (2018). Early detection of diseases in plant tissue using spectroscopy – applications and limitations. *Applied Spectroscopy Reviews*, 53(1), 36-64. <https://doi.org/10.1080/05704928.2017.1352510>

Khan, M. A., Zhao, Y., & Korban, S. S. (2012). Molecular mechanisms of pathogenesis and resistance to the bacterial pathogen *Erwinia amylovora*, causal agent of fire blight disease in Rosaceae. *Plant Molecular Biology Reporter*, 30, 247-260.

Khanal, S., Fulton, J., & Shearer, S. (2017). An overview of current and potential applications of thermal remote sensing in precision agriculture. *Computers and electronics in agriculture*, 139, 22-32. <https://doi.org/https://doi.org/10.1016/j.compag.2017.05.001>

Khattab, A., Habib, S. E., Ismail, H., Zayan, S., Fahmy, Y., & Khairy, M. M. (2019). An IoT-based cognitive monitoring system for early plant disease forecast. *Computers and electronics in agriculture*, 166, 105028.

Kirchgessner, N., Liebisch, F., Yu, K., Pfeifer, J., Friedli, M., Hund, A., & Walter, A. (2017). The ETH field phenotyping platform FIP: a cable-suspended multi-sensor system. *Functional Plant Biology*, 44(1), 154-168. <https://doi.org/https://doi.org/10.1071/FP16165>

Kirk, R., Cielniak, G., & Mangan, M. (2020). L*a*b*Fruits: A Rapid and Robust Outdoor Fruit Detection System Combining Bio-Inspired Features with One-Stage Deep Learning Networks. *Sensors*, 20(1), 275. <https://www.mdpi.com/1424-8220/20/1/275>

Kitić, G., Tagarakis, A., Cselyuszka, N., Panić, M., Birgermajer, S., Sakulski, D., & Matović, J. (2019). A new low-cost portable multispectral optical device for precise plant status assessment. *Computers and electronics in agriculture*, 162, 300-308.

<https://doi.org/https://doi.org/10.1016/j.compag.2019.04.021>

Kodors, S., Lacis, G., Sokolova, O., Zhukovs, V., Apeinans, I., & Bartulsons, T. (2021). Apple scab detection using CNN and Transfer Learning.

Köller, W., Wilcox, W., & Parker, D. (2005). Sensitivity of *Venturia inaequalis* populations to anilinopyrimidine fungicides and their contribution to scab management in New York. *Plant Disease*, 89(4), 357-365.

Konanz, S., Kocsányi, L., & Buschmann, C. (2014). Advanced Multi-Color Fluorescence Imaging System for Detection of Biotic and Abiotic Stresses in Leaves. *Agriculture*, 4(2), 79-95.
<https://www.mdpi.com/2077-0472/4/2/79>

Kumari, D., & John, S. (2020). Sorption Capacity of Pesticides on Soil in a Predominant Apple Cultivation Area. *Soil and Sediment Contamination: An International Journal*, 29(1), 107-119.
<https://doi.org/10.1080/15320383.2019.1684876>

Kuska, M., & Mahlein, A.-K. (2018). Aiming at decision making in plant disease protection and phenotyping by the use of optical sensors. *European Journal of Plant Pathology*, 152, 987-992.
Kyratzis, A. C., Skarlatos, D. P., Menexes, G. C., Vamvakousis, V. F., & Katsiotis, A. (2017).

Assessment of Vegetation Indices Derived by UAV Imagery for Durum Wheat Phenotyping under a Water Limited and Heat Stressed Mediterranean Environment [Original Research]. *Frontiers in Plant Science*, 8. <https://doi.org/10.3389/fpls.2017.01114>

Lanz, B., Dietz, S., & Swanson, T. (2018). The expansion of modern agriculture and global biodiversity decline: an integrated assessment. *Ecological Economics*, 144, 260-277.

Lebourgeois, V., Bégué, A., Labbé, S., Mallavan, B., Prévot, L., & Roux, B. (2008). Can Commercial Digital Cameras Be Used as Multispectral Sensors? A Crop Monitoring Test. *Sensors*, 8(11), 7300-7322. <https://www.mdpi.com/1424-8220/8/11/7300>

Lee, A.-y., Kim, S.-Y., Hong, S.-J., Han, Y.-h., Choi, Y., Kim, M., Yun, S. K., & Kim, G. (2019). Phenotypic Analysis of Fruit Crops Water Stress Using Infrared Thermal Imaging. *Journal of Biosystems Engineering*, 44(2), 87-94. <https://doi.org/10.1007/s42853-019-00020-2>

Lee, D.-H., Back, C.-G., Win, N. K. K., Choi, K.-H., Kim, K.-M., Kang, I.-K., Choi, C., Yoon, T.-M., Uhm, J. Y., & Jung, H.-Y. (2011). Biological Characterization of *Marssonina coronaria* Associated with Apple Blotch Disease. *Mycobiology*, 39(3), 200-205.
<https://doi.org/10.5941/MYCO.2011.39.3.200>

Li, L., Zhang, Q., & Huang, D. (2014). A Review of Imaging Techniques for Plant Phenotyping. *Sensors*, 14(11), 20078-20111. <https://www.mdpi.com/1424-8220/14/11/20078>

Li, L., Zhang, S., & Wang, B. (2021). Plant disease detection and classification by deep learning—a review. *IEEE Access*, 9, 56683-56698.

Li, W., Zhu, X., Yu, X., Li, M., Tang, X., Zhang, J., Xue, Y., Zhang, C., & Jiang, Y. (2022). Inversion of Nitrogen Concentration in Apple Canopy Based on UAV Hyperspectral Images. *Sensors*, 22(9), 3503. <https://www.mdpi.com/1424-8220/22/9/3503>

Li, X., & Li, S. (2022). Transformer Help CNN See Better: A Lightweight Hybrid Apple Disease Identification Model Based on Transformers. *Agriculture*, 12(6), 884. <https://www.mdpi.com/2077-0472/12/6/884>

Lin, Y. (2015). LiDAR: An important tool for next-generation phenotyping technology of high potential for plant phenomics? *Computers and electronics in agriculture*, 119, 61-73. <https://doi.org/https://doi.org/10.1016/j.compag.2015.10.011>

Lindell, C. A., Irish-Brown, A., Rothwell, N. L., & Wallis, A. E. (2023). Pest and disease risk and management in high-density perennial crops: Current knowledge and areas of future research. *Crop Protection*, 165, 106150.

Lindell, C. A., Irish-Brown, A., Rothwell, N. L., & Wallis, A. E. (2023). Pest and disease risk and management in high-density perennial crops: Current knowledge and areas of future research. *Crop Protection*, 165, 106150. <https://doi.org/https://doi.org/10.1016/j.cropro.2022.106150>

Lindenthal, M., Steiner, U., Dehne, H.-W., & Oerke, E.-C. (2005). Effect of Downy Mildew Development on Transpiration of Cucumber Leaves Visualized by Digital Infrared Thermography. *Phytopathology*, 95(3), 233-240. <https://doi.org/10.1094/phyto-95-0233>

Liu, B.-Y., Fan, K.-J., Su, W.-H., & Peng, Y. (2022). Two-Stage Convolutional Neural Networks for Diagnosing the Severity of Alternaria Leaf Blotch Disease of the Apple Tree. *Remote sensing*, 14(11), 2519. <https://www.mdpi.com/2072-4292/14/11/2519>

Liu, P., Choo, K.-K. R., Wang, L., & Huang, F. (2017). SVM or deep learning? A comparative study on remote sensing image classification. *Soft Computing*, 21(23), 7053-7065. <https://doi.org/10.1007/s00500-016-2247-2>

Liu, J., & Wang, X. Plant diseases and pests detection based on deep learning: a review. *Plant Methods* 17, 22 (2021). <https://doi.org/10.1186/s13007-021-00722-9>

Liu, Y., Zhang, Y., Jiang, D., Zhang, Z., & Chang, Q. (2023). Quantitative Assessment of Apple Mosaic Disease Severity Based on Hyperspectral Images and Chlorophyll Content. *Remote sensing*, 15(8), 2202. <https://www.mdpi.com/2072-4292/15/8/2202>

Lopez-Ruiz, N., Granados-Ortega, F., Carvajal, M. A., & Martinez-Olmos, A. (2017). Portable multispectral imaging system based on Raspberry Pi. *Sensor Review*, 37(3), 322-329. <https://doi.org/10.1108/SR-12-2016-0276>

Lozowicka, B., Hrynko, I., Kaczyński, P., Jankowska, M., & Rutkowska, E. (2016). Long-Term Investigation and Health Risk Assessment of Multi-class Fungicide Residues in Fruits. *Polish Journal of Environmental Studies*, 25. <https://doi.org/10.15244/pjoes/61111>

Mace, A., Ridley, L., E., Parrish, G., Barker, I., MacArthur, R., and Rainford, J. (2020) PESTICIDE USAGE SURVEY REPORT 286 ORCHARDS IN THE UNITED KINGDOM 2018

MacHardy, W. E. (1996). Apple Scab, Biology, Epidemiology, and Management. St Paul, Minn USA, APS.

MacHardy, W. E. (2000). Current status of IPM in apple orchards. *Crop Protection*, 19(8), 801-806. [https://doi.org/https://doi.org/10.1016/S0261-2194\(00\)00107-1](https://doi.org/https://doi.org/10.1016/S0261-2194(00)00107-1)

MacHardy, W. E., & Gadoury, D. M. (1989). A revision of Mills' s criteria for predicting apple scab infection periods. *Phytopathology*, 79(3), 304-310.

MacHardy, W. E., Gadoury, D. M., & Gessler, C. (2001). Parasitic and biological fitness of *Venturia inaequalis*: relationship to disease management strategies. *Plant Disease*, 85(10), 1036-1051.

Maduraimuthu, D., Prasad, P. V. V., Boyle, D., & Schapaugh, W. (2011). High-Temperature Stress and Soybean Leaves: Leaf Anatomy and Photosynthesis. *Crop Science*, 51, 2125–2131. <https://doi.org/10.2135/cropsci2010.10.0571>

Maghsoudi, H., & Minaei, S. (2014). A review of applicable methodologies for variable-rate spraying of orchards based on canopy characteristics. *Journal of Crop Protection*, 3(4), 531-542. <http://jcp.modares.ac.ir/article-3-5376-en.html>

Mahlein, A.-K. (2016). Plant disease detection by imaging sensors—parallels and specific demands for precision agriculture and plant phenotyping. *Plant Disease*, 100(2), 241-251.

Mahlein, A.-K., Kuska, M. T., Behmann, J., Polder, G., & Walter, A. (2018). Hyperspectral Sensors and Imaging Technologies in Phytopathology: State of the Art. *Annual Review of Phytopathology*, 56(Volume 56, 2018), 535-558. <https://doi.org/https://doi.org/10.1146/annurev-phyto-080417-050100>

Mahlein, A.-K., Oerke, E.-C., Steiner, U., & Dehne, H.-W. (2012). Recent advances in sensing plant diseases for precision crop protection. *European Journal of Plant Pathology*, 133, 197-209.

Mamaghani, B., & Salvaggio, C. (2019). Multispectral Sensor Calibration and Characterization for sUAS Remote Sensing. *Sensors*, 19(20), 4453. <https://www.mdpi.com/1424-8220/19/20/4453>

Manandhar, A., Zhu, H., Ozkan, E., & Shah, A. (2020). Techno-economic impacts of using a laser-guided variable-rate spraying system to retrofit conventional constant-rate sprayers. *Precision Agriculture*, 21, 1156-1171.

Martinelli, F., Scalenghe, R., Davino, S., Panno, S., Scuderi, G., Ruisi, P., Villa, P., Stroppiana, D., Boschetti, M., & Goulart, L. R. (2015). Advanced methods of plant disease detection. A review. *Agronomy for sustainable development*, 35, 1-25.

Martinez-Guanter, J., Ribeiro, Á., Peteinatos, G. G., Pérez-Ruiz, M., Gerhards, R., Bengochea-Guevara, J. M., Machleb, J., & Andújar, D. (2019). Low-Cost Three-Dimensional Modeling of Crop Plants. *Sensors*, 19(13), 2883. <https://www.mdpi.com/1424-8220/19/13/2883>

Martínez-Toledo, M. V., Salmerón, V., Rodelas, B., Pozo, C., & González-López, J. (1998). Effects of the fungicide Captan on some functional groups of soil microflora. *Applied Soil Ecology*, 7(3), 245-255. [https://doi.org/https://doi.org/10.1016/S0929-1393\(97\)00026-7](https://doi.org/https://doi.org/10.1016/S0929-1393(97)00026-7)

Mary, A. P., Robert, E. R., George, J. C. V., Maxwell, J. G., Ryan, H., Edward, L., & James, F. P. (2017). Laying the foundation to use Raspberry Pi 3 V2 camera module imagery for scientific and engineering purposes. *Journal of Electronic Imaging*, 26(1), 013014. <https://doi.org/10.1117/1.JEI.26.1.013014>

McDonald, D., & Glynn, C. (1994). Difficulties in measuring adoption of apple IPM: a case study. *Agriculture, Ecosystems and Environment (Netherlands)*, 48(3).

Mohanty, S. P., Hughes, D. P., & Salathé, M. (2016). Using Deep Learning for Image-Based Plant Disease Detection [Methods]. *Frontiers in Plant Science*, 7. <https://doi.org/10.3389/fpls.2016.01419>

Mohr, S., Meinecke, S., Feibicke, M., Duquesne, S., Frische, T., & Sahm, R. (2023). Effects of a realistic pesticide spraying sequence for apple crop on stream communities in mesocosms: negligible or notable? *Environmental Sciences Europe*, 35(1), 35. <https://doi.org/10.1186/s12302-023-00739-y>

Morales, A., Guerra, R., Horstrand, P., Diaz, M., Jimenez, A., Melian, J., Lopez, S., & Lopez, J. F. (2020). A Multispectral Camera Development: From the Prototype Assembly until Its Use in a UAV System. *Sensors*, 20(21), 6129. <https://www.mdpi.com/1424-8220/20/21/6129>

Mouron, P., Heijne, B., Naef, A., Strassemeyer, J., Hayer, F., Avilla, J., Alaphilippe, A., Höhn, H., Hernandez, J., Mack, G., Gaillard, G., Solé, J., Sauphanor, B., Patocchi, A., Samietz, J., Bravin, E., Lavigne, C., Bohanec, M., Golla, B., Bigler, F. (2012). Sustainability assessment of crop protection systems: SustainOS methodology and its application for apple orchards. *Agricultural systems*, 113, 1-15. <https://doi.org/https://doi.org/10.1016/j.agsy.2012.07.004>

Mulla, D. J. (2013). Twenty-five years of remote sensing in precision agriculture: Key advances and remaining knowledge gaps. *Biosystems engineering*, 114(4), 358-371.

Murray, J., Fennell, J. T., Blackburn, G. A., Whyatt, J. D., & Li, B. (2020). The novel use of proximal photogrammetry and terrestrial LiDAR to quantify the structural complexity of orchard trees. *Precision Agriculture*, 21(3), 473-483. <https://doi.org/10.1007/s11119-019-09676-4>

Nagy, A., Riczu, P., & Tamás, J. (2014). Spectral analysis of stress symptoms caused by apple powdery mildew (*Podosphaera leucotricha*). *Acta Agraria Debreceniensis* (55), 83-88.

- Nelson, M. R., Orum, T. V., Jaime-Garcia, R., & Nadeem, A. (1999). Applications of geographic information systems and geostatistics in plant disease epidemiology and management. *Plant Disease*, 83(4), 308-319.
- Newton, A., Begg, G., & Swanston, J. (2009). Deployment of diversity for enhanced crop function. *Annals of Applied Biology*, 154(3), 309-322.
- Nguyen, C., Sagan, V., Skobalski, J., & Severo, J. I. (2023). Early Detection of Wheat Yellow Rust Disease and Its Impact on Terminal Yield with Multi-Spectral UAV-Imagery. *Remote sensing*, 15(13), 3301. <https://www.mdpi.com/2072-4292/15/13/3301>
- Nouri, M., Gorretta, N., Vaysse, P., Giraud, M., Germain, C., Keresztes, B., & Roger, J.-M. (2018). Near infrared hyperspectral dataset of healthy and infected apple tree leaves images for the early detection of apple scab disease. *Data in Brief*, 16, 967-971. <https://doi.org/https://doi.org/10.1016/j.dib.2017.12.043>
- O'Connor, J., Smith, M. J., & James, M. R. (2017). Cameras and settings for aerial surveys in the geosciences: Optimising image data. *Progress in Physical Geography: Earth and Environment*, 41(3), 325-344. <https://doi.org/10.1177/0309133317703092>
- Oerke, E.-C. (2006). Crop losses to pests. *The Journal of agricultural science*, 144(1), 31-43.
- Oerke, E.-C. (2020). Remote Sensing of Diseases. *Annual Review of Phytopathology*, 58(Volume 58, 2020), 225-252. <https://doi.org/https://doi.org/10.1146/annurev-phyto-010820-012832>
- Oerke, E. C., Fröhling, P., & Steiner, U. (2011). Thermographic assessment of scab disease on apple leaves. *Precision Agriculture*, 12(5), 699-715. <https://doi.org/10.1007/s11119-010-9212-3>
- Oerke, E.-C., & Steiner, U. (2010). Potential of Digital Thermography Thermography for Disease Control. In E.-C. Oerke, R. Gerhards, G. Menz, & R. A. Sikora (Eds.), *Precision Crop Protection - the Challenge and Use of Heterogeneity* (pp. 167-182). Springer Netherlands. https://doi.org/10.1007/978-90-481-9277-9_11
- Oerke, E.-C., & Steiner, U. (2024). Hyperspectral imaging reveals small-scale water gradients in apple leaves due to minimal cuticle perforation by *Venturia inaequalis* conidiophores. *Journal of Experimental Botany*, 75(10), 3125-3140. <https://doi.org/10.1093/jxb/erae065>
- Oerke, E.-C., & Steiner, U. (2024). Hyperspectral imaging reveals small-scale water gradients in apple leaves due to minimal cuticle perforation by *Venturia inaequalis* conidiophores. *Journal of Experimental Botany*, 75(10), 3125-3140. <https://doi.org/10.1093/jxb/erae065>
- Oerke, E.-C., Steiner, U., Dehne, H.-W., & Lindenthal, M. (2006). Thermal imaging of cucumber leaves affected by downy mildew and environmental conditions. *Journal of Experimental Botany*, 57(9), 2121-2132. <https://doi.org/10.1093/jxb/erj170>

- Oh, C.-S., & Beer, S. V. (2005). Molecular genetics of *Erwinia amylovora* involved in the development of fire blight. *FEMS Microbiology Letters*, 253(2), 185-192. <https://doi.org/10.1016/j.femsle.2005.09.051>
- Olson, D., & Anderson, J. (2021). Review on unmanned aerial vehicles, remote sensors, imagery processing, and their applications in agriculture. *Agronomy Journal*, 113(2), 971-992. <https://doi.org/https://doi.org/10.1002/agj2.20595>
- Olsson, P.-O., Vivekar, A., Adler, K., Garcia Millan, V. E., Koc, A., Alamrani, M., & Eklundh, L. (2021). Radiometric Correction of Multispectral UAS Images: Evaluating the Accuracy of the Parrot Sequoia Camera and Sunshine Sensor. *Remote sensing*, 13(4), 577. <https://www.mdpi.com/2072-4292/13/4/577>
- Omasa, K., Hosoi, F., & Konishi, A. (2006). 3D lidar imaging for detecting and understanding plant responses and canopy structure. *Journal of Experimental Botany*, 58(4), 881-898. <https://doi.org/10.1093/jxb/erl142>
- Pallottino, F., Antonucci, F., Costa, C., Bisaglia, C., Figorilli, S., & Menesatti, P. (2019). Optoelectronic proximal sensing vehicle-mounted technologies in precision agriculture: A review. *Computers and electronics in agriculture*, 162, 859-873. <https://doi.org/https://doi.org/10.1016/j.compag.2019.05.034>
- Papp, D., Gao, L., Thapa, R., Olmstead, D., & Khan, A. (2020). Field apple scab susceptibility of a diverse *Malus* germplasm collection identifies potential sources of resistance for apple breeding. *CABI Agriculture and Bioscience*, 1(1), 16. <https://doi.org/10.1186/s43170-020-00017-4>
- Papp, D., Király, I., & Tóth, M. (2016). Suitability of old apple varieties in organic farming, based on their resistance against apple scab and powdery mildew. *Organic Agriculture*, 6, 183-189.
- Park, K., Hong, Y. k., Kim, G. h., & Lee, J. (2018). Classification of apple leaf conditions in hyper-spectral images for diagnosis of Marssonina blotch using mRMR and deep neural network. *Computers and electronics in agriculture*, 148, 179-187. <https://doi.org/https://doi.org/10.1016/j.compag.2018.02.025>
- Parsa, S., Morse, S., Bonifacio, A., Chancellor, T. C., Condori, B., Crespo-Pérez, V., Hobbs, S. L., Kroschel, J., Ba, M. N., & Rebaudo, F. (2014). Obstacles to integrated pest management adoption in developing countries. *Proceedings of the National Academy of Sciences*, 111(10), 3889-3894.
- Patocchi, A., Wehrli, A., Dubuis, P.-H., Auwerkerken, A., Leida, C., Cipriani, G., Passey, T., Staples, M., Didelot, F., & Philion, V. (2020). Ten years of VINQUEST: first insight for breeding new apple cultivars with durable apple scab resistance. *Plant Disease*, 104(8), 2074-2081.
- Paulus, S. (2019). Measuring crops in 3D: using geometry for plant phenotyping. *Plant Methods*, 15(1), 103. <https://doi.org/10.1186/s13007-019-0490-0>

Paulus, S., Behmann, J., Mahlein, A.-K., Plümer, L., & Kuhlmann, H. (2014). Low-Cost 3D Systems: Suitable Tools for Plant Phenotyping. *Sensors*, 14(2), 3001-3018. <https://www.mdpi.com/1424-8220/14/2/3001>

Peil, A., Bus, V. G., Geider, K., Richter, K., Flachowsky, H., & Hanke, M.-V. (2009). Improvement of fire blight resistance in apple and pear. *Int J Plant Breed*, 3(1), 1-27.

Penvern, S., Simon, S., Bellon, S., Alaphilippe, A., Lateur, M., Lauri, P.-E., Dapena, E., Jamar, L., Hemptinne, J.-L., & Warlop, F. (2012, 2012-07-01). Sustainable orchards' redesign: at the crossroads of multiple approaches 10th European IFSA Symposium, Aarhus, Denmark Aarhus (denmark). <https://hal.science/hal-01268467>

Pethybridge, S. J., & Nelson, S. C. (2015). Leaf Doctor: A New Portable Application for Quantifying Plant Disease Severity. *Plant Disease*, 99(10), 1310-1316. <https://doi.org/10.1094/pdis-03-15-0319-re>

Petkovsek, M. M., Stampar, F., & Veberic, R. (2007). Parameters of inner quality of the apple scab resistant and susceptible apple cultivars (*Malus domestica* Borkh.). *Scientia horticulturae*, 114(1), 37-44. <https://doi.org/https://doi.org/10.1016/j.scienta.2007.05.004>

Phillips, A., Crous, P., & Alves, A. (2007). *Diplodia seriata*, the anamorph of "Botryosphaeria" obtusa. *Fungal Diversity* 25 (2007), 25.

Piechowicz, B., Sieńko, J., Mytych, J., Grodzicki, P., Podbielska, M., Szpyrka, E., Zaręba, L., Piechowicz, I., & Sadło, S. (2021). Assessment of risk to honeybees and honey consumers resulting from the insect exposure to captan, thiacloprid, penthiopyrad, and λ -cyhalothrin used in a commercial apple orchard. *Environmental Monitoring and Assessment*, 193(3), 129. <https://doi.org/10.1007/s10661-021-08913-6>

Pierce, F. J., & Nowak, P. (1999). Aspects of precision agriculture. *Advances in agronomy*, 67, 1-85.

Pineda, M., Barón, M., & Pérez-Bueno, M.-L. (2021). Thermal Imaging for Plant Stress Detection and Phenotyping. *Remote sensing*, 13(1), 68. <https://www.mdpi.com/2072-4292/13/1/68>

Popp, J., Petó, K., & Nagy, J. (2013). Pesticide productivity and food security. A review. *Agronomy for sustainable development*, 33, 243-255.

Pourazar, H., Samadzadegan, F., & Dadrass Javan, F. (2019). Aerial multispectral imagery for plant disease detection: radiometric calibration necessity assessment. *European Journal of Remote Sensing*, 52(sup3), 17-31. <https://doi.org/10.1080/22797254.2019.1642143>

Prabhakar, M., Prasad, Y. G., & Rao, M. N. (2012). Remote Sensing of Biotic Stress in Crop Plants and Its Applications for Pest Management. In B. Venkateswarlu, A. K. Shanker, C. Shanker, & M. Maheswari (Eds.), *Crop Stress and its Management: Perspectives and Strategies* (pp. 517-545). Springer Netherlands. https://doi.org/10.1007/978-94-007-2220-0_16

Prakash, R. M., Saraswathy, G. P., Ramalakshmi, G., Mangaleswari, K. H., & Kaviya, T. (2017, 17-18 March 2017). Detection of leaf diseases and classification using digital image processing. 2017

International Conference on Innovations in Information, Embedded and Communication Systems (ICIIECS),

Pretty, J., & Bharucha, Z. P. (2014). Sustainable intensification in agricultural systems. *Annals of botany*, 114(8), 1571-1596.

Pretty, J. N. (1995). Participatory learning for sustainable agriculture. *World Development*, 23(8), 1247-1263. [https://doi.org/https://doi.org/10.1016/0305-750X\(95\)00046-F](https://doi.org/https://doi.org/10.1016/0305-750X(95)00046-F)

Pretty, J. N. (1997). The sustainable intensification of agriculture. *Natural resources forum*,

Ray, M., Ray, A., Dash, S., Mishra, A., Achary, K. G., Nayak, S., & Singh, S. (2017). Fungal disease detection in plants: Traditional assays, novel diagnostic techniques and biosensors. *Biosensors and Bioelectronics*, 87, 708-723.

Reig, G., Lordan, J., Sazo, M. M., Hoying, S., Fargione, M., Reginato, G., Donahue, D. J., Francescato, P., Fazio, G., & Robinson, T. (2019). Long-term performance of 'Gala', Fuji' and 'Honeycrisp' apple trees grafted on Geneva® rootstocks and trained to four production systems under New York State climatic conditions. *Scientia horticulturae*, 244, 277-293.

Rexhepi, E., Paçe, H., Vrapı, H., Hasani, A., & Kokthi, E. (2018). Scab infection management on apple leaves in western Balkans.

Ridley, L., Mace, A., Stroda, E., Parrish, G., Rainford, J., MacArthur, R. and Garthwaite, D., (2022) PESTICIDE USAGE SURVEY REPORT 297 ORCHARDS IN THE UNITED KINGDOM 2020

Ridley, L., Parrish, G., Chantry, T., Richmond, A., MacArthur, R. and Garthwaite, D., (2024) PESTICIDE USAGE SURVEY REPORT 311 ORCHARDS IN THE UNITED KINGDOM 2022

Ristaino, J. B., Anderson, P. K., Bebbler, D. P., Brauman, K. A., Cunniffe, N. J., Fedoroff, N. V., Finegold, C., Garrett, K. A., Gilligan, C. A., & Jones, C. M. (2021). The persistent threat of emerging plant disease pandemics to global food security. *Proceedings of the National Academy of Sciences*, 118(23), e2022239118.

Roberts, D. P., Short Jr, N. M., Sill, J., Lakshman, D. K., Hu, X., & Buser, M. (2021). Precision agriculture and geospatial techniques for sustainable disease control. *Indian Phytopathology*, 74(2), 287-305.

Rosa, L., Chiarelli, D. D., Rulli, M. C., Dell'Angelo, J., & D'Odorico, P. (2020). Global agricultural economic water scarcity. *Science Advances*, 6(18), eaaz6031. <https://doi.org/doi:10.1126/sciadv.aaz6031>

Rose, D. C., & Chilvers, J. (2018). Agriculture 4.0: Broadening responsible innovation in an era of smart farming. *Frontiers in Sustainable Food Systems*, 2, 87.

Rosell Polo, J. R., Sanz, R., Llorens, J., Arnó, J., Escolà, A., Ribes-Dasi, M., Masip, J., Camp, F., Gràcia, F., Solanelles, F., Pallejà, T., Val, L., Planas, S., Gil, E., & Palacín, J. (2009). A tractor-mounted scanning LIDAR for the non-destructive measurement of vegetative volume and surface area of tree-row plantations: A comparison with conventional destructive measurements. *Biosystems engineering*, 102(2), 128-134.

<https://doi.org/https://doi.org/10.1016/j.biosystemseng.2008.10.009>

Rougerie-Durocher, S., Philion, V., & Szalatnay, D. (2020). Measuring and modelling of apple flower stigma temperature as a step towards improved fire blight prediction. *Agricultural and Forest Meteorology*, 295, 108171.

<https://doi.org/https://doi.org/10.1016/j.agrformet.2020.108171>

Sadeghipoor, Z., Lu, Y. M., & Süsstrunk, S. (2013, 26-31 May 2013). A novel compressive sensing approach to simultaneously acquire color and near-infrared images on a single sensor. 2013 IEEE International Conference on Acoustics, Speech and Signal Processing,

Saleem, M. H., Potgieter, J., & Arif, K. M. (2019). Plant disease detection and classification by deep learning. *Plants*, 8(11), 468.

Sandler, M., Howard, A., Zhu, M., Zhmoginov, A., & Chen, L.-C. (2018). Mobilenetv2: Inverted residuals and linear bottlenecks. *Proceedings of the IEEE conference on computer vision and pattern recognition*, Sankaran, S., Khot, L. R., Espinoza, C. Z., Jarolmasjed, S., Sathuvalli, V. R., Vandemark, G. J., Miklas, P. N., Carter, A. H., Pumphrey, M. O., Knowles, N. R., & Pavek, M. J. (2015). Low-altitude, high-resolution aerial imaging systems for row and field crop phenotyping: A review. *European Journal of Agronomy*, 70, 112-123.

<https://doi.org/https://doi.org/10.1016/j.eja.2015.07.004>

Sankaran, S., Maja, J. M., Buchanon, S., & Ehsani, R. (2013). Huanglongbing (Citrus Greening) Detection Using Visible, Near Infrared and Thermal Imaging Techniques. *Sensors*, 13(2), 2117-2130. <https://www.mdpi.com/1424-8220/13/2/2117>

Sankaran, S., Mishra, A., Ehsani, R., & Davis, C. (2010). A review of advanced techniques for detecting plant diseases. *Computers and electronics in agriculture*, 72(1), 1-13.

Schoofs, H., Delalieux, S., Deckers, T., & Bylemans, D. (2020). Fire Blight Monitoring in Pear Orchards by Unmanned Airborne Vehicles (UAV) Systems Carrying Spectral Sensors. *Agronomy*, 10(5), 615. <https://www.mdpi.com/2073-4395/10/5/615>

Sedlar, A. D., Bugarin, R. M., Nuyttens, D., Turan, J. J., Zoranovic, M. S., Ponjican, O. O., & Janic, T. V. (2013). Quality and efficiency of apple orchard protection affected by sprayer type and application rate. *Spanish Journal of Agricultural Research*, 11(4), 935-944.

<https://doi.org/10.5424/sjar/2013114-3746>

Shadrin, D., Pukalchik, M., Uryasheva, A., Tsykunov, E., Yashin, G., Rodichenko, N., & Tsetserukou, D. (2020). Hyper-spectral NIR and MIR data and optimal wavebands for detection of apple tree diseases. arXiv preprint arXiv:2004.02325.

Shafiekhani, A., Kadam, S., Fritschi, F. B., & DeSouza, G. N. (2017). Vinobot and Vinoculer: Two Robotic Platforms for High-Throughput Field Phenotyping. *Sensors*, 17(1), 214. <https://www.mdpi.com/1424-8220/17/1/214>

Shakoor, N., Lee, S., & Mockler, T. C. (2017). High throughput phenotyping to accelerate crop breeding and monitoring of diseases in the field. *Current Opinion in Plant Biology*, 38, 184-192. <https://doi.org/https://doi.org/10.1016/j.pbi.2017.05.006>

Sharma, A., Kumar, V., Shahzad, B., Tanveer, M., Sidhu, G. P. S., Handa, N., Kohli, S. K., Yadav, P., Bali, A. S., & Parihar, R. D. (2019). Worldwide pesticide usage and its impacts on ecosystem. *SN Applied Sciences*, 1, 1-16.

Shruthi, U., Nagaveni, V., & Raghavendra, B. K. (2019, 15-16 March 2019). A Review on Machine Learning Classification Techniques for Plant Disease Detection. 2019 5th International Conference on Advanced Computing & Communication Systems (ICACCS),

Shuaibu, M., Lee, W. S., Schueller, J., Gader, P., Hong, Y. K., & Kim, S. (2018). Unsupervised hyperspectral band selection for apple Marssonina blotch detection. *Computers and electronics in agriculture*, 148, 45-53. <https://doi.org/https://doi.org/10.1016/j.compag.2017.09.038>

Simko, I., Hayes, R. J., & Furbank, R. T. (2016). Non-destructive Phenotyping of Lettuce Plants in Early Stages of Development with Optical Sensors [Original Research]. *Frontiers in Plant Science*, 7. <https://doi.org/10.3389/fpls.2016.01985>

Simon, S., Brun, L., Guinaudeau, J., & Sauphanor, B. (2011). Pesticide use in current and innovative apple orchard systems. *Agronomy for sustainable development*, 31(3), 541-555.

Singh, S., & Gupta, S. (2016). Digital Image Processing Techniques for Early Detection and Classification of different Diseased Plants. *International Journal of Bio-Science and Bio-Technology*, 8, 61-66. <https://doi.org/10.14257/ijbsbt.2016.8.4.07>

Sishodia, R. P., Ray, R. L., & Singh, S. K. (2020). Applications of remote sensing in precision agriculture: A review. *Remote sensing*, 12(19), 3136.

Skoneczny, H., Kubiak, K., Spiralski, M., Kotlarz, J., Mikiciński, A., & Puławska, J. (2020). Fire Blight Disease Detection for Apple Trees: Hyperspectral Analysis of Healthy, Infected and Dry Leaves. *Remote sensing*, 12(13), 2101. <https://www.mdpi.com/2072-4292/12/13/2101>

Slaton, M. R., Raymond Hunt Jr, E., & Smith, W. K. (2001). Estimating near-infrared leaf reflectance from leaf structural characteristics. *American Journal of Botany*, 88(2), 278-284. <https://doi.org/https://doi.org/10.2307/2657019>

Stafford, J. V. (2000). Implementing precision agriculture in the 21st century. *Journal of agricultural engineering research*, 76(3), 267-275.

Steinberger, E. M., & Beer, S. V. (1988). Creation and complementation of pathogenicity mutants of *Erwinia amylovora*. *Mol. Plant-Microbe Interact*, 1, 135-144.

- Stensvand, A., Gadoury, D. M., Amundsen, T., Semb, L., & Seem, R. C. (1997). Ascospore Release and Infection of Apple Leaves by Conidia and Ascospores of *Venturia inaequalis* at Low Temperatures. *Phytopathology*, 87(10), 1046-1053.
<https://doi.org/10.1094/phyto.1997.87.10.1046>
- Stöcker, C., Bennett, R., Nex, F., Gerke, M., & Zevenbergen, J. (2017). Review of the Current State of UAV Regulations. *Remote sensing*, 9(5), 459. <https://www.mdpi.com/2072-4292/9/5/459>
- Storey, G., Meng, Q., & Li, B. (2022). Leaf Disease Segmentation and Detection in Apple Orchards for Precise Smart Spraying in Sustainable Agriculture. *Sustainability*, 14(3), 1458.
<https://www.mdpi.com/2071-1050/14/3/1458>
- Strange, R. N., & Scott, P. R. (2005). Plant disease: a threat to global food security. *Annu. Rev. Phytopathol.*, 43, 83-116.
- Strickland, D., Carroll, J., & Cox, K. (2020) Apple Powdery Mildew. Retrieved February 5 2021, from <https://ecommons.cornell.edu/items/1df0e373-84e1-4001-a75d-1ca2573359ee>
- Strickland, D. A., Hodge, K. T., & Cox, K. D. (2021). An Examination of Apple Powdery Mildew and the Biology of *Podosphaera leucotricha* from Past to Present. *Plant Health Progress*, 22(4), 421-432. <https://doi.org/10.1094/php-03-21-0064-rv>
- Szegedy, C., Ioffe, S., Vanhoucke, V., & Alemi, A. (2017). Inception-v4, Inception-ResNet and the Impact of Residual Connections on Learning. *Proceedings of the AAAI Conference on Artificial Intelligence*, 31(1). <https://doi.org/10.1609/aaai.v31i1.11231>
- Szkolnik, M. (1978). Techniques involved in greenhouse evaluation of deciduous tree fruit fungicides. *Annual Review of Phytopathology*, 16(1), 103-129.
- Tan, M., & Le, Q. (2021). Efficientnetv2: Smaller models and faster training. *International conference on machine learning*,
- Taye, M. M. (2023). Theoretical Understanding of Convolutional Neural Network: Concepts, Architectures, Applications, Future Directions. *Computation*, 11(3), 52.
<https://www.mdpi.com/2079-3197/11/3/52>
- Taylor, L., & Nitschke, G. (2018, 18-21 Nov. 2018). Improving Deep Learning with Generic Data Augmentation. *2018 IEEE Symposium Series on Computational Intelligence (SSCI)*,
- Thapa, R., Zhang, K., Snavely, N., Belongie, S., & Khan, A. (2020). The Plant Pathology Challenge 2020 data set to classify foliar disease of apples. *Applications in plant sciences*, 8(9), e11390.
- Thapa, R., Zhang, K., Snavely, N., Belongie, S., & Khan, A. (2021). Plant Pathology 2021 - FGVC8 . Kaggle. <https://kaggle.com/competitions/plant-pathology-2021-fgvc8>

Thompson, A. L., Thorp, K. R., Conley, M., Andrade-Sanchez, P., Heun, J. T., Dyer, J. M., & White, J. W. (2018). Deploying a Proximal Sensing Cart to Identify Drought-Adaptive Traits in Upland Cotton for High-Throughput Phenotyping [Methods]. *Frontiers in Plant Science*, 9. <https://doi.org/10.3389/fpls.2018.00507>

Toda, Y., & Okura, F. (2019). How Convolutional Neural Networks Diagnose Plant Disease. *Plant Phenomics*, 2019. <https://doi.org/doi:10.34133/2019/9237136>

Tovar, J. C., Hoyer, J. S., Lin, A., Tielking, A., Callen, S. T., Elizabeth Castillo, S., Miller, M., Tessman, M., Fahlgren, N., Carrington, J. C., Nusinow, D. A., & Gehan, M. A. (2018). Raspberry Pi-powered imaging for plant phenotyping. *Applications in plant sciences*, 6(3), e1031. <https://doi.org/https://doi.org/10.1002/aps3.1031>

Tudi, M., Daniel Ruan, H., Wang, L., Lyu, J., Sadler, R., Connell, D., Chu, C., & Phung, D. T. (2021). Agriculture Development, Pesticide Application and Its Impact on the Environment. *International journal of environmental research and public health*, 18(3), 1112. <https://www.mdpi.com/1660-4601/18/3/1112>

Turkoglu, M., Hanbay, D., & Sengur, A. (2022). Multi-model LSTM-based convolutional neural networks for detection of apple diseases and pests. *Journal of Ambient Intelligence and Humanized Computing*, 13(7), 3335-3345. <https://doi.org/10.1007/s12652-019-01591-w>

Urbanietz, A., & Dunemann, F. (2005). Isolation, identification and molecular characterization of physiological races of apple powdery mildew (*Podosphaera leucotricha*). *Plant Pathology*, 54(2), 125-133. <https://doi.org/https://doi.org/10.1111/j.1365-3059.2005.01156.x>

Ustin, S. L., & Jacquemoud, S. (2020). How the optical properties of leaves modify the absorption and scattering of energy and enhance leaf functionality. *Remote sensing of plant biodiversity*, 349-384.

Vagelas, I., Papadimos, A., & Lykas, C. (2021). Pre-Symptomatic Disease Detection in the Vine, Chrysanthemum, and Rose Leaves with a Low-Cost Infrared Sensor. *Agronomy*, 11(9), 1682. <https://www.mdpi.com/2073-4395/11/9/1682>

Vagelas, I., Papadimos, A., & Lykas, C. (2021). Pre-Symptomatic Disease Detection in the Vine, Chrysanthemum, and Rose Leaves with a Low-Cost Infrared Sensor. *Agronomy*, 11(9), 1682. <https://www.mdpi.com/2073-4395/11/9/1682>

Valle, B., Simonneau, T., Boulord, R., Sourd, F., Frisson, T., Ryckewaert, M., Hamard, P., Briche, N., Dautat, M., & Christophe, A. (2017). PYM: a new, affordable, image-based method using a Raspberry Pi to phenotype plant leaf area in a wide diversity of environments. *Plant Methods*, 13(1), 98. <https://doi.org/10.1186/s13007-017-0248-5>

Verhoeven, G. (2008). Imaging the invisible using modified digital still cameras for straightforward and low-cost archaeological near-infrared photography. *Journal of Archaeological Science*, 35(12), 3087-3100. <https://doi.org/https://doi.org/10.1016/j.jas.2008.06.012>

- Vescovo, L., Wohlfahrt, G., Balzarolo, M., Pilloni, S., Sottocornola, M., Rodeghiero, M., & Gianelle, D. (2012). New spectral vegetation indices based on the near-infrared shoulder wavelengths for remote detection of grassland phytomass. *International Journal of Remote Sensing*, 33(7), 2178-2195. <https://doi.org/10.1080/01431161.2011.607195>
- Virlet, N., Costes, E., Martinez, S., Kelner, J.-J., & Regnard, J.-L. (2015). Multispectral airborne imagery in the field reveals genetic determinisms of morphological and transpiration traits of an apple tree hybrid population in response to water deficit. *Journal of Experimental Botany*, 66(18), 5453-5465. <https://doi.org/10.1093/jxb/erv355>
- Virlet, N., Sabermanesh, K., Sadeghi-Tehran, P., & Hawkesford, M. J. (2016). Field Scanalyzer: An automated robotic field phenotyping platform for detailed crop monitoring. *Functional Plant Biology*, 44(1), 143-153.
- Vishnoi, V. K., Kumar, K., Kumar, B., Mohan, S., & Khan, A. A. (2023). Detection of Apple Plant Diseases Using Leaf Images Through Convolutional Neural Network. *IEEE Access*, 11, 6594-6609. <https://doi.org/10.1109/ACCESS.2022.3232917>
- Vit, A., & Shani, G. (2018). Comparing RGB-D Sensors for Close Range Outdoor Agricultural Phenotyping. *Sensors*, 18(12), 4413. <https://www.mdpi.com/1424-8220/18/12/4413>
- Wallis, A., Carroll, J., & Cox, K. (2020) Fire Blight. Retrieved February 5 2021, from <https://ecommons.cornell.edu/items/079c9763-8cd8-4028-a779-e9c32aeaf584>
- Wang, G., Sun, Y., & Wang, J. (2017). Automatic Image-Based Plant Disease Severity Estimation Using Deep Learning. *Computational Intelligence and Neuroscience*, 2017(1), 2917536. <https://doi.org/https://doi.org/10.1155/2017/2917536>
- Wang, P., Niu, T., Mao, Y., Zhang, Z., Liu, B., & He, D. (2021). Identification of Apple Leaf Diseases by Improved Deep Convolutional Neural Networks with an Attention Mechanism [Original Research]. *Frontiers in Plant Science*, 12. <https://doi.org/10.3389/fpls.2021.723294>
- Weber, R. (2014). Biology and control of the apple canker fungus *Neonectria ditissima* (syn. *N. galligena*) from a Northwestern European perspective. *Erwerbs-Obstbau*, 56(3), 95-107.
- Weber, R. W. S. (2014). Biology and control of the apple canker fungus *Neonectria ditissima* (syn. *N. galligena*) from a Northwestern European perspective. *Erwerbs-Obstbau*, 56(3), 95-107. <https://doi.org/10.1007/s10341-014-0210-x>
- Weber, R. W. S., & Børve, J. (2021). Infection biology as the basis of integrated control of apple canker (*Neonectria ditissima*) in Northern Europe. *CABI Agriculture and Bioscience*, 2(1), 5. <https://doi.org/10.1186/s43170-021-00024-z>
- Wei, Y., Xia, W., Huang, J., Ni, B., Dong, J., Zhao, Y., & Yan, S. (2014). CNN: Single-label to multi-label. arXiv preprint arXiv:1406.5726.

- Whalon, M., & Croft, B. (1984). Apple IPM implementation in North America. *Annual review of entomology*, 29, 435-470.
- White, J. W., & Conley, M. M. (2013). A Flexible, Low-Cost Cart for Proximal Sensing. *Crop Science*, 53(4), 1646-1649. <https://doi.org/https://doi.org/10.2135/cropsci2013.01.0054>
- Wöhner, T., & Emeriewen, O. F. (2019). Apple blotch disease (*Marssonina coronaria* (Ellis & Davis) Davis) – review and research prospects. *European Journal of Plant Pathology*, 153(3), 657-669. <https://doi.org/10.1007/s10658-018-1590-9>
- Wolfert, S., Ge, L., Verdouw, C., & Bogaardt, M.-J. (2017). Big data in smart farming—a review. *Agricultural systems*, 153, 69-80.
- Woolley, J. T. (1971). Reflectance and Transmittance of Light by Leaves. *Plant Physiology*, 47(5), 656-662. <https://doi.org/10.1104/pp.47.5.656>
- Xu, H., Zhu, S., Ying, Y., & Jiang, H. (2006). Application of multispectral reflectance for early detection of tomato disease (Vol. 6381). *SPIE*. <https://doi.org/10.1117/12.685531>
- Xu, X., Yang, J., Thakur, V., Roberts, A., & Barbara, D. J. (2008). Population Variation of Apple Scab (*Venturia inaequalis*) Isolates from Asia and Europe. *Plant Disease*, 92(2), 247-252. <https://doi.org/10.1094/pdis-92-2-0247>
- Xu, X.-M., & Butt, D. (1995). Adem™ a PC-based multiple disease warning system for use in the cultivation of apples. *IV International Symposium on Computer Modelling in Fruit Research and Orchard Management* 416,
- Yadav, A., Thakur, U., Saxena, R., Pal, V., Bhateja, V., & Lin, J. C.-W. (2022). AFD-Net: Apple Foliar Disease multi classification using deep learning on plant pathology dataset. *Plant and Soil*, 477(1), 595-611. <https://doi.org/10.1007/s11104-022-05407-3>
- Yamashita, R., Nishio, M., Do, R. K. G., & Togashi, K. (2018). Convolutional neural networks: an overview and application in radiology. *Insights into Imaging*, 9(4), 611-629. <https://doi.org/10.1007/s13244-018-0639-9>
- Yang, K., Zhong, W., & Li, F. (2020). Leaf Segmentation and Classification with a Complicated Background Using Deep Learning. *Agronomy*, 10(11), 1721. <https://www.mdpi.com/2073-4395/10/11/1721>
- Ye, X., Abe, S., & Zhang, S. (2020). Estimation and mapping of nitrogen content in apple trees at leaf and canopy levels using hyperspectral imaging. *Precision Agriculture*, 21(1), 198-225. <https://doi.org/10.1007/s11119-019-09661-x>
- Yu, R., Luo, Y., Zhou, Q., Zhang, X., Wu, D., & Ren, L. (2021). Early detection of pine wilt disease using deep learning algorithms and UAV-based multispectral imagery. *Forest Ecology and Management*, 497, 119493. <https://doi.org/https://doi.org/10.1016/j.foreco.2021.119493>

- Zanin, A. R. A., Neves, D. C., Teodoro, L. P. R., da Silva Júnior, C. A., da Silva, S. P., Teodoro, P. E., & Baio, F. H. R. (2022). Reduction of pesticide application via real-time precision spraying. *Scientific Reports*, 12(1), 5638. <https://doi.org/10.1038/s41598-022-09607-w>
- Zare, M., Drastig, K., & Zude-Sasse, M. (2020). Tree Water Status in Apple Orchards Measured by Means of Land Surface Temperature and Vegetation Index (LST-NDVI) Trapezoidal Space Derived from Landsat 8 Satellite Images. *Sustainability*, 12(1), 70. <https://www.mdpi.com/2071-1050/12/1/70>
- Zeng, Q., Puławska, J., & Schachterle, J. (2021). Early events in fire blight infection and pathogenesis of *Erwinia amylovora*. *Journal of Plant Pathology*, 103(1), 13-24. <https://doi.org/10.1007/s42161-020-00675-3>
- Zhang, J., Huang, Y., Pu, R., Gonzalez-Moreno, P., Yuan, L., Wu, K., & Huang, W. (2019). Monitoring plant diseases and pests through remote sensing technology: A review. *Computers and electronics in agriculture*, 165, 104943. <https://doi.org/https://doi.org/10.1016/j.compag.2019.104943>
- Zhang, N., Wang, M., & Wang, N. (2002). Precision agriculture—a worldwide overview. *Computers and electronics in agriculture*, 36(2), 113-132. [https://doi.org/https://doi.org/10.1016/S0168-1699\(02\)00096-0](https://doi.org/https://doi.org/10.1016/S0168-1699(02)00096-0)
- Zhang, Z., Wang, X., Lai, Q., & Zhang, Z. (2018). Review of variable-rate sprayer applications based on real-time sensor technologies. *Automation in Agriculture—Securing Food Supplies for Future Generations*. Intech, 53-79.
- Zhang, Z., & Zhu, L. (2023). A Review on Unmanned Aerial Vehicle Remote Sensing: Platforms, Sensors, Data Processing Methods, and Applications. *Drones*, 7(6), 398. <https://www.mdpi.com/2504-446X/7/6/398>
- Zhong, Y., & Zhao, M. (2020). Research on deep learning in apple leaf disease recognition. *Computers and electronics in agriculture*, 168, 105146. <https://doi.org/https://doi.org/10.1016/j.compag.2019.105146>
- Zhu, Y., Yang, G., Yang, H., Wu, J., Lei, L., Zhao, F., Fan, L., & Zhao, C. (2020). Identification of Apple Orchard Planting Year Based on Spatiotemporally Fused Satellite Images and Clustering Analysis of Foliage Phenophase. *Remote sensing*, 12(7), 1199. <https://www.mdpi.com/2072-4292/12/7/1199>
- Zhuang, F., Qi, Z., Duan, K., Xi, D., Zhu, Y., Zhu, H., Xiong, H., & He, Q. (2021). A Comprehensive Survey on Transfer Learning. *Proceedings of the IEEE*, 109(1), 43-76. <https://doi.org/10.1109/JPROC.2020.3004555>

9 Appendices

9.1 Appendix A – Experimental Weather Conditions

The experiments conducted throughout this thesis were performed in a semi-controlled environment that was significantly influenced by external weather conditions. The following section provides information collected during the experimental process. Figure 9.1 displays the temperature recorded within the experimental glasshouse from February 2021 to January 2022. Figure 9.2 shows the humidity levels recorded within the experimental glasshouse over the same period. Tables 9.1 and 9.2 present the external weather conditions recorded on-site at the Hazelrigg Field Station during both rounds of time series acquisition in Experiment 1. Table 9.3 displays the weather conditions recorded on-site during the imaging trials of Experiment 2. Due to technical issues with the TinyTag Data Logger, internal glasshouse conditions were not recorded during 2023.

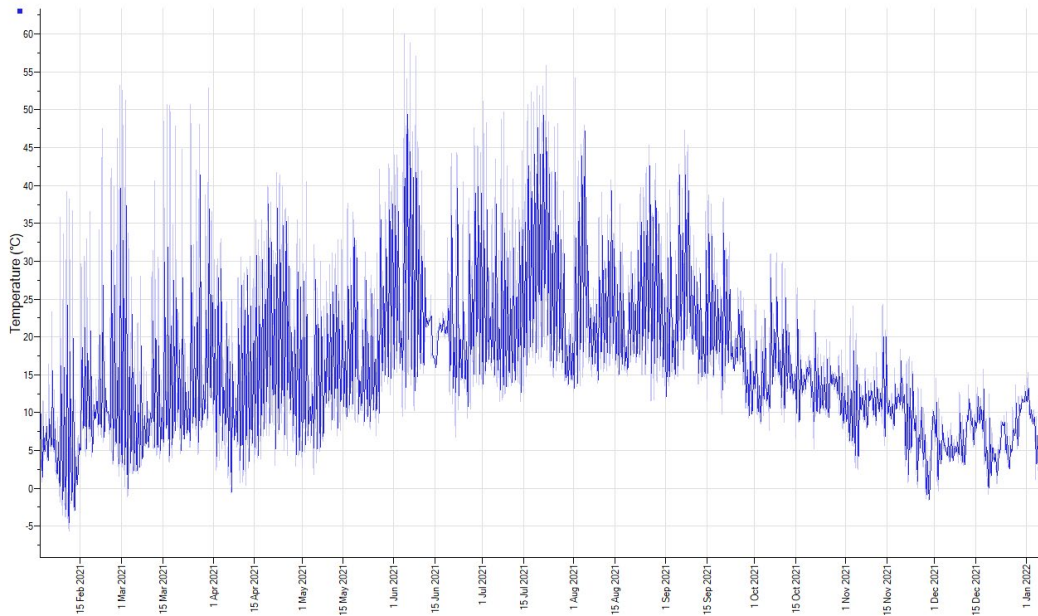


Figure 9.1 Temperature within the Experimental Dome (Feb 2021- Jan 2022) captured by TinyTag Data Logger (Gemini Data Loggers, Chichester, UK)

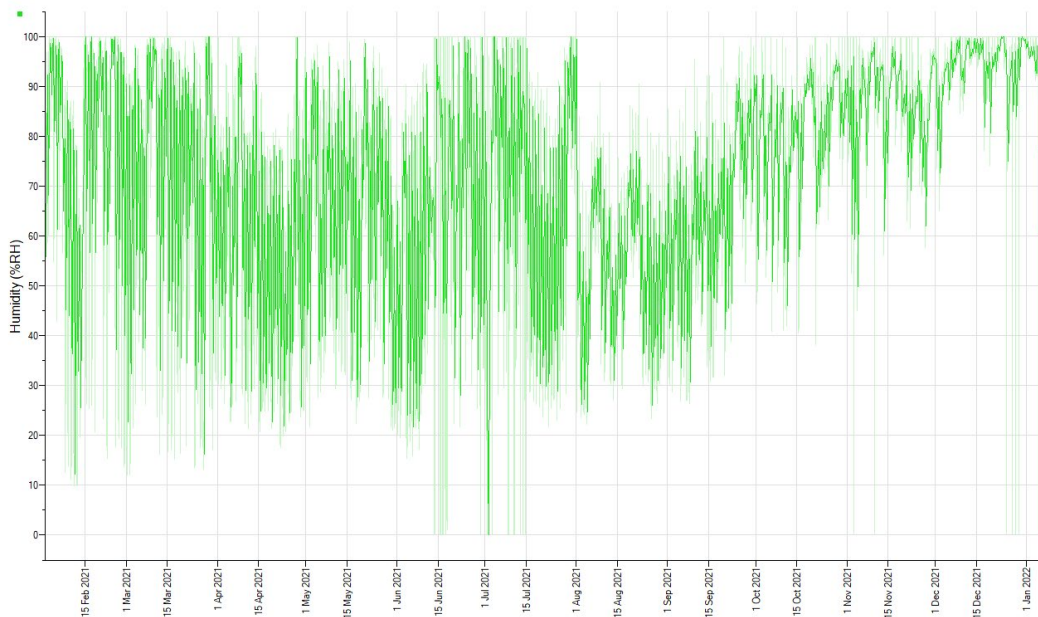


Figure 9.2 Humidity within the Experimental Dome (Feb 2021- Jan 2022) captured by TinyTag Data Logger (Gemini Data Loggers, Chichester, UK)

Date	Total cloud	Present weather	Dry bulb (°C)	Wet bulb (°C)	Max (°C)	Min (°C)	Rainfall (mm)	Sunshine (h)
12/08/21	7	02	15.0	13.7	18.7	13.1	0.0	5.1
13/08/21	4	01	15.9	13.3	18.4	13.2	0.0	10.9
14/08/21	7	02	15.7	14.9	16.6	14.5	4.3	1.5
15/08/21	8	02	16.2	14.6	17.3	12.9	0.0	0.9
16/08/21	8	60	13.9	12.3	16.8	13.0	1.7	4.6
17/08/21	8	53	14.5	14.4	17.4	13.4	1.2	2.3
18/08/21	8	51	13.9	13.8	15.2	13.1	3.7	0.0
19/08/21	7	02	15.2	14.4	17.3	13.2	0.3	0.0
20/08/21	7	02	17.3	16.0	20.0	14.0	1.5	0.0
21/08/21	8	03	16.5	16.0	19.0	15.9	7.8	0.0
22/08/21	7	50	15.8	15.8	19.5	14.8	0.0	5.2
23/08/21	3	03	18.4	15.5	21.8	13.7	0.0	8.4
24/08/21	7	03	16.0	14.4	20.6	11.4	0.0	6.5
25/08/21	3	02	17.3	15.4	19.5	10.8	0.0	10.2
26/08/21	2	02	16.9	14.5	19.4	13.9	0.0	12.2
27/08/21	6	02	13.3	11.4	18.5	7.7	0.0	7.7
28/08/21	1	01	15.8	12.1	18.5	7.9	0.0	11.4
29/08/21	2	03	15.5	13.4	17.7	10.1	0.0	6.9
30/08/21	8	02	14.0	12.0	17.9	12.2	0.0	1.9
31/08/21	7	02	12.9	10.7	16.7	11.4	0.0	0.3
01/09/21	8	02	13.2	12.3	18.6	9.6	0.0	5.3
02/09/21	7	02	14.5	12.4	20.0	10.1	0.0	7.8
03/09/21	8	02	13.1	11.8	15.1	11.2	0.0	0.0
04/09/21	8	02	14.2	12.4	17.7	12.3	0.0	0.3
05/09/21	2	01	17.7	14.9	22.1	12.8	0.1	8.9
06/09/21	8	01	17.3	16.2	20.5	14.8	0.0	2.9
07/09/21	0	02	20.5	18.2	26.2	12.2	0.0	10.9
08/09/21	3	02	23.5	18.4	27.3	18.7	0.0	10.6
09/09/21	8	02	18.5	17.2	21.4	16.2	3.6	0.7
10/09/21	8	02	17.2	17.1	21.3	15.0	0.0	1.5
11/09/21	7	02	17.1	15.9	17.8	15.8	0.0	1.9
12/09/21	8	02	13.4	12.0	16.5	11.6	0.0	0.0
13/09/21	8	15	13.2	11.6	15.1	11.8	0.2	0.0
14/09/21	7	60	14.0	13.0	18.9	13.1	0.0	5.1
15/09/21	1	02	14.9	13.4	18.7	8.6	3.4	10.0

Table 9.1 Weather conditions regarded at 10AM from Hazelrigg Field Station (UK Meteorological Office - Climatological Station Number 7236) during Experiment 1 – Round 1

Date	Total cloud	Present weather	Dry bulb (°C)	Wet bulb (°C)	Max (°C)	Min (°C)	Rainfall (mm)	Sunshine (h)
08/10/21	6	02	15.5	13.2	18.5	12.8	0.0	5.5
09/10/21	8	51	13.3	13.2	15.1	13.3	2.0	0.0
10/10/21	1	02	11.8	11.1	13.9	9.4	0.0	7.1
11/10/21	2	02	12.2	10.8	14.5	8.4	0.2	6.4
12/10/21	7	01	13.9	13.0	15.2	11.6	0.6	0.0
13/10/21	8	20	12.9	12.4	13.4	11.3	0.1	0.1
14/10/21	8	02	12.2	11.2	13.6	11.4	1.2	0.0
15/10/21	1	02	8.8	6.6	12.2	3.7	0.0	9.3
16/10/21	7	20	8.6	8.0	13.8	6.1	6.2	0.3
17/10/21	8	60	11.9	11.8	14.0	8.6	4.3	0.0
18/10/21	8	02	12.3	11.1	15.8	11.0	7.6	0.0
19/10/21	8	53	15.4	15.4	16.9	12.3	5.7	0.0
20/10/21	8	16	10.8	10.3	11.1	9.0	5.8	0.5
21/10/21	1	02	6.4	4.6	10.4	3.2	6.5	8.7
22/10/21	7	81	9.0	8.8	11.4	6.4	0.4	1.6
23/10/21	6	01	10.0	8.5	12.0	8.6	0.4	0.1
24/10/21	8	62	10.0	9.1	12.6	9.4	3.9	0.8
25/10/21	7	15	10.5	10.1	12.6	8.8	5.6	2.4
26/10/21	7	50	10.1	10.0	15.5	8.0	15.6	0.8
27/10/21	8	59	13.5	13.5	15.4	10.0	23.2	0.0
28/10/21	8	03	13.9	12.7	14.8	12.2	9.3	0.0
29/10/21	7	25	13.3	12.2	14.3	11.2	22.6	2.1
30/10/21	7	61	8.5	8.5	11.9	8.0	14.2	2.4
31/10/21	8	63	9.6	8.9	11.4	7.1	32.9	0.1
01/11/21	7	81	9.8	9.3	10.5	7.5	2.9	0.8
02/11/21	7	80	7.4	7.0	10.3	5.5	0.6	2.6
03/11/21	2	02	6.6	5.7	10.0	5.1	0.0	3.9
04/11/21	1	02	4.8	3.4	8.3	2.2	0.0	8.6
05/11/21	8	45	6.2	6.2	11.3	1.5	0.0	0.2
06/11/21	8	02	10.7	9.5	12.3	6.2	4.2	0.0
07/11/21	6	01	9.4	7.4	10.5	7.8	0.1	0.2
08/11/21	8	51	8.0	8.0	13.0	7.5	3.0	0.0
09/11/21	8	53	11.5	11.3	12.7	8.0	10.0	0.0
10/11/21	7	01	9.3	9.3	11.2	8.6	0.2	0.1
11/11/21	6	01	9.6	9.0	11.7	7.6	4.7	1.0

Table 9.2 Weather conditions regarded at 10AM from Hazelrigg Field Station (UK Meteorological Office - Climatological Station Number 7236) during Experiment 1 – Round 2

Date	Total cloud	Present weather	Dry bulb (°C)	Wet bulb (°C)	Max (°C)	Min (°C)	Rainfall (mm)	Sunshine (h)
23/08/23	8	02	16.0	14.0	18.7	14.1	5.2	1.8
24/08/23	7	01	15.4	14.6	17.4	14.8	1.7	8.4
25/08/23	6	15	14.7	13.3	16.7	11.8	10.3	5.4
26/08/23	7	02	13.8	12.5	17.6	10.1	0.1	3.1
27/08/23	8	02	14.2	13.2	15.6	10.5	0.0	0.2
28/08/23	6	15	14.4	11.9	16.1	12.0	1.5	2.2
29/08/23	7	21	14.7	13.4	16.9	13.1	5.1	6.2
30/08/23	3	02	12.9	11.5	16.7	11.1	0.0	9.8
31/08/23	5	03	14.8	13.4	18.8	9.6	0.2	5.0
01/09/23	7	03	15.4	13.9	18.6	13.0	0.0	0.3
02/09/23	1	03	18.8	15.4	20.7	13.1	0.0	10.9
03/09/23	3	05	17.5	16.2	21.1	13.5	0.0	11.1
04/09/23	1	02	21.1	17.8	25.6	12.2	0.0	11.9
05/09/23	1	02	23.0	16.6	26.3	16.8	0.0	10.0
06/09/23	1	02	21.8	18.1	24.6	15.4	0.0	9.6
07/09/23	8	03	21.7	18.7	25.1	17.6	0.0	0.1
08/09/23	7	02	22.2	18.8	26.4	15.9	0.0	8.1
09/09/23	7	02	20.1	19.0	23.3	17.9	0.5	3.7
10/09/23	5	02	23.0	18.6	23.5	14.7	2.5	2.1
11/09/23	8	50	17.2	17.0	17.3	17.1	7.1	0.0
12/09/23	7	01	14.8	13.4	16.0	13.0	0.4	0.0
13/09/23	1	02	14.6	11.3	17.5	7.6	10.3	7.6
14/09/23	6	03	15.2	14.0	17.9	12.2	7.6	5.9
15/09/23	7	01	16.8	15.6	18.5	11.3	0.0	0.0
16/09/23	5	01	15.4	13.2	17.5	12.6	0.0	3.0
17/09/23	8	02	15.7	14.1	18.0	13.6	22.4	0.0
18/09/23	8	65	13.5	13.3	16.2	13.4	18.3	3.2
19/09/23	8	63	16.2	15.5	17.2	9.6	11.0	0.0
20/09/23	8	63	15.6	15.4	16.6	15.2	13.4	3.5
21/09/23	2	02	12.9	11.3	15.2	9.3	10.3	8.7
22/09/23	8	21	11.5	11.0	14.5	9.0	8.0	0.6
23/09/23	7	60	11.3	10.1	16.3	8.6	0.4	4.7
24/09/23	8	02	16.4	15.4	18.4	8.7	4.3	0.1
25/09/23	8	03	16.0	13.9	17.7	12.5	0.0	5.8
26/09/23	6	02	15.7	14.0	17.9	12.4	1.9	6.0
27/09/23	8	15	13.4	11.7	18.0	11.1	8.8	0.5
28/09/23	8	15	14.2	12.4	14.8	13.4	2.2	0.0
29/09/23	6	03	14.0	12.3	15.8	12.0	0.0	7.1
30/09/23	8	02	12.9	11.8	16.3	10.4	7.5	0.0
01/10/23	8	02	16.1	15.8	16.6	10.7	0.0	0.3
02/10/23	7	02	14.0	13.2	14.9	12.2	10.6	0.1
03/10/23	6	03	12.9	11.2	14.5	9.7	0.6	3.6
04/10/23	8	80	13.7	12.2	16.1	12.4	4.7	2.1
05/10/23	8	60	14.0	13.2	15.8	12.8	30.6	0.0
06/10/23	8	02	15.8	15.6	16.6	13.3	2.0	0.0
07/10/23	8	02	15.7	15.0	17.5	15.0	0.0	0.1
08/10/23	8	02	14.9	13.9	19.5	13.2	0.0	Tr
09/10/23	8	46	15.4	15.4	16.5	14.7	0.1	0.1
10/10/23	7	03	16.2	13.2	19.0	12.8	8.0	1.4
11/10/23	8	51	11.2	9.9	11.9	10.2	0.0	0.0
12/10/23	1	02	8.1	6.5	12.7	3.1	7.4	9.1
13/10/23	8	60	10.7	10.6	12.3	8.1	3.3	3.9
14/10/23	4	03	8.9	6.0	10.4	6.6	1.8	6.7
15/10/23	1	02	6.1	3.5	10.8	2.3	0.0	8.2
16/10/23	7	02	7.9	6.1	11.9	3.5	0.0	5.2
17/10/23	6	02	9.6	8.4	13.0	5.7	0.0	3.2
18/10/23	7	02	11.2	9.4	15.6	9.6	7.8	1.7
19/10/23	8	53	13.7	13.4	17.6	11.2	15.6	2.5

Table 9.3 Weather conditions regarded at 10AM from Hazelrigg Field Station (UK Meteorological Office - Climatological Station Number 7236) during Experiment 2

9.2 Appendix B – Convolutional Neural Network Model Code Structure

9.2.1 Chapter 4 Model Code

The following code was used in Chapter 4 to train MobileNetV2 and EfficientNetV2L models to classify the ADID dataset. The pre-trained models are imported from the Keras packages and fine-tuned on the ADID training set. The retrained model is employed to classify all images in the ADID testing set and provide confidence values in a CSV-format spreadsheet. All hyperparameters were optimised by trial and improvement by assessing performance on a validation dataset of publicly sourced imagery.

```
import numpy as np
import pandas as pd
from sklearn.preprocessing import MultiLabelBinarizer
import tensorflow as tf
from tensorflow.keras.layers import BatchNormalization,
GlobalAveragePooling2D, Input, GlobalMaxPooling2D
import keras
from tensorflow.keras.preprocessing.image import ImageDataGenerator
import tensorflow.keras.layers as L
from keras.models import Sequential, Model

strategy = tf.distribute.get_strategy()

# variables

depth = 3
EPOCHS = 20
BS = 6
IMG_SHAPE = (1200, 900, 3)
SEED = 100

# pathways
train_paths = r"C:\Users\bleas\Documents\CHAPTER4\ADID\ADID_Train"
train =
pd.read_csv(r"C:\Users\bleas\Documents\CHAPTER4\ADID\ADID_Train.csv")
test_paths = r"C:\Users\bleas\Documents\CHAPTER4\ADID\ADID_Test"
test = pd.read_csv(r"C:\Users\bleas\Documents\CHAPTER4\ADID\ADID_Test.csv")

label_split = train.labels_mc.apply(lambda x: x.split())
trans_label = MultiLabelBinarizer().fit(label_split)
labels_mc = pd.DataFrame(trans_label.transform(label_split),
columns=trans_label.classes_)
labels_mc.head()
print()

# multilabel
```

```

train['labels_mc'] = train['labels_mc'].apply(lambda string: string.split('
'))
train
s = list(train['labels_mc'])
mlb = MultiLabelBinarizer()
trainx = pd.DataFrame(mlb.fit_transform(s), columns=mlb.classes_,
index=train.index)
#trainy = trainx.sum()
print(trainx.columns)
print(trainx.sum())
print()

labels_mc = pd.concat([train['image_id'], labels_mc], axis=1)
labels_mc.head()
print()

label2id = {
    'complex' : 0,
    'frogeye_leaf_spot' : 1,
    'healthy' : 2,
    'powdery_mildew' : 3,
    'rust' : 4,
    'scab' : 5
}

NUM_CLASS = len(label2id)

datagen = ImageDataGenerator(
    rescale=1 / 255.0,
    preprocessing_function=None, # You can add your custom preprocessing
function here if needed
    data_format=None,
    validation_split=0.0, # Set the validation_split to the desired value
for splitting your data
    rotation_range=20, # Random rotation of the image in the range of
-30 to 30 degrees
    width_shift_range=0.1, # Random horizontal shift of the image
    height_shift_range=0.1, # Random vertical shift of the image
    shear_range=0.1, # Shear transformations
    zoom_range=0.1, # Random zooming inside the image
    horizontal_flip=True, # Randomly flip the image horizontally
    vertical_flip=True # Don't flip the image vertically
)

train_data = datagen.flow_from_dataframe(
    train,
    directory=train_paths,
    x_col="image_id",
    y_col='labels_mc',
    color_mode="rgb",
    class_mode="categorical",
    batch_size=BS,
    shuffle=True,
    seed=100,
    image_size=(1200,900))

def build_lr_fn(lr_start=0.0001, lr_end=0.00001, num_epochs=9):
    def lr_fn(epoch):
        if epoch < num_epochs:
            lr = lr_start - (lr_start - lr_end) * epoch / num_epochs
        else:

```

```

        lr = lr_end
    return lr

    return lrfn

lrfn = build_lrfn()
STEPS_PER_EPOCH = labels_mc.shape[0] // BS
lr_schedule = tf.keras.callbacks.LearningRateScheduler(lrfn, verbose=1)

class_count = len(list(train_data.class_indices.keys())) # to define number
of classes in dense layer

from tensorflow.keras.applications import EfficientNetV2L

base_model = EfficientNetV2L(include_top=False, weights="imagenet",
input_shape= IMG_SHAPE, input_tensor=Input(shape=(1200, 900, 3)))

model = Sequential([
    base_model,
    L.GlobalAveragePooling2D(),
    L.BatchNormalization(),
    L.Dense(NUM_CLASS,
            kernel_initializer=keras.initializers.RandomUniform(seed=SEED),
            bias_initializer=keras.initializers.Zeros(), name='dense_top',
activation='softmax')
])

metrics = [
    keras.metrics.CategoricalAccuracy(name='accuracy'),
    keras.metrics.Precision(name='precision')]

model.compile(optimizer='adam', loss='categorical_crossentropy', metrics=
[metrics])

# Freezing the weights
for layer in model.layers[:-1]:
    layer.trainable=False

model.summary()

history = model.fit(train_data,
                    epochs=EPOCHS,
                    steps_per_epoch=train_data.samples//BS,
                    callbacks=lr_schedule,
                    validation_data=validation_data)

datagen_test = ImageDataGenerator(
    rescale=1 / 255.0,
    preprocessing_function=None, # You can add your custom preprocessing
function here if needed
    data_format=None,
)

test_data = datagen_test.flow_from_dataframe(

```



```

test,
directory=test_paths,
x_col="image_id",
y_col="labels_mc",
color_mode="rgb",
class_mode="categorical",
batch_size=BS,
shuffle=False,
seed=100,
image_size=(1200,900))

probabilities = model.predict(test_data, steps=len(test_data))

preds = model.predict(test_data)
preds = preds.tolist()
y_pred = np.argmax(preds, axis=1)

indices = []
for pred in preds:
    temp = []
    for category in pred:
        if category >= 0.5:
            temp.append(pred.index(category))
    if temp != []:
        indices.append(temp)
    else:
        temp.append(np.argmax(pred))
        indices.append(temp)

print(indices)

labels_mc = (train_data.class_indices)
labels_mc = dict((v, k) for k, v in labels_mc.items())

testlabels_mc = []

for image in indices:
    temp = []
    for i in image:
        temp.append(str(labels_mc[i]))
    testlabels_mc.append(' '.join(temp))
print(testlabels_mc)
df = test

res = pd.DataFrame()
res['NUM_ID'] = df['num_id']
res['image_id'] = test['image_id']
res['SOURCE'] = test['source']
res['TRUE_labels_mc'] = test['labels_mc']
res['CNN_labels_mc'] = testlabels_mc
res['complex'] = probabilities[:, 0]
res['frogeye_leaf_spot'] = probabilities[:, 1]
res['healthy'] = probabilities[:, 2]
res['powdery_mildew'] = probabilities[:, 3]
res['rust'] = probabilities[:, 4]
res['scab'] = probabilities[:, 5]

model.save("CHAPTER4_EfficientNetV2L_labels_mc.hdf5")

res.to_csv("CHAPTER4_EfficientNetV2L_labels_mc_Predictions.csv",
index=False)

```

9.2.2 Chapter 5 Model Code

9.2.2.1 Model Fine-Tuning

The following code was used in Chapter 5 to train MobileNetV2, InceptionResNetV2 and EfficientNetV2L models to classify the final apple disease dataset. The pre-trained models are imported from the Keras packages and fine-tuned on the training set. The retrained model is employed to classify all images in the testing set and provide confidence values in a CSV-format spreadsheet. All hyperparameters were optimised by trial and improvement by assessing performance on a validation dataset of publicly sourced imagery.

```
#IMPORT PYTHON PACKAGES
import numpy as np
import pandas as pd
from sklearn.preprocessing import MultiLabelBinarizer
import tensorflow as tf
from tensorflow.keras.layers import BatchNormalization, GlobalAveragePooling2D,
Input, GlobalMaxPooling2D
import keras
from tensorflow.keras.preprocessing.image import ImageDataGenerator
import tensorflow.keras.layers as L
from keras.models import Sequential

# INITIAL MODEL PARAMETERS
strategy = tf.distribute.get_strategy()
depth = 3
EPOCHS = 12
BS = 6
IMG_SHAPE = (1200, 1200, 3)
SEED = 1000

# DATASET PATHWAYS
train_paths = r"C:\Users\bleas\Documents\TRIALS\FINAL\TOTAL\TRAIN"
train = pd.read_csv(r"C:\Users\bleas\Documents\TRIALS\FINAL\TOTAL\TRAIN.csv")
test_paths = r"C:\Users\bleas\Documents\TRIALS\FINAL\TOTAL\TEST"
test = pd.read_csv(r"C:\Users\bleas\Documents\TRIALS\FINAL\TOTAL\TEST.csv")

#READ TRAINING DATASET ANNOTATIONS
label_split = train.labels.apply(lambda x: x.split())
trans_label = MultiLabelBinarizer().fit(label_split)
labels = pd.DataFrame(trans_label.transform(label_split),
columns=trans_label.classes_)
labels.head()
print()

train['labels'] = train['labels'].apply(lambda string: string.split(' '))
train

s = list(train['labels'])
mlb = MultiLabelBinarizer()
trainx = pd.DataFrame(mlb.fit_transform(s), columns=mlb.classes_,
index=train.index)
print(trainx.columns)
print(trainx.sum())
print()

#DISPLAY LABEL DISTRIBUTION
```

```

labels = pd.concat([train['image_id'], labels], axis=1)
labels.head()
print()

label2id = {
    'FROGEYE' : 0,
    'HEALTHY' : 1,
    'MILDEW' : 2,
    'RUST' : 3,
    'SCAB' : 4
}
NUM_CLASS = len(label2id)

#TRAINING DATASET AUGMENTATION
datagen = ImageDataGenerator(
    rescale=1 / 255.0,
    preprocessing_function=None,
    data_format=None,
    validation_split=0.0, # NO VALIDATION SPLIT
    rotation_range=20, # RANDOM ROTATION OF THE IMAGE
    width_shift_range=0.1, # RANDOM HORIZONTAL SHIFT OF THE IMAGE
    height_shift_range=0.1, # RANDOM VERTICAL SHIFT OF THE IMAGE
    shear_range=0.1, # RANDOM SHEAR TRANSFORMATIONS
    zoom_range=0.1, # RANDOM ZOOM TRANSFORMATIONS
    horizontal_flip=True, # RANDOMLY FLIP IMAGE HORIZONTALLY
    vertical_flip=True # RANDOMLY FLIP IMAGE VERTICALLY
)

#TRAINING DATASET GENERATOR
train_data = datagen.flow_from_dataframe(
    train,
    directory=train_paths,
    x_col="image_id",
    y_col='labels',
    color_mode="rgb",
    class_mode="categorical",
    batch_size=BS,
    shuffle=True,
    seed=1000,
    image_size=(1200,1200))

#VALIDATION DATASET GENERATOR (FOR HYPERPARAMETER ADJUSTMENT)
validation_data = datagen.flow_from_dataframe(
    train,
    directory=train_paths,
    x_col="image_id",
    y_col='labels',
    color_mode="rgb",
    class_mode="categorical",
    batch_size=BS,
    shuffle=True,
    seed=1000,
    image_size=(1200,1200))

#BUILD LEARNING RATE
def build_lr_fn(lr_start=0.0001, lr_end=0.00001, num_epochs=9):
    def lr_fn(epoch):
        if epoch < num_epochs:
            lr = lr_start - (lr_start - lr_end) * epoch / num_epochs
        else:
            lr = lr_end
        return lr
    return lr_fn

lr_fn = build_lr_fn()
STEPS_PER_EPOCH = labels.shape[0] // BS

```

```

lr_schedule = tf.keras.callbacks.LearningRateScheduler(lrfn, verbose=1)

class_count = len(list(train_data.class_indices.keys())) # to define number of
classes in dense layer

#IMPORT PRE-TRAINED MODEL FROM KERAS
from tensorflow.keras.applications import EfficientNetV2L

# BUILD PRE-TRAINED MODEL FOR FURTHER TRAINING
base_model = EfficientNetV2L(include_top=False, weights="imagenet", input_shape=
IMG_SHAPE, input_tensor=Input(shape=(1200, 1200, 3)))

model = Sequential([
    base_model,
    L.GlobalMaxPooling2D(),
    L.Dense(NUM_CLASS,
            kernel_initializer=keras.initializers.RandomUniform(seed=SEED),
            bias_initializer=keras.initializers.Zeros(), name='dense_top',
activation='sigmoid') #SIGMOID FUNCTION FOR MULTILABEL APPROACH
])

#TRAINING PERFORMANCE METRICS PER EPOCH
metrics = [
    keras.metrics.CategoricalAccuracy(name='accuracy'),
    keras.metrics.Precision(name='precision')]
model.compile(optimizer='adam', loss='binary_crossentropy', metrics=[metrics])

# FREEZE MODEL WEIGHTS (FOR TRANSFER LEARNING)
for layer in model.layers[:-1]:
    layer.trainable=False
model.summary()

#DISPLAY PERFORMANCE METRICS PER EPOCH
history = model.fit(train_data,
                    epochs=EPOCHS,
                    steps_per_epoch=train_data.samples//BS,
                    callbacks=lr_schedule,
                    validation_data=validation_data)

#TEST DATASET GENERATOR
datagen_test = ImageDataGenerator(
    rescale=1 / 255.0,
    preprocessing_function=None,
    data_format=None,)

test_data = datagen_test.flow_from_dataframe(
    test,
    directory=test_paths,
    x_col="image_id",
    y_col="labels",
    color_mode="rgb",
    class_mode="categorical",
    batch_size=BS,
    shuffle=False,
    seed=1000,
    image_size=(1200,1200))

# CNN PREDICTION OUTPUT FOR TEST DATASET
probabilities = model.predict(test_data, steps=len(test_data))
preds = model.predict(test_data)
preds = preds.tolist()
y_pred = np.argmax(preds, axis=1)

# PREDICTION THRESHOLD SET TO CONFIDENCE 0.5
indices = []
for pred in preds:
    temp = []
    for category in pred:

```

```

        if category >= 0.5:
            temp.append(pred.index(category))
    if temp != []:
        indices.append(temp)
    else:
        temp.append(np.argmax(pred))
        indices.append(temp)
print(indices)

labels = (train_data.class_indices)
labels = dict((v, k) for k, v in labels.items())
testlabels = []

for image in indices:
    temp = []
    for i in image:
        temp.append(str(labels[i]))
    testlabels.append(' '.join(temp))
print(testlabels)
df = test

#CSV FILE FORMAT
res = pd.DataFrame()
res['NUM_ID'] = df['NUM_ID']
res['IMAGE_ID'] = test['image_id']
res['SOURCE'] = test['SOURCE']
res['TRUE_LABELS'] = test['labels']
res['CNN_LABELS'] = testlabels
res['FROGEYE'] = probabilities[:, 0]
res['HEALTHY'] = probabilities[:, 1]
res['POWDERY_MILDEW'] = probabilities[:, 2]
res['RUST'] = probabilities[:, 3]
res['SCAB'] = probabilities[:, 4]
# PREDICTIONS SAVED TO CSV FILE
res.to_csv("EfficientNetV2L_MULTISPECTRALAPPLEDISEASE_Predictions.csv",
index=False)

# TRAINED MODEL SAVED
model.save("EfficientNetV2L_MULTISPECTRALAPPLEDISEASE.hdf5")

```

9.2.3 Pre-Trained CNN Classifier

The following code loaded a pre-trained model to classify imagery within a new dataset. It was used specifically in Chapter 5 to classify localised imagery in Section 5.3.3.

```
#IMPORT PYTHON PACKAGES
import numpy as np
import pandas as pd
import tensorflow as tf
from tensorflow.keras.preprocessing.image import ImageDataGenerator
from tensorflow.keras.models import Sequential, load_model

# INITIAL MODEL PARAMETERS
strategy = tf.distribute.get_strategy()
depth = 3
EPOCHS = 12
BS = 6
IMG_SHAPE = (1200, 1200, 3)
SEED = 1000

# DATASET PATHWAYS
test_paths = r"C:\Users\bleas\Documents\TRIALS\FINAL\TOTAL\TEST_CROPPED"
test = pd.read_csv(r"C:\Users\bleas\Documents\TRIALS\FINAL\TOTAL\TEST.csv")

#LOAD PRE-TRAINED MODEL FROM FILE
loaded_model =
load_model(r"C:\Users\bleas\PycharmProjects\GPU\EfficientNetV2L_MULTISPECTRALAPPLIED
ISEASE.hdf5")

#TEST DATASET GENERATOR
datagen_test = ImageDataGenerator(
    rescale=1 / 255.0,
    preprocessing_function=None,
    data_format=None, )

test_data = datagen_test.flow_from_dataframe(
    test,
    directory=test_paths,
    x_col="image_id",
    y_col="labels",
    color_mode="rgb",
    class_mode="categorical",
    batch_size=BS,
    shuffle=False,
    seed=1000,
    image_size=(1200, 1200))

# CNN PREDICTION OUTPUT FOR TEST DATASET
probabilities = loaded_model.predict(test_data, steps=len(test_data))
preds = loaded_model.predict(test_data)
preds = preds.tolist()
y_pred = np.argmax(preds, axis=1)

indices = []
for pred in preds:
    temp = []
    for category in pred:
        if category >= 0.5:
            temp.append(pred.index(category))
    if temp != []:
        indices.append(temp)
    else:
        temp.append(np.argmax(pred))
        indices.append(temp)
```

```

print(indices)
labels = (train_data.class_indices)
labels = dict((v, k) for k, v in labels.items())
testlabels = []

for image in indices:
    temp = []
    for i in image:
        temp.append(str(labels[i]))
    testlabels.append(' '.join(temp))
print(testlabels)
df = test

#CSV FILE FORMAT
res = pd.DataFrame()
res['NUM_ID'] = df['NUM_ID']
res['IMAGE_ID'] = test['image_id']
res['SOURCE'] = test['SOURCE']
res['TRUE_LABELS'] = test['labels']
res['CNN_LABELS'] = testlabels
res['FROGEYE'] = probabilities[:, 0]
res['HEALTHY'] = probabilities[:, 1]
res['POWDERY_MILDEW'] = probabilities[:, 2]
res['RUST'] = probabilities[:, 3]
res['SCAB'] = probabilities[:, 4]

# PREDICTIONS SAVED TO CSV FILE
res.to_csv("EfficientNetV2L_MULTISPECTRALAPPLEDISEASE_Predictions_2.csv",
index=False)

```

9.3 Appendix C – Convolutional Neural Network Classification Results

9.3.1 Model Training Metrics

Each model was fine-tuned on the primary and secondary data within the training set until it reached convergence. During the training process, the output for learning rate, loss, accuracy, F1 score, and training duration was provided for each epoch. Tables 9.4 and 9.5 display the training metrics for fine-tuning the MobileNetV2 and EfficientNetV2L models, as discussed in Chapter 4. Tables 9.6, 9.7, and 9.8 present the training metrics for fine-tuning the MobileNetV2, InceptionResNetV2, and EfficientNetV2L models, as discussed in Chapter 5.

Chapter 4 MobileNetV2 Training Metrics					
Epoch	Learning Rate	Loss	Accuracy	F1 Score	Duration (s)
1	1.00E-07	1.878	0.2713	0.1231	428
2	7.60E-07	1.7275	0.3123	0.1633	405
3	1.42E-06	1.4426	0.4382	0.2904	397
4	2.08E-06	1.148	0.5863	0.484	403
5	2.74E-06	0.8877	0.6971	0.6466	396
6	3.40E-06	0.6989	0.7646	0.7334	386
7	4.06E-06	0.5704	0.8061	0.7801	388
8	4.72E-06	0.4876	0.8325	0.8106	384
9	5.38E-06	0.4217	0.8543	0.8351	387
10	6.04E-06	0.3685	0.8747	0.857	391
11	6.70E-06	0.3242	0.8883	0.8713	388
12	7.36E-06	0.2865	0.9024	0.8888	389
13	8.02E-06	0.25	0.9166	0.9026	391
14	8.68E-06	0.2176	0.9294	0.9174	390
15	9.34E-06	0.1898	0.9377	0.9263	393
16	1.00E-05	0.162	0.9485	0.9393	394
17	8.02E-06	0.1359	0.9593	0.9515	394
18	6.44E-06	0.1174	0.966	0.9588	392
19	5.17E-06	0.1036	0.9704	0.965	389
20	4.16E-06	0.0943	0.9739	0.9683	389

Table 9.4 MobileNetV2 training metrics (Chapter 4)

Chapter 4 EfficientNetV2L Training Metrics					
Epoch	Learning Rate	Loss	Accuracy	F1 Score	Time per Epoch (s)
1	1.00E-07	1.7731	0.217	0.1884	1727
2	7.60E-07	1.3408	0.5185	0.4218	1759
3	1.42E-06	0.8406	0.7091	0.6383	1784
4	2.08E-06	0.5796	0.8019	0.7735	1842
5	2.74E-06	0.451	0.8456	0.8223	1945
6	3.40E-06	0.3536	0.8832	0.8613	1780
7	4.06E-06	0.2802	0.9076	0.8893	1740
8	4.72E-06	0.2097	0.9318	0.917	1694
9	5.38E-06	0.1636	0.9472	0.9343	1685
10	6.04E-06	0.1262	0.9584	0.948	1672
11	6.70E-06	0.0967	0.9691	0.9617	1670
12	7.36E-06	0.0787	0.9744	0.9684	1680
13	8.02E-06	0.0677	0.979	0.9746	1671
14	8.68E-06	0.0587	0.9809	0.9767	1673
15	9.34E-06	0.0544	0.9825	0.978	1679
16	1.00E-05	0.0479	0.9838	0.9796	1683
17	8.02E-06	0.0364	0.9875	0.9846	1682
18	6.44E-06	0.0276	0.9903	0.9883	1679
19	5.17E-06	0.0229	0.9912	0.9893	1676
20	4.16E-06	0.0174	0.9933	0.9917	1686

Table 9.5 EfficientNetV2L training metrics (Chapter 4)

Chapter 5 MobileNetV2 Training Metrics					
Epoch	Learning Rate	Loss	Accuracy	Precision	Time per Epoch (s)
1	0.0001	0.2817	0.7557	0.7501	796
2	9.00E-05	0.1548	0.8659	0.8697	781
3	8.00E-05	0.1153	0.8986	0.9055	758
4	7.00E-05	0.0951	0.9154	0.923	764
5	6.00E-05	0.0846	0.9248	0.933	761
6	5.00E-05	0.0761	0.9295	0.9393	749
7	4.00E-05	0.0651	0.9394	0.9485	749
8	3.00E-05	0.0591	0.9415	0.9536	749
9	2.00E-05	0.0531	0.9482	0.9585	749
10	1.00E-05	0.0497	0.9507	0.9597	770
11	1.00E-05	0.0471	0.9527	0.9635	780
12	1.00E-05	0.0469	0.9524	0.9626	753

Table 9.6 MobileNetV2 training metrics (Chapter 5)

Chapter 5 InceptionResNetV2 Training Metrics					
Epoch	Learning Rate	Loss	Accuracy	Precision	Time per Epoch (s)
1	0.0001	0.1659	0.8445	0.8562	814
2	9.00E-05	0.0875	0.9195	0.9314	800
3	8.00E-05	0.0657	0.9379	0.9499	783
4	7.00E-05	0.0527	0.9479	0.9603	796
5	6.00E-05	0.0437	0.9534	0.967	791
6	5.00E-05	0.0345	0.9614	0.9748	786
7	4.00E-05	0.0277	0.9657	0.9797	787
8	3.00E-05	0.0208	0.9699	0.9839	787
9	2.00E-05	0.0163	0.9716	0.9872	789
10	1.00E-05	0.0131	0.9766	0.99	786
11	1.00E-05	0.0116	0.9763	0.9921	792
12	1.00E-05	0.0102	0.9772	0.9927	789

Table 9.7 InceptionResNetV2 training metrics (Chapter 5)

Chapter 5 EfficientNetV2L Training Metrics					
Epoch	Learning Rate	Loss	Accuracy	Precision	Time per Epoch (s)
1	0.0001	0.1754	0.8347	0.865	1345
2	9.00E-05	0.1067	0.904	0.9221	1277
3	8.00E-05	0.0857	0.9214	0.9375	1276
4	7.00E-05	0.0699	0.9357	0.9497	1275
5	6.00E-05	0.0585	0.9429	0.9577	1275
6	5.00E-05	0.0477	0.9499	0.9667	1276
7	4.00E-05	0.0402	0.9548	0.9705	1278
8	3.00E-05	0.0329	0.9627	0.9771	1274
9	2.00E-05	0.0269	0.9675	0.981	1272
10	1.00E-05	0.0219	0.9711	0.9844	1271
11	1.00E-05	0.019	0.9729	0.9865	1278
12	1.00E-05	0.0186	0.974	0.9868	1273

Table 9.8 EfficientNetV2 training metrics (Chapter 5)

9.3.2 Classification Results

9.3.2.1 Chapter 4 Classification Results

Label	MobileNetV2				EfficientNetV2L			
	TP	TN	FP	FN	TP	TN	FP	FN
Complex	527	5059	121	93	549	5051	129	71
Frogeye Leaf Spot	655	5055	54	36	666	5060	49	25
Healthy	1885	3646	126	143	1897	3624	148	131
Powdery Mildew	209	5568	9	14	206	5572	5	16
Rust	556	5151	64	29	555	5155	60	30
Scab	1539	3904	243	114	1498	3967	180	155

Table 9.9 Classification results for the full ADID Dataset

Label	MobileNetV2				EfficientNetV2L			
	TP	TN	FP	FN	TP	TN	FP	FN
RGB	97	306	76	33	65	332	50	65
NIR	135	252	98	27	130	268	82	32

Table 9.10 Classification results for the multispectral ADID subset

9.3.2.2 Chapter 5 Classification Results

Validation Data												
Model	MobileNetV2				InceptionResNetV2				EfficientNetV2L			
Label	TP	TN	FP	FN	TP	TN	FP	FN	TP	TN	FP	FN
FROGEYE	830	3477	42	51	831	3471	48	50	855	3469	50	26
HEALTHY	1247	3061	55	37	1257	3055	61	27	1245	3105	11	39
MILDEW	226	4140	13	21	238	4147	6	9	247	4122	31	0
RUST	616	3719	24	41	623	3717	26	34	635	3719	24	22
SCAB	1409	2820	80	91	1405	2852	48	95	1448	2845	55	52

Table 9.11 Classification results for the validation data

Multispectral Data (Whole-Plant)												
Model	MobileNetV2				InceptionResNetV2				EfficientNetV2L			
Label	TP	TN	FP	FN	TP	TN	FP	FN	TP	TN	FP	FN
RGB Control	0	1036	64	0	0	1022	78	0	0	1022	78	0
RGB Experimental	223	463	26	338	257	474	15	354	348	442	47	263
NIR Control	0	1064	36	0	0	1078	22	0	0	1078	22	0
NIR Experimental	293	473	6	328	343	475	4	278	401	467	11	221

Table 9.12 Classification results of fine-tuned CNN for multispectral imagery (whole-plant)

Multispectral Data (Localised)												
Model	MobileNetV2				InceptionResNetV2				EfficientNetV2L			
Label	TP	TN	FP	FN	TP	TN	FP	FN	TP	TN	FP	FN
RGB Control	0	1041	59	0	0	1068	32	0	0	1026	74	0
RGB Experimental	352	464	25	239	360	484	5	251	516	444	45	95
NIR Control	0	1065	35	0	0	1032	68	0	0	1079	21	0
NIR Experimental	521	474	5	100	547	464	15	74	549	470	9	72

Table 9.13 Classification results for multispectral imagery (localised)

EfficientNetV2L Control									
Sample	RGB				NIR				
	TP	TN	FP	FN	TP	TN	FP	FN	
C01	0	55	0	0	0	55	0	0	
C02	0	53	2	0	0	51	4	0	
C03	0	50	5	0	0	55	0	0	
C04	0	40	15	0	0	53	2	0	
C05	0	53	2	0	0	55	0	0	
C06	0	53	2	0	0	55	0	0	
C07	0	49	6	0	0	55	0	0	
C08	0	43	12	0	0	53	2	0	
C09	0	48	7	0	0	53	0	0	
C10	0	55	0	0	0	55	0	0	
C11	0	55	0	0	0	55	0	0	
C12	0	52	3	0	0	55	0	0	
C13	0	55	0	0	0	55	0	0	
C14	0	54	1	0	0	55	0	0	
C15	0	55	0	0	0	55	0	0	
C16	0	53	2	0	0	52	3	0	
C17	0	51	4	0	0	55	0	0	
C18	0	48	7	0	0	49	6	0	
C19	0	53	2	0	0	53	2	0	
C20	0	49	5	0	0	53	2	0	

Table 9.14 EfficientNetV2L classification results for Control samples

EfficientNetV2L Experimental (Full-Scale)								
Sample	RGB				NIR			
	TP	TN	FP	FN	TP	TN	FP	FN
E01	16	11	0	28	20	11	0	24
E02	10	18	19	8	3	36	1	15
E03	17	19	13	6	10	29	3	13
E04	5	31	6	13	1	37	0	16
E05	14	29	4	8	13	30	2	10
E06	21	21	1	12	28	21	1	5
E07	29	12	0	14	38	11	0	6
E08	25	20	0	10	28	18	2	7
E09	20	19	0	16	32	18	0	5
E10	18	16	0	21	17	16	0	22
E11	8	32	0	15	15	32	0	8
E12	14	34	3	4	13	35	1	6
E13	24	15	0	16	28	13	0	14
E14	27	19	0	9	29	17	0	9
E15	9	32	0	14	20	32	0	3
E16	7	32	0	16	14	32	0	9
E17	27	12	0	16	33	12	0	10
E18	22	30	1	2	17	31	0	7
E19	14	21	0	20	22	17	1	15
E20	21	19	0	15	19	20	0	16

Table 9.15 EfficientNetV2L classification results for Experimental samples (whole-plant)

EfficientNetV2L Experimental (Localised)								
Sample	RGB				NIR			
	TP	TN	FP	FN	TP	TN	FP	FN
E01	38	11	0	6	36	11	0	8
E02	17	15	22	1	17	37	0	1
E03	20	25	7	3	22	27	5	1
E04	18	31	6	0	17	37	0	1
E05	17	33	0	5	22	32	1	1
E06	29	20	2	4	33	21	0	0
E07	41	12	0	2	44	11	0	0
E08	30	20	0	5	30	19	1	5
E09	31	19	0	5	34	18	0	3
E10	23	16	0	16	33	16	0	6
E11	21	32	0	2	21	31	1	2
E12	17	33	4	1	17	36	0	2
E13	33	15	0	7	32	13	0	10
E14	31	19	0	5	37	17	0	1
E15	18	31	1	5	23	32	0	0
E16	16	31	1	7	19	32	0	4
E17	39	12	0	4	39	12	0	4
E18	23	30	1	1	20	31	0	4
E19	26	20	1	8	28	17	1	9
E20	28	19	0	8	25	20	0	10

Table 9.16 EfficientNetV2L classification results for Experimental samples (localised)

9.4 Appendix D - Multispectral Time Series Imagery

The aim of this research was to develop a remote sensing system capable of detecting apple scab infections early under natural illumination conditions. Through the acquisition of time series imagery, it was demonstrated that high-resolution multispectral imagery (VIS-NIR) had significant diagnostic potential throughout the development of apple scab symptoms on plants. The following figures (Figure 9.3 – Figure 9.20) provide examples of apple scab symptom development and progression on seedling S17 in Experiment 1, as well as a range of examples for control (C07), training (T23) and experimental (E06 and E09) samples from ‘large’, ‘medium’ and ‘small’ sizes in Experiment 2.



Figure 9.3 Experiment 1 'Sample (S)' time series 7-21 d.p.i. (Sample S17)



Figure 9.4 Experiment 1 'Sample (S)' time series 22-35 d.p.i. (Sample S17)

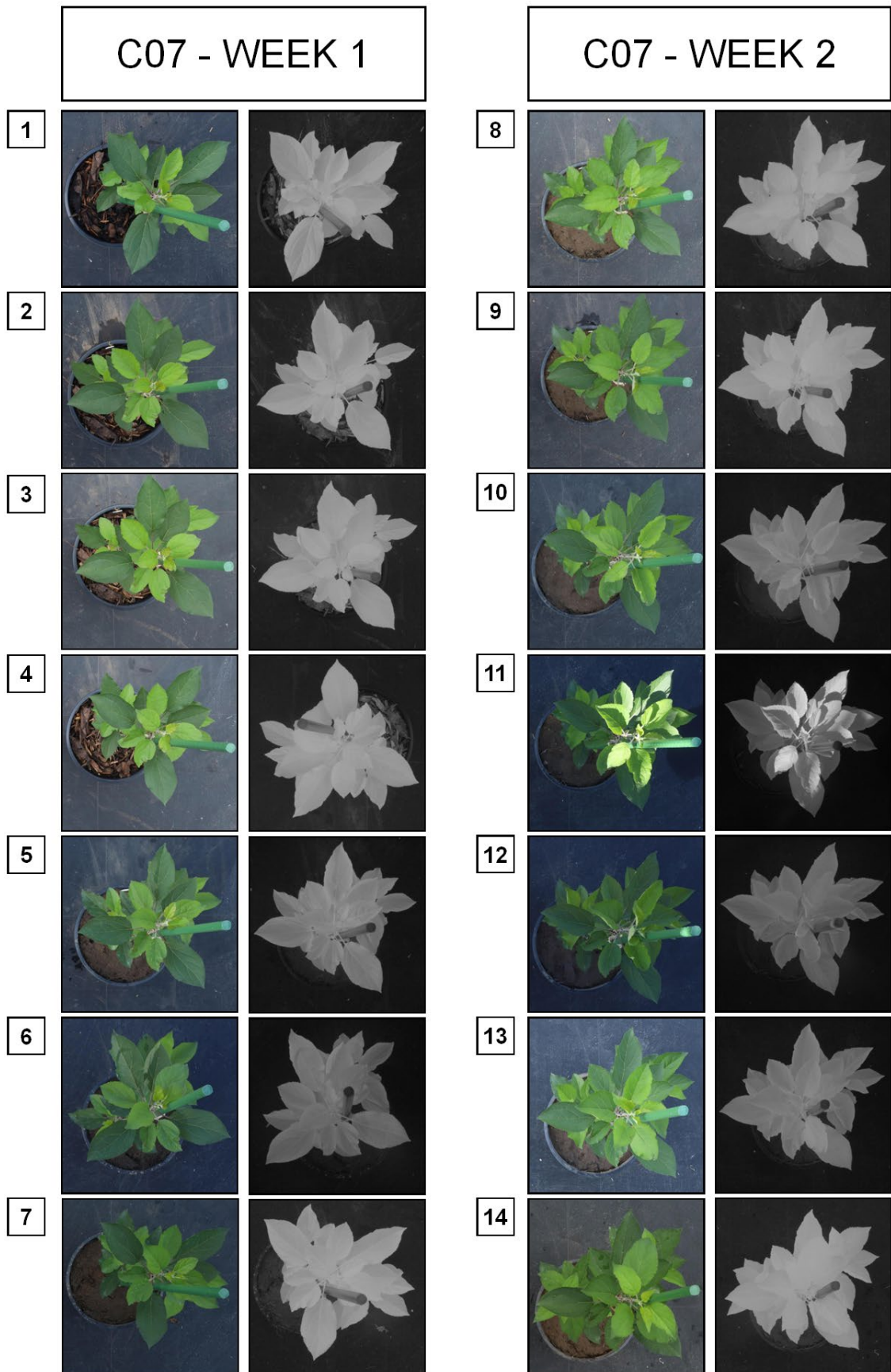


Figure 9.5 Experiment 2 'Control (C) - large' time series 1-14 d.p.i. (Sample C07)

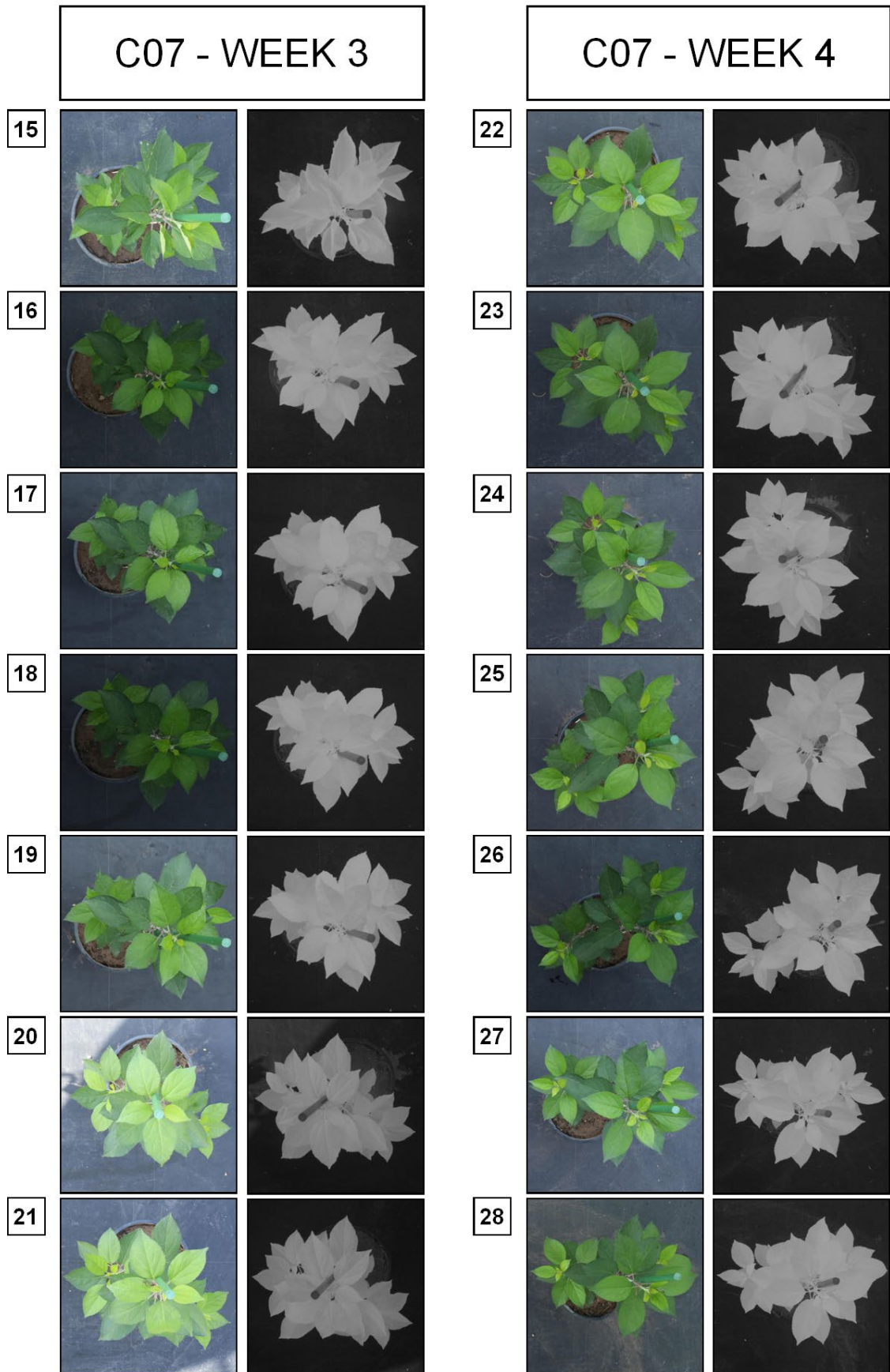


Figure 9.6 Experiment 2 'Control (C) - large' time series 15-28 d.p.i. (Sample C07)

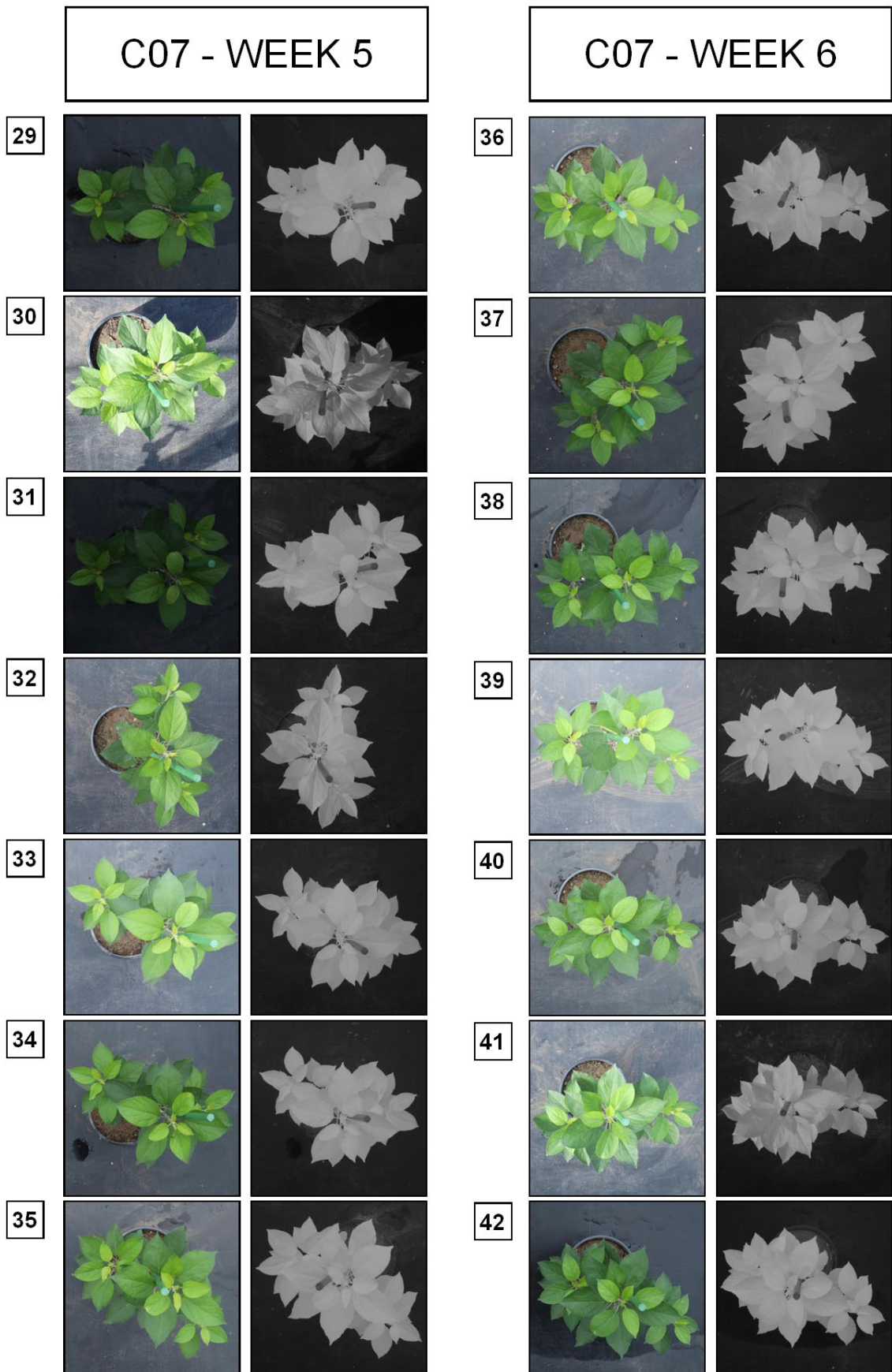
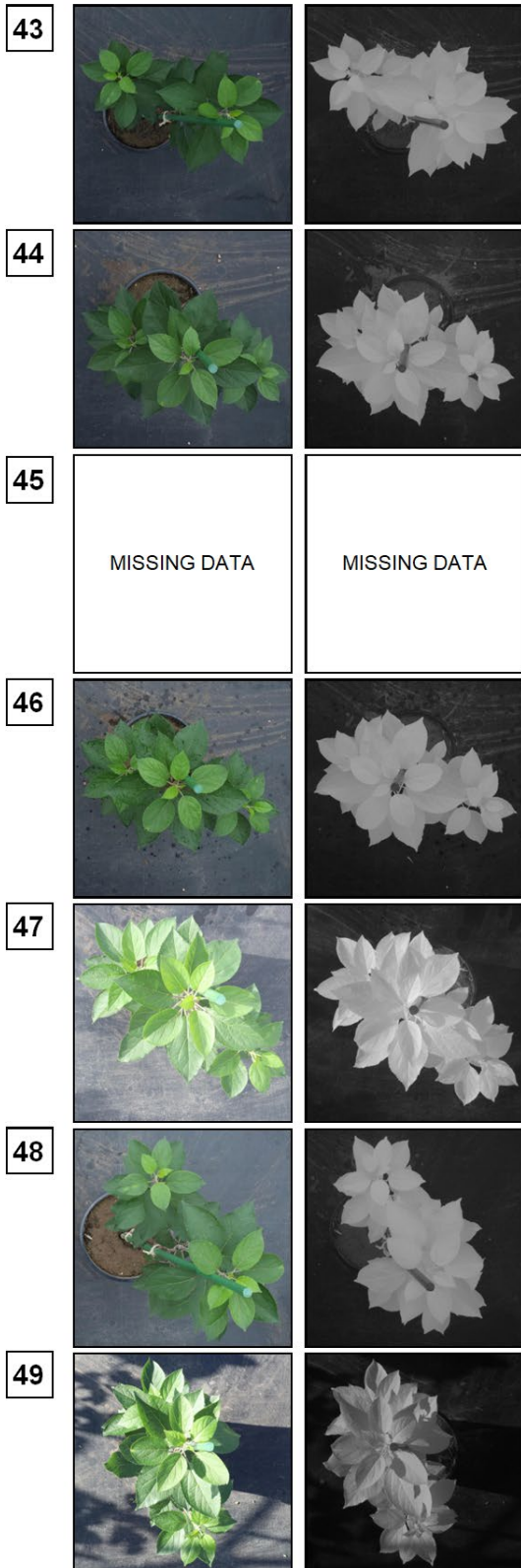


Figure 9.7 Experiment 2 'Control (C) - large' time series 29-42 d.p.i. (Sample C07)

C07 - WEEK 7



C07 - WEEK 8

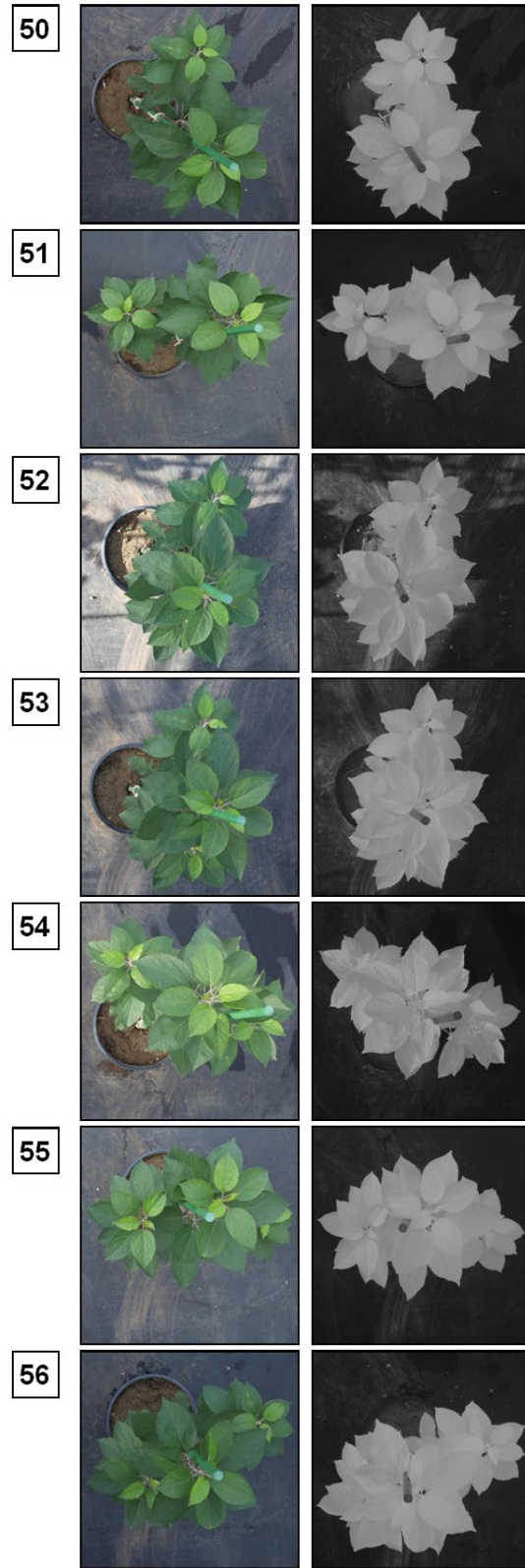


Figure 9.8 Experiment 2 'Control (C) - large' time series 43-56 d.p.i. (Sample C07)

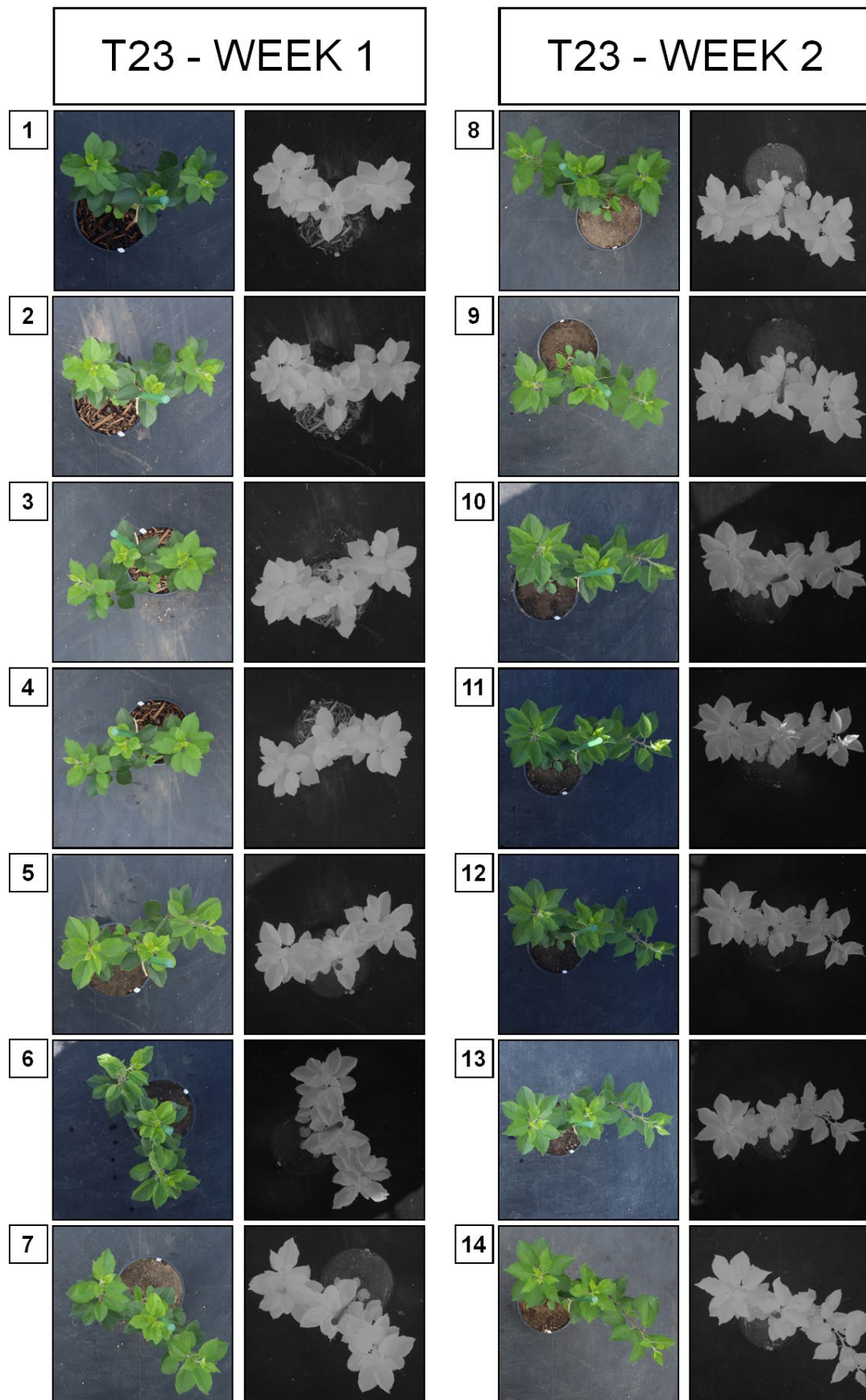


Figure 9.9 Experiment 2 'Training (T) - large' time series 01-14 d.p.i. (Sample T23)

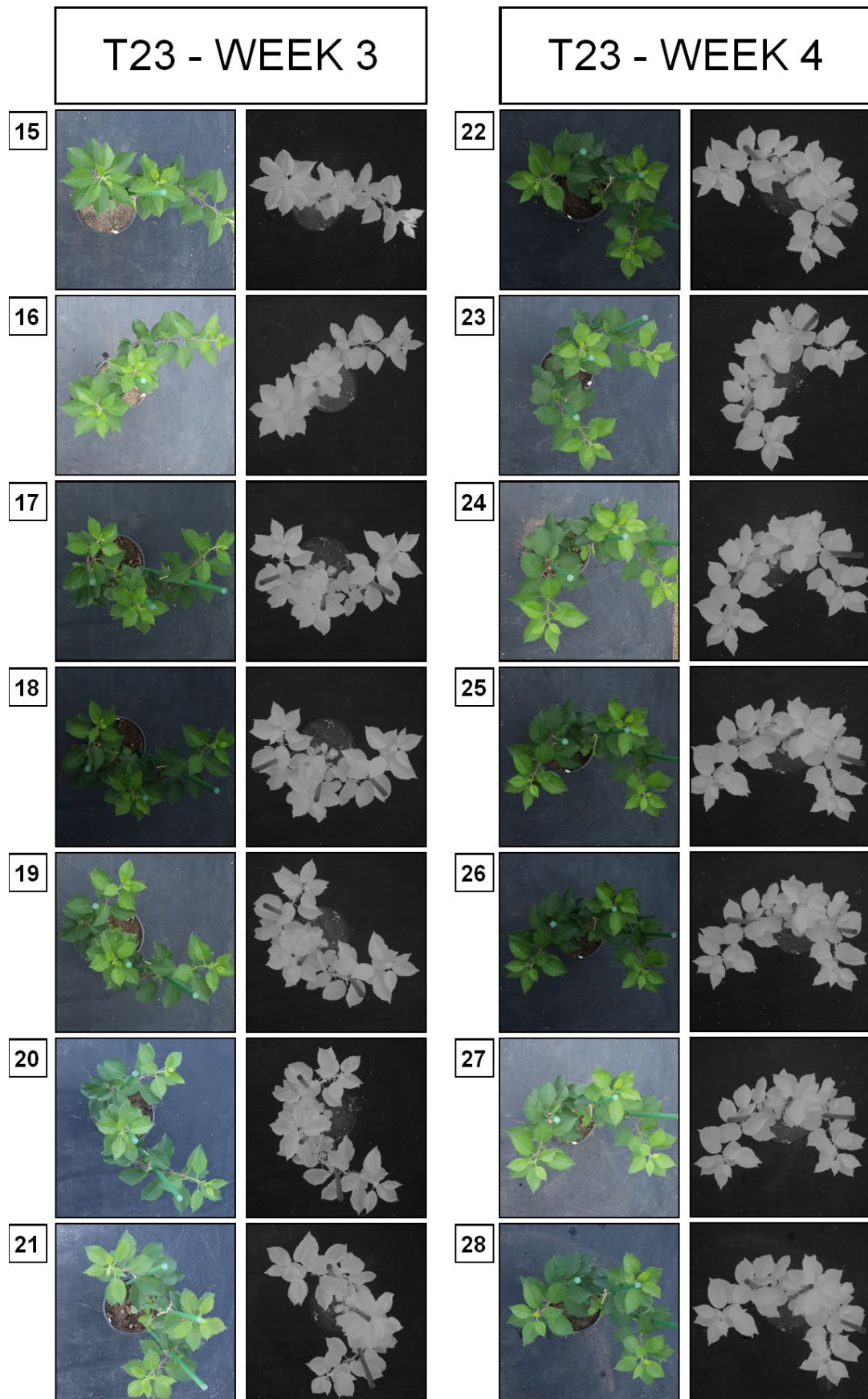


Figure 9.10 Experiment 2 'Training (T) - large' time series 15-28 d.p.i. (Sample T23)

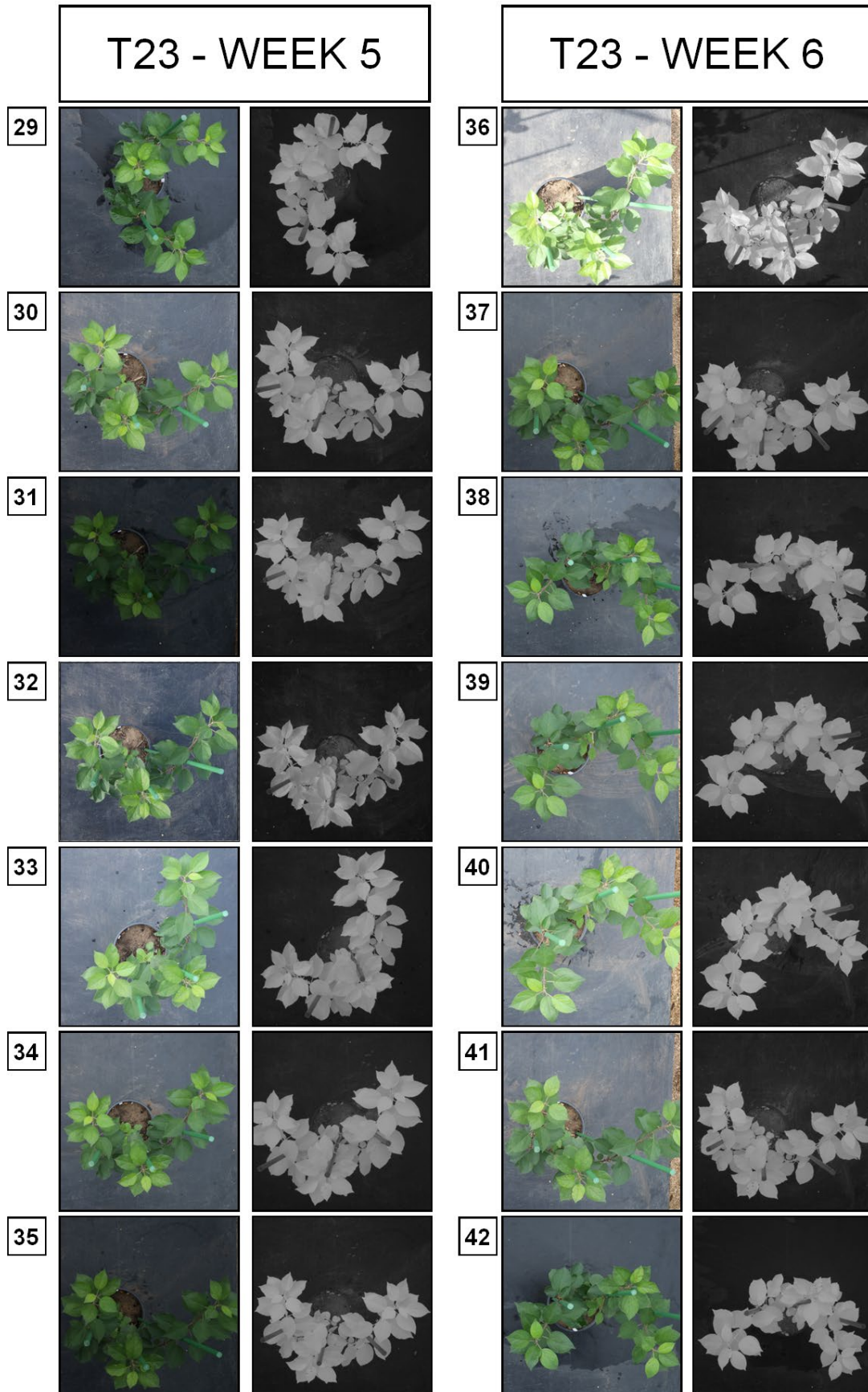


Figure 9.11 Experiment 2 'Training (T) - large' time series 29-42 d.p.i. (Sample T23)

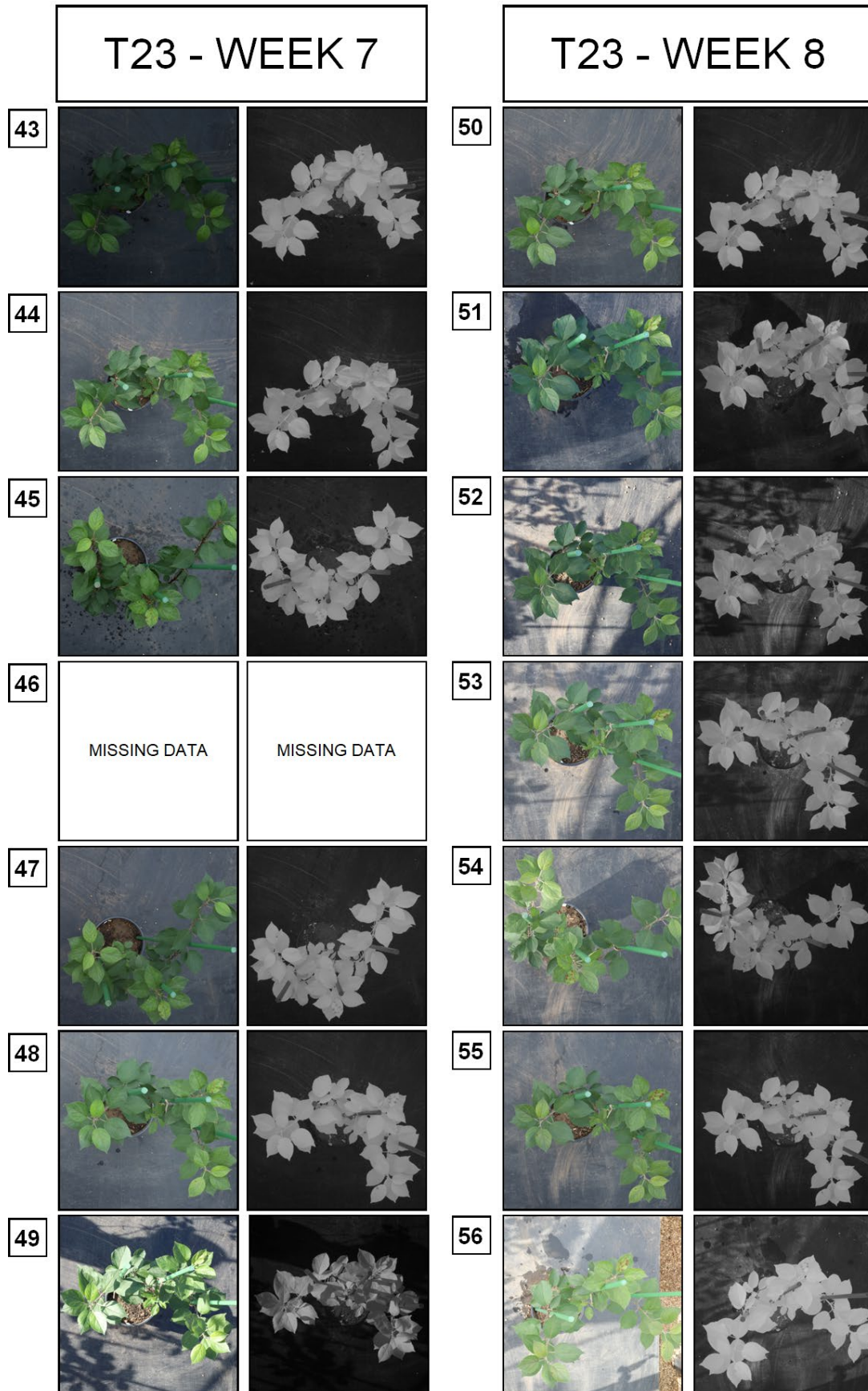


Figure 9.12 Experiment 2 'Training (T) - large' time series 43-56 d.p.i. (Sample T23)

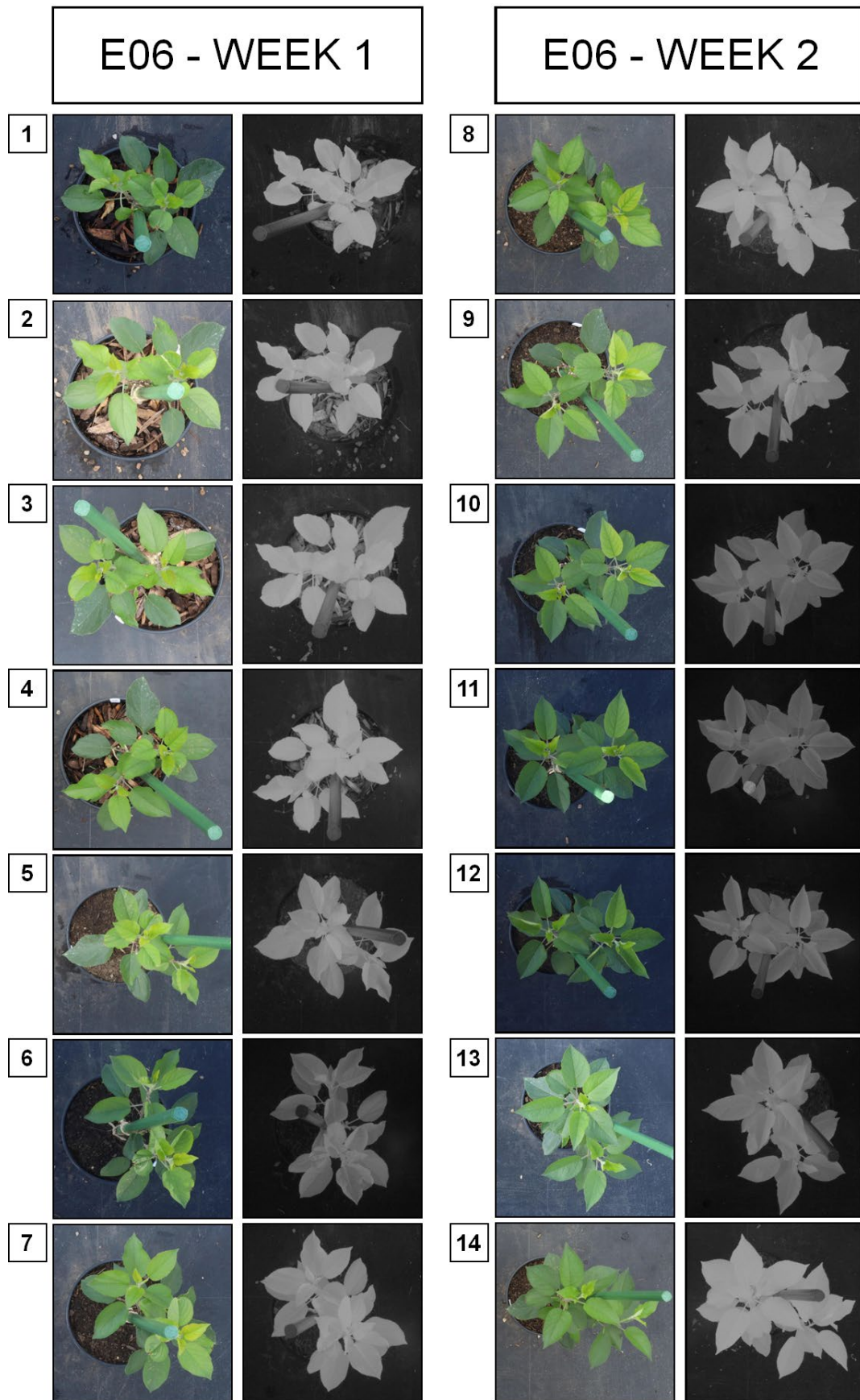


Figure 9.13 Experiment 2 'Experimental (E) - medium' time series 01-14 d.p.i. (Sample E06)

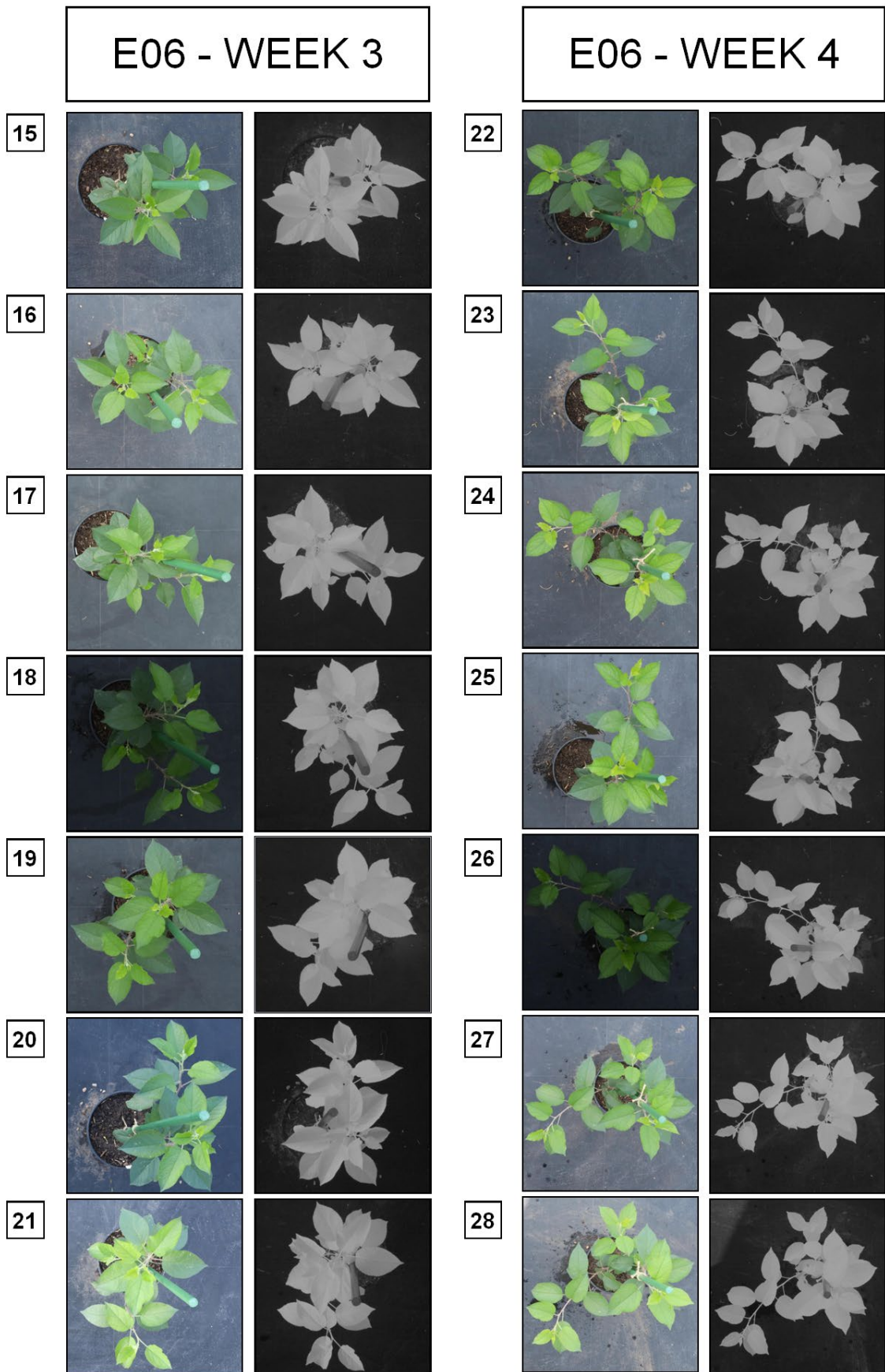


Figure 9.14 Experiment 2 'Experimental (E) - medium' time series 15-28 d.p.i. (Sample E06)

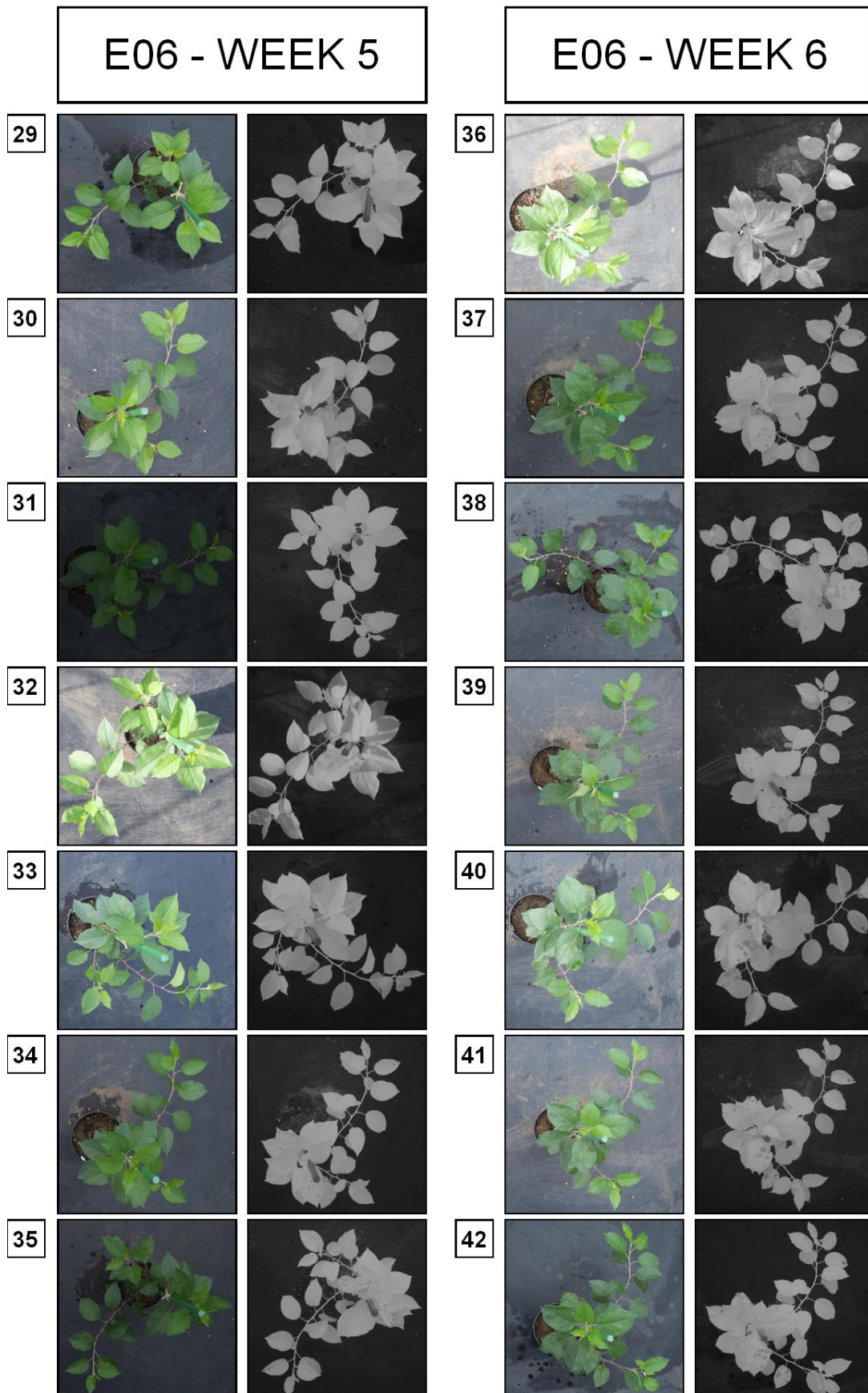


Figure 9.15 Experiment 2 'Experimental (E) - medium' time series 29-42 d.p.i. (Sample E06)

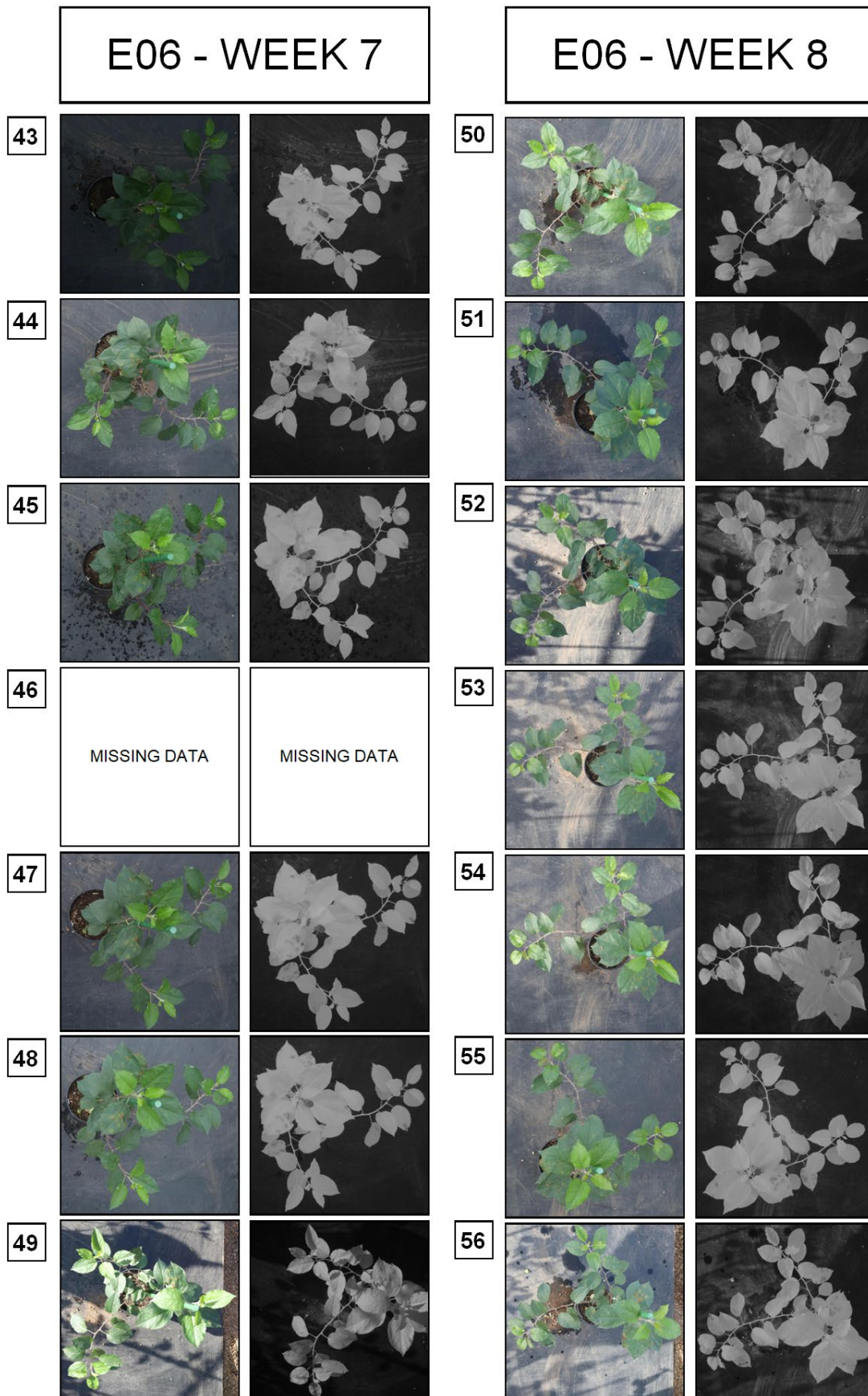


Figure 9.16 Experiment 2 'Experimental (E) - medium' time series 43-56 d.p.i. (Sample E06)



Figure 9.17 Experiment 2 'Experimental (E) - small' time series 01-14 d.p.i. (Sample E09)



Figure 9.18 Experiment 2 'Experimental (E) - small' time series 15-28 d.p.i. (Sample E09)

E09 - WEEK 5

E09 - WEEK 6

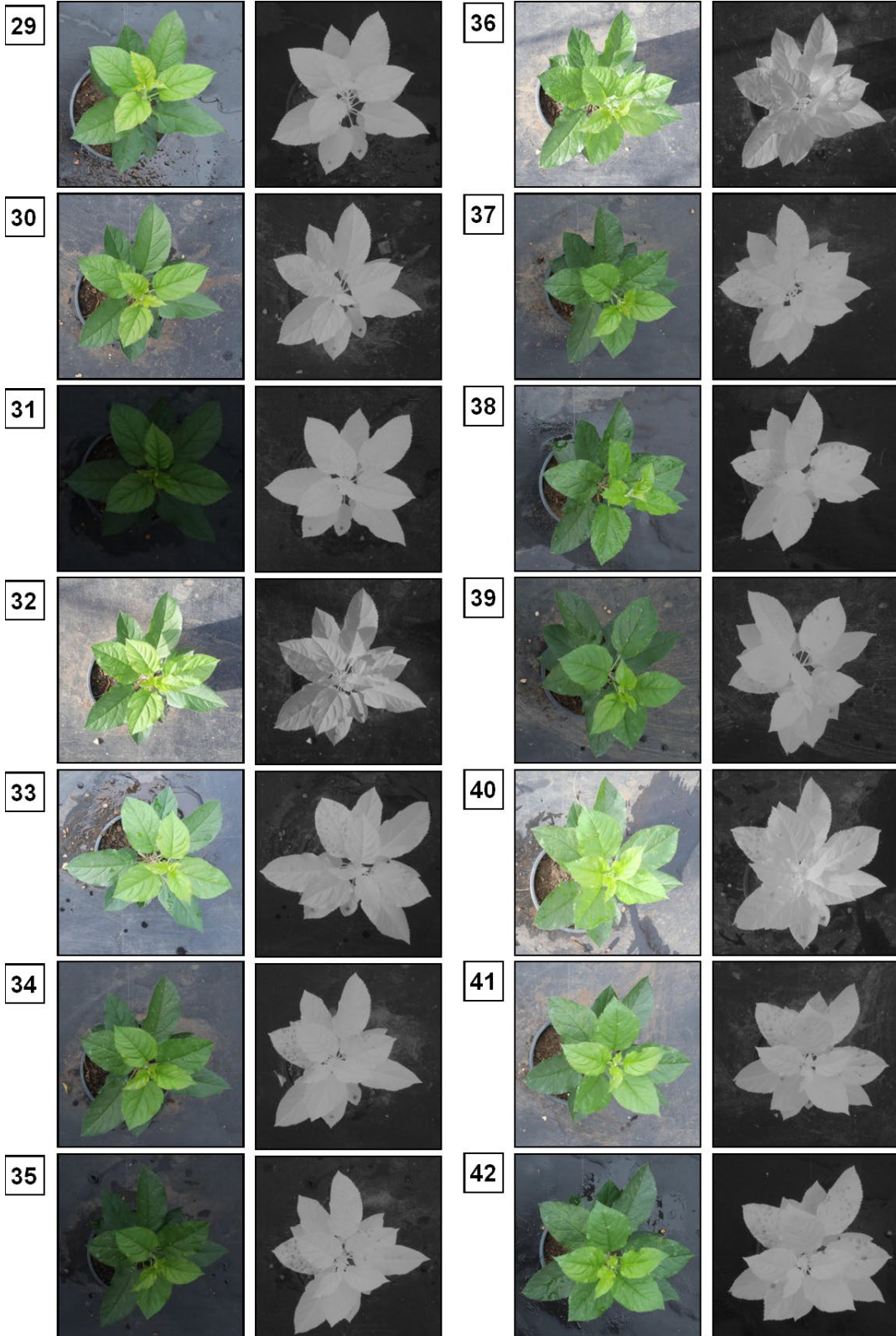


Figure 9.19 Experiment 2 'Experimental (E) - small' time series 29-42 d.p.i. (Sample E09)

E09 - WEEK 7

E09 - WEEK 8

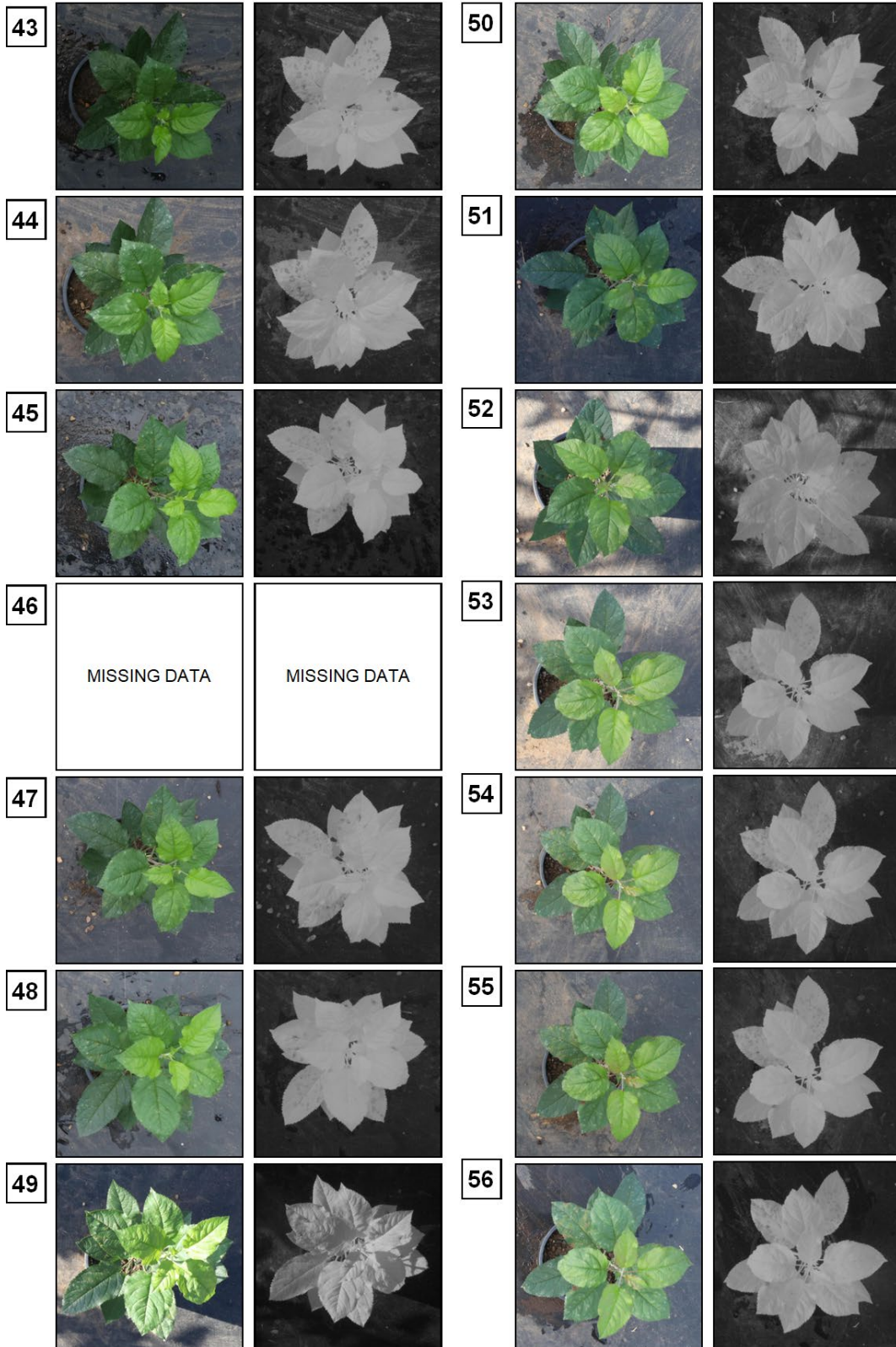


Figure 9.20 Experiment 2 'Experimental (E) - small' time series 43-56 d.p.i. (Sample E09)